ABSTRACT

Title of Dissertation: EVALUATING SURFACE MECHANISMS FOR CATALYTIC COMBUSTION OF H_2 AND CH_4 ON Pd CATALYSTS

Seyed-Abdolreza Seyed-Reihani, Doctor of Philosophy, 2005

Dissertation directed by: Associate Professor Gregory Jackson
Department of Mechanical Engineering

Applications of fuel-lean catalytic combustion for power generation and exhaust heat recovery have raised the desire for reactor optimization. Such optimization requires adequately detailed surface chemistry models to predict reactor performance over a broad range of conditions relevant to the application. This study presents experimental studies in well-defined micro-reactors for catalytic combustion of CH_4 and H_2 on γ-Al_2O_3 supported Pd catalysts, which are used to evaluate and refine surface chemistry mechanisms. The experimental results are compared to predictions by a transient numerical model for a catalytic channel flow with intra-phase diffusion in the porous washcoat support. Mechanisms for low temperature (< 250ºC) combustion of H_2 under excess O_2 and for relatively high temperature (> 400ºC) CH_4 combustion under excess O_2 have been developed and evaluated by comparison of experimental results in well-defined microreactors with transient model predictions.

Low-temperature catalytic combustion over Pd-catalysts of very lean H_2/O_2 mixture diluted in N_2 has been studied in the catalytic washcoat micro-reactor with transient exhaust monitoring using mass spectrometry. Experimental results reveal the important features of the Pd-H_2-O_2 surface chemistry under excess O_2, particularly the effects of competitive adsorption/desorption of both the reactants and H_2O product. Results show that H_2 conversion depends on equivalence ratio at temperatures ≤ 125°C and on H_2O vapor < 125°C. A proposed multi-step surface chemistry predicts based on detailed elementary reaction steps with thermodynamic reversibility and surface species interaction potentials captures the trends for conversion with respect to inlet temperature and water vapor. Intrinsic low dimensional manifolds (ILDM) were identified for the heterogeneous Pd-H_2-O_2 kinetics and the results show how specific species equilibration define the slowest modes in the catalytic reaction system.

For the fuel lean CH_4 oxidation over supported Pd catalysts, isothermal time-on-stream microreactor experiments and heating/cooling cyclic tests from 400°C to 850°C revealed the effects of PdO reduction/reoxidation on CH_4 combustion kinetics. Test results with different H_2O concentration revealed that competitive CH_4 and H_2O adsorption impacts on the activity only under catalyst conditions dominated by PdO. A detailed Pd-CH_4-O_2 surface mechanism predicts the impact of Pd reduction/reoxidation on CH_4 oxidation rates. A post-process sensitivity analysis reveals the important reactions steps and provides a means for improving the detailed mechanism for predicting the complex hysteretic kinetics of CH_4 oxidation on Pd.

EVALUATING SURFACE MECHANISMS FOR CATALYTIC COMBUSTION OF H_2 AND CH_4 ON Pd CATALYSTS

by

Seyed-Abdolreza Seyed-Reihani

Dissertation submitted to the Faculty of the Graduate School of the
University of Maryland, College Park in partial fulfillment
of the requirements for the degree of
Doctor of Philosophy
2005

Advisory Committee:

Associate Professor Gregory Jackson, Chairman/Advisor
Professor Reinhard Radermacher
Professor Gottlieb S. Oehrlein
Associate Professor Kenneth Kiger
Assistant Professor Elias Balaras

Dedicated to my wife, Zahra

, with all my respect and love

, and our dear daughter Hosna

Acknowledgements

It is my great pleasure to express my sincere gratitude to my advisor, Dr. Gregory Jackson for his invaluable help throughout my Ph.D. program. I could not have completed my dissertation without his guidance and patience. I am very thankful for all amount of time that he dedicated to me. His experience and deep insight in catalytic combustion has largely helped me finishing my Ph.D. dissertation. I would also like to thank the other members of my advisory committee, Dr. Reinhard Radermacher, Dr. Gottlieb Oehrlein, Dr. Kenneth Kiger and Dr. Elias Balaras for their valuable comments and suggestions for improvement. I thank my friends and colleagues in the Reacting Flow Lab, Fuel Cell Research Center and Catalyst Lab for their companionship and help. I would also like to thank my Iranian friends Reza Zarkesh and Dr. Reza Roodsari for their support when I studied in University of Maryland. I am thankful to my brother-in-law, Mohammad, and Reza Kazemi who helped me to improve my presentation. I am deeply indebted to my family in particular, my wife and my sweetie daughter, Hosna for all their love, support and sacrifice that provided my unending inspiration throughout this effort. Finally, but not at the least I am very thankful to my mom and sister for their spiritual support. I sorely missed my late Dad who taught me real values of our transient lives. May God bless him.

The study reported in this dissertation was supported by funds provided by:

- National Science Foundation: Dr. Farley Fisher, Program Manager
- Office of Naval Research: Tom Swean, Program Manager
- Alstom Power Research Center: Dr. Tim Griffin, Program Manager

that, I am thankful for their financial support.

Table of Contents

List of Tables

List of Figures

List of Abbreviation

a_{cat}	Surface area of catalyst per volume of washcoat
a_{ch}	Geometric surface area of channel per volume of channel
a_{wc}	Interface surface area of washcoat with channel per volume of washcoat
A_i	Pre-exponential factor
$\overline{C}_{Pk,b}$	Molar specific heat capacity for k^{th} species in catalyst bulk
$\overline{C}_{Pk,s}$	Molar specific heat capacity for k^{th} species on catalyst surface
$C_{Pk,g}, C_{Pk,gs}$	Specific heat capacity for gas species k in channel and washcoat
$C_{P,sub}, C_{P,wc}$	Specific heat capacity for washcoat and reactor substrate
$\overline{C_{P,s}}$	Effective specific heat capacity for washcoat, substrate, catalyst, and gas in washcoat
$\overline{C_{P,g}}$	Effective specific heat capacity for gas in channel
d_{hyd}	Hydraulic diameter of channel
$D^M{}_k$	Mixture-averaged diffusion coefficient
$D^M{}_{kj}$	Ordinary multi-component diffusion coefficient
D_{ij}	Binary diffusion coefficient
$D^T{}_k$	Thermal diffusion coefficient
E_{act}	Activation energy per unit mole
f	Factor used in equation for Stefan velocity

$h_{k,g}, h_{k,gs}$	Specific enthalpy of the kth species in the channel and washcoat
$h_{k,gm}$	Average specific enthalpy of species k between channel and washcoat
h_T	Heat transfer coefficients
$\vec{j}_k$	Diffusion flux of the kth species (= $\rho Y_k \vec{V}_k$)
$\vec{j}^{\,d}$	Ordinary diffusion part in mass flux of gas phase $\vec{j}_k$
$\vec{j}^{\,T}$	Thermal diffusion (Soret effect) part in mass flux of gas phase $\vec{j}_k$
$\vec{j}^{\,P}$	Pressure diffusion (Soret effect) part in mass flux of gas phase $\vec{j}_k$
$\vec{j}_q$	Heat flux of gas phase by conduction, Dufour effect and mass diffusion
$\vec{j}^{\,c}$	Heat conduction in heat flux of gas phase $\vec{j}_q$
$\vec{j}^{\,D}$	Mass diffusion heat flux of gas phase $\vec{j}_q$
k_{r_i}	Backward rate constant
k_{f_i}	Forward rate constant
K_{c_i}	Chemical equilibrium constant
K_b^f	Index of the first bulk-phase species
K_b^l	Index of the last bulk-phase species
K_s^f	Index of the first surface-phase species
K_s^l	Index of the last surface-phase species
Nu_k	Sherwood number for mass transfer of species k between channel and washcoat

$Nu_{k,i}$	Sherwood number constants for mass transfer correlation
Nu_T	Nusselt number for heat transfer between channel and washcoat
$Nu_{T,i}$	Nusselt number constants for heat transfer correlations
P_g , P_{gs}	Pressure in the channel flow and washcoat
q_i	Rate of progress of the i^{th} reaction
$\overline{R}$	Universal gas constant
$\dot{s}_k$	Molar production rate of k^{th} species per unit surface area
Sh_k	Sherwood number for the k^{th} species
S_k	Sticking coefficient
t	Time
T_g , T_s	Temperature in the channel flow and washcoat
T_{in}	Temperature in the inlet of channel
T_{ext}	Temperature of external gas phase over the porous layer
u_g	Mean axial velocity in the channel flow
u_{in}	Mean axial velocity in the inlet of channel
$\overline{V}$	Average Stefan velocity from the channel flow to the washcoat
$\vec{V}_k$	Diffusion velocity
v_{sub}	Volume of substrate to volume of washcoat
W_k	Molecular weight of the k^{th} species
W_g , W_{gs}	Mean molecular weight of mixture in channel and washcoat

W_{gm}	Average mean molecular weight between channel and washcoat
x	Axial distance
x_k	Non-dimensional distance for mass transfer correlations
x_T	Non-dimensional distance for heat transfer correlation
$X_{k,b}$	Mole fraction of the k^{th} bulk species
X_k	Mole fraction of the k^{th} gas phase species in channel
$X_{H2O,ext}$	Mole fraction of H_2O in external gas phase over washcoat
$Y_{k,g}$, $Y_{k,gs}$	Mass fraction of gas phase species k in the channel and washcoat
$Y_{k,gm}$	Average mass fraction of gas species k between channel and washcoat
$YV_{k,g}$	Mass weighted diffusion velocity of species k from channel to washcoat
β_i	Temperature exponent in Arrhenius rate equation
Γ_{cat}	Surface site density of the catalyst
ε	Porosity of catalytic washcoat
λ_s	Effective thermal conductivity of solid reactor substrate with washcoat
ρ_g , ρ_{gs}	Gas phase density in the channel flow and washcoat
ρ_{gm}	Average gas phase density between the channel flow and washcoat
ρ_{wc} , ρ_{sub}	Solid phase density of washcoat and reactor substrate
$\theta_{k,s}$	Surface site fraction of the k^{th} surface species
Θ_k^T	Thermal diffusion coefficient for the k^{th} species
σ_{cat}	Dispersion of catalyst

ϕ	Equivalence ratio
$\dot{\omega}_k$	Molar production rate of k^{th} species from gas-phase reactions

Chapter 1

Introduction to Catalytic Combustion and Modeling

1.1 The importance of catalytic combustion

Since the late 1950's catalytic combustion has been under investigation for its capability in removing volatile organic compounds (VOC) by total oxidation (Lopez et al. 2001). A decade later heat generation by this method and its application towards minimizing emission and NO_x in the combustion process has become of significant interest. Catalytic combustion also has potential to broaden lean stability limit of peak flame temperature less than 1500°C without significant formation of pollutant where lean premixed homogeneous combustion is not possible (Etemad et al. 1999).

Catalytic combustion of natural gas over Pd has potential for many industrial applications, e.g. gas turbines and boilers, due to its ultra-low emissions of NO_x, CO and unburned hydrocarbons (Forzatti 2003). Catalytically assisted combustion of natural gas is a promising technology in generating energy at higher yields and in a more environmentally friendly way than thermal combustion (Ozawa et al. 2003). Gas turbines as sources of power generation, used broadly throughout the industry, show a big room for implementing catalytic combustion to achieve ultra-low NOx emissions (Fant et al. 2000).

Catalytic combustion is not limited to hydrocarbons. Catalytic combustion of H_2 over Pt, as a typical problem, also has been investigated extensively numerically and experimentally to understand reaction kinetics and present transport phenomena (Fernandes et al. 1999). Among all the candidates for possible alternative fuels, hydrogen

has a priority due to its high contents of energy and environmental friendliness. Hydrogen has a great potential for use in fuel cells in anode side.

Modeling of catalytic combustion has exhibited great challenges due to large disparity in length and time scales ranging from quantum, to atomistic, to mesoscopic, to macroscopic (Raimondeau and Vlachos 2002). There are coupling mechanisms between scales. Figure 1.1 depicts the range of present length scales in a monolithic catalytic reactor.

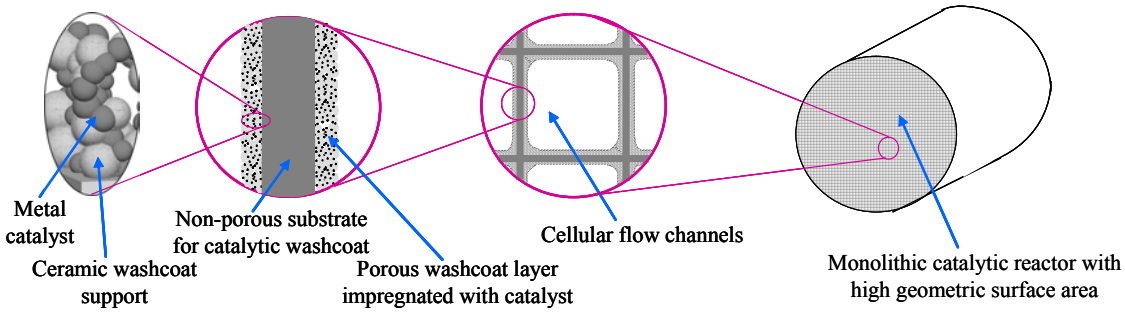

Figure 1.1 Length scales involved in a monolithic catalytic reactor

A catalyst consists of a series of dispersed small active metal/metal oxide particles (usually transitional metals) on an inert and porous support with very high surface area, e.g., 200 m^2/g. The support holds the metal in place, so the catalyst is easy to separate from the reacting mixture. Materials like aluminum oxide (alumina), silicon dioxide (silica), activated carbon and zeolites (alumino silicates) are used as support with pore size in order of 1 μm. A critical property of supported catalysts is that they have high dispersion (fraction of atoms on the surface). The numerical model developed in the current study is based on the mean field (MF) theory and covers meso-scale length scales

in a catalytic reactor. It assumes infinity Fickian diffusion on the catalyst surface and removes all spatial non-uniformity on the catalyst surface.

Predictions of numerical models are strongly reliable on detailed surface chemistry. The chemistry of reactions is modeled by elementary reactions on a molecular level in the gas phase and on the surface phase. In the current study, surface chemistry mechanisms will be developed for catalytic combustion of H_2 and CH_4 on Pd-based catalysts. Intrinsic low dimensional manifold, (ILDM) as a powerful tool is used to analyze the developed surface chemistry.

1.2 Background

1.2.1 Hydrogen combustion on Pd catalysts

Hydrogen has great potential for use in fuel cells and in ultra-low emission catalytic combustion systems with exhaust temperatures well below 1000°C. Use of it accompanies an important reduction in NO_x, CO and CO_2 emissions (Sheng et al. 2002). The oxidation of hydrogen on different metal catalysts has been studied for a number of decades (Lischka and Gross 2002). Among the metals, Pd has shown a great activity for different applications such as heating applications and fuel cell anode exhaust.

Recently low temperature catalytic combustion of H_2 on supported noble Pd catalyst has been under investigation for applications such as deep-sea diver heating during long duration, breathing air humidification. This heating technique is expected to minimize the power and space requirements that must be dedicated to diver thermal protection within swimmer delivery vehicles or free-swimming missions (Nuckols 2000). Figure 1.2 shows a schematic design of this apparatus.

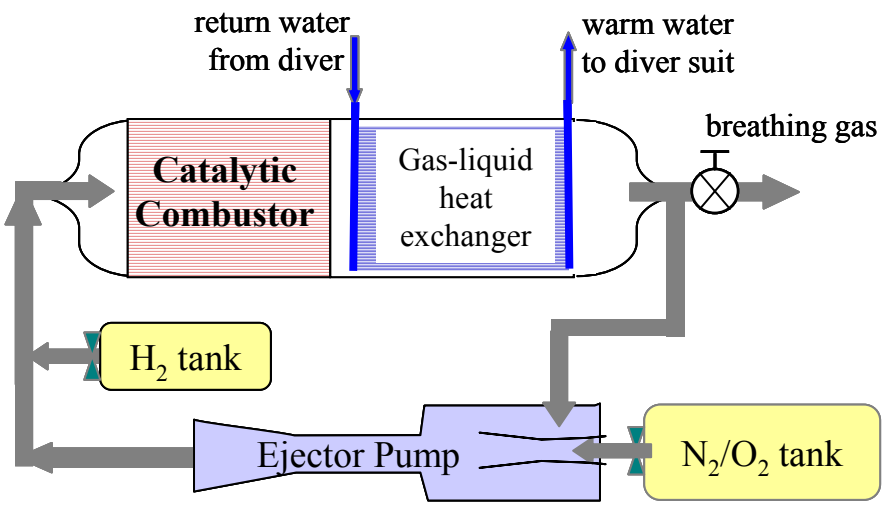

Design courtesy of Prof. M. Nuckols
U.S. Naval Academy, Annapolis, MD

Figure 1.2 Deep sea diver heating and breathing gas humidification

As the other application H_2 combustion on metals such as Pt/Pd in anode side of a proton-exchange membrane fuel cell (PEMFC) (Emonts 1999), has brought a great motivation to understand catalytic oxidation of H_2 in low temperatures. PEMFC has shown promising to be an efficient and clean alternative to fuel combustion for primary power generation for stationary and mobile source applications (Farrauto et al. 2003). They are about twice as fuel efficient as the internal combustion engines with negligible emission. Figure 1.3 shows H_2 combustion in fuel cell anode exhaust generating heat for steam reformer to produce H_2-rich reformate.

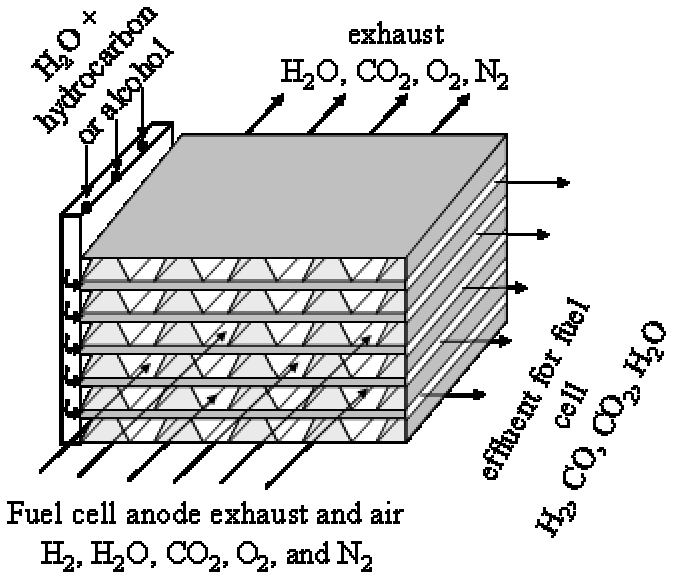

Figure 1.3 Fuel cell anode exhaust for steam reforming

Interest in low-temperature H_2 catalytic combustion, however, it is not limited to potential applications. As with homogeneous chemical mechanisms, where H_2-O_2 chemistry provides a critical subset of larger mechanisms for hydrocarbon combustion, the heterogeneous chemistry of H_2 and O_2 on specific catalysts such as polycrystalline PdO_x also provides a key subset of reactions necessary for building larger surface chemistry mechanisms for oxidation of CH_4 and higher hydrocarbons which is the most important aspect of the current research. The current study employs a well-characterized, temperature-programmed reactor to explore the surface chemistry for H_2 combustion on Pd catalysts at low inlet temperature, T_{in}, and equivalence ratio, ϕ, and to provide a launching point for mechanism refinement and development of larger mechanisms for hydrocarbon combustion on Pd catalysts (Kramer et al. 2003).

Recently, catalytic combustion of H_2 has found application in nuclear power plants. In case of a severe accident, Pd-based catalyst of H_2 combustion can control the risk of an explosion in a nuclear power plant (Morfin et al. 2004).

Interaction of H_2 with metal surfaces has served as a model system for the investigation of fundamental reaction steps at surfaces, both experimentally as well as theoretically(Lischka and Gross 2002). Non-activated dissociation of H_2 on Pd as a unique capability and its high solubility and mobility in Pd have been resulted in several technologies such as H_2 storage, gas sensors and H_2 purification devices (Nutzenadel et al. 2000). Pd exposed to H_2 can undergo a strong reconstruction of the electronic structure of the surface and lead to the formation of non-stoichiometric PdH_x (Shaikhutdinov et al. 2001). For example at room temperature Pd can be loaded with H_2 to make a compound $PdH_{0.83}$ only by exposing metal surface by H_2(Cobden et al. 1999). Formation of PdH_x is related with the increase of the lattice constant by a factor 3.5%. At T < -70°C a monolayer of dissociated H atoms occupying the 4-fold hollow surface sites is readily saturated on Pd(100)(Fogelberg and Petersson 1996). In atmospheric pressure of H_2 thickness of hydrogen layer formed over the Pd film is estimated 50nm. It has been shown by TPD plots three distinct signals, a sharp low-temperature signal denoting desorption of surface chemisorbed hydrogen (β-phase) and a broad desorption signal indicating subsurface hydrogen (α_1-phase) at low H_2 pressure and bulk H solid solution (α_2-phase) at high H_2 pressure(Fogelberg and Petersson 1996).

The reaction on Pt, Pd and Ag is of special importance, since water as the product of the reaction easily desorbs, leaving the surface accessible for further adsorption of the reactant (Ljungstrom et al. 1989). Catalytic combustion of hydrogen under lean

conditions is of particular interest for the understanding of the chemical reactions on catalyst metal. Also in lean hydrogen-oxygen mixtures, modeling of the mass transport in the gas phase is much simpler, if the physical properties of gas mixture such as temperature and density do not change considerably as a result of the chemical reaction (Johansson and Ekedahl 2001).

1.2.2 Methane oxidation on Pd catalysts

Noble metal catalysts such as Pt, Rh and Pd and their metal oxides are the most active systems at low and high reaction temperatures of alkanes. Palladium is also used in exhaust clean-up and in catalytic removal of volatile organic compounds (VOC) (Farrauto 1997). This shows a high oxidation activity of Pd even under very fuel lean conditions that is not possible for the most other noble metal catalysis. For combustion of light hydrocarbons like methane several investigations suggested supported palladium on alumina or zirconia to be the best catalyst, although Rh and Pt are known to be efficient for higher hydrocarbons (Farrauto et al. 1992). It is well known both metallic and oxide phases are active in catalytic activation (double activity). The oxide form of Pd is considered as the most active phase (Burch 1997; Ciuparu et al. 2002).
Catalytic activity of supported palladium for CH_4 combustion is related to different parameters including support material, weight percentage of Pd, dipersivity of catalyst and reactor temperature.

Catalytically assisted combustion of natural gas with a minimum emission of NO_x, CO and hydrocarbons is a promising technology for gas turbine industry (Forzatti 2003; Ozawa et al. 2003). Numerous demonstrations and even recent field operation in

working gas turbines (Kajita and Betta 2003) have shown that lean catalytic combustion with Pd-based catalysts as the front end section of the reactor can provide reliable steady-state performance at low adiabatic reaction temperatures (T_{ad} < 1200ºC). These reactors have relied on Pd-based catalyst for light-off at low inlet temperatures T_{in} and in many cases alternative channel coating for managing reactor temperatures over the front-end Pd-based catalyst (Forzatti 2003). Figure 1.4 shows a schematic of one kind of hybrid catalytic combustor for gas turbine engine applications, which provides motivation for this study. The premixed air/fuel (CH_4) stream is fed to catalytic combustor for partial conversion to complete combustion products before entering a homogeneous burnout region where the remaining un-burnt fuel is ideally consumed (Fant et al. 2000).

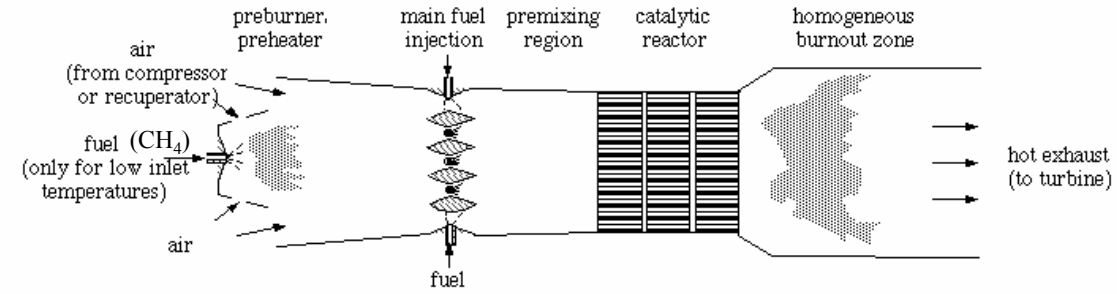

Figure 1.4 Schematic of hybrid catalytic combustor for gas turbine

At catalytic oxidation conditions, surface and bulk state of Pd supported catalysts at low reactor temperatures are composed almost entirely of PdO_x which are very active for CH_4 oxidation. At temperatures higher than 700°C, it's believed the stable phase is in the form of metal Pd with low activity. The change in the catalyst activity, results from the change in crystal structure and the electronic properties of the catalyst surface (Lyubovsky and Pfefferle 1999; Perdigon-Melon et al. 2003). It has been shown at

temperature range 200 thru 700 °C state of the catalyst surface is dominantly in its most active form, PdO_x , stable up to 750 °C in air at 1 atm (Farrauto et al. 1992). It has been indicated the rate limiting step of CH_4 oxidation in net oxidized environment below 700 °C on the Pd-based supported catalysts is related to the density of oxide vacancy Pd(sb) and oxygen occupied sites O(sb) (Wolf et al. 2003). It is observed, that the low temperature CH_4 oxidation on Pd-based catalysts can be assisted by metallic phase of Pd catalyst (Carstens et al. 1998).

Thermodynamically stable phases of Pd-supported catalysts, by reactor temperature and oxygen partial pressure, during CH_4 catalytic combustion has been studied extensively by different researchers. The complex behavior of CH_4 combustion on the Pd-supported catalysts is associated with the Pd oxidation-reduction. Hysteresis loop over temperature range from 600 °C to 800 °C in the oxidation of CH_4 over Pd catalyst supported on γ-Al_2O_3 was observed by different researchers (Farrauto et al. 1992; Salomonsson et al. 1995; Groppi et al. 1999; Forzatti 2003; Lyubovsky et al. 2003). TGA experiments indicate that at standard air O_2 partial pressures PdO decomposes to Pd at temperatures higher than 750 °C during heating cycle, but re-oxidation of metal on the cooling cycle doesn't start until temperature drops well below 650 °C (Farrauto et al. 1992; Datye et al. 2000; Wolf et al. 2003). The hysteresis loop in CH_4 combustion on Pd-supported catalyst is believed to depend upon the transformation between different phases of Pd-based catalysts. The same loop was confirmed by McCarty where the hystresis is attributed to the formation of a relatively stable saturated layer of chemisorbed oxygen which prevents of nucleation and growth of the active surfaces of bulk PdO and inhibits the rate of oxidation of methane. The extent of bulk Pd reoxidation

is strongly temperature and support dependent (McCarty 1995). Groppi et al. concluded the observed hystresis loop originated from two phenomena: (1) the reactivity of PdO is higher than metallic Pd, (2) the temperature threshold for the onset of the PdO → Pd transformation differs from that of the reverse Pd → PdO (Groppi et al. 1999). Significant drop in catalytic activity of CH_4 at temperatures higher than 700°C over alumina supported Pd catalysts is due to decomposition of PdO (Sekizawa et al. 1993). Complete transformation at higher temperatures generates crystalline metal particles, which are relatively resistant to oxidation during the cooling and thereby cause the Pd reduction/oxidation hystresis. It was reported that at temperatures higher than 800 °C, that the Pd-supported catalyst in reduced form is much more active to complete CH_4 oxidation than the oxidized form (Lyubovsky and Pfefferle 1998; Lyubovsky and Pfefferle 1999). Study of the catalyst microstructure by TEM during methane oxidation on alumina supports has revealed that the PdO → Pd transformation is initiated at the surface and causes small patches of Pd metal to form on the surface of the PdO (Datye et al. 2000). However, complete transformation during heating cycle generates single crystal metal particles, to be oxidized harder upon cooling cycle.

In the first attempt to model oxidation-reduction kinetics of polycrystalline Pd foil over a broad range of temperature, it was suggested that the observed behavior can be explained in terms of a kinetically controlled process at lower temperatures with a low barrier and a diffusion-controlled process at higher temperatures with a high activation. In the intermediate temperature range the system displays a complex kinetic behavior with apparent negative activation energy. It means catalyst activity increases while temperature decreases. This behavior is caused by a transition between the reaction and

the diffusion controlled processes (McCarty 1995; Lyubovsky and Pfefferle 1998; Lyubovsky and Pfefferle 1999; Veser et al. 1999; Ciuparu et al. 2002).

Previous studies indicated that PdO reacts in a Mars-van Krevelan redox mechanism during catalytic oxidation of CH_4 at temperatures less than 600 °C (Muller et al. 1997; Fujimoto et al. 1998; Au-Yeung et al. 1999). This redox mechanism has a key role in the activity of supported Pd for oxidation of CO and CH_4. CO oxidation is an intermediate surface reaction during CH_4 combustion. Repeated oxidation/reduction cycles are also responsible for the occurrence of temporal oscillations in CO oxidation over Pd catalyst. These oscillations occur over a range of $0.05 < P_{co}/P_{o2} < 2$ ratios and a temperature range 230-350 °C (Bassett and Imbihl 1990). It has been shown that kinetic oscillations in CO oxidation are generated by slow formation/removal of subsurface lattice oxygen. Imbihl setup a mathematical model which involves the formation of a subsurface of species and a periodic emptying and refilling of this subsurface oxygen reservoir (Bassett and Imbihl 1990). The model was extended to consider repulsive interactions between adsorbed oxygen atoms which changes the activation energy for subsurface oxygen formation (Hartmann et al. 1994). This model has the potential to give a good qualitative agreement with the experimental results.

There is a general agreement that the oxidation of CH_4 over PdO is strongly inhibited by H_2O and to a lesser extent by CO_2 (Ciuparu et al. 2002). Assuming a power rate law expression, dependence on H_2O was -1 over the whole studied range (Ribeiro et al. 1994; Fujimoto et al. 1998). For CO_2 was about zero below 0.5% CO_2 at low temperature (<500°C) and about -2 above 0.5% CO_2 (Ribeiro et al. 1994). Fujimoto et al. showed that low temperature CH_4 oxidation rates on Pd catalysts supported on ZrO_2

depend weakly on O_2 concentration (0.1±0.1 order), but are proportional to CH_4 concentration (1.1±0.1 order). For CO_2, they found the exponent was -2 only when CO_2 concentration is high (3-5 %) (Fujimoto et al. 1998). Study of effect of water on the activity of alumina-supported Pd catalysts in the catalytic combustion of CH_4 in the temperature range 180 – 515 °C revealed the apparent wet activation energy, 151±15 kJ/mol, was much higher than that of dry one, 86 kJ/mol. This rise in the catalytic activation energy was attributed to competitive adsorption between CH_4 and H_2O. Also, they found a nearly first order (1±0.1) in CH_4, a nearly zeroth order (0.1±0.1) in O_2 , an order of -0.8±0.2 in water vapor and a zeroth order in the partial pressure of CO_2 under all conditions (van Giezen et al. 1999; Ibashi et al. 2003). Ibashi et al. reports the orders for H_2O and CO_2, -0.32 and -0.25 respectively (Ibashi et al. 2003). It looks like Ibashi data is influenced by mass transfer since the numbers are so different. For alumina-supported palladium catalysts, a very weak inhibition effect of activity in the presence of 20% CO_2 was found that completely disappear when water was added to the feed (Burch and Loader 1994). Water inhibition effect on supported Pd catalyst for CH_4 combustion is strongly temperature dependent for equilibration of the adsorption/desorption of water. Under continuous inlet water flow inhibition effect is important to higher temperatures due to readsorption, but stronger at lower temperatures($T < 500$ °C) (Ciuparu and Pfefferle 2001; Groppi 2003; Ibashi et al. 2003). This suggests that experiment with water in the feed cannot be used to predict the behavior of real systems. Therefore, correcting the data for water inhibition effect is not straightforward (Ciuparu et al. 2001). The effect of water on activity of Pd-supported catalyst in reduced form is lower than that of the oxidized form and slowly restorable. This means water inhibition effect is not due

to deactivation of the catalyst (Ciuparu and Pfefferle 2001; Groppi 2003; Ibashi et al. 2003). It has been demonstrated that water inhibition effect is suppressed by using Pd catalysts supported by ZrO_2 instead of Al_2O_3, although, Pd-supported on ZrO_2 has as high an initial activity as Pd-supported on Al_2O_3. In other words dehydroxilation of the PdO surface is faster in the presence of high oxygen mobility support like ZrO_2 which restrains morphological changes in Pd particles due to formation of inactive surface species $Pd(OH)_2$ that effectively blocks access of CH_4 to the active surface site (Nomura et al. 1999; Ibashi et al. 2003).

1.2.3 Detailed surface chemistry mechanisms for catalytic combustion

Uncertainties in the thermodynamics and rate parameters governing surface chemistry limit the effectiveness of many surface mechanisms to a narrow range of conditions. The thermochemistry of surface species in catalytic combustion can be influenced by strong interaction potentials between various adsorbed species. Interaction potentials can lead to segregation of surface species as illustrated in CO and H_2 oxidation on Pt using Monte-Carlo simulations (Kissel-Osterrieder et al. 2000; Raimondeau and Vlachos 2002). However, under conditions where surface adsorbates are small and relatively mobile, mean field approximations may provide a computationally efficient approach for modeling complex phenomena on catalyst surfaces, such as oscillatory (Imbihl and Ertl 1995) or hysteretic reaction rates (McCarty 1995) observed in combustion on Pd-based catalysts.

Numerous applications of Pd-based catalytic combustion have motivated recent studies to build surface chemistry mechanisms with species interaction potentials for Pd-

based catalysts. A recent review of Pd-based catalytic combustion (Ciuparu et al. 2002) provides a thorough discussion of the outstanding questions raised by experimental studies regarding complex interactions of O, H, and C_1 species on Pd/PdO_x surfaces. Recent studies have developed mean-field approaches to simulate hysteresis in oxidation/reduction cycles of Pd/PdO_x catalysts (Wolf et al. 2003) and the impact of stoichiometry on low temperature oxidation of H_2 over Pd-based catalyst (Kramer et al. 2003). Developing the requisite surface thermochemistry for catalytic combustion of hydrocarbons on Pd-based catalysts will be predicated by the identification of the critical processes and equilibria in smaller subset mechanisms for $Pd/O_2/H_2$ (Kramer et al. 2003) as well as $Pd/O_2/CO$ (Imbihl and Ertl 1995). Through detailed modeling of CH_4 and H_2 combustion on supported Pd-catalysts, the current study will seek a better understanding of properties of catalysts and operating conditions in order to obtain better catalytic combustion performance for practical applications of the catalytic combustion.

In heterogeneous catalysis, the knowledge of the kinetics of chemical reactions, i.e., of the way in which the rates of reactions depend on process conditions, forms the basis for the design and optimization of both catalysts and chemical reactors. Within the steady-state frame, only lumped kinetic parameters can be estimated from a regression of steady-state kinetic data (Schuurman and Mirodatos 1997). It is possible to validate proposed surface reaction mechanisms by detailed modeling of reaction kinetics and transport phenomena, and data collected from carefully designed and simple catalytic combustion experiments. In this way, Fernandes et al. have studied autothermal behavior of platinum catalyzed hydrogen oxidation in fuel lean and fuel rich conditions (Fernandes et al. 1999). The stagnation flow geometry is modeled using multicomponent transport

and detailed surface and gas phase reactions. In their mechanistic surface reactions, repulsive interactions between hydrogen and oxygen chemisorbed species, H(s) and O(s), are implemented linearly in the desorption barrier.

Ignition, extinction and multiple steady-states in surface reactions are important in many applications like partial oxidation reactors for chemical synthesis and catalytic removal of pollutants. These instabilities limit the regime of operation of many industrial catalytic reactors and play a major role in reactor and process safety (Vlachos and Bui 1996). Global one-step surface chemistry fails to predict experimental results in complex coupling between gas-phase and surface processes. Study of oxidation of lean H_2 over Pt in a stagnation-point flow reactor has shown that Pt inhibition of homogeneous ignition and depletion of O_2 caused by fast diffusion of H_2 as compared to O_2 cannot be predicted with simple one-step chemistry (Vlachos and Bui 1996). Such lumped surface chemistry steps are fitted to experimental data and are applicable over a narrow window of conditions. Understanding of intimate coupling between surface and gas phases will accelerate significantly technological advances in catalytic combustion technology for gas turbines and other applications. Detailed and validated surface mechanisms are needed for predictive process modeling. To achieve such a goal, and to improve the control and design of these inherently nonlinear processes, there is obviously a need to model these complex processes and validate the detailed mechanistic surface chemistry. It is the major challenge in developing predictive models for catalytic combustion (Vlachos and Bui 1996; Bui et al. 1997).

Surface reaction mechanism have been tested and validated for a few very simple molecules such as H_2 and CO over the Pd or Pt supported catalysts. Detailed surface

mechanisms have been presented for the oxidation on Pt-based catalysts of CO (Raimondeau and Vlachos 2002), H_2 (Bui et al. 1997), and CH_4 (Deutschmann et al. 1998; Goralski and Schmidt 1999; Aghalayam et al. 2003) and more recently, the oxidation on Pd-based catalysts of CO (Peskov et al. 2003) , H_2 (Kramer et al. 2003), and CH_4 as well (Sidwell et al. 2003) on Pd. For a molecule like CH_4, over the Pd-based catalyst it has been a matter of debate. Applications of catalytic combustion for gas turbines (Forzatti and Groppi 1999) or utility burners and catalytic exhaust aftertreatment have led to several efforts to develop detailed multi-step mechanisms for complete oxidation of relatively small molecules such as CH_4. The surface chemistry, which must incorporate the complex interactions between CH_4 oxidation kinetics and catalyst oxidation/reduction cycles (Ciuparu et al. 2002), requires detailed multi-step reaction schemes where different steps becoming rate limiting at different reactor inlet temperatures (T_{in}) and CH_4 equivalence ratios (φ). However, Pd/PdO_x transition can cause significant transient variation in catalytic combustion activity particularly when surface temperatures rises above 800ºC (McCarty 1995; Ciuparu et al. 2002).

1.2.4 Numerical modeling of catalytic combustion

Modeling of catalytic reactors can help to understand better what governs the reaction rates (conversion of fuel) and to predict operation in regimes where experiments are difficult or dangerous. Modeling may be of great use for sizing the reactor, understanding its behavior in operations and predicting the effect of changing operation conditions (Canu and Vecchi 2002). Catalytic surface reactions and in some cases gas phase reactions along with simultaneous interphase and intraphase heat and mass transfer can lead to very complex behavior. Numerical simulation can be an effective tool for

assessing the performance of a catalytic reactor. To have a quantitative understanding of catalytic combustion, the mathematical model should provide capability to analyze the elementary chemical and transport processes at the interface of gas–surface and to relate them to surrounding gas phase. The achieving of the detail of the reactor behavior makes necessary a better agreement between experimental and flow field model with a detailed chemistry. By leveling a better agreement between experimental and modeled flow field, details of the reactor behavior can be elucidated.

Figure 1.5 illustrates a single monolitic channel is used to show all physical processes. In general, a mathematical model should include the following physical and chemical processes:

- Catalytic surface reactions in catalytic wall and homogeneous gas phase reactions
- Heat, mass and momentum transfer by convection and diffusion in the gas phase and in the interphase between gas and catalyst surface
- Heat and mass diffusion within the porous catalyst layer (washcoat)
- Heat conduction, axially and radially, and radiation in the solid non-porous substrate

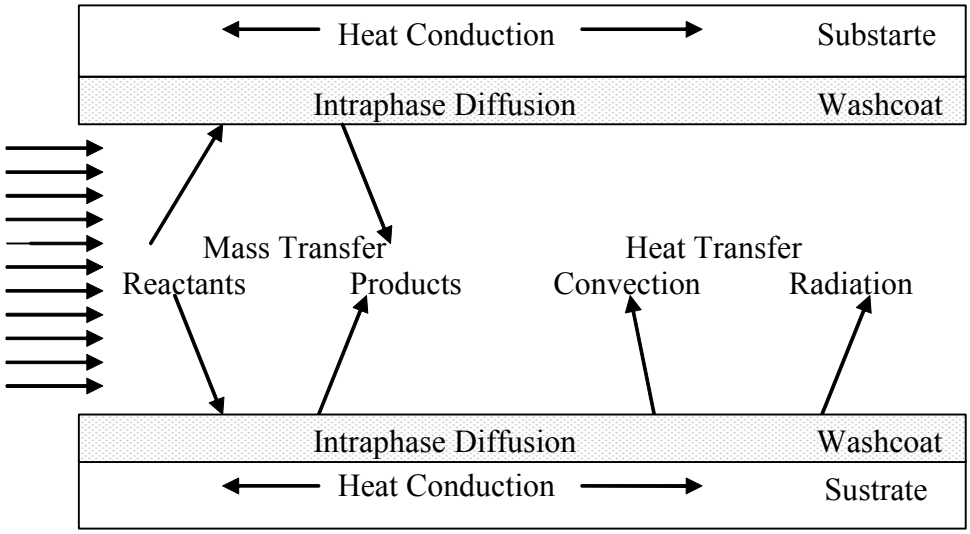

Figure 1.5 Schematic of reaction and transport processes in a monolithic channel

All these phenomena are strongly interacted due to the intense thermal effects associated with the exothermicity of catalytic surface reactions. Generally speaking surface reactions are dominant by the following sub-processes:

1. diffusion of reactants from gas phase channel flow to the gross exterior porous surface of catalyst
2. molecular/Knudsen intradiffusion of reactants to the interior porous structure of washcoat
3. adsorption of the reactants onto the catalyst surface
4. heterogeneous catalytic surface reactions
5. desorption of chemically adsorbed products away from the surface
6. transfer of products from the interior catalyst pores to the external surface of catalyst by diffusion mechanisms
7. diffusion of products into the gas phase channel flow

During an exothermic oxidation reaction, relatively low temperature of gas phase reactants and high mass transfer gradients at the entrance to the monolithic channel, surface reactions usually control the behavior of reactor called kinetically controlled region. Because of heat release of surface chemical reactions, the temperature of the catalyst wall as well as the gas flow increases and all diffused reactants will be depleted as the rate of surface reactions increase exponentially. Accordingly, the downstream portion of channel that is more likely controlled by mass transfer rate is called diffusion-controlled region.

In recent years modeling of reacting flows raised many challenging points. There is a broad range of time and length scales in a catalytic reactor that control various processes. Reactor length scales span several orders of magnitude from the largest length scales associated with reactor length down to the small length scales associated with the catalyst particle sizes (on the order of a few nanometer). Large ranges of time scales causes the governing partial differential equations for catalytic oxidation reactors to be very stiff.

Lumped and distributed models are the two types of numerical modeling in catalytic combustion. In the lumped model, a one-dimensional model is based on lumping of the cross-sectional and peripheral distributed variables into appropriate average values such as plug flow model. However, in the distributed model, variables account for the distribution over the cross section and periphery such as 2D channel flow configuration; stagnation point flow and flat plate boundary layer flow, for both steady state and transient flows. Following are the main elements of the aforementioned models:

- Identification of different regimes of catalytic combustion and distribution of dominant species
- Characterization of catalytic ignition (diffusion control) and extinction (kinetic control) of different fuels in a range of operating pressures and temperatures as a function of fuel-to-air ratio and effect of different heat transfer modes
- Thermal efficiency of catalyst by fuel conversion

1.2.4.1 Plug flow models

Plug flow models assume zero radial gradient in the gas flow conditions. They can be used to study axial variations and mass transfer limited conversion for a given reactor. Such models have been used to show that for limiting fuel reactants with Lewis number less than unity such as hydrogen (Hegedus 1975).

Referring to the plug flow model, CO oxidation over Pt monolithic single channel under simultaneous heat and mass transfer conditions and global chemical reaction was studied. The predicted CO concentration along the channel by plug flow model with constant Nusselt number is in a very good agreement with a 2D steady-state model (Heck 1976). Whereas, in a comparison of results from plug flow model (lumped) and 2-D model (distributed) showed, plug flow model can not predict wall temperature profile correctly due to additional uncertainties in estimating local heat and mass transfer in light-off region and in the presence of very fast physico-chemical phenomena that departs from standard correlations in the literature because of entrance and surface reaction effects. However, plug flow model could show a rather sophisticated surface-reaction

mechanism. The 2D applied model was a laminar flow in a circular channel in steady state and fully developed condition. However, for long enough monolith reactors, plug flow model can predict gas exit temperatures comparably well depending strongly upon the correlation for estimation of heat and mass transfer coefficients (Groppi et al. 1995; Groppi et al. 1995). An interesting comparison has been attempted by Raja et al (Raja et al. 2000). They have compared the solution of the full Navier-Stokes equations with that of the isothermal catalyst PLUG code, which is a part of the CHEMKIN (Kee 1998) software package. Under some flow conditions, in mass-transfer limited region, the plug-flow model significantly overpredicts the conversion rates. Mass-transfer coefficients can potentially extend the applicability of plug-flow model, although there appears to be no simple quantitative correlation to determine them. Based on the competing time scales for convective and diffusive transport in the axial and radial directions, they could get practical bounds, in low and high Reynolds numbers, on range over which the plug-flow assumptions are valid. In laminar flow regime, the bound of validity is $\frac{D_h}{L} \prec\prec \mathrm{Re}_{D_h}\, Sc \prec\prec \frac{L}{D_h}$. For the lean fuel-air mixture, the plug-flow model should be valid in the range $0.02 << \mathrm{Re_D} << 50$. At fully turbulent flows the range can be written $\frac{D_h}{L} \prec\prec \mathrm{Re}_{D_h}\, Sc_T \frac{\nu}{\nu_T} \prec\prec \frac{L}{D_h}$. For a typical catalytic-channel flow model it will be $0.02\mathrm{Re_D} << \mathrm{Re_D} << 50\mathrm{Re_D}$.

Plug flow models have been used for analyzing of annular reactors. McCarty proposed a novel reactor consisting of a ceramic tube deposited with a thin catalyst layer co-axially placed internally to a quartz tube to form an annular chamber where the gas flows to achieve a minimal impact of diffusion phenomena on kinetic measurements

(McCarty 1995). The annular configuration appears as a valuable alternative to fixed-bed reactors with a high pressure drop for characterizing catalytic materials and for studying reaction kinetics in the range of high space velocities (low residence time) and high reaction temperatures. CO combustion over Pt-based supported catalyst and CH_4 combustion of supported Pd over Al_2O_3 and ZrO_2 were investigated using annular reactor (Beretta et al. 1999; Groppi et al. 2001; Groppi 2003; Ibashi et al. 2003). In this mathematical model, gas phased and catalyst phases are considered with a 1D or 2D descriptions, respectively. The included assumptions are: 1) fully developed laminar flow in the annulus, 2) planar geometry of the active washcoat, 3) negligible pressure drop.

1.2.4.2 Multi-dimensional flow models

As gas phase flow velocity in the catalytic channel increases, boundary layer approximations become increasingly valid. Under these conditions, elliptic Navier-Stokes equations transform to parabolized equations leading to much more efficient computational solution. It has been shown both Navier-Stokes and boundary layer model in Reynolds numbers of 200 and 2000 yield results that are in very good agreement (Raja et al. 2000).

Modeling at various level of sophistication can cover some of the physical phenomena occurring in the system. As an example, concentration of minor species which are largely controlled by the gas phase chemical behavior, in boundary layer model are underpredicted or overpredicted in comparison to full Navier-Stokes equations. In these conditions elliptic 2D model should be used (Raja et al. 2000).

To investigate the role of axial heat transfer by radiation in a single channel of a honeycomb structure monolithic catalytic channel with a negligible pressure drop, a 2D finite element simulator developed by Hayes et a. indicates that the contribution of heat radiation is lower than that of the wall conduction in ceramic monolith because of the typical high aspect ratio of monolith channels (Hayes et al. 1992). Thus it can be safely ignored except for heat dispersion effects at the catalyst ends. Negligible effect of radiation heat transfer in channels with high aspect ratios is confirmed in another study (Boehman 1998). The primary effects of radiation heat transfer are to smooth the temperature gradients that arises from catalyst light-off and to advance the light-off front forward in the channel flow (Boehman 1998). In another attempt the contribution of radiation was simulated by enhancing the value of solid conduction in the form of "effective conductivity", to study the effects of hydrodynamical development, gas property variations, wall heat conduction and radiation in monolith combustors (Groppi et al. 1995). Their results have shown: 1) hydrodynamic development has made a short delay of the light-off, 2) assumption of constant gas properties are not sufficiently accurate, particularly in predicting the outlet gas temperature, 3) backward heat conduction by wall conduction should be implemented in the modeling, 4) contribution of the homogeneous gas phase reaction is negligible 5) weak dependence of monolith behavior on radiation heat transfer, with the primary effect of radiation being on the position of the steady state light off profile moved upstream only slightly (Groppi et al. 1995; Groppi et al. 1999).

Catalytic combustion of a mixture of CH_4 and air in a square monolith channel, with a structured catalyst layer, and a global kinetic equation has been analyzed by 2D

and 3D models using commercial softwares. A comparison of different 2D approximations with a full 3D model, which predicts a different ignition behavior, shows the latter is needed to properly describe actual input data. This proved the relevance of the flow and geometry (corners) conditions, particularly with respect to the importance of the chemistry. It was shown that the decrease in the combustion rate at a higher conversion is mostly a chemical effect, instead of a diffusion limitation. This means a need for a better description of surface chemistry (Canu and Vecchi 2002).

FLUENT, as a commercial code, has been used in modeling of catalytic reactors. In a study, a 2D elliptic model for short contact time reactors with detailed surface and gas phase chemistry is analyzed. Result for partial oxidation of CH_4 on Rh and Pt –coated monoliths, has shown at the catalyst entrance an extremely rapid variation of temperature, velocity and transport coefficients occurs and complete oxidation products are formed. CH_4 conversion and syngas selectivity decreases with increasing flow velocity and increases by increasing CH_4/O_2 ratio. In atmospheric pressure gas phase reactions can be neglected but for pressures higher than 10 atmospheres it makes a big contribution. The same model was used to study the Pt-catalyzed partial oxidation of ethane to ethylene (Deutschmann and Schmidt 1998; Zerkle et al. 2000). Hydrogen assisted catalytic combustion of CH_4 over Pt has been investigated by the same model. The light-off is primarily controlled by the catalyst temperature that is a result of the heat release due to catalytic hydrogen oxidation. The higher the hydrogen the sooner the light-off (Deutschmann et al. 2000). The 3D simulation of natural gas conversion in monolithic catalysts by FLUENT including the detailed reaction mechanisms allows to study catalyst

behavior in more detail. Results show very strong axial and radial gradients in temperature profiles due to chemical reactions and heat transport (Deutschmann 2001).

Effect of gas phase chemistry is investigated by solving full Navier-Stokes in an axisymmetric channel flow. It was found gas phase reactions has only a small effect on the prediction of major species concentration and a very strong influence on the concentration of minor species (Raja et al. 2000).

The catalytic combustion of methane/air on Pd-based catalysts at gas turbine relevant conditions is simulated with a 2D elliptic fluid mechanical code. It includes global gas and surface chemistry as well as detailed transport and heat loss mechanisms. It has been shown at inlet temperatures $T < 700$ °C, a global catalytic kinetic step provides very good agreement between the measured and predicted fuel conversion over a broad range parameter variations including channel hydraulic diameter, channel length, pressure and inlet temperature. In some specific conditions the absolute temperature rise across the catalyst becomes essentially independent of pressure, very desirable for many practical systems (Carroni et al. 2003).

The effect of turbulent flow was investigated on catalytically stabilized combustion of lean hydrogen/air mixture in plane channels with Pt-coated isothermal walls. 2D elliptic model included surface and gas phase chemistries. The approach is based on a two-layer κ-ε turbulent model, a Favre-avergae moment closure, a presumed Gaussian probability density function for gaseous reactions and a laminar-like closure for surface reactions. Results shows gaseous combustion inhibits turbulence substantially, resulting in higher turbulent transport for the leaner mixtures (Mantzaras et al. 2000).

The light-off of catalytic partial oxidation of methane on a Rh-based alumina supported catalyst was studied in a short contact time flow reactor using a recently developed computer code, DETCHEM. Model solves 2D equations of heat and mass included by elementary-step based reaction mechanisms for surface and gas phase reactions. Results showed the reaction zone moves from rear face to the front face of the monolith during ignition. At the steady-state, oxygen is the primary adsorbed species in the catalyst entrance region, where total oxidation occurs. Along the channel oxygen surface concentration decreases rapidly and steam reforming leads to an increase in syngas selectivity (Schwiedernoch et al. 2003).

Most of these studies investigated steady-state modeling and all have used a one-step chemistry or detailed surface chemistry on Pt catalysts. However, Pd catalysts are being used in a broad range of temperatures for different fuel/air mixtures. Complex behavior of Pd in the well-known hysteresis loop demands the development of the detailed surface chemistry mechanism for Pd in low temperatures and high temperatures. To do so, a transient mathematical modeling to capture all time scales will be developed.

1.3 Analysis of surface chemistry by ILDM

The application of ILDM's has been well studied for gas-phase chemistry as introduced by Maas and Pope(Maas and Pope 1992). However, limited work has been presented on the use of ILDM's for complex surface chemistry with one notable exception (Yan and Maas 2000) where ILDM's were applied to reduce a surface mechanism for CH_4 oxidation over Pt.

The current study employs ILDM's for interpreting surface chemistry mechanisms for low temperature combustion of H_2 over supported Pd-catalysts. Two alternative mechanisms are modified from a previously published mechanism (Kramer et al. 2003), and do well at capturing the effects of H_2O on H_2 conversion under conditions of excess O_2. A model problem based on a uniform porous washcoat-supported catalyst was established as a dynamical system for capturing the coupling of surface chemistry with the gas-phase in a differential reactor. ILDM's associated with the surface chemistry are identified and associated with the catalyst behavior in the differential reactor.

1.4 Objectives of the study

The proposed research here is aimed at furthering our understanding of H_2 and CH_4 combustion on supported Pd-catalysts by:

1) doing experiments of Pd-H_2 and Pd-CH_4 combustion in a broad range of inlet temperatures and fuel concentrations
2) proposing detailed surface chemistry for H_2 and CH_4 catalytic combustion on Pd
3) developing integrated effectiveness 1-D model using heat and mass transfer correlations for evaluating the proposed surface thermochemistries
4) validating the numerical model by comparing results with the experimental data
5) developing dynamic model to implement ILDM method for analyzing Pd-H_2 surface chemistry
6) refining Pd-CH_4 surface chemistry using sensitivity analysis

Figure 1.6, depicts the above objectives and their inter-relationship.

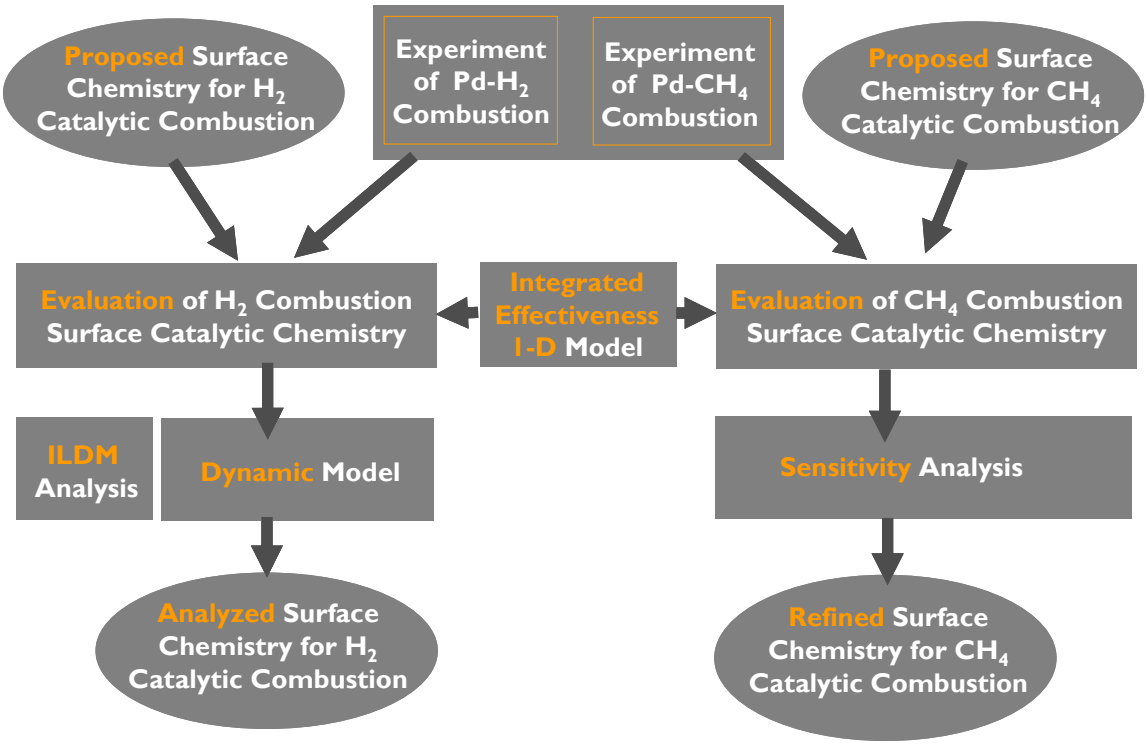

Figure 1.6 Schematic of research objectives and inter-dependencies

In order to accomplish the above tasks, this thesis is developed based on the following chapters:

In Chapter 2, experimental setup for catalyst studies is shown. Then experimental tests for H_2 combustion on Pd-based supported catalyst including temperature programmed reaction (TPR) and time on stream (TOS) tests are presented and discussed. Finally experimental results are presented for Pd catalyst in reduced/oxidized forms and their differences in energy levels are discussed.

In Chapter 3, balance continuous equations in gas phase and discretized washcoat model are presented. Then homogeneous and heterogeneous chemical reaction mechanisms are introduced. Secondly, necessity of mass and heat transfer correlations are discussed and boundary conditions for the quasi-1D model are specified. Numerical methods for solving continuous model are also presented. The difficulty for time-integration of the catalytic reacting flow leads to adopting either the full implicit time integration methods or the time-splitting techniques. Both need an efficient stiff ordinary differential equations (ODE) solvers. Gear-type BDF solver and LIMEX solvers are introduced. In last part of the chapter sample numerical results of the model is validated against the experimental results.

In Chapter 4, surface chemistry for H_2 oxidation on supported Pd-based catalyst in oxidized status has been proposed. Comparing predictions of numerical model and experimental results evaluates validity of the numerical model and surface chemistry model including surface species thermodynamics.

In Chapter 5, theoretical dynamic model is described. Then, numerical solution of manifold is presented and ILDM code is verified. Transient analysis of Pd-H_2-O_2 surface chemistry by dynamic model provides some useful information about competition between different time scales. Then, based on the ILDM analysis controlling processes of the surface chemistry at different operational conditions are discussed.

In Chapter 6, experimental results of TPR and TOS tests for CH_4 in dry/wet inlet flows are shown. To assess the proposed surface chemistry for Pd-CH_4, numerical and experimental results are compared.

In Chapter 7, surface chemistry of Pd-CH_4 is analyzed by calculating of first order linear sensitivity coefficients.

In Chapter 8, a short summary of results is presented. Finally, some recommendations are made for direction of future works.

Chapter 2

Experimental Results for Pd-H_2

2.1 Introduction

Validation of catalytic reactor models and associated surface chemistry mechanisms necessitate having experiments data. The existence of uncertainties in inlet data and parameters of catalytic reactor models makes it necessary to run well-characterized experiments. These uncertainties include: 1) definition of surface reaction chemistry and thermodynamics; 2) the difficulties in characterizing catalytic surface area; 3) mass and heat transfer correlations.

Experiments for surface chemistry are often performed in differential reactors with low conversion and thus, insignificant variation in reactant flow conditions across the reactor. Sometimes difficulty in measuring small conversions accurately requires a compromise in experiments where reactor residence times are high enough to get good real-time conversion measurements. In this way, to get H_2 oxidation kinetics at low temperatures on supported Pd catalysts a novel reactor was designed and tested. Real-time analysis of the effluent was done using a quadrupole mass spectrometer (QMS). Supported Pd-metal catalysts consist of small Pd particles on an inert support. Support is there to hold the metals in place, and to spread out the catalyst over more surface area. Supports tend to be high-surface-area materials such as alumina in the current study.

2.2 Experimental setup

2.2.1 Reactor design for kinetic studies

A catalytic reactor is composed of a geometric reactor, substrate, housing and the catalytic support and material. The main issue in designing the reactor is to create a controlled experimental test facility that makes possible measuring of catalyst activity over a range of different inlet conditions. The following design features are incorporated in reactor:

- Temperature measurements and controllable reactor temperature
- Optical access to the catalyst
- Material with high durability for temperature and humidity
- Inlet uniform mixture
- Exhaust gas sampling for real time analysis
- Substrate with high thermal conductivity for uniform temperature
- Ability to achieve very low residence time with negligible pressure drop

Following the aforementioned design criteria, the annular reactor was designed and parts are assembled. The annular configuration in the experiments has shown to meet the criteria in the bulleted list (McCarty 1995; Groppi et al. 2001). The components of reactor include: quartz tube as housing, the mixing zone, inlet and outlet fittings, isokinetic sampling exhaust, catalytically coated inert ceramic tube. The schematic of annular reactor is shown in Figure 2.1.

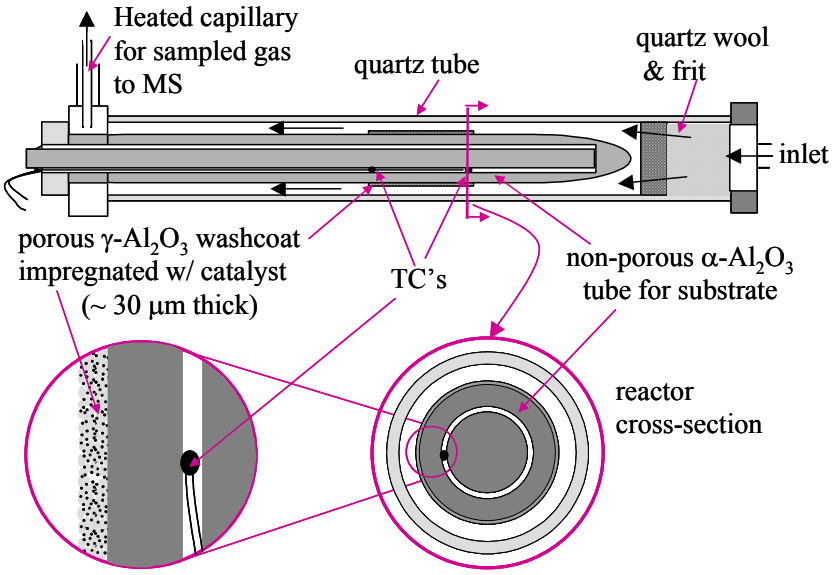

Figure 2.1 Schematic of annular flow reactor

2.2.2 Reactor description

The well-designed reactor makes an ideal tool for measuring of kinetics of H_2 oxidation on supported Pd-catalyst. It provides partial conversion of H_2 and maximum heat loss of the reactor to the surrounding to have an isothermal reactor which is preferred for analysis of kinetics data. The reactor geometry provided an annular flow with hydraulic diameter 0.5 mm. The housing of reactor is the outer quartz tube (10 mm in diameter). The inner non-porous α-Al_2O_3 tube (9.5 mm in diameter) was centrally located inside the quartz tube using nuts and ferrules such that the flow passed through a narrow annulus. The narrow annulus for the flow allowed for low residence time which suppressed the influence of mass transfer for most temperatures used for examining H_2 oxidation kinetics in the present study. Mass transfer limited conversion at typical inlet conditions was calculated to range from 65 to 85% by using mass transfer correlations from a previous study of catalytic oxidation in a similar annular flow reactor (Beretta et

al. 1999). Mass transfer limits were approached for most conditions when inlet temperature $T_{in} \geq 125°C$ (Table 2.1).

Supported precious metal catalyst (Pd) was impregnated into a thin porous γ-Al_2O_3 washcoat layer (30-40 μm thick), coated on the outside of the non-porous tube. The catalytically coated region was chosen to be 20 mm long to have relatively high conversions so that uncertainties in measured H_2 and/or H_2O mole fractions in the reactor effluent were less problematic for calculating H_2 conversion. For all cases presented here the Pd catalyst maintained its bulk oxide state (no bulk effects) except for experiments where the catalyst was intentionally reduced before combustion began.

The flow reactor was placed inside a split-tube furnace to maintain near isothermal conditions at the selected inlet temperature, T_{in}. Temperature rise along the catalytic section was monitored by two K-type thermocouples placed inside the α-Al_2O_3 support tube such that the thermocouples made contacted the tube inner wall at axial locations corresponding to the upstream and downstream boundaries of the catalytic section. Low thermal resistance of the α-Al_2O_3 support tube in radial direction ($< 2.9 \times 10^{-3}$ m °C/W) allows the temperatures in both ends of catalytic section can be measured with these thermocouples. During conditions of relatively high conversion, the rise in surface temperature (< 20°C above the inlet temperature) was monitored by thermocouples. To further minimize the temperature rise along the reactor length, N_2 balance – generally $X_{N2}/X_{O2}=20$ (ratio of mole fraction of O_2 and N_2) – was used and ϕ (equivalence ratio) was held at 0.05 or 0.1. Higher ϕ may have also resulted in significant subsurface O removal from the oxidized PdO bulk.

H_2, O_2, and N_2 flows were controlled using electronic mass flow controllers from Brooks Instrument (±1% full scale). H_2O was added to the flow by bubbling a portion of the O_2/N_2 mixture through a temperature-controlled saturator upstream of the H_2 injection which occurred just upstream of the furnace entrance. Figure 2.2 shows a layout of the experiment showing the location and plumbing of the flow

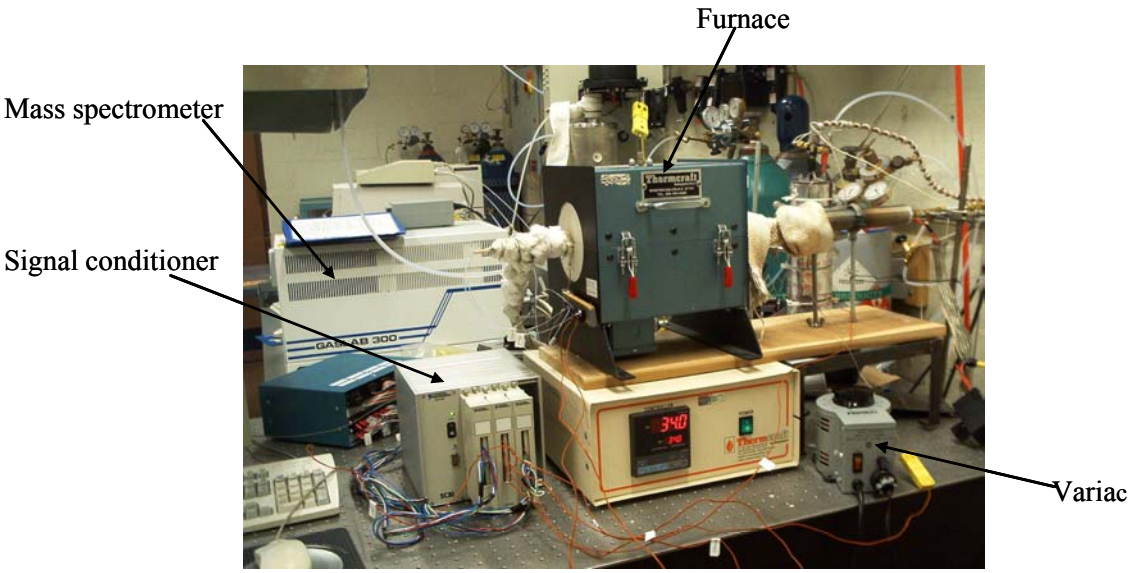

Figure 2.2 Photograph of the experimental setup

2.3 Catalyst preparation and characterization

Optical microscopy is the most commonly used method of obtaining washcoat thickness. Thickness of catalyst estimated by optical microscopy was 20 μm. Surface area of support is another important parameter have a large effect on the dispersivity of catalyst. Surface area is used by catalyst manufacturers to monitor the activity and stability of catalyst. A standardized procedure for determining the internal surface area of a porous material with surface area greater than 1 or 2 m^2/gm is based on the

isothermal adsorption of N_2 at liquid N_2 temperature onto the internal surfaces of support. Surface area for the γ-Al_2O_3 washcoat support based on the multipoint BET method, estimated 10.3 m^2/gm.

More important than the γ-Al_2O_3 washcoat area is the catalyst surface area per volume of washcoat (a_{cat}). This is related to catalyst dispersion (σ), the fraction of accessible Pd atoms at the surface, through the following equation.

$$a_{cat} V_{wc} \left(\frac{\Gamma}{\sigma} \right) W = M \tag{2.1}$$

Where V_{wc}, Γ, W , M show volume of washcoat (cm^3), surface site density (mol/cm^2), molecular weight of catalyst and weight of catalyst, respectively.

The catalyst preparation technique must disperse the catalytic components in such a way as to maximize their availability to reactants. When this is done effectively, catalyst particles on the size of a few nanometer to a few tens of nanometers are present. The most common procedure for dispersing the catalyst species within the carrier (porous washcoat) is by impregnating an aqueous solution containing a salt (precursor) of the catalytic element (Burch and Urbano 1995). In this study, washcoat was prepared by suspending 0.01µm γ-Al_2O_3 particles in slurry with aluminum nitrate solution. Then catalyst was prepared by applying solution of palladium nitrate (precursor) to the washcoat using a capillary impregnation (incipient wetness) approach. The catalyst was calcined in air at 500°C for 8 hrs and then at 300°C with a low flow of O_2 inside the tube furnace to ensure that the Pd was in a fully oxidized state.

Transmission Electron Microscopy (TEM) as the easiest way can be used to measure the size of metal particles. The dark spots on the positive images indicate catalyst particles. Figures 2.3 and 2.4 show two TEM's of Pd crystallites on γ-Al_2O_3. The sizes of the Pd crystallites range between 5 and 10 nm. Assuming a spherical shape for the crystallites, the percent dispersion can be calculated. For the used sample turned out dispersion to be 6-7%. It should be mentioned that this method gives only a small fraction of the catalyst not the entire the sample.

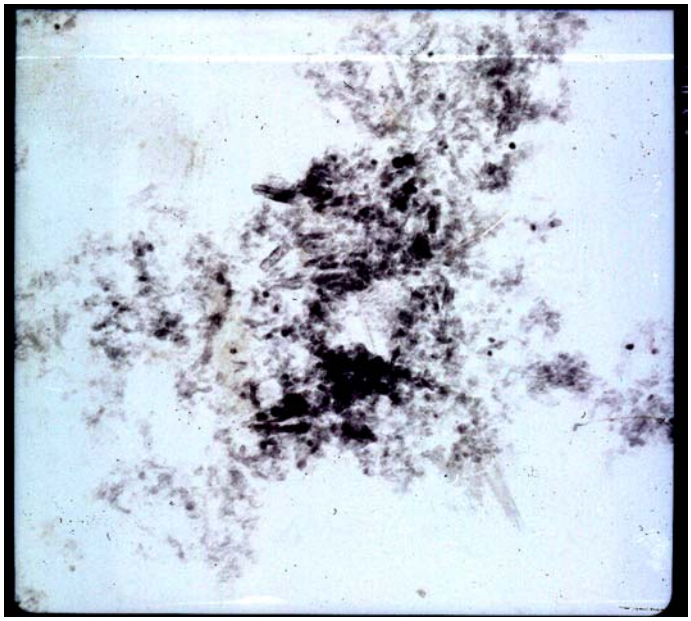

Figure 2.3 Microgram of agglomerated Pd crystallite on a γ-Al_2O_3 support

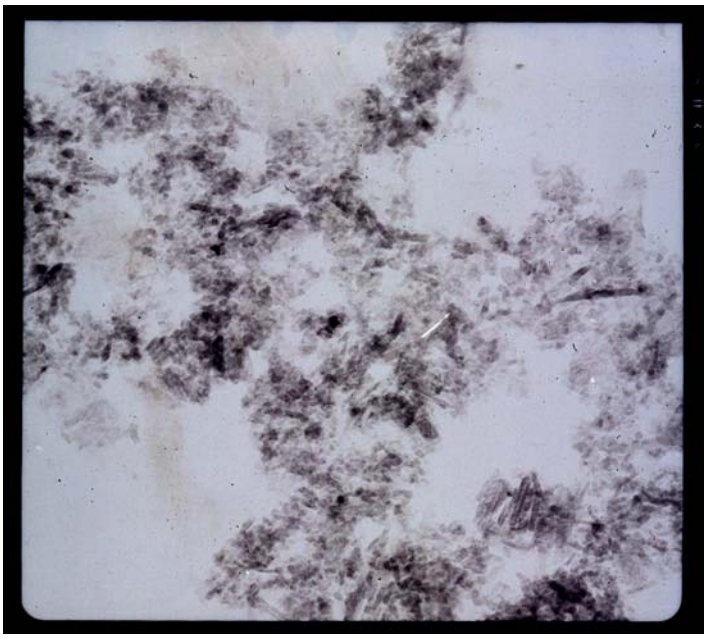

Figure 2.4 Microgram of Pd crystallites on a γ-Al_2O_3 support

In preparing the sample for TEM, the Figure 2.3 is made without using surface tension suppressor, therefore the catalyst particles got agglomerated. To have more uniform distribution of Pd particles, sample was diluted by Methanol.

2.4 Combustion of H_2 on PdO catalyst

Results of H_2 catalytic combustion on Pd-based supported catalysts are presented here. To assess the repeatability of experimental results, some tests were designed and run. Time on stream (TOS) runs were repeated between fuel flow cycled on and off for several minutes. To recover initial conditions of catalyst surface status experiments were run between intervals of running N_2/O_2 mixtures for ten minutes to precondition the catalyst. Extremely repeatable results were obtained during cyclic TOS tests for H_2 oxidation with inlet conditions of T_{in} = 200°C, u_{in} = 10 m/s and ϕ = 0.1 represented in

Figure 2.5. Transient real-time results from QMS continuous measurements are used to calculate conversion based on measured H_2/O_2 ratio. It was found if H_2O mole fraction (X_{H2O}) remained below 5%, accumulation of H_2O inside the QMS did not affect the exhaust gas composition measurements for H_2 and O_2.

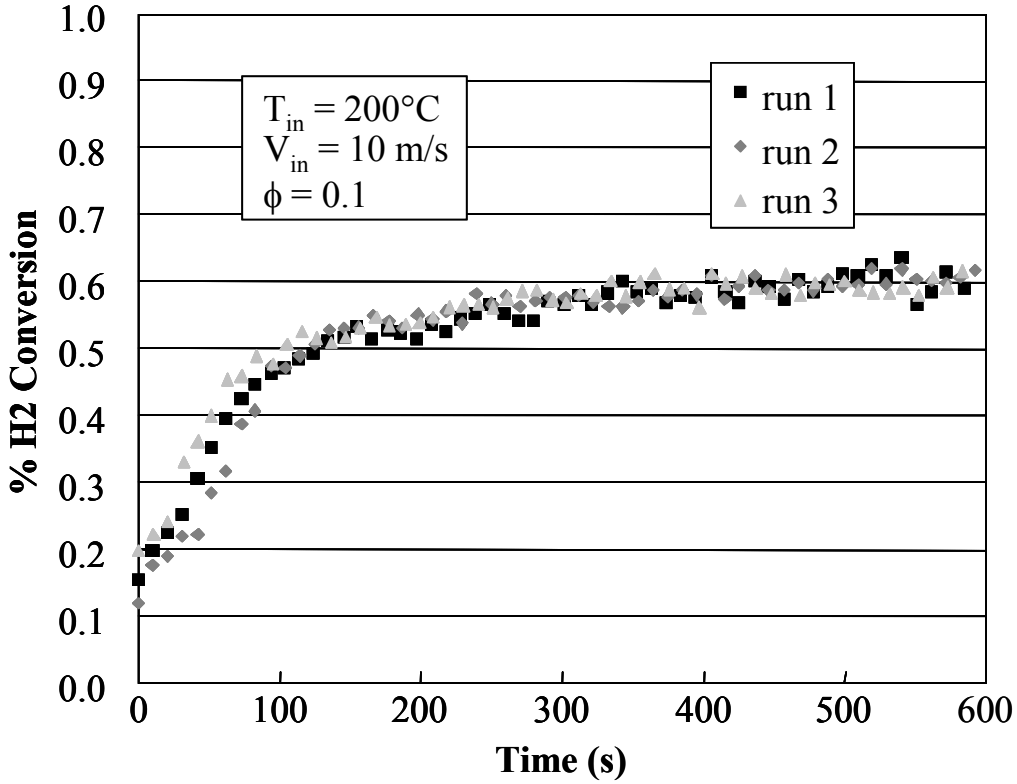

Figure 2.5 Repeatability of experimental results

2.4.1 Temperature programmed reaction tests

TPR tests can yield information the nature of the adsorbed products, the presence of reacting sites and the catalyst selectivity as a function of temperature. In TPR test an

oxidized catalyst is submitted to a programmed temperature rise, while a reactive mixture is flowing over the catalyst.

Because of the rapid kinetics of H_2 catalytic combustion, low temperature studies in flow reactors are necessary to observe conditions where surface kinetics are not masked by intraphase mass transfer limitation. Temperature programmed reactor studies were performed for $\phi = 0.05$ and 0.1 by ramping reactor inlet temperature from 50 to 250ºC at 5ºC/min. Experimental result profiles of H_2 conversion with respect to temperature extracted from real-time gas exhaust analysis are plotted in Figure 2.6. The curves show an impact of H_2 gas-phase concentration on conversion at low T_{in} where conversion is < 0.3. Around 120°C, all curves begin to converge and rise relatively rapidly with T_{in} until an apparent mass-transfer limited conversion is settled down at ≈70% near T_{in} =200°C. For T_{in} >200°C, mass transfer limits conversion which begins to show a weak increase for the dry feeds and minimal to no increase for wet feed. The flattening of conversion with increased T_{in} for the wet feeds suggests an inhibitory effect of H_2O on H_2 oxidation in the higher temperature range. This inhibition is similar to H_2O inhibition for CH_4 light-off over Pd catalysts at higher T_{in} (Chapter 5), but it is not clear that these are the same mechanisms.

In TPR test in lower temperature (< 100°C) as it shown in Figure 2.6, there is a catalytic effect, particularly for dry feed. It seems there is a jump in conversion. It is not clear what makes that change in the conversion. One possible explanation can be related to the rate limiting step which is water desorption and is favored by low temperature. For wet feed, due to differential condition with respect to water, this effect has been suppressed.

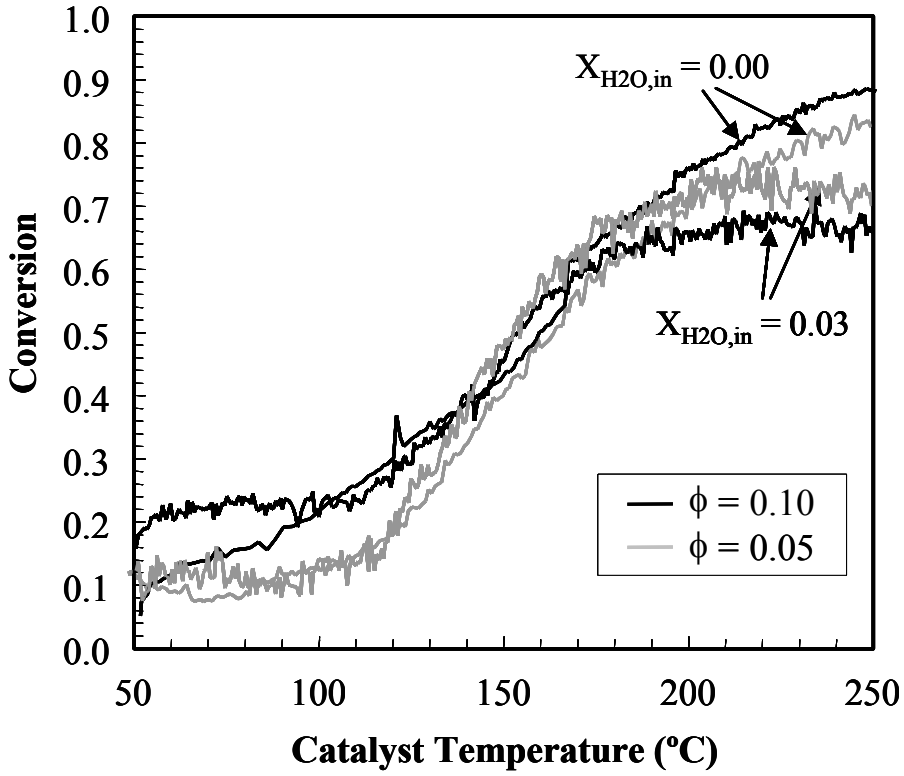

Figure 2.6 TPR tests with heating rate of 5 °C/min, catalyst initially fully oxidized, u_{in} = 10 m/s, X_{N2}/X_{O2} = 20

2.4.2 Time on stream (TOS) tests

In the first set of TOS experiments, effects of inlet temperature T_{in}, equivalence ratio ϕ and inlet water content $X_{H2O,in}$ were studied as shown in Figure 2.7. Table 2.1 provides a matrix of different test conditions. For $T_{in} \leq 125$ °C, wet inlet causes transient slow decay in conversion which is unnoticeable for dry feed. This is possibly related to slow equilibration of water adsorption/desorption or water encouraging. And in this region of inlet temperature conversion is proportional to equivalence ratio both for wet/dry inlet flows. In other words, it suggests an effective order of 2 for H_2

concentration. For $T_{in} \geq 150$ °C where mass transport begins to impact conversion, increased inlet water reduces the time scales to rise to steady state conversion, but the steady-state conversions do not depend on $X_{H2O,in}$ offering no inhibitory effect of water at lower temperature. In comparison to Figure 2.6 this can be seen for low temperature.

Table 2.1 TOS test conditions for catalyst initially fully oxidized
u_{in} =10 m/s, X_{N2}/X_{O2} = 20

Inlet Temperature T_{in}(°C)	$X_{H2O,in}$ (%)		Equivalence Ratio (ϕ)	
100	0		0.05	0.1
125	0	2.1	0.05	0.1
150	0	2.5	0.05	0.1
200	0		0.05	0.1

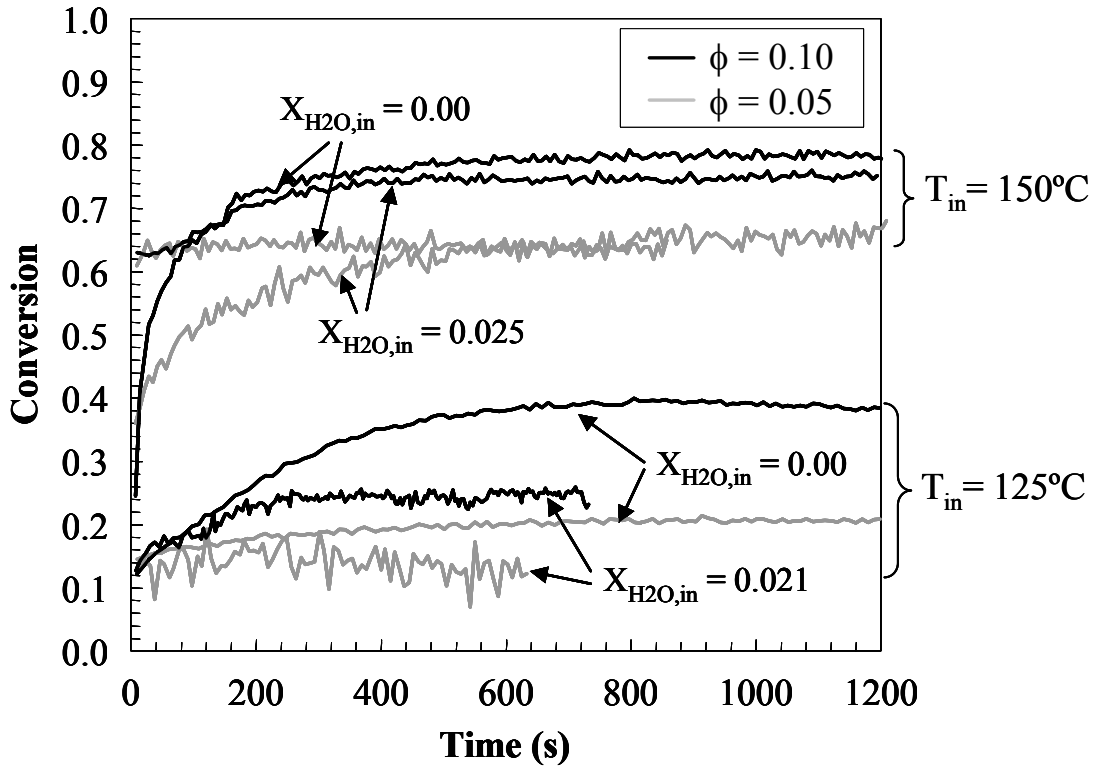

Figure 2.7 The effect of wet feed on TOS conversion for catalyst initially fully oxidized
u_{in} = 10 m/s, X_{N2}/X_{O2} = 20, at $T_{in} \leq 125$°C, $\Delta T_{reactor} < 15$°C

TOS experiments with dry inlet feeds at inlet constant temperatures ranging from 100-200 °C are presented in Figure 2.8. For $T_{in} \leq 125$ °C, initial conversion is independent from H_2 concentration (an effective order of 1 for H_2 concentration), but subsequently it rises based on increased H_2 molar concentration. This can be related to the increased oxide vacancy with increased H_2 content. Therefore rate

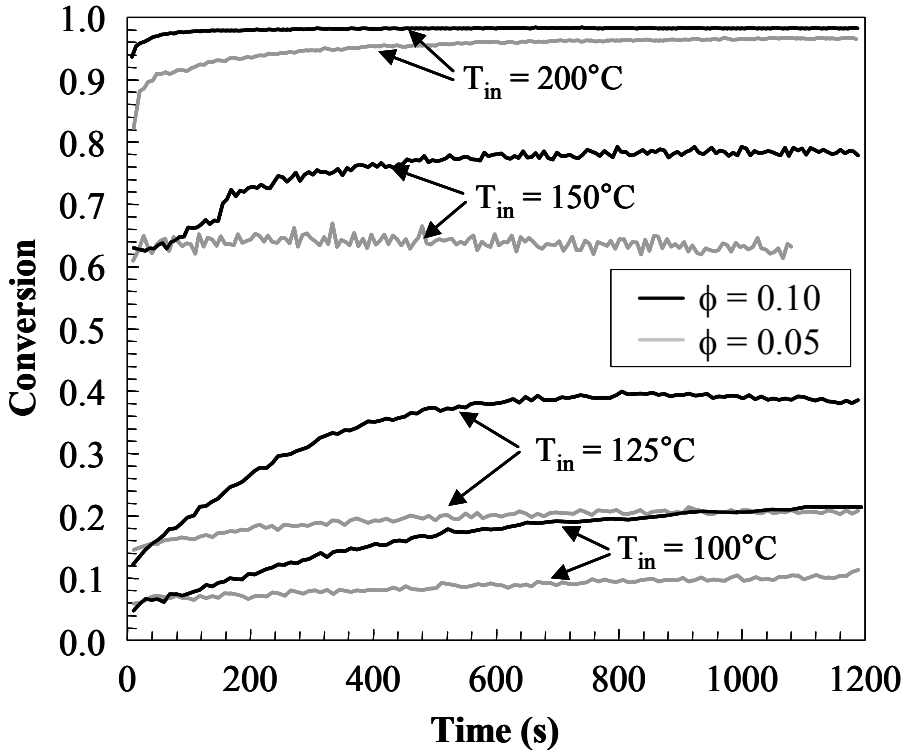

Figure 2.8 TOS experiments in different inlet temperatures for catalyst initially fully oxidized u_{in} = 10 m/s, X_{N2}/X_{O2} = 20, at $T_{in} \leq 125$°C, $\Delta T_{reactor} < 15$°C

controlling reaction with PdO_x dominant surface is:

$$H_2 + 2Pd(sb) + O(sb) \Rightarrow H_2O + 3Pd(sb) \tag{2.2}$$

$$Effective\ \ Rate = k_{reac}\left[H_2\right] \times X^2_{Pd(sb)} \tag{2.3}$$

where, Pd(sb), O(sb), $[H_2]$ and $X_{Pd(sb)}$ show electronically deficient vacancy in surface oxide, 4-fold coordinated O-atom on Pd surfaces, molar concentration of H_2 and mole fraction of surface vacancy, respectively. This means there is a positive feedback with increased H_2 concentration. For $T_{in} \geq 150$ °C, conversion is strongly impacted by mass transfer.

To evaluate impact of initial oxidation state of Pd-based catalyst on conversion, a set of experiments were run where PdO_x catalyst was completely reduced to Pd metal at 400 °C by H_2 flow diluted with N_2 before combustion experiments. In Figure 2.9 transient conversion curves are compared for pre-reduced and oxidized Pd catalysts. The curves indicate a large increase in the activity of the reduced catalyst. In the reduced case, the surface chemistry may likely be controlled by chemisorbed species, such that the rate-limiting step is not H_2 adsorption but perhaps O_2 chemisorption or H_2O adsorption/desorption. It is expected that surface energy levels will change with changes in the sub/surface catalyst state. Nonetheless, the experimental results dictate that the controlling chemical mechanisms for H_2 combustion on polycrystalline PdO surfaces are completely different from the controlling surface mechanisms for H_2 combustion on metallic Pd particles.

Based on the experimental results of H_2 conversion over reduced/oxidized catalysts in Figure 2.9, it can be said pre-reduced Pd has much greater activity than pre-oxidized catalyst. It shows high conversion at temperatures less than 50°C. The increased kinetics rates for H_2 oxidation on the reduced metal catalyst has caused mass transfer limits to be reached at a temperature around 100°C. In other words, pre-reduced catalyst has shifted mass transfer limited conversion to lower temperatures in comparison to

initially oxidized catalyst. Wet feed greatly impacts conversion on reduced Pd due to adsorption of H_2O on metallic Pd, but the effect of inlet water is less severe for initially oxidized catalyst. Possibly, this can be related to higher activation barriers for occupying the active sites by water content in oxidized catalyst.

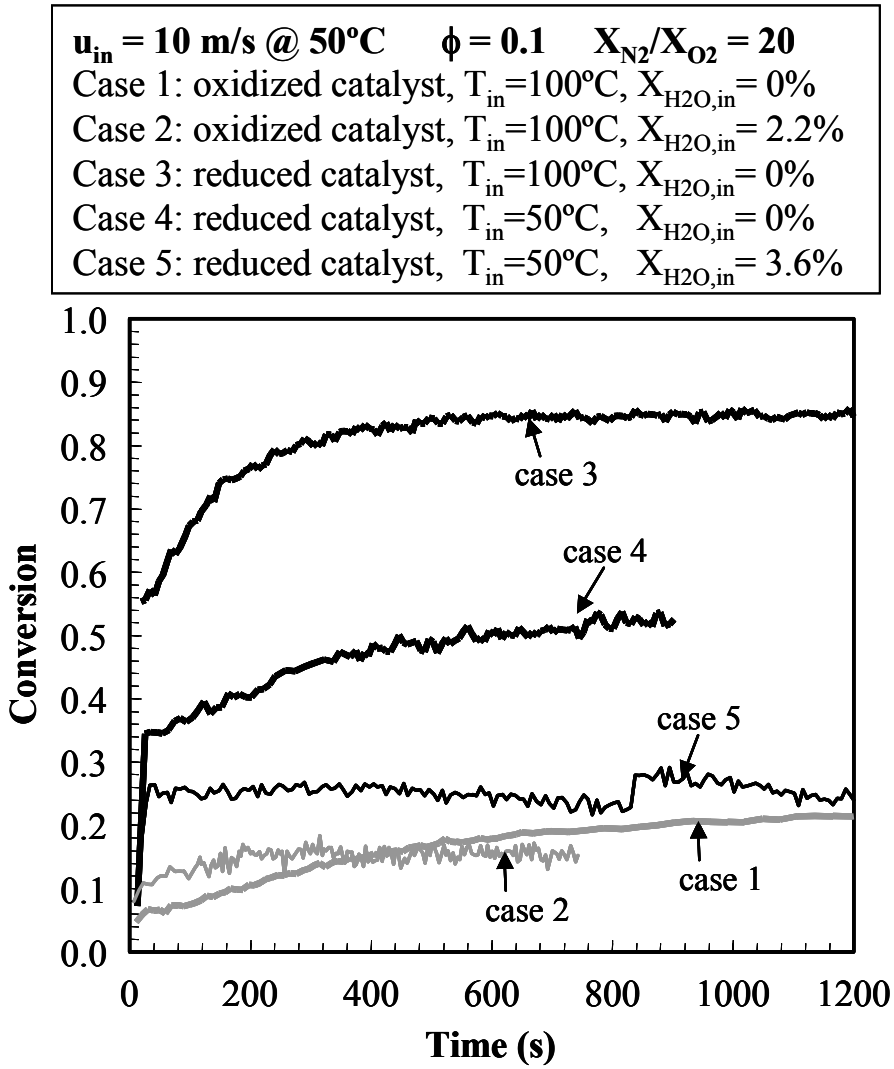

Figure 2.9 Comparison of conversion of H_2 over reduced/oxidized catalysts

2.5 Conclusion

Although H_2 catalytic combustion presents one of the simplest surface chemistry scenarios, it has revealed that the fast surface kinetics of this simple system at low temperature present a significant challenge to surface and combustion scientists for developing predictive tools for catalytic reactor design. Careful analysis of temperature-programmed reactor experiments and transient light-off tests provide a basis for developing a preliminary surface chemistry mechanism. It also serves to provide insight into the importance of surface condition on catalyst activity during the development of detailed surface chemistry mechanisms for oxidation reactions. In the following chapter, using the kinetically rich experimental experiments a numerical model will be developed. The model will explore different surface chemistry models.

Chapter 3

Numerical Channel Flow Model

3.1 Introduction

Mathematical modeling has been considered as a key tool in the development of the catalytic combustor technology for natural gas fuel gas turbines. To be applicable over a wide range of temperature, pressure and equivalence ratio, catalytic combustion models need adequately detailed kinetics to capture kinetically controlled processes such as ignition, catalyst phase shifts and extinction. Along with kinetics, adequate transport models both in the gaseous flows and as necessary porous catalyst supports must capture transport controlled phenomena such as mass transfer limited conversions. Detailed surface chemistry places rigorous demands on numerical models for the catalyst layer and has encouraged simplified models with no discretization in the direction of the depth of the catalyst layer – thereby ignoring the potential influence of intraphase diffusion in the pores of the catalyst support. Models with detailed mechanisms have incorporated non-porous catalyst layers (Bui et al. 1997; Deutschmann et al. 1998; Goralski and Schmidt 1999) or uniform properties throughout a porous support layer (Kramer et al. 2003; Sidwell et al. 2003). The question has remained as to the effects of intraphase diffusion on numerical model predictions with detailed surface chemistry for catalytic combustors and exhaust aftertreatment oxidation reactors, where supported washcoats typically range in thickness from 15-60 μm (Farrauto 1997).

The effects of intra-phase diffusion for channel-flow oxidation reactors with thin washcoats has been investigated in literature with simple single-step kinetic mechanisms in numerical simulations of porous washcoat with discretization in the direction normal to

the washcoat support (Hayes et al. 1995; Leung et al. 1996; Wanker et al. 2000; Groppi et al. 2001; Hayes et al. 2001). In these models, heterogeneous reactions are quantified by single-step rate expressions using either a simple power-law equation (Hayes et al. 1995; Leung et al. 1996; Wanker et al. 2000) and/or Langmuir-Hinshelwood expression (Leung et al. 1996; Groppi et al. 2001; Hayes et al. 2001). Results from these models indicate that intraphase diffusion in the washcoat layer has a much more significant impact on controlling mass transfer to the catalyst and thus impacting mass transfer limits than does diffusion in the channel flow to the external washcoat surface. The catalyst effectiveness factor η is defined by the ratio of the integrated reaction rate throughout the non-uniform porous washcoat layer to the idealized reaction rate if the layer were at the same uniform conditions as its outer surface. A reduction in η from the ideal value of 1.0 quantifies the importance of intraphase diffusion. In previous numerical models using single-step reactions, η fell off sharply from 1.0 even for washcoat thicknesses δ_{wc} as small as 10 μm in some cases (Hayes et al. 2001). The predicted drop in η with increasing temperature for a given oxidation reactor largely depends on the modeled diffusivity of reactants in the porous washcoat, and results show that inaccurate kinetic rate expressions can be derived in these cases if intraphase diffusion is neglected (Hayes et al. 1999; Groppi et al. 2001).

The previous modeling results on effectiveness of catalytic washcoats in exothermic oxidation reactors suggest that the models using multi-step mechanisms, which have neglected intraphase diffusion or avoided it with non-porous catalyst models, should be reconsidered to assess how diffusion in the washcoat impacts predictions with more complex mechanisms. The complex behavior of some catalytic reactions –

particularly on Pd-based catalysts, such as oscillatory oxidation of CO (Imbihl and Ertl 1995), non-monotonic (with temperature) combustion rates of CH_4 (Ciuparu et al. 2002), and sub-surface-sensitive oxidation of H_2 (Kramer et al. 2003) – raises questions as to how effectiveness models can be incorporated with detailed surface chemistry mechanisms. A model has been developed to address these issues, and the model is used to assess look at detail multi-step surface mechanisms for Pd-based catalytic combustion of H_2 at temperatures < 250°C. Then, it was investigated how effectiveness can be readily used for simplifying models of porous washcoat layers typical of monolithic catalytic oxidation reactors. Low-temperature catalytic combustion of H_2 on Pd catalysts is used to look at effectiveness for a multi-step mechanism as a function of temperature, H_2/O_2 ratios and δ_{wc}. The study uses a numerical model with a discretized washcoat layer normal to the surface of the washcoat support. The model results are used to evaluate whether analytical models for effectiveness relating surface reaction rates to intraphase diffusion rates can be used to characterize effectiveness.

3.2 Governing equations

3.2.1 Channel flow model

To assess surface mechanisms for combustion on supported Pd catalysts, a numerical model for a single channel reactor has been developed to compare with experimental results. Figure 3.1 represents an axial volume element of channel flow model. Channel has a porous washcoat supporting dispersed catalyst. The governing equations for low *Mach* number gas phase reactive flow are derived from the general

Navier-Stokes equations of a compressible reacting flow together with transport equations for species.

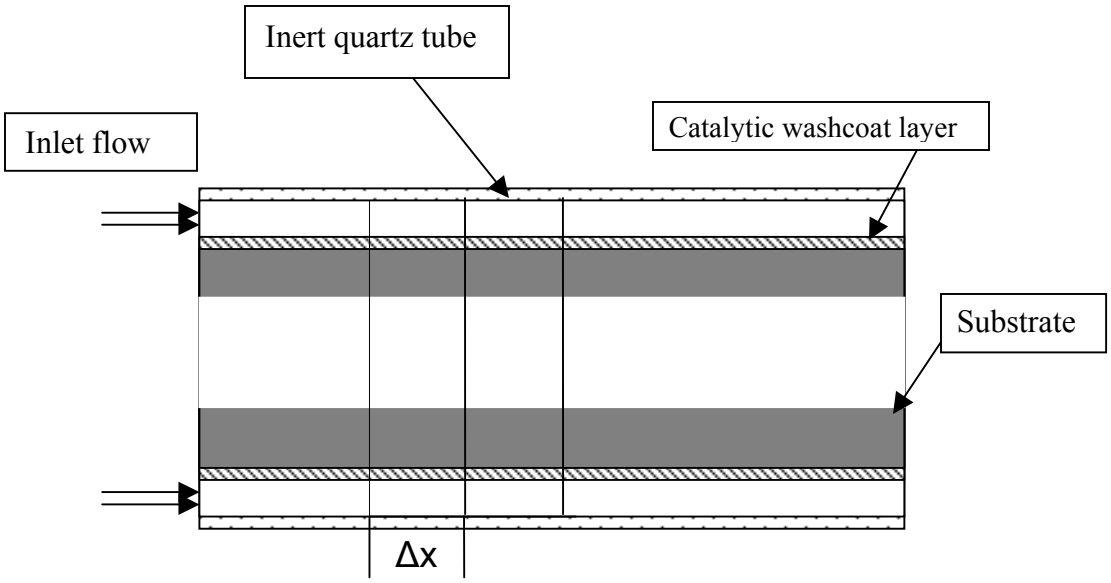

Figure3.1 Volume element for channel flow model

To develop conservation equations for transient quasi-1D plug flow model some simplifications in general Navier-Stokes equations are implemented. In the studied reactor the fluid velocity through annular flow reactor is much smaller than the sound speed ($Ma < 0.05$ in the current study). Since the low velocity and small diameter of channel (less than 1 mm) lead to a very small Reynolds numbers (less than 50 in the current study), laminar channel flow can be assumed in modeling the catalytic channel flow.

In the quasi-1D channel flow model, temperature and species radial gradients between the channel and the washcoat layer, heat and mass transfer coefficients are calculated from some empirical correlations for *Nu* and *Sh* numbers in catalytic oxidation reaction conditions depending on the hydrodynamic, thermal and concentration boundary layer developments to make the 1D model match the real situations(Groppi et al. 1995). Although, in the current study thermal boundary layer is assumed thermally fully developed which is not correct for entrance region, it was found the thermal entrance length is limited to less than 10% of reactor length.

To reduce the computational complexity of the channel flow thermal diffusion in the axial direction of channel flow has not been considered here as a reasonable assumption for gaseous flows due to their low conductivity. The final implemented simplification in general Navier-Stokes equations is based on the previous study including compressible flow model developed in our lab (Zhu 2001). It was found isobaric condition along the convective-dominated channel flow is a valid assumption in this range of Mach number. Also, contribution of axial viscous stress due to dilation of fluid element is negligible. Under these conditions, model allows density variations to be evaluated by ideal gas equations, and the continuity equation can be decoupled from the momentum equation. In other words, for a given pressure, the velocity can be determined from the continuity equation alone. Also, the reasonable approximation of isobaric flow avoids limitations on the integration time-step caused by pressure-velocity-density coupling in fully compressible flow models. All assumptions for quasi-1D model are highlighted in the following:

- laminar flow in the channel

- isobaric condition inside the channel
- negligible contribution of axial viscous stress due to fluid dilation element
- only radial gradient in inter-phase between channel and washcoat
- calculation of heat and mass transfer coefficients from empirical correlations

In nonreacting flows the fluid velocity normal and tangential to a solid wall is zero. However, if there are chemical reactions at the wall, then the normal velocity can be non-zero. This is so-called Stefan flow velocity, $\overline{V}$, occurring when there is a net mass flux between the surface and the gas flow. In deriving conservation equations for channel gas flow, effect of convective Stefan velocity of gas phase species at the inter-phase of channel and washcoat layer is added to diffusive velocities, $YV_{k,g}$, of the gas species. Stefan velocity arises from surface reactions or density changes in the porous washcoat layer.

Following the assumptions, the conservation equations for channel gas flow can be written in the following form:

$$\frac{\partial \rho_g}{\partial t} + \frac{\partial \left(\rho_g u_g\right)}{\partial x} = a_{ch} \rho_{gm} \overline{V} \tag{3.1}$$

$$\rho_g \frac{\partial Y_{k,g}}{\partial t} + \rho_g u_g \frac{\partial Y_{k,g}}{\partial x} = -a_{ch}\left(\rho_{gm} Y V_{k,g} - \rho_{gm} \overline{V}\left(Y_{k,gm} - Y_{k,g}\right)\right) + W_k \dot{\omega}_{k,g} \tag{3.2}$$

$$\rho_g \overline{C}_{P,g} \frac{\partial T_g}{\partial t} + \rho_g u_g \sum_k Y_{k,g} \frac{\partial h_{k,g}}{\partial x} = a_{ch} h_T \left(T_s - T_g\right) - a_{ch} \rho_{gm} \sum_k \left(\left(h_{k,gm} - h_{k,g}\right) Y V_{k,g}\right)$$
$$- \sum_k \left(h_{k,g} W_k \dot{\omega}_{k,g}\right) + a_{ch} \rho_{gm} \overline{V} \sum_k \left(Y_{k,gm} \left(h_{k,gm} - h_{k,g}\right)\right) \tag{3.3}$$

where u_g, gas velocity in channel flow is calculated from equation 3.1 and density of gas phase ρ_g is calculated from ideal gas equation for gas mixture in the channel flow. In conservation equation of gas phase species, $Y_{k,g}$, equation 3.2, transient and convection terms are balanced by diffusion and Stefan velocities from washcoat and generation term $\dot{\omega}_k$ due to gas phase reactions. ρ_{gm}, average gas density is used to calculate the interphase mass transport through channel surface area per volume of channel, a_{ch}. Conservation of energy, equation 3.3, includes heat transfers due to interphase mass transfer, convection heat transfer between channel and washcoat by h_T, heat transfer coefficient and convection of energy due to bulk flow. $\rho_g \overline{C}_{P,g}$ is the effective specific heat capacity of the gas phase species.

To calculate production term in gas phase, $\dot{\omega}_k$ (molar reaction rates per unit volume) and in surface phase, $\dot{s}_k$ (molar reaction rates per unit area) all elementary chemical reactions either in gas or surface phase can represented in the following general equilibrium form:

$$\sum_{k=1}^{K} \upsilon'_{ki} \chi_k \Leftrightarrow \sum_{k=1}^{K} \upsilon''_{ki} \chi_k \qquad i = 1, \ldots\ldots, I \tag{3.4}$$

Where χ_k is the chemical symbol for the *k-th* species. υ'_{ki} and υ''_{ki} are the stoichiometric coefficients for species k in elementary *i-th* reaction acting as reactant or products in

forward or backward reactions, respectively. Based on the principle of microscopic reversibility, any molecular (mechanistic) process and the reverse of that process occur on the average at the same rate (Hill 1977). The production rate $\dot{\omega}_k$ ($\dot{s}_k$ for surface phase reactions) for each species *k* is the sum of the rate of production for all reactions involving the k-th species.

$$\dot{\omega}_k \text{ (or } \dot{s}_k) = \sum_{i=1}^{I} (\upsilon''_{k,i} - \upsilon'_{k,i}) q_i \qquad i = 1, \ldots\ldots, I \tag{3.5}$$

and the rate-of-progress variable q_i for the *i*-th reaction is given by the difference of the forward rates and the reverse rates:

$$q_i = k_{f_i} \prod_{k=1}^{K} [X_k]^{\upsilon'_{ki}} - k_{r_i} \prod_{k=1}^{K} [X_k]^{\upsilon''_{ki}} \tag{3.6}$$

where k_{f_i} and k_{b_i} are the forward and backward reaction rate constants for the *i*th reaction step. $[X_k]$ for the gas phase species is the molar concentration (mole/cm^3) and for surface species surface concentration (mole/cm^2). The forward reaction rate constant k_{f_i} for *I* reactions are assumed to have the modified Arrhenius expression

$$k_i = A_i T^{\beta_i} \exp\left(-\frac{E_i}{RT}\right) \tag{3.7}$$

where E_i represents the barrier energy, A_i the pre-exponential factor and β_i the temperature exponent. For reversible reactions backward rate constants k_{r_i} are related to the forward rate constants k_{f_i} through the equilibrium constants K_{c_i} by

$$K_{c_i} = \frac{k_{f_i}}{k_{r_i}} \tag{3.8}$$

3.2.2 Discretized washcoat model

In catalytic combustion modeling, porous washcoat layer has an important role. In order to assess the interdependence of intra-phase diffusion and complex surface chemistry, a numerical model of a porous catalytic washcoat has been developed.

For the current study pressure drop are neglected. Also, the convection of gas phase species and energy inside the washcoat layer is neglected due to very small pressure drop in the washcoat. In other words, compared with channel flow velocity, Darcy's velocity in porous is very small. Furthermore, washcoat is thin and therefore inside the boundary layer. Also, molecular diffusion in the axial direction is not accounted for because it is much smaller than diffusion through the thickness of washcoat. The storage and redistribution of heat in the washcoat and substrate are considered axially and radially for the catalytic light-off transient modeling. The model incorporates complex surface chemistry for a supported catalyst with a specified surface area to washcoat volume ratio $a_{cat,}$ catalyst dispersion σ_{cat} and density of active sites on catalyst Γ_{cat} (moles/cm2). The inert catalyst support is a porous matrix with a defined porosity ε and a thickness δ_{wc} that extends above a non-porous reactor substrate as indicated in the schematic shown in Figure 3.2. For this configuration as illustrated bigger in Figure 3.3, the transient conservation equations that govern temperature T_s, gas phase mass fractions, Y_k, catalyst surface species site fractions θ_k and catalyst bulk phase species $X_{k,b}$ are discretized in the direction y of the washcoat height. Gas phase density ρ, and the Stefan velocity $\overline{V}$ down through the washcoat are solved for by including the

ideal gas law and the transient mass conservation for each washcoat cell in the set of model equations.

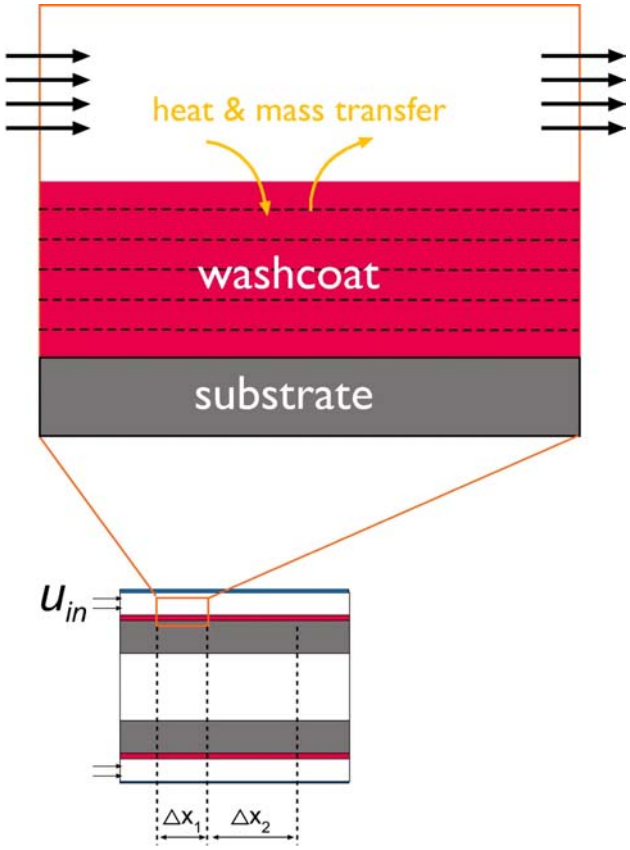

Figure 3.2 Axial element of discretized washcoat model

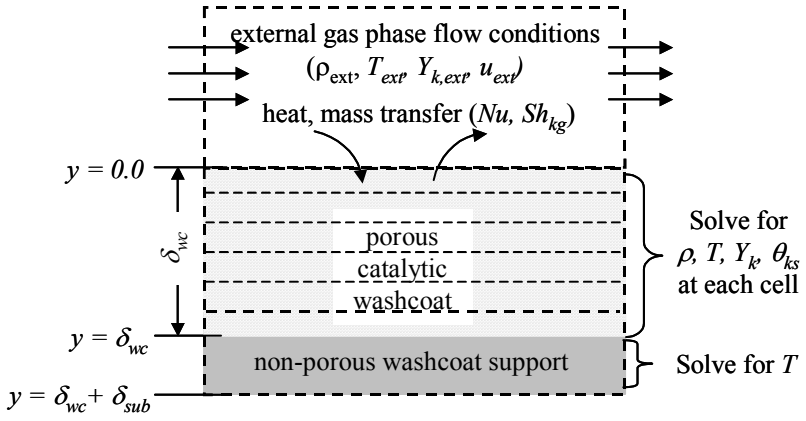

Figure 3.3 Schematic (not in scale) of discretized washcoat

With the defined variable the governing conservation equations of mass, gas phase species, surface site fraction and bulk mole fraction in the porous catalytic washcoat can be written as follows:

$$\varepsilon \frac{\partial \rho}{\partial t} + \varepsilon \frac{\partial (\rho \overline{V})}{\partial y} = a_{cat} \sum_{k=1}^{k_{gas}} \left(W_k \dot{s}_k \right) \tag{3.9}$$

for $k = 1, \ldots, K_{gas}$

$$\varepsilon \rho \frac{\partial Y_k}{\partial t} = \varepsilon \dot{\omega}_k W_k + a_{cat} \dot{s}_k W_k - a_{cat} Y_k \sum_{k=1}^{k_{gas}} \left(W_k \dot{s}_k \right) - \varepsilon \frac{\partial \left(\rho \left(Y V_k + Y_k \overline{V} \right) \right)}{\partial y} \tag{3.10}$$

$$\Gamma_{cat} \frac{\partial \theta_{k,s}}{\partial t} = \dot{s}_k \qquad k = K_{gas}+1, \ldots, K_{gas}+K_{surf} \tag{3.11}$$

$$\frac{(1-\sigma_{cat})\Gamma_{cat}}{\sigma_{cat}} \frac{\partial X_{k,b}}{\partial t} = \dot{s}_k \qquad k = K_{gas}+K_{surf}+1, \ldots, K_{gas}+K_{surf}+K_{bulk} \tag{3.12}$$

Radial convective and radiative heat losses out of the reactor substrate are allowed in the model. However, radiation inside the channel is neglected, because it has a small contribution in redistribution of generated heat due to exothermic surface reactions(Boehman 1998). Another reasonable assumptions made to simplify the governing equations is thermal equilibration between the solid and gas phase temperatures in each washcoat cell.

$$\left(\overline{\rho C_{p,s}}\right)\frac{\partial T_s}{\partial t} = -a_{cat}\sum_{k=1}^{k_{gas}+k_{surf}}\left(h_k \dot{s}_k W_k\right) - \varepsilon\sum_{k=1}^{k_{gas}}\left(h_{k,gs}\dot{\omega}_{k,gs}W_k\right) - \varepsilon\frac{\partial\left(\rho\sum_{k=1}^{k_{gas}}\left(h_k\left(YV_k + Y_k\overline{V}\right)\right)\right)}{\partial y} + \frac{\partial\left(\left(\varepsilon\lambda_{gas} + (1-\varepsilon)\lambda_{solid}\right)\frac{\partial T}{\partial y}\right)}{\partial y} \tag{3.13}$$

$$\overline{\rho C_{P,s}} = \varepsilon\rho_{gs}\sum_k\left(C_{Pk,gs}Y_{k,gs}\right) + a_{cat}\Gamma_{cat}\left(\sum_k\left(\overline{C}_{Pk,s}\theta_{k,s}\right) + \frac{1-\sigma_{cat}}{\sigma_{cat}}\sum_k\left(\overline{C}_{Pk,b}X_{k,b}\right)\right) + (1-\varepsilon)\rho_{wc}C_{P,wc} + v_{sub}\rho_{sub}C_{P,sub} \tag{3.14}$$

where $\overline{\rho C_{p,s}}$ is the effective specific heat capacity of the combined solid (catalyst surface, bulk, and inert support) and gas-phase materials in each cell of the washcoat matrix. Stefan velocity $\overline{V}$ arises through the catalyst layer due to surface reactions or density changes in ρ in the porous layer. $\overline{V}$ can be calculated from mass conservation.

$$\rho_{gm}\overline{V} = \left(\varepsilon\rho_{gs}T_{gs}^{-1}\frac{\partial T_{gs}}{\partial t} + a_{cat}\sum_k\left(W_k\dot{s}_{k,gs}\right) + \varepsilon\rho_{gs}W_{gs}\sum_k W_k^{-1}\frac{\partial Y_{k,gs}}{\partial t}\right)/\, fa_{wc}$$
$$f = 1 + \sum_k\left(W_{gs}W_k^{-1}\left(Y_{k,gm} - Y_{k,gs}\right) + \varepsilon\rho_{gs}Y_{k,gm}\left(\overline{\rho C_{P,s}}T_s\right)^{-1}\left(h_{k,gm} - h_{k,gs}\right)\right) \tag{3.15}$$

As it was mentioned in previous section, production terms due to surface reactions are calculated based on equation 3.5. In this study, activation barriers of some of elementary surface reactions are modified by the coverage (concentration) of some other surface species due to repulsion or attraction forces. For these surface chemical reactions, the rate constant of the Arrhenius expression is modified by the concentration of surface species and/or bulk species.

$$k_{f_i} = A_i T^{\beta_i} \exp\left(-\frac{E_i}{RT}\right) \prod_{k=K_s^f\left(N_s^f\right)}^{K_b^l\left(N_b^l\right)} 10^{\eta_{ki}\theta_k(n)} \left(\theta_k(n)\right)^{\mu_{ki}} \exp\left(-\frac{\varepsilon_{ki}\theta_k(n)}{RT}\right) \tag{3.16}$$

where three coverage parameters η_{ki} μ_{ki} and ε_{ki} are for species *k* and reaction *i*. The product in the equation runs over only those surface species that are specified as contributing to the coverage modification. Using the modified rate expression the activation energy is a function of the coverage:

$$E = E_i + \sum_{k=K_s^f\left(N_s^f\right)}^{K_b^l\left(N_b^l\right)} \varepsilon_{ki}\theta_k(n) \tag{3.17}$$

For reactions with coverage dependency, reverse rate constant is calculated from equation 3.8.

For adsorption reactions, adsorption rate of gas phase species are commonly (Warnatz 1999) described in terms of a sticking coefficient S_k, ($0 \leq S_k \leq 1$), the probability that a molecule sticks when colliding with the surface will result in adsorption. To convert sticking coefficients to the usual mass-action kinetic rate constants, the relation currently used is

$$k_{f_i} = \frac{S_k}{1-\frac{S_k}{2}} \frac{1}{\Gamma_{tot}^m} \sqrt{\frac{RT}{2\pi W_k}} \tag{3.18}$$

$$m = \sum_{i=1}^{N_s} \nu'_{ik} \tag{3.19}$$

where Γ_{tot} (mol /cm^2) is the total surface site concentration summed over all surface phase, and *m* is the sum of all the stoichiometric coefficients of reactants that are surface species.

In the current study diffusion velocities are based on CHEMKIN software(Kee 1998). Dealing of transport properties are usually formulated in two different levels. At the full multicomponent level, each species diffusion velocity is calculated from $\vec{j}_k = \rho Y_k \vec{V}_k$, including three components ordinary diffusion, $\vec{j}_k^{\,d}$, thermal diffusion (Soret effect), $\vec{j}_k^{\,T}$ and pressure diffusion, $\vec{j}_k^{\,p}$.

$$\vec{j}_k = \rho_k V_k = \vec{j}_k^{\,d} + \vec{j}_k^{\,T} + \vec{j}_k^{\,p} \tag{3.20}$$

where

$$\vec{j}_k^{\,d} = \rho W_k \overline{W}^{-2} \sum_{j \neq k} D_{kj}^M W_j \nabla X_j \tag{3.21}$$

$$\nabla X_j = \sum_{i=1}^{N} \left[X_i X_j (V_i - V_j) D_{ij}^{-1} \right] \tag{3.22}$$

$$\vec{j}_k^{\,T} = -D_k^T \nabla(\ln T) \tag{3.23}$$

$$\vec{j}_k^{\,p} = \rho W_k \overline{W}^{-2} \sum_{j \neq k} D_{kj} W_j \left(X_j - Y_j \right) \nabla(\ln p) \tag{3.24}$$

where $\overline{W}$ mean molecular weight of mixture, the D_{kj}^{M} are ordinary multicomponent diffusion coefficient which depend on the concentrations and can be calculated from the binary diffusion coefficients, D_{ij}. However, thermal diffusion is important for light species, e.g. H_2, at low temperatures and will be implemented in the current study (Warnatz 1999).

Calculation of D_{kj}^{M} and D_{k}^{T} are very time consuming, although sum of diffusive fluxes is guaranteed to sum to zero. It means mass is always conserved. Also, multicomponent diffusion velocity, equation 3.20 depends on the concentration gradients of all the remaining species. Therefore, alternative approach of transport velocities can be calculated based on mixture-averaged level. In this approach $\vec{j}_k$ is written in the following method(Kee 1998):

$$\vec{j}_k = -\rho D_k^M \overline{W}^{-1} \nabla(W_k X_k) - \rho D_k^M (1 - W_k \overline{W}^{-1}) Y_k \nabla(\ln p) - D_k^T \nabla(\ln T) \tag{3.25}$$

where D_k^M denotes a mean diffusion coefficient for the diffusion of species *k* into the mixture of the remaining species. It can be calculated from the binary diffusion coefficients D_{jk} by the following formulation:

$$D_k^M = (\sum_{j \neq k} \frac{X_j}{D_{jk}})^{-1} (1 - Y_k) \tag{3.26}$$

The thermal diffusion coefficients D_k^T for light species are evaluated in a relatively fast way through the thermal diffusion ratio which can be defined such as the thermal diffusion velocity is given by,

$$V_k^T = -D_k^M \Theta_k X_k^{-1} \nabla(\ln T) \tag{3.27}$$

Assuming no pressure diffusion, the mixture-average diffusion flux is written:

$$\vec{j}_k = -\rho D_k^M \overline{W}^{-1} \nabla(W_k X_k) - \rho W_k \overline{W}^{-1} D_k^M \Theta_k \nabla(\ln T) \tag{3.28}$$

Mixture-averaged formulation is adequate in cases where one species is present in large excess (such as a carrier or diluent gas). Although, the mixture-averaged transport approximation is inadequate for some applications, it has some properties that make it attractive for numerical computation. It is significantly less computationally intensive than the full-multicomponent transport formulation. Also, the mixture-averaged diffusion velocity of species *k* (equation 3.28) depends explicitly on the concentration gradient of species *k*. However, a consequence of using mixture-averaged transport formulation is that mass is not always conserved. Therefore, at the mixture-averaged level of closure of the transport formulation some corrective measures must be taken. In the current study, due to highly diluted flows, the second formalism has been followed.

The heat flux vector in multicomponent reacting flows, $\vec{j}_q$ accounts for heat conduction, heat flux by Dufour effect and heat flux by diffusion.

$$\vec{j}_q = \vec{j}_q^{\,c} + \vec{j}_q^{\,D} + \vec{j}_q^{\,d} \tag{3.29}$$

These three parts are calculated from the following equations:

$$\vec{j}_q^{\,c} = -\lambda \nabla T \tag{3.30}$$

$$\vec{j}_q^{\,D} = \overline{W} RT \sum_k \sum_{j \neq i} \frac{D_k^T}{\rho D_{kj} W_k W_j} \left(\frac{Y_j}{Y_k} \vec{j}_k - \vec{j}_j \right) \tag{3.31}$$

$$\vec{j}_q^{\,d} = \sum_k h_k \vec{j}_k \tag{3.32}$$

where λ is the mixture thermal conductivity, D_k^T is the coefficient of thermal diffusion, D_{kj} is the binary diffusion coefficients. Usually the Dufour effect is negligible in combustion processes. Therefore, the heat flux vector can be written:

$$\vec{j}_q = -\lambda \nabla T + \sum_k h_k \vec{j}_k \tag{3.33}$$

In this study diffusion velocity in washcoat model is calculated based on mixture-averaged method from the following equation:

$$V_k = -\frac{1}{X_k} D_k^M \frac{\partial X_k}{\partial y} - \frac{D_k^M \Theta_k}{X_k} \frac{1}{T} \frac{\partial T}{\partial y} \tag{3.34}$$

To calculate diffusion of mass from channel flow to washcoat layer, equation 3.34 can be written in the following form by using definition of *Nu* and *Sh* numbers:

$$YV_{k,g} = D_k (d_{hyd} W_{gm})^{-1} \left(Sh_k \left(Y_{k,g} W_g - Y_{k,gs} W_{gs} \right) + \Theta_k^T W_k T_{gm}^{-1} \left(T_g - T_{gs} \right) \right) \tag{3.35}$$

where,

$$Nu_T = \frac{h_T \lambda_g}{d_{hyd}} \qquad \text{and} \qquad Sh_k = \frac{h_{m,k} D_k}{d_{hyd}}$$

3.2.3 Correlations for interphase heat and mass transfer

The respective *Nu* and Sh_k numbers characterize the transport of heat mass transfer through the gas zone. In general the Sh_k and *Nu* numbers are dependent on the flow field surrounding the catalyst. To model catalytic combustion systems using 1D channel model interphase gas-solid mass transfer correlations are necessary due to discontinuity at the wall. This is critical in points with high activity or region where catalyst activity is controlled by mass diffusion process. 1D channel flow models can overpredict catalyst activity because of overestimating local heat and mass transfer coefficients in the presence of very fast variation in generated heat fluxes (Groppi et al. 1999). For kinetically controlled regions where rates are primarily controlled by surface kinetics, accurate heat and mass transfer correlations are not as important. However, the limits of kinetically controlled and mass transfer controlled regions is much less delineated than implied in literature. However, mass transfer rate limiting step dominants the downstream portion of the channel (Pfefferle and Pfefferle 1987). The transition from kinetic control to mass transfer control has been referred to in the literature usually as the "light-off" point. At that point there is sharp increase in temperature and correlations for Sh_k and *Nu* numbers become difficult (Hayes and Kolaczkowski 1994).

There has been a number of investigation both experimental and of heat and mass transfer in catalytic monoliths. In deriving an empirical expression for Sh_k and *Nu*, dominancy of kinetic or mass transfer should be considered, since it makes discrepancy between experimental and numerical results as is the case in Hayes et. al paper (Hayes

and Kolaczkowski 1994). Young and Finlayson analytically calculated the Sh_k and Nu numbers for fully developed flow for the boundary conditions of constant wall concentration/temperature or constant wall mass/heat flux. These numbers are higher at the entrance because boundary layers have not yet developed. Correlations for a combination of numerical solution for developing laminar flow and fully developed flow are proposed by Hawthorn, in the following form:

$$Sh = B(1 + C(D_h / L)\,\mathrm{Re}\,Sc) \tag{3.36}$$

B and C are constants depending on the geometry of channel cross-section and surface roughness, respectively. For square channels, in asymptotic conditions, B is 2.976 and C 0.078 for smooth surfaces. However, B is 3.66 for circular channels and C for automobile monolith catalysts is reported to be 0.095 (Hayes and Kolaczkowski 1994; Uberoi and Pereira 1996; Holmgren and Andersson 1998). Uberoi et. al proposed the following empirical model for the mass transfer limited performance for the CO oxidation reaction in a square channel honeycomb catalysts:

$$Sh = 2.696(1 + 0.139\,\mathrm{Re}\,Sc\frac{D_h}{L})^{0.81} \tag{3.37}$$

The correlation is suitable for describing the catalytic performance in removing nitric oxide selectively from power plant effluents. The model predicts higher *Sh* numbers than the theoretical values for laminar flow because it attempts to qualitatively incorporate turbulence(Uberoi and Pereira 1996).

In another attempt, the following expression was derived for gas-solid mass transfer in CO oxidation in monoliths based on the experimental measurements and 3D

CFD simulations. The considered geometry was a square monolith channel with rounded corners.

$$Sh = 3.53 \exp(0.0298 \,\mathrm{Re} \frac{D_h}{L} Sc) \tag{3.38}$$

At high flow rates, measured conversions were higher than that of simulated one. The relation shows higher *Sh* numbers compared with analytical values for laminar flow, due to turbulence effects.

It the above expressions heat and mass transfer coefficients are evaluated over the length L and fail to capture changes of coefficients along the length of channel. Therefore, the better method is to find *Sh* and *Nu* numbers as a function of reactor length. In the results, Colburn analogy between heat and mass transfer are well satisfied (Groppi et al. 1995). Before light-off point the reaction is kinetically controlled, the heat flux is very low. Therefore, *Nu* is close to the value of the solution of the Graetz problem for constant wall heat flux, Nu_H. After light-off point, the wall temperature is close to the adiabatic reaction temperature accordingly the constant wall temperature solution of Graetz problem, Nu_T is approached. It has been pointed out that *Nu* calculated based on the gas bulk temperature compares well with constant property solutions both for constant wall temperature and for constant wall heat flux (Groppi et al. 1995). In light-off region both heat flux and wall temperature are rapidly increasing and the boundary conditions are completely different fro those of the classical Graetz problem. Based on these discussion, the following correlations are proposed for square channels(Groppi et al. 1995):

$$Nu_T = 2.977 + 6.854\exp(-4249x^*)(1000x^*)^{-0.5174}$$
$$Nu_H = 3.095 + 8.9336\exp(-6.7275x^*)(1000x^*)^{-0.5386} \quad (3.39)$$

The dimensionless axial coordinate is defined as $x^* = x/(D_h Pe_g)$. For heat transfer $x_T = x\lambda_{g,in}/(u_{in}\rho_{g,in}C_{p,g,in}d_{hyd}^2)$ and for mass transfer $x_k = xD_{k,in}/(d_{hyd}^2 u_{in})$ are. Heck et al. stated that in the reactor entrance region up to the point of light-off, the *Nu* and *Sh* numbers corresponding to the condition of constant wall heat flux should be used. The light-off increases *Nu* and Sh_k, for which the values corresponding to constant wall temperature should be used (Hayes and Kolaczkowski 1999). Results from a 2D model of a single channel of a monolith reactor used to evaluate the values of the Nusselt and Sherwood numbers under reaction conditions, shows that lumped models generally fail in predicting the wall temperature profile (light-off position). However, for a sufficiently long monolith segment, gas exit temperature predicted by 1D model shows good agreement with those evaluated by 2D model if convenient correlations are used. Groppi et al. proposed that a better solution for *Nu* in a system with chemical reaction at the wall was obtained by interpolating between Nu_T and Nu_H using the following interpolation equation:

$$\frac{Nu - Nu_H}{Nu_T - Nu_H} = \frac{DaNu}{(Da + Nu)Nu_T} \quad (3.40)$$

The Damkohler number, *Da*, is the ratio of reaction rate to diffusion rate and depends on the reaction kinetics (for $Da \rightarrow 0$, $Nu = Nu_H$, for $Da \rightarrow \infty$, $Nu = Nu_T$). In another paper a 2D model for a circular channel with an axisymmetric flow shows the values of the

Nusselt and Sherwood numbers for the case in which chemical reaction occurs at the wall are not the same as those observed in either the constant wall temperature or the constant wall heat flux cases. Also, a simple interpolation between the value for constant wall temperature and constant wall heat flux using the Damkohler number calculated at inlet reactor conditions does not predict exactly the observed value of Nusselt number. Calculating of Nu and Sh_k numbers needs to include the effects of simultaneous development of thermal, concentration and hydrodynamic boundary layers. In monolith channels with non-axisymmetric flow situation is likely to be more complex, because of the possibility of variable reaction rate around the perimeter of the channel (Hayes and Kolaczkowski 1999).

For flow in an annular reactor, Nu and Sh_k numbers are strongly dependent on the channel geometrical parameters including radii ratio and the eccentricity. For our reactor, problem is equivalent to the thermal problem of heat transfer inside an annular duct with adiabatic external wall and internal wall at constant temperature (boundary condition of the third kind). In co-axial tube with zero eccentricity, the asymptotic mass transfer coefficient decreases with increasing of radii ratio. Eccentricity is expected to influence both the asymptotic value mass transfer coefficient and its decay by increasing the axial coordinate. The following expressions are proposed for Nu and Sh_k numbers in CO combustion over Pt-supported catalyst on alumina in an annulus flow by neglecting entrance effect (Beretta et al. 1999):

$$Nu = 2.227 + 10.079\exp(-23.806x^*)(1000x^*)^{-0.35} \tag{3.41}$$

$$Sh = 2.845 + 37.64\exp(-21.57x^*)(1000x^*)^{-0.35} \tag{3.42}$$

For the same geometry by accounting for entrance effect the following expression for *Sh* number is proposed (Ibashi et al. 2003):

$$Sh = 2.845 + 6.874\exp(-57.2x^*)(1000x^*)^{-0.488} \tag{3.43}$$

In annular geometry, mass transfer coefficient can be derived on the basis of the analogy with the Graetz problem, for an annular geometry with a radii ratio pretty close to 1 and with one adiabatic wall. Assuming fully developed velocity profile at the inlet, and fully developed concentration profile inlet effects can be neglected. Therefore, Sh_k can be assumed a constant (Groppi et al. 2001; Groppi et al. 2001).

3.2.4 Reactor boundary conditions

For the equations governing the porous washcoat layer, axial thermal conduction along the tube walls was included. This required boundary conditions for the energy equation at both ends of the reactor, which were defined by approximate thermal conductivity losses along the support tube. Convective and radiative heat losses terms to the outer non-reactive quartz tube wall were included in the gas flow energy equation. Both heat loss terms were necessary for the model to match observed low ΔT's (< 20ºC) across the reactor at conditions of high H_2 conversion. At the inlet of channel, either velocity profile or the profile of mass flow flux can be given. Also, at the inlet mass fraction of gas species and temperature of the mixture are fixed.

For the current study, numerical results are compared to experiments from annular reactor configuration where the catalytic washcoat was placed on the inner wall of an annular flow passage as presented in other previous studies (McCarty 1995; Groppi et al.

2001; Kramer et al. 2003). At the bottom of the washcoat two boundary conditions have been established for the species and temperature derivatives:

$$\left(\frac{\partial Y_k}{\partial y}\right)_{y=\delta_{wc}} = 0.0 \qquad \text{for } k = 1, \ldots, K_{gas} \tag{3.44}$$

$$\left(\frac{\partial T}{\partial y}\right)_{y=\delta_{wc}+\delta_{sub}} = 0.0 \tag{3.45}$$

Since axial thermal conduction along the tube walls was included in equations governing the porous washcoat layer, this required boundary conditions for the energy equation at both ends of the reactor, which were defined by approximate thermal conductivity losses along the support tube. Also, inlet conditions for gas phase species are specified. A convective heat loss term to the outer non-reactive quartz tube wall was included in the gas flow energy equation. Both heat loss terms were necessary for the model to match observed low ΔT's (< 20ºC) across the reactor at conditions of high H_2 conversion.

$$\begin{aligned} &\text{for } \mathrm{Y_{k,g}} \quad Y_{k,g} = Y_{k,g,in} \\ \text{at } x = x_{in} \quad &\text{for } \mathrm{T_g} \quad \dot{m}\overline{C}_{P,g}\left(T_g - T_{g,in}\right) = \left(a_{sb} + a_{ch}\right)h_{T,in}\left(T_s - T_g\right) \\ &\text{for } \mathrm{T_s} \quad \left(a_{sb} + a_{ch}\right)h_{T,in}\left(T_s - T_g\right) = \left(a_{sb} + a_{ch}\right)\lambda_s\left(\frac{dT_s}{dx}\right) \end{aligned} \tag{3.46}$$

$$\text{at } x = x_{ex} \quad \text{for } \mathrm{T_s} \quad \left(a_{sb} + a_{ch}\right)h_{T,ex}\left(T_s - T_g\right) = \left(a_{sb} + a_{ch}\right)\lambda_s\left(\frac{dT_s}{dx}\right) \tag{3.47}$$

3.2.5 Property evaluation and surface kinetic mechanism

Gas-phase transport properties vary with composition and temperature based on CHEMKIN algorithms and standard JANAF tables are used to model gas-phase thermodynamic properties with respect to temperature. Because conditions in the current study include significant dilution of the reactants, a mixture-averaged form of the binary diffusion coefficient D_{km} is used for diffusion into and through the porous washcoat. The washcoat pores are substantially larger than the molecular mean free path and thus Knudsen diffusion is assumed to have a negligible impact on diffusion in the washcoat. The accuracy of this assumption in large part depends on the specific washcoat microstructure.

The results from catalytic washcoat and channel models are strongly influenced by the detailed surface chemistry mechanism. For the numerical model, surface chemistry for H_2 oxidation on supported Pd-based catalyst under low temperature conditions (< 250ºC) and excess O_2 is chosen as the reaction system. The chemistry of reactions is modeled by elementary reactions on a molecular level both in the gas phase and on the surface phase. The modified Arrhenius equations are used to describe the temperature dependence of the reaction rates. For some surface reactions, heats of reaction and thus activation energy barrier are impacted by interaction potentials of neighboring surface species in a mean field modeling approach. To preserve thermodynamic consistency in the surface chemistry mechanism forward and reverse activation energy barriers, $E_{act,i,f}$ and $E_{act,i,r}$ respectively, are related to each other by equation 3.48 where h_k^0 is species formation enthalpy and ε_{jk} is the surface interaction potentials.

$$E_{act,i,r} = E_{act,i,f} - \sum_{k=1}^{k_{gas}} \left(\nu_{ki} h_k^0 \right) - \sum_{k=k_{gas}+1}^{k_{gas}+k_{surf}} \left(\nu_{ki} \left(h_k^0 + \sum_{j=k_{gas}+}^{k_{gas}+k_{surf}} \left(\varepsilon_{kj} \theta_j \right) \right) \right) \tag{3.48}$$

The second summation adds the heat of reaction using a mean field approximation for the energy due to interaction potentials, and this brings coverage dependencies in $E_{act,i,f}$ and/or $E_{act,i,r}$. It has been shown for small and relatively mobile surface adsorbates a mean field approximation with the use ε_{jk} times the mean surface site fraction θ_j for the interaction potential is a reasonable computationally efficient approach for modeling complex phenomena on catalyst surfaces like oscillatory CO oxidation on Pd-based catalysts (Imbihl and Ertl 1995). The ability for mean field approaches to capture the kinetic behavior of H_2 oxidation on supported Pd-based catalyst under low temperature conditions (< 250°C) and excess O_2 is investigated here by using the numerical model described in Chapter 3.

3.3 Numerical methods

The various physical and chemical processes in catalytic combustion result in a broad range of different time scales. Physical processes like convection and diffusion are in the range of milliseconds to microseconds. However, chemical time scales either surface reaction or homogeneous one cover a range over ten magnitudes of orders from 10^{-10}second for surface adsorption/desorption to more than minutes for slow bulk diffusion reactions(nucleation) depending on the combustor operating conditions (Maas and Pope 1992). Disparity in different time scales involved in chemical and physics processes makes the set of equations governing catalytic combustion very stiff. This

means transient numerical model must capture different physical and chemical processes to model actual behavior of catalytic combustion over a wide range of conditions.

3.3.1 Discretization of governing equations

The first task in solving the problem is to discretize the governing conservation equations. In this research, spatial discretization is performed with the conservative finite volume approach on a non-uniform grid. Non-uniform mesh spacing in axial direction allows us to capture changes in heat and mass transfer in the entry region and to save integration time when analyzing long-term behavior of reactor. Also, the front end of the reactor is kinetically controlled region and most of surface reactions occur. Numerical experiments with compressible flow model shows that grid points and their distribution do not have much effect on the final results (Zhu 2001). The variable grid used in x-direction in this study to analyze a 10 mm reactor is defined as 4 first grids with $\Delta x = 0.1$ and 3 next drids with $\Delta x = 0.2$. For y-direction a uniform mesh spacing is used.

In this method solution variables are stored at the cell centers. Diffusion flux at the cell interface is calculated through finite difference methods in which the diffusion coefficients are computed based on cell interface values.

The convective terms such as $\rho u \partial h/\partial x$, for better convergence, are differenced by first order upwind method. The u velocity is always positive in the current study (slowing from the inlet at $x = 0$ toward the end of reactor), so the upwind differencing is formed in the following form:

$$\rho \mathrm{u} \frac{\partial h}{\partial x} \approx \rho_{\mathrm{j}} u_j \frac{h_j - h_{j-1}}{x_j - x_{j-1}} \tag{3.49}$$

Upwind differences cause substantial artificial diffusion, especially on coarse mesh network. The second derivative diffusion terms, such as that in the energy equation are approximated by the following second order central difference:

$$\frac{\partial}{\partial y}(\lambda\frac{\partial T}{\partial y}) \approx (\frac{2}{y_{j+1}-y_{j-1}})(\lambda_{j+1/2}\frac{T_{j+1}-T_j}{y_{j+1}-y_j} - \lambda_{j-1/2}\frac{T_j-T_{j-1}}{y_j-y_{j-1}}) \tag{3.50}$$

The coefficient λ in this formula are evaluated using the average of the dependent variables between mesh points. The diffusive terms in the species conservation equations are like to the diffusive term in the energy equation. However, they are expressed in terms of diffusion velocities, they are approximated as:

$$\frac{\partial \rho Y_k V_k}{\partial y} \approx \frac{\rho_{j+1/2}Y_{k,j+1/2}V_{k,j+1/2} - \rho_{j-1/2}Y_{k,j-1/2}V_{k,j-1/2}}{y_{j+1/2}-y_{j-1/2}} \tag{3.51}$$

The mixture-averaged diffusion velocities are differenced by the following equations:

$$(Y_k V_k)_{j+1/2} \approx -(D_{km}\frac{W_k}{\overline{W}})_{j+1/2}(\frac{\partial X_k}{\partial y})_{j+1/2} - (D_{km}\Theta_k\frac{W_k}{\overline{W}})_{j+1/2}(\frac{1}{T}\frac{\partial T}{\partial y})_{j+1/2} \tag{3.52}$$

3.3.2 Transient integration method

The finite-difference representation of the defining equations forms a set of differential/algebraic equations (DAE's) which are integrated using a stiff ODE solver, e.g. LIMEX, or Gear-type stiff ODE solvers. This approach to finite-difference form of time dependent PDE's is sometimes called the method of lines (MOL) (Heath 2002). The DAE's are written in general form $g(y, y', t) = 0$, where y, y' represent the components

of the solution and their time derivatives and t is time. In the current study the DAE can be written in its semi-explicit form, or an ODE with constraints,

$$\begin{aligned} y' &= f(t,y,y') \\ 0 &= g(t,y,y') \end{aligned} \tag{3.53}$$

Since DAE involves a mixture of differentiations and integrations, it may be necessary to differentiate repeatedly to get an explicit ODE system for all the unknowns. This turns out to be true unless the problem is singular (singular Jacobian matrix) (Ascher 1998). The number of differentiation needed for this transformation is called the index of DAE. In the current study since our set of DAE's are in semi-explicit (Hessenberg) form, index of the system is 1 (Ascher 1998). Solution vector of variables, y in the current study for each cell is composed as follows including temperature, density, gas phase species in channel flow, and all temperature, density, gas phase species in the porous washcoat layer, surface site fraction of surface spaecies and mole fraction of bulk species :

$$\vec{y} = (T_g, \rho_g, Y_1, \ldots, Y_{kgas-1}, T_{gs}, \rho_{gs}, Y_{1s}, \ldots, Y_{(kgas-1)s}, Z_1, \ldots, Z_{ksurf-1}, X_1, \ldots, X_{kbulk-1})^T \tag{3.54}$$

Numerical time integration of the stiff equations is very time consuming. Due to stability criterion explicit time-integration methods show time steps much smaller than that of the adequate representation of the solution vector. Implicit time-integration methods reduce time limitations in explicit methods have been used in many cases. It is well known theses methods can reach steady state much faster than explicit methods due to large allowable time steps, whereas they need a very expensive computations to calculate large number of inverse matrix. However, the highly stiff nature of reactive source terms dictates implicit time integration to ensure numerical stability. To preserve

time accuracy, particularly in unsteady processes, explicit methods show an advantage over the implicit methods.

Another approach for stiff equation involves a split integration of the convective, diffusive and reactive terms (Strang 1968). It means they can be integrated separately in time using different methods, either implicit or explicit. Although time splitting is easily implemented, it presents convergence probles for flows with high unsteadiness. In this method, chemical source terms are solved by a stiff equation solver and convective and dissipative terms are integrated by an efficient flow solver. By using algorithm react, mix and react to do integration of a single time step, method preserve second order accuracy. However, it is difficult in this method to determine the convenient time step such that flow-field and chemical source term integrators match each other (Fedkiw et al. 1997).

With modern numerical techniques several stiff ODE packages have been developed. In practice, explicit methods applied to a stiff system can require very small values for the step size that roundoff or computation time can become critical factors. For this reason, all stiff ODE solvers are based upon implicit numerical schemes. Deuflhard et. al has developed LIMEX method for the general differential algebraic equations (Deuflhard et al. 1987). In this study, LIMEX solver was used. This solver is based on semi-implicit methods. Semi-implicit methods avoid solving the expensive nonlinear algebraic system by linearizing the implicit equations such as implicit Euler method. This method may not be always stable. The semi-implicit method is recommended for stiff systems (Bader 1983). Bader and Deuflhard implemented semi-implicit midpoint rule and Richardson idea of extrapolation for order and stepsize control to provide a method to solve stiff ODE's. This approach has been shown to be comparable to full implicit

solver such as DASSL for relatively accurate calculations and much faster(Zhu 2001). The time discretization of the linearly implicit extrapolation method LIMEX solves general differential-algebraic systems (DAEs) of the form(Deuflhard et al. 1987):

$$\vec{\vec{B}}(t,\vec{y})\vec{y}' = \vec{f}(t,\vec{y}) \tag{3.55}$$

$\vec{\vec{B}}$ is a *(n,n)*-matrix of rank less or equal n. General conditions for the applicability of LIMEX are a regular matrix pencil $\vec{\vec{B}} + h\vec{\vec{A}}$ with $\vec{\vec{A}}$ the Jacobian of the residual of the DAE and an index of the DAE less or equal 1. The discretization of LIMEX is based on the elementary linearly implicit Euler discretization:

$$\begin{aligned}\vec{\vec{B}}(t_k,\vec{y}_k)\vec{y}')_{y=y_k} + \frac{\partial(\vec{\vec{B}}(t_k,\vec{y}_k)\vec{y}')_{y=y_k}}{\partial\vec{y}}(\vec{y}_{k+1}-\vec{y}_k) \\ = \vec{f}(t_k,\vec{y}_k) + \frac{\partial\vec{f}(t,\vec{y})_{y=y_k}}{\partial\vec{y}}(\vec{y}_{k+1}-\vec{y}_k)\end{aligned} \tag{3.56}$$

Now by using finite difference in time the following equation can be written:

$$\begin{aligned}\vec{\vec{B}}(t_k,\vec{y}_k)(\vec{y}_{k+1}-\vec{y}_k)h^{-1} + \frac{\partial(\vec{\vec{B}}(t_k,\vec{y}_k)\vec{y}')_{y=y_k}}{\partial\vec{y}}(\vec{y}_{k+1}-\vec{y}_k) \\ = \vec{f}(t_k,\vec{y}_k) + \frac{\partial\vec{f}(t,\vec{y})_{y=y_k}}{\partial\vec{y}}(\vec{y}_{k+1}-\vec{y}_k)\end{aligned} \tag{3.57}$$

by manipulating of the equation we have:

$$(\vec{\vec{B}}(t_k,\vec{y}_k) - h\frac{\partial(\vec{f}-\vec{\vec{B}}\vec{y}')_{y_k,t_k}}{\partial\vec{y}})(\vec{y}_{k+1}-\vec{y}_k) = h\vec{f}(t_k,\vec{y}_k) \tag{3.58}$$

And the Jacobian matrix of the residual is defined: $\vec{\vec{J}} = \frac{\partial(\vec{f} - \vec{\vec{B}}\vec{y}')_{y_k, t_k}}{\partial \vec{y}}$. Combined with extrapolation this one-step method permits an adaptive control of stepsize and order. Within the extrapolation process one computes for a basic stepsize h approximations $T_{j,1}$ for $\vec{y}(t_0 + h)$ using the described discretization above with step-sizes $h_j = h / j, j = 1, ...,$ j(max). Then the extrapolation tableau recursively defines higher order approximations $T_{j,k}$:

$$T_{j,k} = T_{j,k-1} + \frac{T_{j,k-1} - T_{j-1,k-1}}{j/(j-k+1)-1} \qquad k = 1, \ldots\ldots, j \tag{3.59}$$

The subdiagonal differences $T_{j,j} - T_{j,j-1}$ are taken as error estimates. In time integration of quasi-1D catalytic full channel model, LIMEX has been used to integrate the whole set of discretized equations simultaneously in each time step. The efficiency of LIMEX is strongly dependent on the calculation of Jacobian matrix and on the solution of the linear systems, since it requires many times calculation of Jacobian and its inverse. The Jacobian matrix involves the derivatives of the discretized convection, diffusion and source terms to the solution variables. For the 1D model, this matrix has a banded structure and for upwind and central differencing scheme used in this study is a block tridiagonal.

3.4 Sample results

With these evaluations, the above conservation, the transient equations are discretized in the *x*- and *y*-directions using first order differences for the convective flux terms and second order differences for the diffusive terms. The equations are integrated numerically with respect to time using the numerical integration scheme LIMEX until a steady-state solution is found. For H_2 over supported Pd catalysts, steady-state solutions are achieved before 1200s and thus transient integration was carried out to 1200s. For the H_2 oxidation, numerical integration of the coupled equations for the channel flow model time steps was limited to time steps ≤ 0.1 s. For a 2 cm long reactor as used in the companion experimental study, a variable-spacing grid of 10 cells (finer near the reactor entrance) was sufficient to capture transient behavior of the surface along the reactor axis. Details of the experimental setup are covered completely in Chapter 2. Local heat and mass transfer from the channel flow to the porous washcoat layer are calculated using Graetz number correlations developed for reacting flows as discussed above. The model calculates average temperature, density, and species fractions both in the channel flow and in the porous washcoat layer, which is modeled as radially discretized finite volumes. Surface site fractions on the washcoat catalyst are also calculated.

The transient H_2 conversion and outlet temperature are shown in Figure 3.4 under the condition defined in Table 3.1. There exists a delay between the maximum temperature at the outlet and the maximum H_2 conversion of the reactor due to the heat storage for warming-up of the reactor walls. The heat capacity of the reactor causes a drop in H_2 conversion after 11s. Figure 3.5 shows transient surface site fractions of surface species Pd oxide, O(sb) and hydroxyl, OH(sb). It indicates a larger downstream

portion of reactor experiences reduction of the Pd catalyst. Surface hydroxyl starts to build up fast after 1s and consequently due to H2O equilibration, it reaches to a steady state level. Interestingly, two surface species, O(sb) and OH(sb) after around 2s show the same monotonicity in their behavior before getting to a steady-state level.

Table 3.1 - Flow conditions and physical parameters of the annular reactor

Physical Parameters:	
Length of the reactor	2.0 cm
Porosity of washcoat	0.5
Density of solid phase of washcoat	3.94 g/cm^3
Site density per unit washcoat surface area	1.75e-09 sites/cm^2
Dispersion of the Catalyst	10 %
Wall thermal conductivity	0.22 W/(cm.K)
Washcoat Thickness	30 µm
Annular channel height	0.068 cm
Specific heat at constant volume	0.765 kJ/kg.K
Specific area in washcoat	2000 cm^{-1}
Inlet Flow Conditions for Case of H_2	
Pressure	1atm
Temperature	100°C
Velocity	10.0m/s
H_2 mole fraction	0.0190
O_2 mole fraction	0.0460
N_2 mole fraction	0.9350

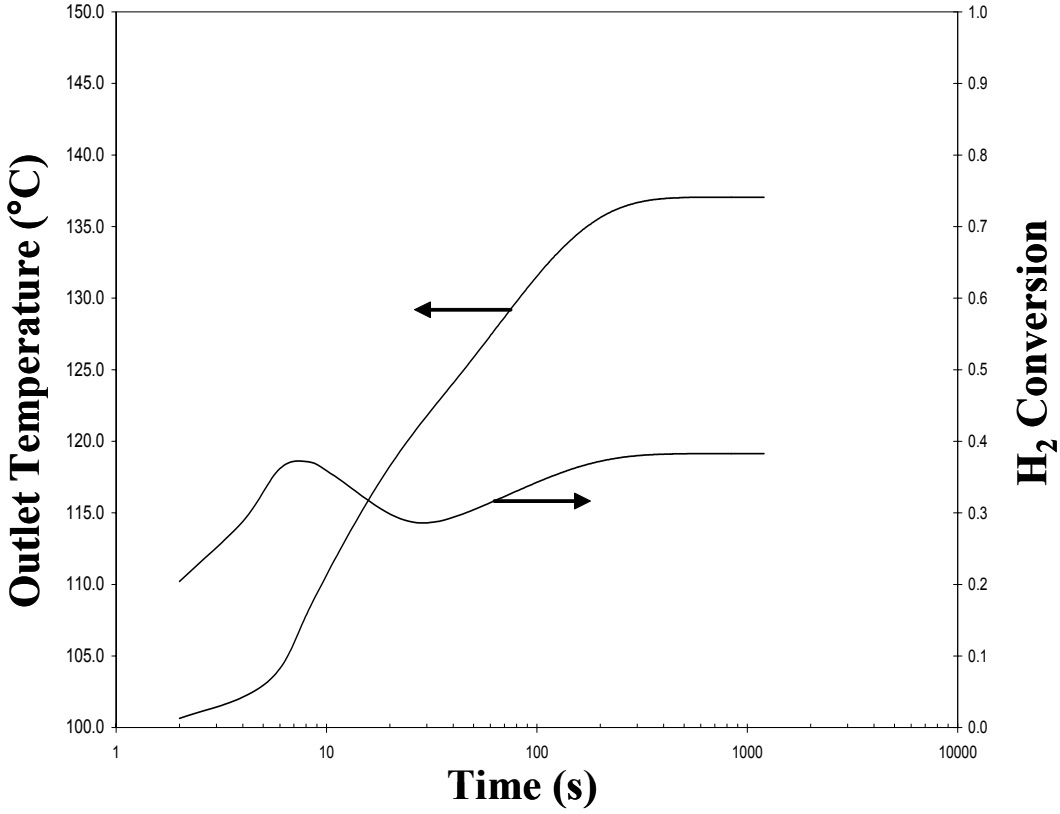

Figure 3.4 Comparison of experimental results and numerical predictions of H_2 conversion

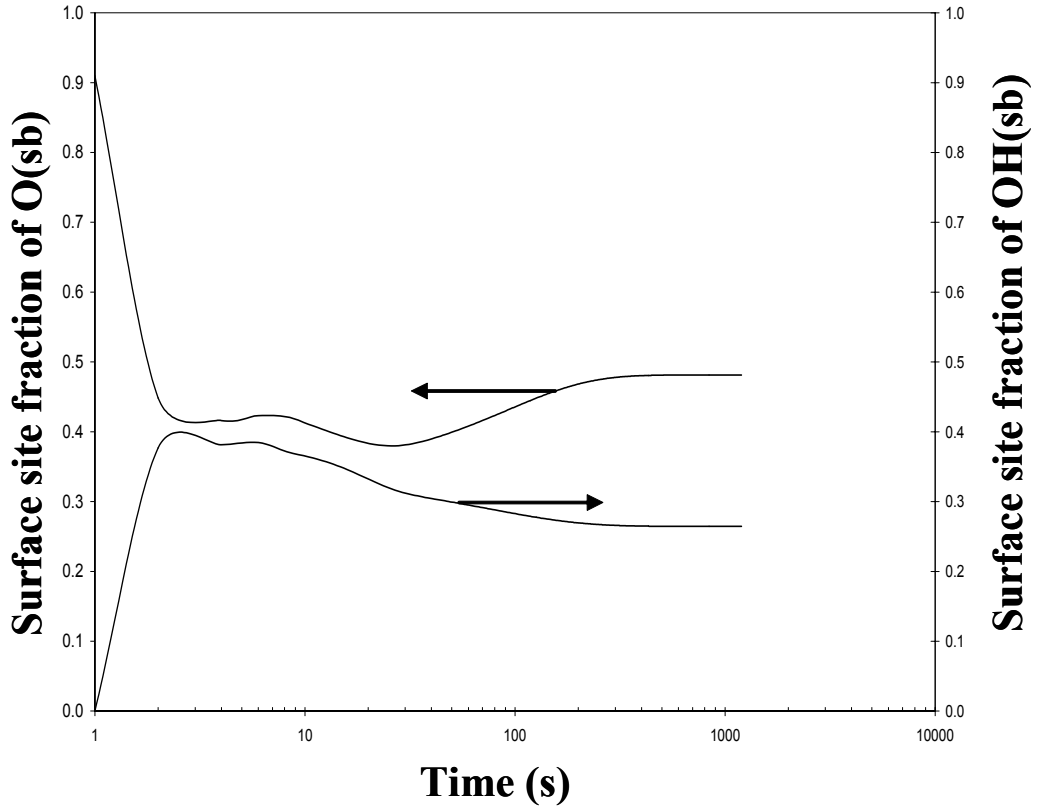

Figure 3.5 Comparison of experimental results and numerical predictions of O(sb) and OH(sb) surface site fractions

3.5 Conclusion

A mathematical model was developed to explore effect of diffusion mechanism inside the washcoat. The model was integrated to a channel flow model to evaluate reactor behavior during different operational conditions. Importance of surface chemistry mechanism and heat/mass transfer correlations were discussed. Due to stiffness of the system of discretized governing algebraic/differential equations, stiff ODE solver was applied. Finally, some sample results were presented to show how numerical results can elaborate transient behavior of reactor.

Chapter 4

Validation of Reactor Model for Pd-H_2-O_2

4.1 Introduction

In the development of full reactor model for catalytic reacting channel flows, some simplifications have been made to speed up the computer simulations. These along with some uncertainties in surface reaction chemistry, thermochemistry of surface species and catalytic surface properties make it necessary that model be compared with experimental results. In the current chapter, at first surface chemistry mechanism for low temperature H_2 combustion over Pd-based catalysts has been proposed. Then the developed model in Chapter 3 was used to look at the kinetically controlled problem of H2 oxidation over supported Pd-catalysts at very low temperatures. Finally, based on comparison of experimental results with model predictions validity of surface chemistry mechanism is explored.

4.2 Pd-H_2-O_2 surface chemistry mechanism

The detailed chemistry mechanism for this study has been adapted from Kramer et. al (Kramer et al. 2003). The surface chemistry is derived from a previous Pd-O2 mechanism that has been validated with extensive experimental studies. This previous study based on TGA/MS experiments developed and validated a mechanism for oxidation and reduction of supported Pd polycrystalline Pd (Wolf et al. 2003). This Pd-O_2 mechanism was validated for a temperature range from 200 to 1200°C and provided the Pd-O surface chemistry used in the existing mechanism.

A preliminary Pd-H_2-O_2 mechanism for O_2-net environment,(Kramer et al. 2003) reflected trends in catalyst light-off but unable to predict the inhibition of H_2O and the impact of fuel equivalence ratio ϕ on conversion. Some experimental results for steady-state conversion for a range of inlet temperatures and ϕ = 0.05 and 0.1, $X_{N2,in}/X_{O2,in}$ = 20 in dry/wet feeds are presented in Chapter 2. As discussed in Chapter 2, H_2O in the inlet feed reduces conversion for ϕ = 0.1. Additionally, conversion rises more rapidly for ϕ = 0.1 than that for ϕ = 0.05. To further refine the preliminary mechanism (Kramer et al. 2003), the catalytic channel model (Kramer et al. 2003) was used in a parametric study to evaluate what surface thermodynamic parameters and expected surface species interaction potentials could be adjusted to capture the observed trends in H_2 conversion with respect to ϕ and $X_{H2O,in}$. No changes were made to validated Pd-O_2 surface chemistry except that interaction potentials between H-containing surface species and the Pd-O species were added for the full H_2 oxidation surface mechanism.

A brief overview of the Pd-O_2 mechanism and the additional H-containing mechanism is given here. The surface chemistry mechanism differentiate between two different surface Pd-O atomic interactions(Veser et al. 1999): 1) surface Pd oxide (O(sb)) and 2) chemisorbed O atom on Pd metal (O(s)). Surface oxide vacancies on (1 0 0) surface of Pd is depicted in Figure 4.1 (Wolf et al. 2003). As shown, O_2 is adsorbed dissociatively onto metallic Pd(s) and Pd(sb) forms two different Pd-O interactions O(s) and O(sb), respectively. Reactions as indicated by R# in Figure 4.1 are shown in Table 4.1. Accordingly, to make consistency inclusion of two Pd-O species also makes the mechanism include two Pd-H surface species in agreement with the present experimental observations(Dus and Nowicka 1998): 1) H(sb), which is a H atom resting in a Pd oxide

vacancy and 2) H(s) which is chemisorbed H(s). In the same way, two surface species for Pd-OH and Pd-H_2O are considered.

Table 4.2 presents species formation enthalpies relative to zero energy levels for standard gas-phase enthalpies and pure Pd metal. As seen in the Table 4.2, each surface species has two possible interactions with Pd depending on whether it is bound to a vacancy in the surface oxide (O(sb)) layer or whether it is chemisorbed onto metallic Pd.

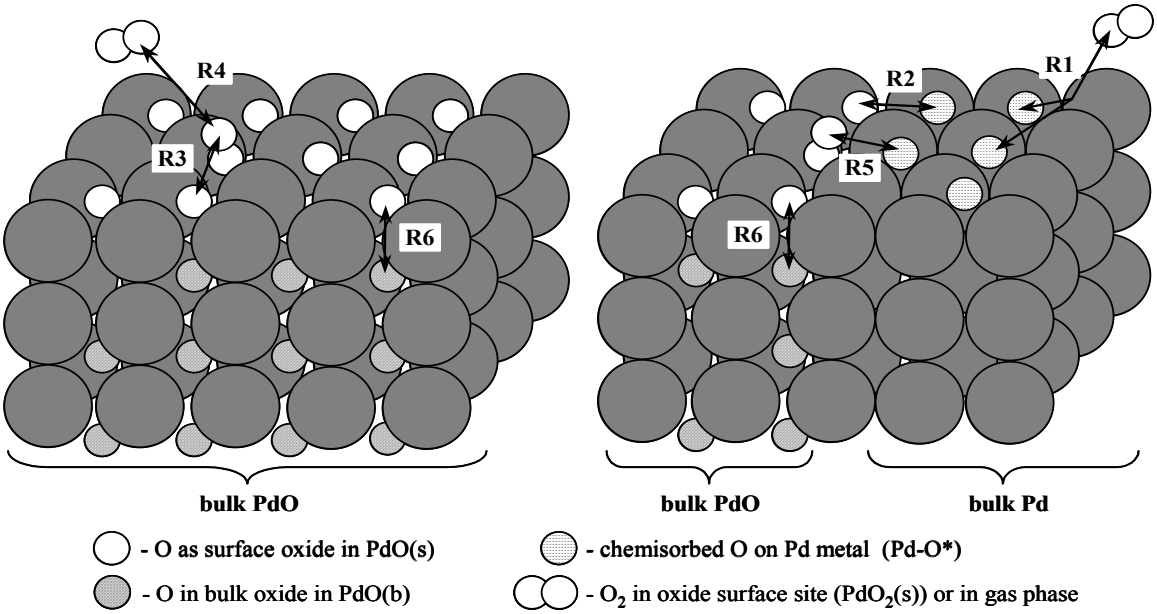

Figure 4.1 Illustration of reactions for O and Pd atoms (Wolf et al. 2003)

Table 4.1 Reactions as indicated by R# in Figure 4.1

Reaction #	Reactants	Products
R1	O2 + 2Pd(s)	2O(s)
R2	O(s)	O(sb)
R3	2O(sb)	O2(sb) + Pd(sb)
R4	O2(sb)	O2 + Pd(sb)
R5	O(sb) + O(s)	O2(sb) + Pd(s)
R6	O(sb) + Pd(b)	O(b) + Pd(sb)

Since O(sb) is the predominant species for net oxidizing environments at temperatures in the current study, the (sb) species will play a more important role in modeling the H_2 combustion.

Table 4.2 Gas-phase and surface species enthalpies relative to standard gas phase enthalpies

Species	h_k^0 **(at 25ºC in kJ/gmol)**
H_2	0.0
O_2	0.0
H_2O	-241.8
N_2	0.0
Pd(s)	0.0
Pd-O(s)	$-115.0+57.5\theta_{O(s)}+29\theta_{OH(s)}$
Pd-O(sb)	-115.0
Pd(sb)	$-35.0+208\theta_{Pd(sb)}+208\theta_{H2O(sb)}+104\theta_{H(sb)}+104\theta_{OH(sb)}$
Pd-O_2(sb)	-105.0
Pd-H(s)	$-42.0+8\theta_{H(s)}$
Pd-OH(s)	$-214.0+29\theta_{O(s)}+14.5\theta_{OH(s)}$
Pd-H_2O(s)	-302.0
Pd-H(sb)	$-52.0+104\theta_{Pd(sb)}+104\theta_{H2O(sb)}+52\theta_{H(sb)}+52\theta_{OH(sb)}$
Pd-OH(sb)	$-224.0+104\theta_{Pd(sb)}+104\theta_{H2O(sb)}+52\theta_{H(sb)}+52\theta_{OH(sb)}$
Pd-H_2O(sb)	$-322.0+208\theta_{Pd(sb)}+208\theta_{H2O(sb)}+104\theta_{H(sb)}+104\theta_{OH(sb)}$

The refined Pd-O_2-H_2 mechanism, like the mechanism from which it id derived, (Kramer et al. 2003) has not taken into consideration the impact of bulk PdO reduction or the formation of bulk PdH. Such changes in the bulk of the catalyst will the impact the surface enthalpies of all species as observed for the PdO mechanism (Wolf et al. 2003) and CO oxidation on Pd versus PdO (Meusel et al. 2001). Thus conversion at conditions of relatively high ϕ (> 0.3), where it is suspected that bulk reduction and hydride formation are likely, are unlikely to be captured by the following proposed mechanism.

However, it can be extended straightforwardly to conditions involving bulk PdO reduction (Wolf et al. 2003). Actually, the presented experimental results in Chapter 2, do suggest that the controlling mechanism for H_2 combustion on PdO are substantially different from the controlling mechanisms for H_2 combustion on metallic Pd particles.

Using the mechanism, predictions were validated against the complex experimental trends shown in Figure 4.2 for H_2 conversion as a function of ϕ and $X_{H2O,in}$.

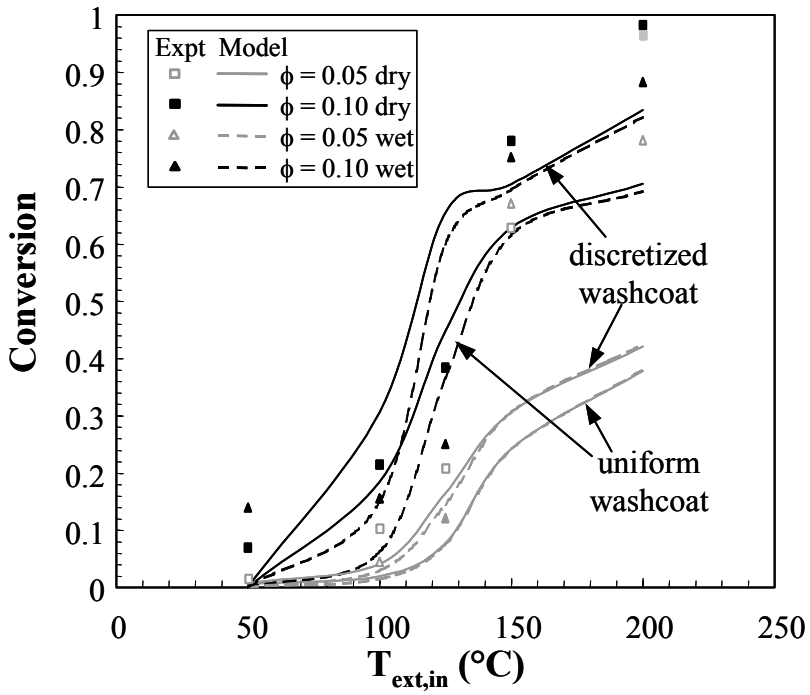

Figure 4.2 Experimental measurements and numerical predictions

The principle difference between the current mechanism from the mechanism of Kramer et. al includes a decrease in the surface enthalpy of OH(sb) and H_2O(sb) by 10 and 20 kJ/gmol respectively and the addition of interaction potentials between all of the (sb) species. Although, the self-repulsions for chemisorbed O(s) and H(s) are well documented in the literature (Rinnemo et al. 1997), interaction potentials associated with

the (sb) species are uncertain and to be calculated from detailed atomistic modeling which is an area of ongoing research (Lopez et al. 2004) or use of semi-empirical techniques, such as the bond order conservation (BOC), known as unity bond index-quadratic exponential potential (UBI-QEP) or Polanyi free energy relations and first principle density functional theory (DFT) (Mhadeshwar et al. 2003). Intuitively they are related to an electron affinity of the unsatisfied oxide vacancy, and thus, strengths of the repulsive interactions can be adjusted by the extent that the adsorbate reduces the electron rich condition in the Pd(sb) configuration. In this regard, OH(sb) is given half the repulsive force of Pd(sb), due to share a single electron between the Pd and OH adatom. The repulsion between H(sb) and H_2O(sb) species are much less certain and were varied in the mechanism as indicated in Table 4.2. The complete surface reaction mechanism is given in Table 4.3. The mechanism includes 12 elementary reversible reactions with six adsorption/desorption reactions.

H_2 conversion is most sensitive to adsorption/desorption reaction rates of H_2 and H_2O, which are related to the surface enthalpy of H(sb), OH(sb) and H_2O(sb). To observe temperature dependency of sticking coefficients for both O_2 and H_2, they are assumed to decay with $T^{-0.5}$ (Yagi et al. 1999). In particular, model runs revealed conversion depends strongly on the ratio of H_2 and O_2 adsorption on oxide vacancies under the excess O2 conditions relevant to the current study. To get conversion in low temperatures, H_2 adsorption is modeled to occur dissociatively on vacancy/oxide pairs (reaction 4f). Experimental evidences show that ratio of sticking coefficients of H_2/O_2 on Pd must be near 5:1 to predict Pd-based H_2 sensor performance (Soderberg and Lundstrom 1983). However, to match measurements in this study the ratio of H_2 sticking coefficient on both

Table 4.3 Pd-O_2-H_2 surface chemistry mechanism used in numerical code

Reactions	**A factor or Stick coeff.** (UNITS - G,CM,S)	$\mathbf{E_{ACT}}$ (KJ/MOL)
Adsorption/Desorption Reactions		
1f) O_2+2Pd(s) ⇒ 2O(s)	$0.8*T^{-0.5}$	0.0
1r) 2O(s) ⇒ O_2+2Pd(s)	$5.7*10^{21}$	230 –115ΘO(s)
2f) O_2+Pd(sb) ⇒ O_2(sb)	$1.0*T^{-0.5}$	0.0
2r) O_2(sb) ⇒ O_2+Pd(sb)	$1.0*10^{13}$	70
3f) H_2+2Pd(s) ⇒ 2H(s)	$6.4*T^{-0.5}$	0.0
3r) 2H(s) ⇒ H_2+2Pd(s)	$5.7*10^{21}$	84 –16θH(s)
4f) H_2+Pd(sb)+O(sb) ⇒ H(sb)+OH(sb)	$8.0*T^{-0.5}$	0.0
4r) OH(sb)+H(sb) ⇒ H_2+Pd(sb)+O(sb)	$5.7*10^{21}$	126
5f) H_2O+Pd(s) ⇒ H_2O(s)	0.50	0.0
5r) H_2O(s) ⇒ H_2O+Pd(s)	$1.0*10^{13}$	60.2
6f) H_2O+Pd(sb) ⇒ H_2O(sb)	0.50	0.0
6r) H_2O(sb) ⇒ H_2O+Pd(sb)	$1.0*10^{13}$	45.2
Reversible Surface Reactions		
7) O(s) ⇔ O(sb)	$5.0*10^{11}$	90
8) O_2(sb)+Pd(sb) ⇔ 2O(sb)	$5.7*10^{21}$	0.0
9) O_2(sb)+Pd(s) ⇔ O(sb)+O(s)	$5.7*10^{21}$	185 – 57.5θO(s)
10) H(s)+Pd(sb) ⇔ H(sb)+Pd(s)	$5.7*10^{21}$	50
11) H(s)+O(s) ⇔ OH(s)+Pd(s)	$5.7*10^{21}$	45
12) H(s)+OH(s) ⇔ H_2O(s)+Pd(s)	$5.7*10^{21}$	55
13) OH(s)+OH(s) ⇔ H_2O(s)+O(s)	$5.7*10^{21}$	102
14) OH(sb)+Pd(s) ⇔ H(s)+O(sb)	$5.7*10^{21}$	97 + 8θH(s)
15) H(s)+OH(sb) ⇔ H2O(sb)+Pd(s)	$5.7*10^{21}$	40
16) OH(sb)+Pd(sb) ⇔ H(sb)+O(sb)	$5.7*10^{21}$	122
17) H_2O(sb)+Pd(sb) ⇔ H(sb)+OH(sb)	$5.7*10^{21}$	121
18) OH(sb)+OH(sb) ⇔ H_2O(sb)+O(sb)	$5.7*10^{21}$	81

the metal and the oxide vacancies to the O_2 sticking coefficient was increased to nearly 8 to 1. This has been qualitatively verified, where even in O_2-rich environment, supported PdO particles can undergo partial reduction at low temperatures when H_2 equivalence ratios are > 0.2.

Single atom desorption pre-exponentials were set equal to a typical typical frequency of the vibration of the bond for surface adatoms (10^{13} s^{-1}) (Warnatz 1999). For bimolecular surface reactions pre-exponentials are set equal to a typical frequency factor divided by the average site density, which equals $1.75*10^{-9}$ mol/cm^2. This has been shown to be acceptable (Wolf et al. 2003).

The reversible surface reactions (reactions 7-18) for converting adsorbed H species to H_2O are shown in Table 4.3. The reaction rates are evaluated based on thermodynamic consistency with the enthalpies including interaction potentials in Table 4.2 and the approximation that reaction entropy changes are zero. This latter approximation results in constant pre-exponential factors between the forward and reverse surface reactions.

Contribution of gas phase chemistry mechanism for the low temperature and low ϕ conditions was tested by including in the model simulation a detailed gas-phase chemistry mechanism for homogeneous H_2 combustion (Yetter et al. 1991). Including the gas phase chemistry in both the channel flow and the washcoat pores increased H_2 conversion by less than 1% at the highest temperature (250°C) modeled in this study. Increase in conversion was negligibly small for lower temperature and thus gas phase chemistry was not included in most simulations.

4.3 Comparison of numerical and experimental results

The surface mechanism in Table 4.3 implemented with the channel flow model follows quite well the complex trends in experimental observations with respect to $T_{ext,in}$ and $X_{H2O,in}$ for ϕ = 0.05, 0.1 as indicated in Figure 4.2. To observe the importance of

modeling a radially discretized washcoat vs. a uniform washcoat, the catalytic channel model was run in two different modes: 1) with a washcoat discretized into 15 radial layers and 2) a washcoat which is considered uniform in the radial direction. The simulated reactor follows the experimental geometry as indicated in Table 4.4 and the model is discretized axially into 10 cells of variable length as stated in Chapter 3.

Table 4.4 Flow conditions and physical parameters of the annular reactor

Physical Parameters	
Length of the reactor	2.0 cm
Porosity of washcoat	0.5
Density of solid phase of washcoat	3.94 g/cm^3
Site density per unit washcoat surface area	1.75e-09 sites/cm^2
Dispersion of the Catalyst	10 %
Wall thermal conductivity	0.22 W/(cm.K)
Washcoat Thickness	30 μm
Annular channel height	0.068 cm
Specific heat at constant volume	0.765 kJ/kg.K
Specific area in washcoat	2000 cm^{-1}
Inlet Flow Conditions for Case of H_2	
Pressure(atm)	1
Temperature(K)	373.15 – 473.15
Velocity (m/s)	10.0
H_2 (mol %)	1.90 %
O_2 (mol %)	4.60 %
N_2 (mol %)	93.50 %

The results show the good ability of the model to match the light-off in conversion between 100 and 150°C for the experimental conditions with both ϕ. Furthermore, the mechanism captures the observed H_2O inhibition for $T_{ext,in}$ < 150°C for ϕ = 0.1. The model also shows trends qualitatively for higher temperature conversion where mass transfer becomes rate-limiting. The lower impact of H_2O on conversion at these conditions is shown both in the simulations and the experiments. However, the model underpredicts conversions for ϕ = 0.05 at these temperatures where mass transport

begins to impact the conversion in the catalyst. That may be attributed to the limitations of the 1-D correlations for the mass transfer to the washcoat and by an uncertainty of surface chemistry in under-predicting of the vacancy creation rates at the lower ϕ. This suggests that the diffusive transport models based on the Graetz correlation for accounting for transport from the gas to the catalytic channel may need improvement or be replaced with a multi-dimensional flow model.

In Figure 4.2, the discretized washcoat predicts a higher H_2 conversion than the uniform washcoat results for an equal inlet condition. This discrepancy arises because the uniform washcoat doesn't have any mechanism to evaluate influences the H_2 concentration at the washcoat/channel interface by diffusion into the washcoat. The addition of ordinary diffusion model into/through the washcoat with the discretized model results in the gradient of gas phase H_2 species through the washcoat layer with higher H_2 concentration in the outer cells of the washcoat near the channel flow and causes higher predicted conversion than that by the uniform washcoat. This indicates that conversion calculated from uniform washcoat and multiplied by a simple effectiveness factor will not necessarily capture the effects of intra-pore diffusion on catalyst performance, particularly within the context of complex surface chemistry mechanisms.

In order to compare more experimental data with model, result of TPR experiment (Figure 2.6) are compared with model for $\phi = 0.1$ with $X_{H2O,in} = 0.0$ and $X_{H2O,in} = 0.03$. The results are depicted in Figure 4.3 and Figure 4.4. Model captures rise from low conversion to high conversion between 100-150°C in both wet and dry cases. Model does not show conversion in temperatures less than 80°C in particular for wet flows. In Figure 4.3, for T > 200°C H_2 conversion in the dry feed continues to rise, but

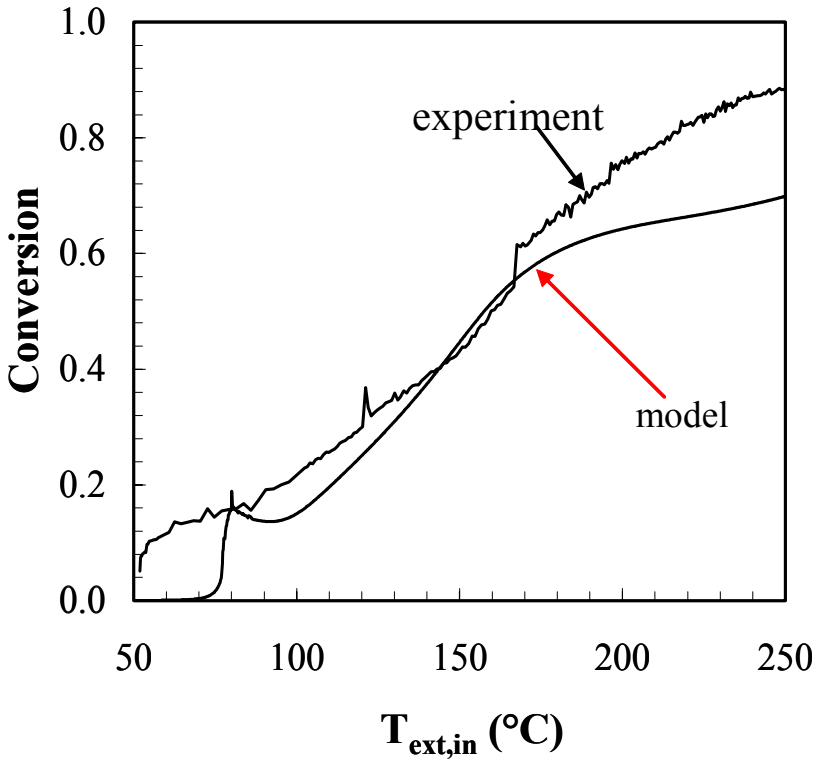

Figure 4.3 Model prediction of H_2 conversion for $\phi = 0.1$ and $X_{H2O,in} = 0.0$ in TPR test

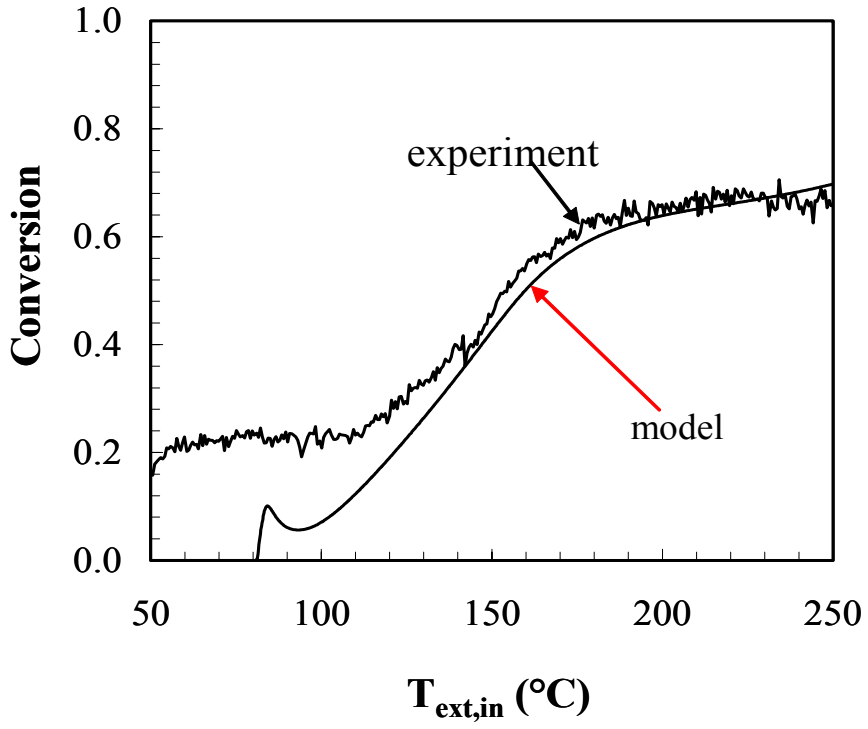

Figure 4.4 Model prediction of H_2 conversion for $\phi = 0.1$ and $X_{H2O,in} = 0.03$ in TPR test

more slowly than during light-off phase, possibly due to rising mass transfer rates and model follows qualitatively in this region, whereas, conversion for inlet feed with 3% H_2O shows a plateau after 200°C.

4.4 Catalytic washcoat effectiveness for H_2 combustion

To characterize conditions in which intra-pore diffusion in the washcoat is significant, a single axial slice model with the discretized washcoat into 20 meshes was run with external flow conditions equivalent to the inlet conditions for the cases presented in Figure 4.2.

Analysis of the solution includes the calculation of the apparent effectiveness factor η, which is based on the reaction rate of the limiting reactant, H_2. From the steady state concentration profile across the washcoat layer, η is found from the following equation:

$$\eta = \frac{\int_0^{\delta_{wc}} \dot{s}_{H_2}(Y_k, \theta_k, T)dy}{\delta_{wc}\dot{s}_{H_2@cell\#1}} \tag{4.2}$$

Because it is of interest to assess whether conventional effectiveness correlations based on Thiele modulus ϕ_T can be adapted for complex chemistry models, a definition for ϕ_T is given as follows:

$$\phi_{\mathrm{T}} = \delta_{wc}\sqrt{\frac{\dot{s}_{H_2@cell\#1}a_{cat}W_{H_2}}{\rho Y_{H_2}D_{H_2}}} \tag{4.3}$$

All parameters in equation 4.3 are calculated at the outermost washcoat cell of the discretized catalyst support layer, which is in contact with the external channel flow. This allows for the possibility of using a Thiele modulus correlation for a simplified model wherein the catalytic washcoat is modeled by conditions in a single cell only.

To asses the impact of surface chemistry in the depth of the washcoat, the model was run for some of the conditions. Profiles of surface site fractions with respect to dimensionless depth in the washcoat are plotted in Figures 4.5a-4.5f. The plots include steady state profiles of the site fractions of the three most dominant surface species – O(sb), OH(sb), and OH(s) – and the site fractions Pd(sb), oxide vacancy, and Pd(s), open metallic site. The plots in Figure 4.5 also show the fraction of H_2 remaining in the gas phase ($Y_{H2}/Y_{H2,ext}$) through the depth of the washcoat.

Comparison of Figures 4.5a and 4.5b indicate that the thicker 80 μm washcoat at T_{ext} = 125°C results in a lower Y_{H2} in the deeper regions of the washcoat and thus lower reduced vacancy and increased oxide site fractions in the deeper layers. It means, there should be a reduction in surface activity for H_2 oxidation. Correspondingly, there is a drop in effectiveness from 60% to 40% with the increase in washcoat thickness from 40 to 80 μm.

Figures 4.5a and 4.5c show that wet feed in the external gas flow at T_{ext} = 125°C and at ϕ = 0.1, does not greatly change the distribution of the major surface species. At this temperature in the light-off range, adding H_2O in the gas phase reduces vacancy concentrations by increased H_2O adsorption and thus H_2O(sb) and H_2O(s) site fractions. This lowers activity and conversion from the catalyst layer. For the lower ϕ = 0.05, shown in Figure 4.5d, vacancy concentrations are significantly decreased due to less H_2

oxidation and thus O(sb) removal. This explains the reduced H_2 consumption for the lower ϕ at $T_{ext} < 150°C$. Combined with the surface site fraction profiles in Figure 4.5d and 4.5f, this suggests a need to improve the surface chemistry mechanism with respect to H_2 adsorption and it relationship to the site fractions of Pd(sb) and Pd(s).

The impact of temperature on surface site fractions is illustrated by Figure 4.5e and 4.5f. It shows that the increase in temperature to 150°C results in increased activity with increased vacancy concentrations for both $\phi = 0.1$ and $\phi = 0.05$ respectively. However, significant gradients through the depth of a 40 μm begin to appear for the $\phi = 0.1$ case due to the increased activity at this condition. This results in a drop in η. For the dry $\phi = 0.1$ case $\eta = 0.45$, whereas at the same temperature the dry $\phi = 0.05$ case has an $\eta = 0.9$. This implies that a simple surface chemistry model with a first order reaction rate expression for H_2 will not predict conversion as a function of ϕ. Furthermore discretized washcoat models may be necessary to interpret measurements for evaluating surface chemistry mechanisms in supported washcoat catalysts, particularly under conditions of high conversion.

Figure 4.6 represents conversion as calculated by the gas phase Y_{H2} at the washcoat/channel flow interface for a range of washcoat thicknesses for channel flow conditions of $\phi = 0.05$ and 0.1 for dry feed. The results suggest that at low conversion, conversion is proportional to δ_{wc}. However, as conversion begins to rise rapidly between 100 and 150°C, the proportionality between conversion and δ_{wc} doesn't exist because intra-pore diffusion mechanism is slower than to replenish the thicker washcoat layers at the higher conversion rates.

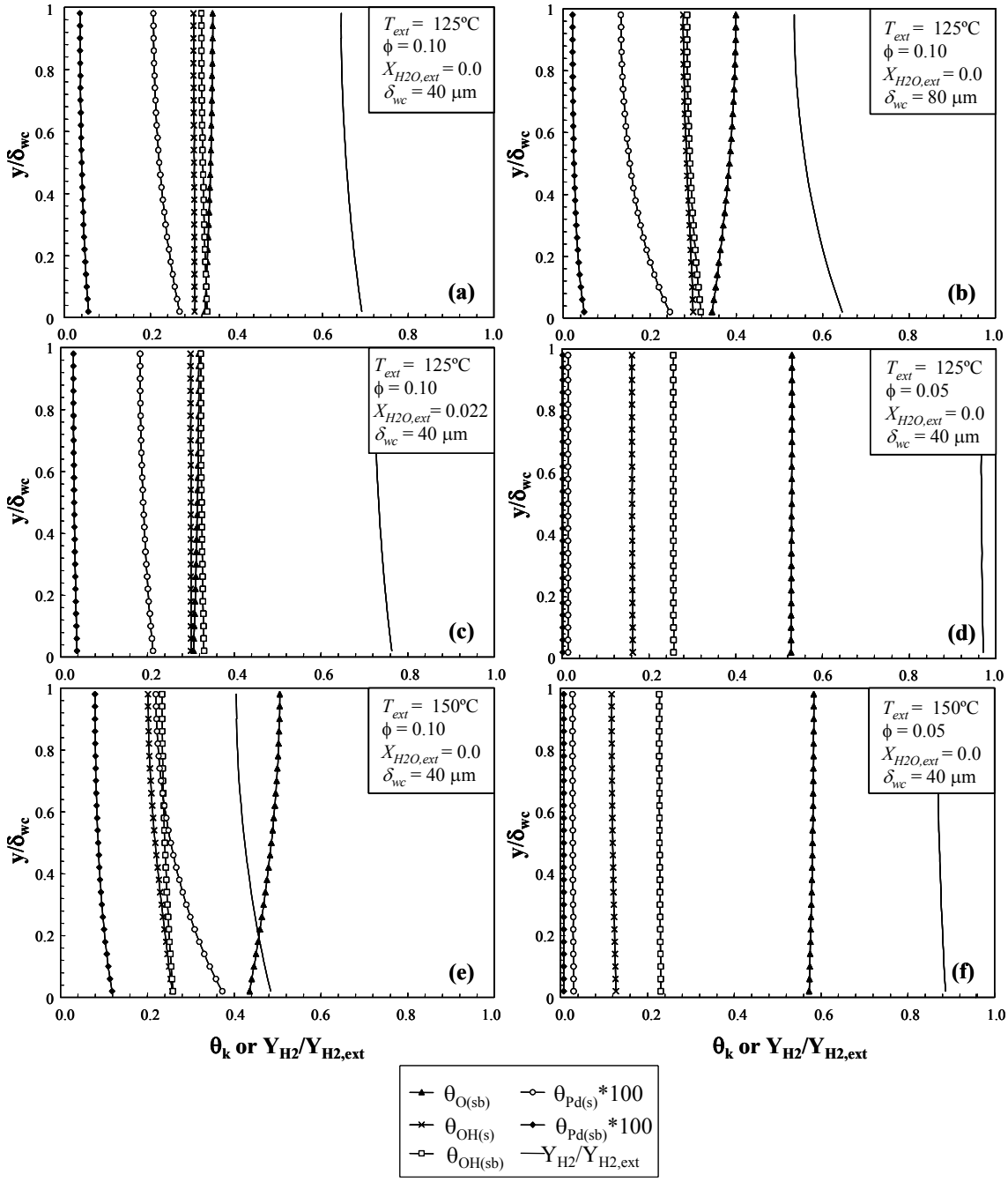

Figure 4.5 Major surface species for a range of condition

At higher temperatures different washcoat thickness (or catalyst loading) doesn't show any impacts on conversion. These temperatures are correspondent to external mass transfer limits that control conversion. The conversion plots vs. T_{ext} in Figure 4.6 indicate

that this limit is reached more slowly by the thinner washcoats with lower catalyst loading. This is a reminder that the temperature at which external mass transfer limitations dominate for any given surface chemistry mechanism depends strongly not only on channel geometry but also on washcoat geometry as well.

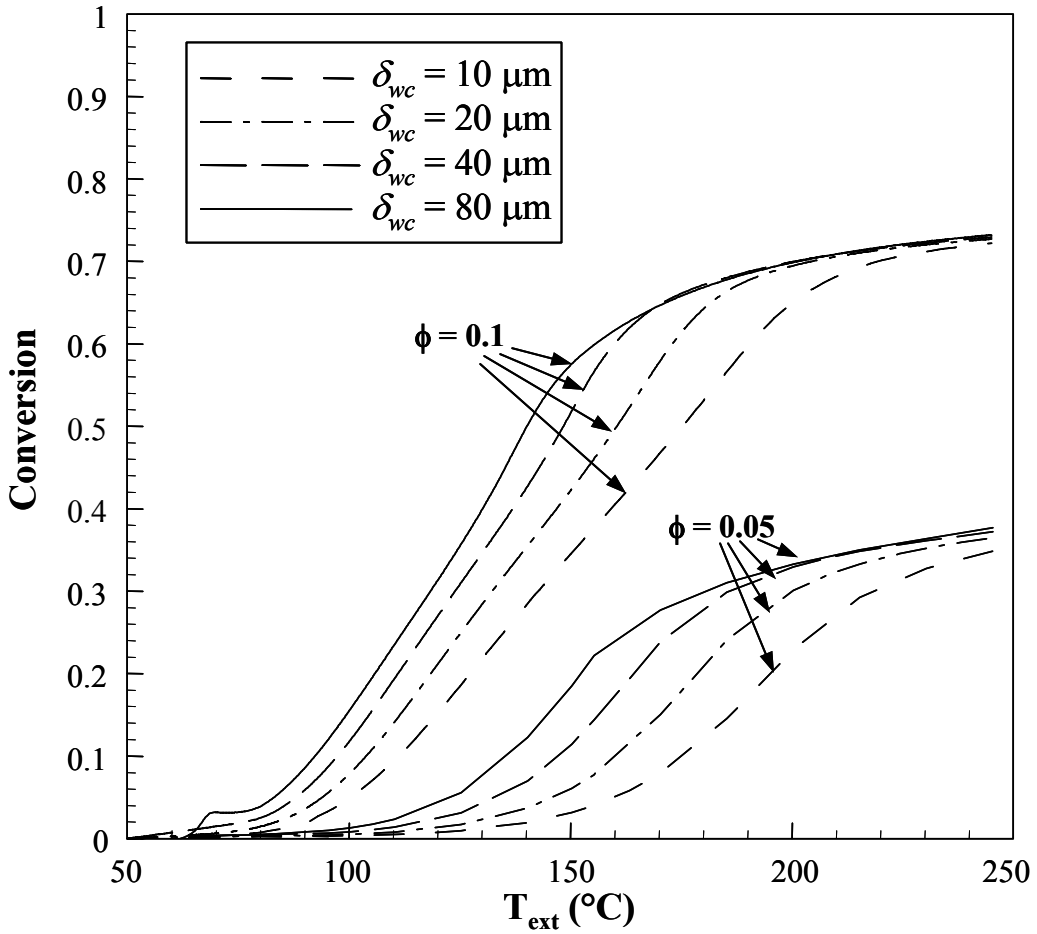

Figure 4.6 Conversion vs. T_{ext} for discretized washcoat layer at different thicknesses

Figure 4.7 shows a plot of calculated effectiveness for the dry inlet conditions plotted in Figure 4.6. As expected, η falls off with increasing δ_{wc}. However, for the ϕ = 0.1 cases, the multi-step surface chemistry results in more complex behavior of η with respect to T_{ext} than observed with single-step chemistry mechanisms. This arises because

of the change in surface conditions/activity through the washcoat depth become significant for $T_{ext} \geq 125°C$. Because the H_2 oxidation reaction creates vacancies (Pd(sb)) by removing O(sb) sites. It has an autocatalytic nature with increased H_2 oxidation rates as ϕ and T increases. For the $\phi = 0.05$ cases, the behavior of η vs. T_{ext} for the different δ_{wc} in Figure 4.7 follows trends much more similar to those derived from simple reaction rate expressions (Hayes et al. 1999), because the lower ϕ does not provide as significant vacancy creation and associated autocatalytic behavior.

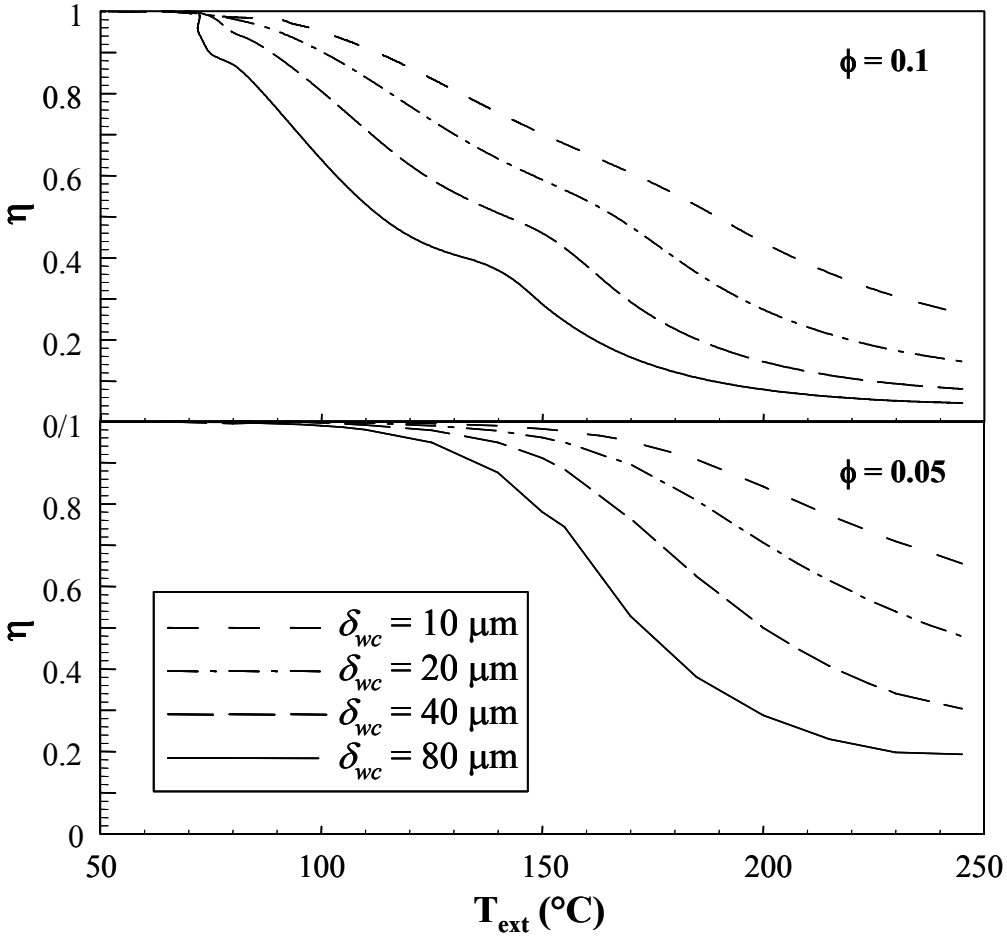

Figure 4.7 Effectiveness vs. T_{ext} at different thickness of washcoat

To investigate impact of gas phase H_2O catalyst effectiveness, Figure 4.8 is generated. It plots η vs. T_{ext} for δ_{wc} = 20 μm for increasing $Y_{H2O,ext}$ using the one-dimensional washcoat model. Interestingly, the effectiveness is only influenced by $Y_{H2O,ext}$ at T_{ext} < 200°C where slower adsorption/desorption rates of H_2O increase site fractions of H_2O(sb) and H_2O(s). The increased effectiveness with increased $Y_{H2O,ext}$ at the lower temperatures is derived from the slower H_2 oxidation rates with the increased surface H_2O blocking vacancies for H_2 adsorption. It means inside the washcoat layer gradients of H_2 decreases.

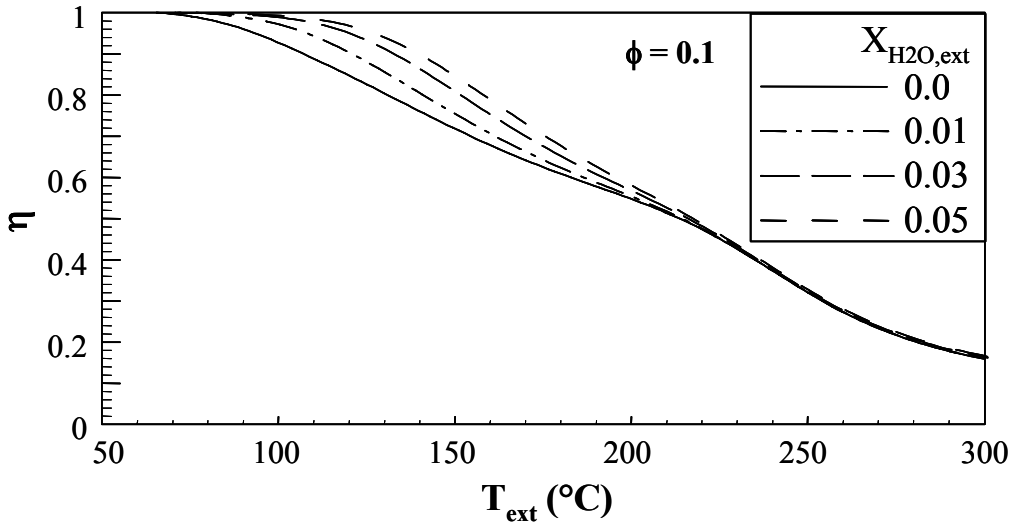

Figure 4.8 Effect of inlet water on the effectiveness with δ_{wc} = 20 μm and ϕ = 0.1

In most catalytic reactor studies with porous washcoats, effectiveness models are used in place of discretized porous media models. The question then arises can a fundamental relationship be used to model catalyst effectiveness for variations in Y_{H2O} and T along the channel axis. In this regard, the catalytic channel model with the discretized washcoat was run for several conditions with δ_{wc} = 30 μm (similar to experimental conditions in Figure 4.2). With the significant changes in gas-phase and

surface species and temperature along the channel length, effectiveness shows a complex behavior for $\phi = 0.1$ with increasing T. For $T \geq 150°C$, most of the H_2 oxidation occurs over the first 0.5 cm of the reactor. Thus an effectiveness model must be most accurate in this front-end region. Clearly a constant effectiveness model will not work well for predicting conversion from the complex H_2 oxidation surface mechanism along the first 0.5 cm. Only under conditions where overall conversion through the channel is relatively small (such as $T_{ext,in} < 125°C$ for $\phi = 0.1$ and $T_{ext,in} < 150°C$ for $\phi = 0.05$ does a constant η model look to be a reasonable approximation even for the relatively thin (30 μm) washcoat used for Figure 4.9. This result suggests that attempts to validate complex mechanisms with experimental measurements in washcoat reactors must take care to operate at relatively low conversions if uniform washcoat or catalyst surface conditions are assumed. However, increased conversion cases are often needed for mechanism validation to assess how the catalyst responds to changes in oxidation potential or product concentrations in the gas phase. Thus, careful modeling of the washcoat and its effectiveness are highly recommended for such validation studies.

In practice, conventional approach for modeling effectiveness without the complications of discretizing the catalytic washcoat depth often the use of the Thiele modulus ϕ_T, defined in the equation 4.3. ϕ_T provides a measure of the ratio of the rate of limiting reactant consumption and the diffusion rate of the limiting reactant into the porous catalyst layer. Equation 4.3 is designed on the assumption that H_2 is consumed in a first order reaction, which might appear reasonable since all H_2 adsorption reactions are first order with respect to Y_{H2}. However, as discussed earlier, under conditions of higher conversion, there is positive feedback of the H_2 oxidation reaction due to the net creation

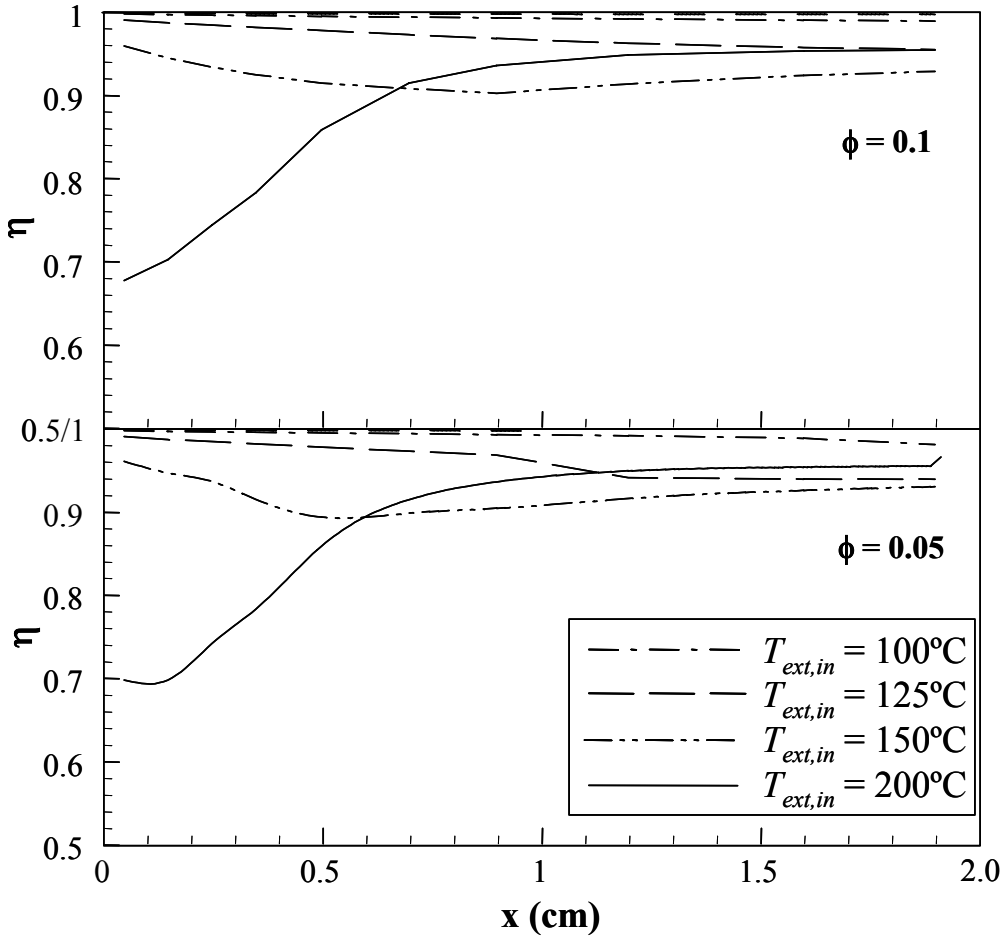

Figure 4.9 Effectiveness vs. axial distance along the channel

of vacancies (particularly Pd(sb) or Pd(s)) that means the H_2 oxidation remove O(sb), OH(sb), or OH(s) from the surface faster than they are replenished. This positive feedback pushes the effective order of H_2 oxidation slightly > 1.

A plot of ϕ_T vs. T_{ext} for a range of δ_{wc} is given in Figure 4.10. For the fixed ϕ = 0.1, the shape of the Thiele modulus curves calculated from the 1-D washcoat model does not vary significantly with washcoat thickness. A similar trend for ϕ_T vs. T_{ext} is observed for ϕ = 0.05. Although ϕ_T shows relatively smooth behavior with respect to T_{ext} and δ_{wc}, the earlier plot of effectiveness η vs. T_{ext} suggests that a simple relationship between the

first order ϕ_T and η may not be readily found for the complex surface chemistry mechanism.

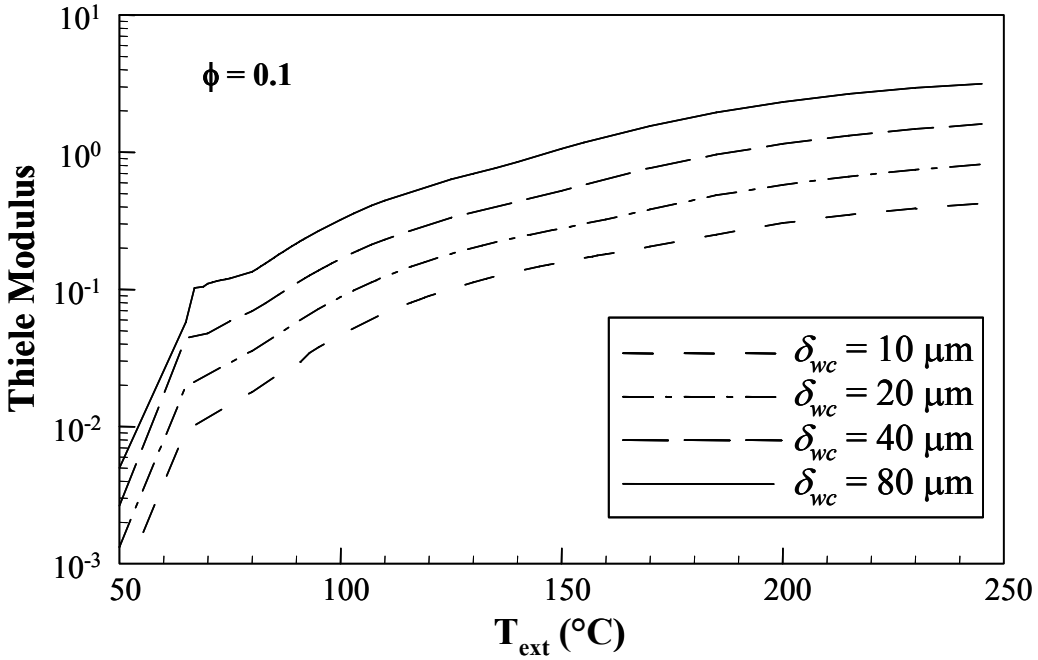

Figure 4.10 Thiele modulus vs. T_{ext} at different thicknesses

Theoretical models for washcoat at nearly isothermal conditions (as is the case for the thin washcoats in the current model) indicate that η should vary approximately as $\tanh(\phi_T)/\phi_T$. (Farrauto 1997). The application of such a simple relationship working with a complex mechanism would provide an ideal approach to simplifying channel flow reactor models and providing a computationally efficient means of incorporating effectiveness into catalytic reactor flow models with detailed chemistry. Thus, for the current study, the local washcoat model was used to investigate η vs. ϕ_T for a range of flow conditions. Figure 4.11 indicates that although the basic shape of the theoretical

tanh(ϕ_T)/ϕ_T curve is followed by the data, the non-linear effects of H_2 on conversion and similarly η result in a steeper drop-off in η with increasing ϕ_T. While an effective Thiele modulus could perhaps be defined with a quasi-reaction rate expression that involves H_2 to a power > 1.0 but < 2.0, the significant scatter in the data over the limited range of conditions presented in Figure 4.11 suggest that this may not provide a very accurate approach to model η. In general, Figure 4.11 does not show clear trends for η vs. ϕ_T other than the general shape with the rapid fall-off in η as ϕ_T increases above 0.1. Thus, for the current Pd-H_2-O_2 mechanism, a one-parameter effectiveness correlation may not be adequate for modeling η, and the importance of a discretized washcoat is evident for conditions where η drops significantly below 1.0.

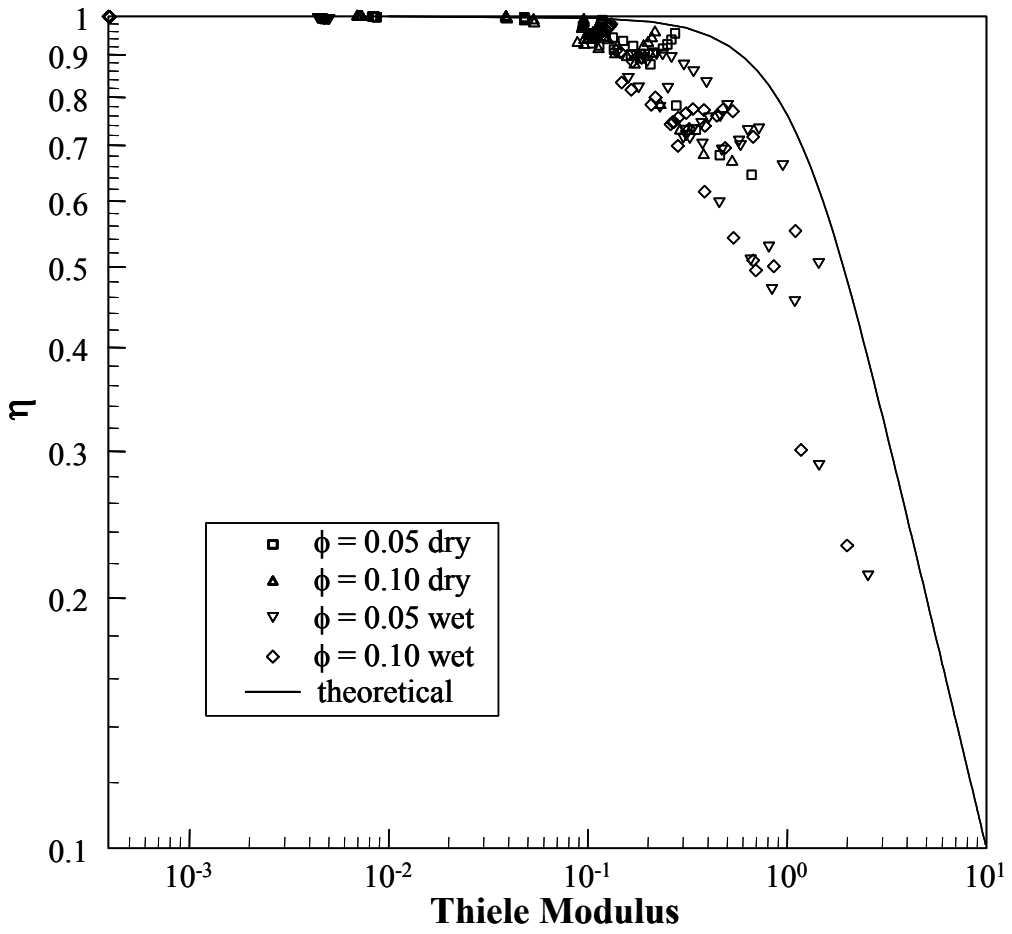

Figure 4.11 Local effectiveness vs. local Thiele modulus

4.5 Conclusion

Careful analysis of temperature-programmed reactor experiments and transient light-off tests provide a basis for developing a preliminary surface chemistry mechanism. In this chapter the proposed surface chemistry for H_2 oxidation over Pd-supported catalysts is validated through a discretized washcoat model. It has been shown to capture the experimental trend of H_2 conversion a discretized washcoat model is necessary. As shown in the validation for the detailed Pd-H_2-O_2 mechanism used herein, a discretized washcoat model can lead to changes in conversion predictions in comparison to uniform

washcoat models for a catalytic reactor, even for a washcoat thickness as low as 30 μm. Also, it was explored effectiveness of washcoat at temperatures < 200°C by increasing external water content, increases. Furthermore, a simple constant effectiveness model does not readily capture the observed changes in predictions between a uniform and a radially discretized washcoat model. It also serves to provide insight into the importance of looking at catalyst effectiveness during the development of detailed surface chemistry mechanisms for oxidation reactions and further to warn against neglecting the role of effectiveness and its impact upon conversions for thin washcoat reactors in studies for validating complex surface mechanisms.

Chapter 5

Transient Analysis of Pd-H_2-O_2 Surface Chemistry by ILDM

5.1 Introduction

Developing the requisite surface thermochemistry for catalytic combustion of hydrocarbons on Pd-based catalysts will be predicated by the identification of the critical processes and equilibria in smaller subset mechanisms for Pd/O_2/H_2 (Kramer et al. 2003) as well as Pd/O_2/CO (Imbihl and Ertl 1995). In this chapter intrinsic low-dimensional manifold (ILDM) analysis is used to investigate the complex interactions of Pd/O_2/H_2 in proposed catalytic combustion mechanisms to gain understanding for validating the mechanisms. The application of ILDM's has been studied for gas-phase chemistry as an efficient tool of chemical mechanism reduction (Maas and Pope 1992).

5.2 Methods for reduction and analysis of surface chemistry

Modeling of spatially inhomogeneous systems includes the solution of the kinetic differential equations several thousand times for tens of hundreds of species. The use of detailed and comprehensive chemical models introduces a large number of chemical species, which make the governing equation system very large and often computationally stiff thereby demanding a prohibitive amount of computational resources for all, but the simplest of flows. Reduction of the number of reactions or species may speed up computational times by several orders (Turanyi 1994). Until the last twenty years, detailed reaction mechanisms were not suitable for numerical simulation of most

combustion processes and catalytic oxidation. Therefore, reduction of large reaction mechanisms, as a better approach is often required.

There are diverse timescales in a set of reactions where some of them are long and have much less degree of freedom. Reduction means the identification of a subset of reactions and species groups which can follow the dynamic response of the full reaction mechanisms. It is obvious that importance of reactions depends on time scales of interest. Identifying and eliminating unimportant reactions is not always easily recognized in large reaction mechanisms. It is more instructive to reduce a mechanism to its minimum in order to see how species interact and how coupling can occur between reactions.

Over many years several methods have become available for the reduction of large mechanisms successfully involving either removal of species and reactions or lumping of species into groups. Reduction schemes often use a combination of those two approaches to make considerable simplifications (Brown 1997). A good review of those methods is presented by Tomlin et al. (Tomlin 1997). Most reduction techniques are based on the concept of separation of timescales, although some of them are simply based on deleting unimportant reactions from the detailed reaction mechanism by assuming some reactions are fast or in equilibrium.

In a homogeneous reaction mechanisms, there is a widely different relaxation timescales from a few seconds to nanoseconds (Maas and Pope 1992). This is the reason that makes governing ordinary differential equations (ODE) for evolutionary processes, e.g. the chemical reactions, stiff. This leads to huge computations on supercomputers, often impractical. Therefore, it becomes necessary to reduce the stiffness addressed by chemistry. Range of chemical time scales is wider than transport time scales associated

with molecular transport and bulk advective flows, which are in the range of milliseconds to microseconds. Equilibration of fast chemical processes can occur in less than one integration time step, if the time step is based solely on fluid flows equilibrated. If these equilibrations even have multiple equilibrium states, such large time step integration may head to inaccurate simulations.

One of the fundamental questions frequently addressed in chemical kinetics literature is the minimal number of state variables needed to represent the characteristic behavior of large scale systems. Quasi steady state assumption (QSSA), partial equilibrium (PE) and intrinsic low dimensional manifolds (ILDM) are based on time scales of the system (Turanyi 1988; Maas and Pope 1992). Other approaches include conservation relations, lumping of species, sensitivity analysis and substituting differential equations by input-output relations (repro-modelling). Handrock-Meyer et al., have presented an algorithm, based on the theory of invariant integral manifold, to estimate local minimal number of state variables to characterize behavior of long time dynamics in a multi-scale system (Handrock-Meyer et al. 2001). They have shown their method can be used to justify mathematically quasi-steady state approximation and quasi-equilibrium reaction methods. They have shown the existence of a locally invariant manifold in state space which is exponentially attracting.

The method of ILDM was applied to reduce chemical kinetics of homogeneous gas phase reactions (Maas and Pope 1992). ILDM is similar to lumping techniques combining explicitly elementary species concentrations into a smaller number of "lumped" parameters based on the eigenmodes of the dynamical kinetic equations. With ILDM's, fast chemical equilibration processes can be locally identified by eigenmode

analysis and then decoupled from dynamic integration of the system. Therefore, the reduced chemical kinetics can be described by only few slow chemical processes. In a state space description, trajectories of the state (defined by the temperatures and species distributions in the reactor) collapse to low-dimensional subspaces (local attractors) defined as hyper surfaces in chemical space. Movement along these manifolds defines a reduced number of variables that define the chemical evolution of the system (Skodje and Davis 2001). The movement towards the low dimensional subspace is usually very fast, as the fast reactants bring the chemical composition of the system to the attracting manifold in composition space. These are referenced to as relaxation processes. After relaxation, trajectories move within the low-dimensional subspaces governed by the slow processes defining the asymptotic dynamics. For some of detailed homogeneous combustion mechanisms, dynamic dimension needed to describe the essential features was found to be two or three, e.g., atmospheric premixed laminar H_2/air flat flame (Buki et al. 2002).

Along the ILDM, the trajectories develop orthogonal to the rapidly contracting directions. If fast relaxing time scales are not significant except for establishing equilibrium, the dynamical system can be described by the low-dimensional manifold, i.e., the ILDM. The manifold method used successfully for reducing homogeneous gas phase kinetics in laminar and turbulent combustion flows (Norris and Pope 1995; Gicquel et al. 1999; Singh et al. 2001; Landenfeld et al. 2002; Fiorina et al. 2003). Recently ILDM has been applied successfully in gas phase chemistry used to deposit silicon carbide in chemical vapor deposition method (CVD) (de Persis et al. 2004).

Although, application of ILDM's has been well studied for gas-phase chemistry there has been limited work on the use of ILDM's for complex surface chemistry with one notable exception (Yan and Maas 2000) where ILDM's were applied to reduce a surface mechanism for CH_4 oxidation over Pt. The current chapter presents ILDM's for interpreting surface chemistry mechanisms for the low temperature oxidation of H_2 over the supported Pd-catalysts. The impact of surface chemistry modifications on the system dynamical response is investigated by looking at the mechanism in Chapter 4 and a slightly modified mechanism. By using a model problem based on a uniform porous washcoat-supported catalyst a dynamical system is established for investigating the surface chemistry in a differential reactor. ILDM's associated with the surface chemistry are identified and associated with the catalyst behavior in the differential reactor.

5.3 Theoretical dynamic model

To investigate ILDM analysis of the surface chemistry mechanism, the discretized washcoat model in Chapter 3 is formulated as a uniform differential reactor, looking at a single axial cell, such that the system of governing equations can be identified as a dynamical system dependent only on local conditions. Such a reactor model maintaining the coupling between the gas-phase transport and surface reactions is illustrated by the schematic shown in Figure 5.1.

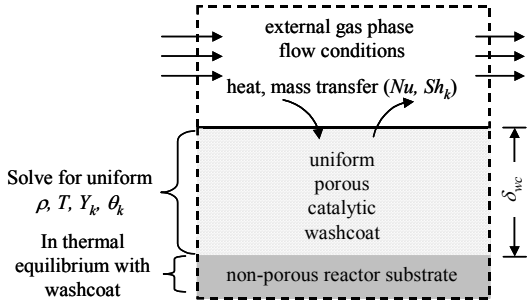

Figure 5.1 Schematic illustrating an axial slice from the channel flow model (dynamic model)

The dynamic model was used to look at the response of a porous catalytic washcoat layer in thermal equilibrium with a reactor substrate. Fixing the external flow conditions transforms the calculations into a dynamical system and allows for the ILDM's associated with the catalytic combustion chemistry to be clearly identified.

Detailed gas-phase chemistry as well as chemistry is incorporated in the model. The governing equations are covered in section 3.2.2. Here, equations for the uniform porous washcoat, are simplified. Conservation of gas phase species, equation 5.1, ($k = 1, k_{gas}$), surface species, equation 5.2 and energy equation, equation 5.3 are in the following:

$$\rho\varepsilon\frac{\partial Y_k}{\partial t} = \varepsilon\dot{\omega}_k W_k + a_{cat}\left(\dot{s}_k W_k - Y_k\sum_{k,g}\left(W_k\dot{s}_k\right)\right) + a_{wc}\overline{\rho}YV_k - a_{wc}\overline{\rho}V(\overline{Y}_k - Y_k) \quad (5.1)$$

where the overbar implies mean conditions between the washcoat and the external flow.

$$\Gamma_{cat}\frac{\partial\theta_k}{\partial t} = \dot{s}_k \qquad k = K_{gas}+1,\ K_{gas}+K_{surf} \quad (5.2)$$

$$\begin{aligned}\left(\overline{\rho C_p}\right)\frac{\partial T}{\partial t} &= -a_{cat}\sum_{k,g}\left(h_k\dot{s}_k W_k\right) - \varepsilon\sum_{k,g}\left(h_k\dot{\omega}_k W_k\right) - a_{cat}\sum_{k,s}\left(h_k\dot{s}_k W_k\right) \\ &+ a_{wc}h_T(T_{ext}-T) + a_{wc}\overline{\rho}\sum_{k,g}((\overline{h}_k - h_k)YV_k) - a_{wc}\overline{\rho}V\sum_{k,g}(\overline{h}_k\overline{Y}_k - h_k Y_k)\end{aligned} \quad (5.3)$$

where the weighted specific heat capacity $\overline{\rho C_p}$ includes the gas and solid phases.

$$\overline{\rho C_{P,s}} = \varepsilon \rho_{gs} \sum_k \left(C_{Pk,gs} Y_{k,gs} \right) + a_{cat} \Gamma_{cat} \sum_k \left(\overline{C}_{Pk,s} \theta_{k,s} \right) + (1-\varepsilon) \rho_{wc} C_{P,wc} + v_{sub} \rho_{sub} C_{P,sub} \tag{5.4}$$

Conservation of bulk phase species are not necessary in this model, because the examined mechanism for Pd-H2-O2 catalytic combustion does not incorporate bulk phase transformations as discussed in Chapter 4.

To clarify evaluation of the ILDM's that govern the surface chemistry mechanism, heat and mass transport are determined with fixed external flow conditions such that the dynamical response of the system is controlled strictly by changes within the washcoat media. Thermal and species diffusive fluxes are modeled with the use of *Nu* and Sh_k number correlations described in Chapter 3. These fluxes at the interface between the channel flow and the outer washcoat surface are defined by the following equations:

$$YV_k = D_{km} Sh_k (Y_{k,ext} - Y_k) / d_{hyd} \qquad k = 1, \ldots, K_{gas} \tag{5.5}$$

$$h_T (T_{ext} - T) = Nu \lambda_{gas} (T_{ext} - T)_{y=0} / d_{hyd} \tag{5.6}$$

The transient conservation equations for the uniform washcoat cell with fixed channel flow conditions are integrated numerically with respect to time using the numerical integration scheme LIMEX until time t = 1000 s, at which point for all non-oscillatory cases a steady-state solution has been reached. This numerical model is used

to study the surface chemistry mechanism presented in Chapter 3 and a modified version presented in Table 5.1 and 5.2. Table show Table 5.1 shows the thermochemistry and Table 5.2 the reaction mechanism. The difference between the two thermochemistries are the higher stability of OH(sb) and H_2O(sb) on isolated vacancies resulting in a higher desorption barrier for H_2O from the oxide surface and increase in interaction potentials between H-containing and the original Pd-O species such as H(sb) and H_2O(sb) in the modified surface chemistry. Altered numbers are bolded in Table 5.1. But both surface reaction mechanisms have the highest sensitivity for H_2 conversion toward adsorption/desorption reaction rates. To enforce thermodynamic consistency, changes in the surface species' enthalpies h_k and their interaction potentials ε_{jk} lead to changes in the activation energy barriers and their coverage dependencies, from equation 3.48. The variations in the mechanism can be accepted within the present uncertainties in surface thermochemistry without significantly shifting the channel flow model predictions. It should be noted that these mechanisms are only studied for predicting H_2 combustion at low ϕ where there is no bulk PdO reduction.

The two surface mechanisms capture the trends in experimental observations for $\phi = 0.1$ for the range of temperature shown in Figure 4.2 (based on Table 4.2) and Figure 5.2 (based on the Table 5.2) and have qualitative agreement with the observations for $\phi =$ 0.05. The presented result in Figure 5.2 does not include gas phase combustion. Table 5.3 shows physical parameters and test conditions in the differential reactor.

As a sample numerical transient model results, Figures 5.3a and 5.3b show predictions using modified surface chemistry mechanism in Table 5.2, transient

Table 5.1 Gas-phase and surface species enthalpies in modified surface chemistry relative to standard gas phase enthalpies

Species	h_k^0 **(at 25°C in kJ/gmol)**
H_2	0.0
O_2	0.0
H_2O	-241.8
N_2	0.0
Pd(s)	0.0
Pd-O(s)	$-115.0+57.5\theta_{O(s)}+29\theta_{OH(s)}$
Pd-O(sb)	-115.0
Pd(sb)	$-35.0+208\theta_{Pd(sb)}+\mathbf{147}\theta_{H2O(sb)}+\mathbf{208}\theta_{H(sb)}+104\theta_{OH(sb)}$
Pd-O_2(sb)	-105.0
Pd-H(s)	$-42.0+8\theta_{H(s)}$
Pd-OH(s)	$-214.0+29\theta_{O(s)}+14.5\theta_{OH(s)}$
Pd-H_2O(s)	-302.0
Pd-H(sb)	$\mathbf{-57.0}+\mathbf{208}\theta_{Pd(sb)}+\mathbf{147}\theta_{H2O(sb)}+\mathbf{208}\theta_{H(sb)}+\mathbf{104}\theta_{OH(sb)}$
Pd-OH(sb)	$\mathbf{-229.0}+104\theta_{Pd(sb)}+\mathbf{73.5}\theta_{H2O(sb)}+\mathbf{104}\theta_{H(sb)}+52\theta_{OH(sb)}$
Pd-H_2O(sb)	$-322.0+\mathbf{147}\theta_{Pd(sb)}+\mathbf{104}\theta_{H2O(sb)}+\mathbf{147}\theta_{H(sb)}+\mathbf{73.5}\theta_{OH(sb)}$

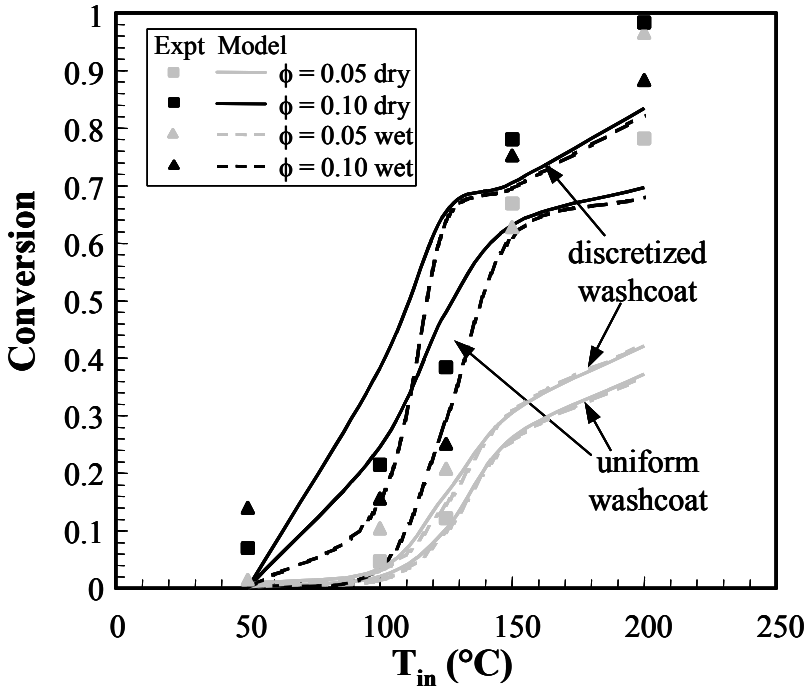

Figure 5.2 Comparison of experimental conversion vs. T_{in} and numerical models for the modified surface chemistry (Table 5.2)

Table 5.2 Pd-O_2-H_2 modified surface chemistry mechanism used in ILDM study

Reactions	A or stick coef.	E_{act} [kJ/mol] for Mech. A
Adsorption/Desorption Reactions		
1f) $O_2+2Pd(s) \Rightarrow 2O(s)$	$0.8*T^{-0.5}$	0.0
1r) $2O(s) \Rightarrow O_2+2Pd(s)$	$5.7*10^{21}$	$230 - 115\theta_{O(s)}$
2f) $O_2+Pd(sb) \Rightarrow O_2(sb)$	$1.0*T^{-0.5}$	0.0
2r) $O_2(sb) \Rightarrow O_2+Pd(sb)$	$1.0*10^{13}$	70
3f) $H_2+2Pd(s) \Rightarrow 2H(s)$	$6.4*T^{-0.5}$	0.0
3r) $2H(s) \Rightarrow H_2+2Pd(s)$	$5.7*10^{21}$	$84 - 16\theta_{H(s)}$
4f) $H_2+Pd(sb)+O(sb) \Rightarrow H(sb)+OH(sb)$	$8.0*T^{-0.5}$	0.0
4r) $OH(sb)+H(sb) \Rightarrow H_2+Pd(sb)+O(sb)$	$5.7*10^{21}$	$136 + C_{4r}$[a]
5f) $H_2O+Pd(s) \Rightarrow H_2O(s)$	0.50	0.0
5r) $H_2O(s) \Rightarrow H_2O+Pd(s)$	$1.0*10^{13}$	60.2
6f) $H_2O+Pd(sb) \Rightarrow H_2O(sb)$	0.50	0.0
6r) $H_2O(sb) \Rightarrow H_2O+Pd(sb)$	$1.0*10^{13}$	$55.2 + C_{6r}$[a]
Reversible Surface Reactions		
7) $O(s) \Leftrightarrow O(sb)$	$5.0*10^{11}$	90
8) $O_2(sb)+Pd(sb) \Leftrightarrow 2O(sb)$	$5.7*10^{21}$	0.0
9) $O_2(sb)+Pd(s) \Leftrightarrow O(sb)+O(s)$	$5.7*10^{21}$	$185 - 57.5\theta_{O(s)}$
10) $H(s)+Pd(sb) \Leftrightarrow H(sb)+Pd(s)$	$5.7*10^{21}$	50
11) $H(s)+O(s) \Leftrightarrow OH(s)+Pd(s)$	$5.7*10^{21}$	45
12) $H(s)+OH(s) \Leftrightarrow H_2O(s)+Pd(s)$	$5.7*10^{21}$	55
13) $OH(s)+OH(s) \Leftrightarrow H_2O(s)+O(s)$	$5.7*10^{21}$	102
14) $OH(sb)+Pd(s) \Leftrightarrow H(s)+O(sb)$	$5.7*10^{21}$	$102 + 8\theta_{H(s)}$
15) $H(s)+OH(sb) \Leftrightarrow H_2O(sb)+Pd(s)$	$5.7*10^{21}$	$40 + C_{15f}$[a]
16) $OH(sb)+Pd(sb) \Leftrightarrow H(sb)+O(sb)$	$5.7*10^{21}$	122
17) $H_2O(sb)+Pd(sb) \Leftrightarrow H(sb)+OH(sb)$	$5.7*10^{21}$	121
18) $OH(sb)+OH(sb) \Leftrightarrow H_2O(sb)+O(sb)$	$5.7*10^{21}$	81

[a] Coverage dependencies: $C_{4r} = -104\theta_{Pd(sb)} - 73.5\theta_{H2O(sb)} - 104\theta_{H(sb)} - 52\theta_{OH(sb)}$

$C_{6r} = 61\theta_{Pd(sb)} + 43\theta_{H2O(sb)} + 61\theta_{H(sb)} + 30.5\theta_{OH(sb)}$, $C_{15f} = 43\theta_{Pd(sb)} + 30.5\theta_{H2O(sb)} + 43\theta_{H(sb)} + 21.5\theta_{OH(sb)}$

profiles of H_2 conversion in the washcoat ($= 1 - Y_{H2}/Y_{H2,ext}$) and surface site fractions (θ_k) for the differential washcoat reactor under both dry and wet ($X_{H2O,ext} = 0.022$) conditions at $T_{ext} = 100$ºC, $\phi = 0.1$, and $X_{N2,ext}/X_{O2,ext} = 20$ in order to maintain relatively small temperature rise. The θ_k plotted in Figure 5.3 show a transition from an initially oxidized

Table 5.3 Flow conditions and physical parameters of the differential reactor

Physical Parameters	
Length of the reactor	1.0 cm
Porosity of washcoat	0.5
Density of solid phase of washcoat	3.94 g/cm^3
Site density per unit washcoat surface area	1.75e-09 sites/cm^2
Dispersion of the Catalyst	10 %
Wall thermal conductivity	0.22 W/(cm.K)
Washcoat Thickness	10 µm
Substrate thickness	75 µm
Specific heat at constant volume	0.765 kJ/kg.K
Specific area in washcoat	2000 cm^{-1}
Catalyst loading	5.5 mg/cm^3
Inlet Flow Conditions for Case of H_2	
Pressure(atm)	1
Temperature(°C)	100 – 200
Velocity (m/s)	10.0
H_2 (mol %)	1.90 %
O_2 (mol %)	4.60 %
N_2 (mol %)	93.50 %

catalyst with $\theta_{O(sb)}$ = 0.9 to conditions where the surface has significant coverage of OH(sb) and OH(s). For the dry case, this transition leads to oscillatory behavior (of the surface site fractions and the H_2 conversion). While mild oscillations were observed in the mass spectrometer measurements in the catalyst channel experiments for some conditions, the oscillations were minimal compared to those shown in Figure 5.3a. These oscillations are so significant here because the reactor is a differential slice. In a full channel flow simulation using the modified surface chemistry mechanism in Table 5.2 under the same condition conditions, results show significantly damped oscillations (< 10% of mean H_2 conversion) due to the production of H_2O along the channel. These values are comparable to some fluctuations observed in. Addition of H_2O in the gas phase suppresses the oscillations as indicated by the wet case in Figure 5.3b. The rapid (< 1 s) changes of H_2 conversion would likely only be observed in a differential reactor, of order

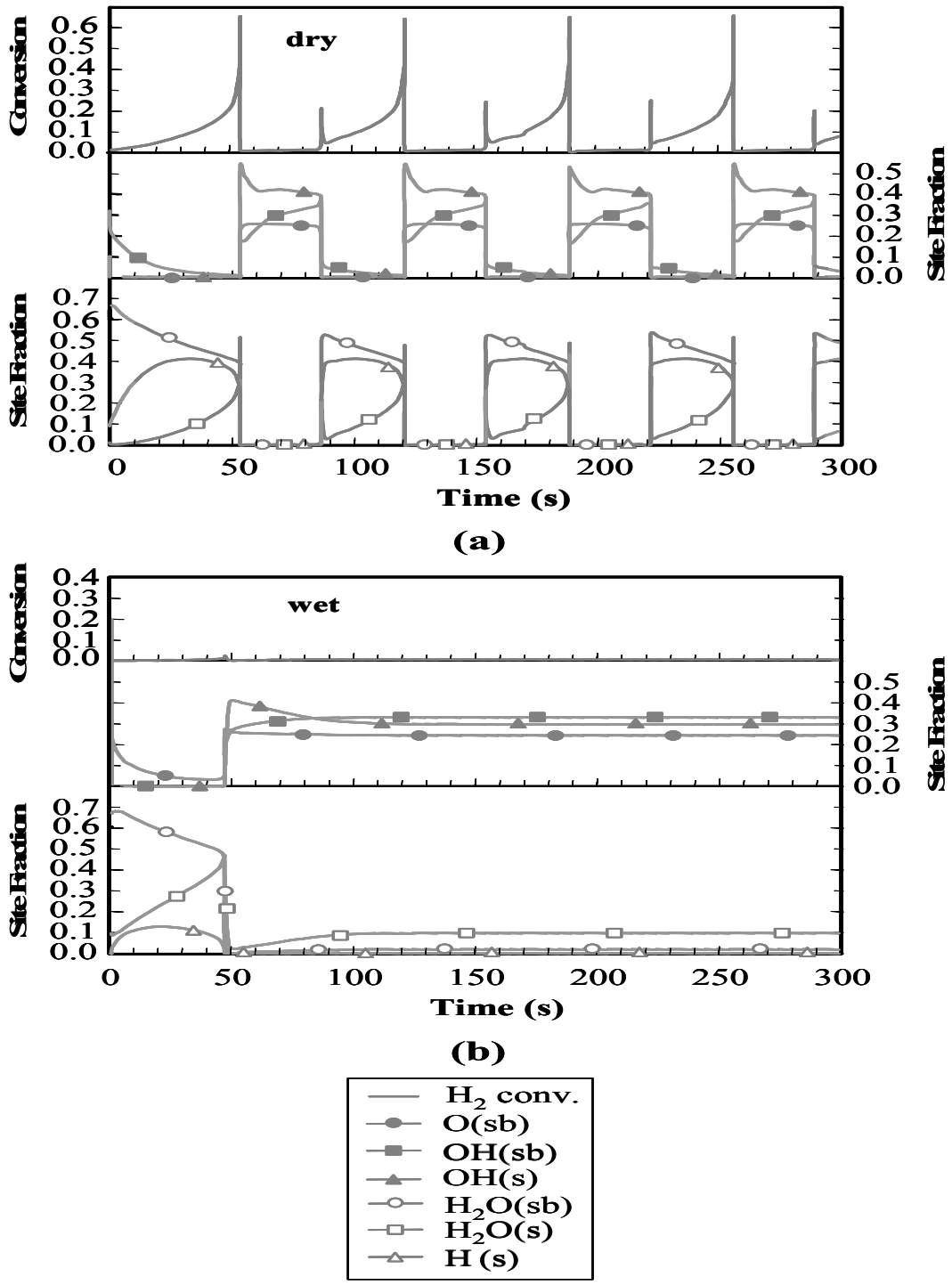

Figure 5.3 Transient profiles of H_2 conversion in the wascoat and surface site fractions in uniform differential reactor at T_{ext} = 100ºC and ϕ = 0.1 with modified surface chemistry mechanisms for (a) dry and (b) wet ($X_{H2O,ext}$ = 0.022) conditions

1 mm in length, because variation in gas and surface conditions lengthwise along longer reactors will mask the effects of sharp local transitions on exhaust gas measurements. This suggests the value of differential reactors to test kinetic mechanisms, but the difficulty in realizing such short contact differential reactors arises because it is difficult to measure conversions in flow even when conversion is large in the washcoat pores.

All the results in Figure 5.3 for both the dry and wet cases indicate multiple time scales from << 1 s to > 10 s impacting the surface site fractions and similarly the H_2 conversion with respect to time. The multiple time scales and the oscillatory behavior illustrated in Figure 5.3 suggest that ILDM's may provide insight to this system by isolating the slower time scale processes.

5.4 Numerical solution of manifold

The ILDM method is based on a reaction trajectory in state space which quickly converges to a low dimensional manifold represented by a smaller number of variables n_s (species). Then only n_s ODE's are solved for n variables based on original dynamical system equations.

In chemical systems the ODE's will have conserved quantities such as total mass, and possibly other vanishing linear combinations of rates. These conserved linear quantities correspond to hyper surfaces in composition (i.e. phase) space and the motion on this hyper surface can be described with a reduced set of dynamical variables, restricted to the intersection of these hyper planes associated with the constant values of the conserved quantities. The full set of dynamical variables, can be recovered using the constants that parametrize the hyper planes. As time increases, the phase space flow

becomes more constrained and the number of variables needed to define the evolution reduces toward some final value M. This low dimensional manifold is a solution of a functional equation derived from the transient differential equations for the reactions. At vanishing decay rate the slow manifold becomes a line of equilibrium states (stagnation point of the stiffly coupled system of ODEs) (Roussel 1990).

Some formal techniques use singular perturbation theory to remove transient species from the mechanism resulting inherent separation of time scales. To this end, the governing equations 5.1 thru 5.3 for the uniform porous catalytic washcoat can be written as:

$$\frac{\partial \vec{y}}{\partial t} = \vec{\vec{B}}^{-1}(\vec{y})\left(\vec{\Gamma}(T_{ext}, Y_{k,ext}, \vec{y}) + \vec{\Omega}(\vec{y})\right) = \vec{F}(\vec{y}) \tag{5.6}$$

where, $\vec{y}$ the solution vector includes T, Y_k, and θ_k in the catalytic washcoat. $\vec{\vec{B}}(\vec{y})$ denotes the matrix multiplier of the transient derivatives, $\vec{\Gamma}$ denotes flux terms due to diffusion and Stefan velocity convection to/from the external flow, and $\vec{\Omega}$ is the local source terms due to reactions. Because T_{ext} and $Y_{k,ext}$ are fixed in this problem, the derivatives are simply a function $\vec{F}$ of the washcoat state specified by $\vec{y}$.

To identify the time-scales of this system around a point in state space, the Jacobian $\vec{\vec{F}}_{\vec{y}}$ is calculated. Eigenvalues and eigenvectors (or directions in the state-space associated with each eigenvalue) are evaluated. The eigenvalues and eigenvectors of Jacobian of velocity function $\vec{F}$ describe the time evolution of small displacements with respect to a representative trajectory passing through a point in phase space. The absolute value of the real part of each negative eigenvalue gives the corresponding reciprocal

relaxation time while the eigenvectors system gives the principal axes in the co-moving frame.

A common property of the spectrum of the Jacobian in stiff ODEs is real negative and nondegenerate eigenvalues. The Jacobian can be transformed into fast and slow subspaces according to the following equations (Schmidt et al. 1998; Buki et al. 2002):

$$\begin{pmatrix} \hat{Z}_f \\ \hat{Z}_s \end{pmatrix} \vec{\vec{F}}_y(\vec{y}) \begin{pmatrix} Z_f & Z_s \end{pmatrix} = \begin{pmatrix} \lambda_f & 0 \\ 0 & \lambda_s \end{pmatrix} \tag{5.7}$$

where.

$$\begin{pmatrix} \hat{Z}_f \\ \hat{Z}_s \end{pmatrix} \begin{pmatrix} Z_f & Z_s \end{pmatrix} = I \tag{5.8}$$

Z_f and $\hat{Z}_f$ are invariant right and left subspaces vectors respectively, associated with the n_f eigenvalues (λ_f) having the most negative real parts, and Z_s and $\hat{Z}_s$ are invariant right and left subspaces vectors respectively associated with the n_s eigenvalues (λ_s)having the least negative real parts. The ILDM's are the loci in state space for which there is essentially no movement in the fast directions. In other words, for $\vec{F}$ to exist in the slow subspace, it must be orthogonal to the orthogonal complement of the slow subspace (Kaper and Kaper 2002). In the Maas-Pope algorithm, low dimensional attractive manifold is defined based on the attractivity of points in phase space where n_f fastest eigenvectors along the kinetic flow make no projection. The n_s-dimensional ILDM is orthogonal to the transient decay directions, thus represent a pure asymptotic motion (Skodje and Davis 2001). In other words, derivatives of fast variables are assumed to be

zero. Therefore, the dynamic system is represented by differential-algebraic system under specific conditions.

The method to calculate invariant subspaces for the dynamical equations governing the catalytic washcoat for this study follows the same method implemented previously for gas phase chemistry (Maas 1998; Handrock-Meyer et al. 2001; Kaper and Kaper 2002; Nafe and Maas 2002). The Schur form decomposition of the Jacobian is calculated, and the Schur vectors are sorted such that the eigenvalues of the system appear in the diagonal in ascending order of their real parts is done by applying a sequence of Givens rotations (Demmel 1997). Thus, the real Schur decomposition will be in the following form:

$$\vec{\vec{F}}_y(\vec{y}) = \begin{pmatrix} Q_f & Q_s \end{pmatrix} \begin{pmatrix} \hat{N}_f & \hat{N}_{fs} \\ 0 & \hat{N}_s \end{pmatrix} \begin{pmatrix} Q_f^T \\ Q_s^T \end{pmatrix} \tag{5.9}$$

where Q_f and Q_s are the basis vectors of the fast subspace and its orthogonal complement, respectively. Since the fast and slow subspaces are not necessarily orthogonal to each other, the orthogonal complement of the slow subspace cannot always form a basis for the fast subspace. Therefore, a separate basis for the fast subspace is found according to the following equation:

$$\begin{pmatrix} \hat{Z}_f \\ \hat{Z}_s \end{pmatrix} = \begin{pmatrix} I & -X \\ 0 & I \end{pmatrix} \begin{pmatrix} Q_f^T \\ Q_s^T \end{pmatrix} \tag{5.10}$$

where X is calculated from solving the Sylvester equation:

$$\hat{N}_f X - X\hat{N}_s = -\hat{N}_{fs} \tag{5.11}$$

There are different methods to assess how close a trajectory point in state space is to a given n-dimensional manifold. In the current paper, the state y(t) is away from state y^n, where y^n is the state obtained starting from y(t) and assuming the system progress with frozen slow modes:

$$\vec{Z}^{-1}\frac{\partial \vec{y}}{\partial \tau} = \begin{pmatrix} I & 0 \\ 0 & 0 \end{pmatrix} \vec{Z}^{-1}\vec{F}(\vec{y}) \tag{5.12}$$

The above system of equations as well as the standard system equations is solved using the LIMEX transient integration scheme (Deuflhard et al. 1987), to determine if a given state space point in solving equation 5.6 is on a set of ILDM's of dimension n_s.

The power in the ILDM's, particularly for the complex surface chemistry of the current problem, lies in the identification of the slow mode directions Z_s and the associated eigenvalues of these directions. These modes, will be a function of the composition on state space location and will identify the critical combination of surface and gas-phase species which control the slowest time scales that are revealed in the calculations of the full system identified in equation 5.6. Thus, the ILDM analysis for the complex surface chemistry should first observe the response of the full system to extract the catalytic system behavior for a range of conditions and then explore what low dimensional manifolds are associated with the slower time scale phenomena.

5.5 Verification of the ILDM analysis

To characterize the Pd-H_2-O_2 surface chemistry presented in Table 4.1 and Table 4.2 and assess the complexities associated with the strong species interaction potential, several transient integrations for a range of external flow conditions and initial surface

species distributions were performed. To identify ILDM's, a range of initial surface conditions were studied with the full system of equations with $\phi = 0.1, 0.05$, $T_{ext} = 150$ °C, and $X_{H2O,ext} = 0.0$. The initial conditions were characterized by different site fractions of the dominant surface species O(sb), OH(sb) and OH(s). These three species typically cover more than 90% of catalyst surface. To show surface state for oxidized or reduced catalyst, two different colors were used. When surface is initially covered by (sb) species ($\theta_{O(sb)} + \theta_{OH(sb)} > 0.6$), red color shows surface is predominantly oxidized. If surface initially is mostly covered by OH(s) or ($\theta_{O(sb)} + \theta_{OH(sb)} < 0.5$), blue color shows surface is predominantly reduced. Figures 5.4 show how trajectories in the O(sb) versus OH(sb) plane behave for 7 different initial surface conditions and for two different ϕ's at $T_{in} = 150$°C. It is noted that initial conditions nearer the origin have larger initial fractions of OH(s) and thus start from a more reduced state.

As seen in Figure 5.4a and 5.4b, trajectories from different initial conditions quickly collapse to a single manifold for both different initial H_2 concentrations. But slowest modes change with ϕ. However, these manifolds are not connected. It was observed after a time of 1000 s. In other words, after 1000 s slowest modes in dry gas flow are not equilibrated. It was observed they connected to each other before 2000 s. This suggests that the characteristics times associated with these manifolds are extremely large.

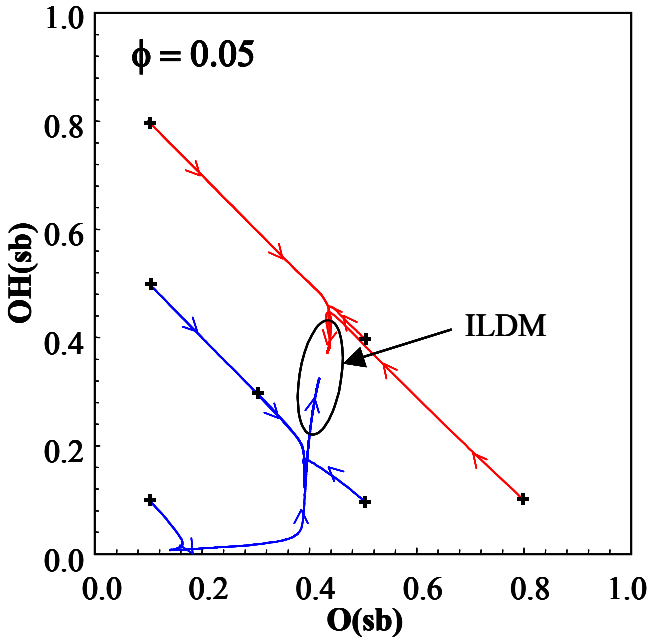

Figure 5.4a Projection of trajectories onto the OH(sb) vs. O(sb) plane for different initial surface conditions, T_{ext} = 150ºC, X_{N2}/X_{O2}= 20 , $X_{H2O,ext}$= 0.0
Red: initially more oxidized, Blue: initially more reduced

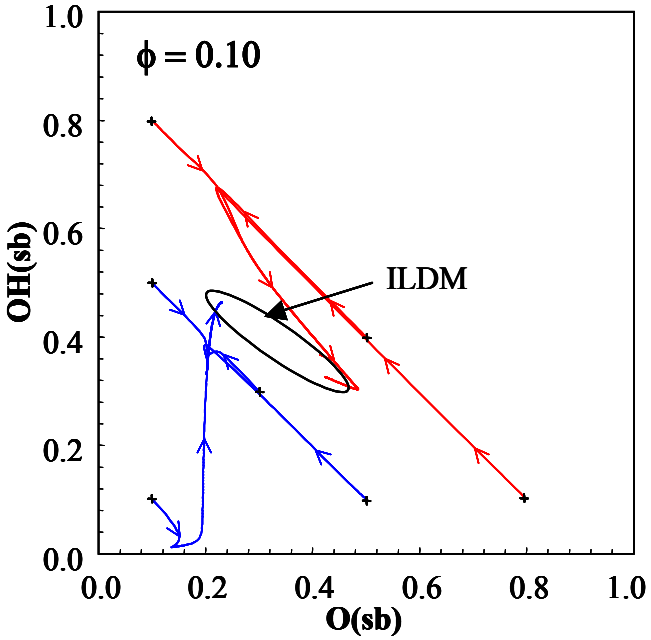

Figure 5.4b Projection of trajectories onto the OH(sb) vs. O(sb) plane for different initial surface conditions, T_{ext} = 150ºC, X_{N2}/X_{O2}= 20 , $X_{H2O,ext}$= 0.0
Red: initially more oxidized, Blue: initially more reduced

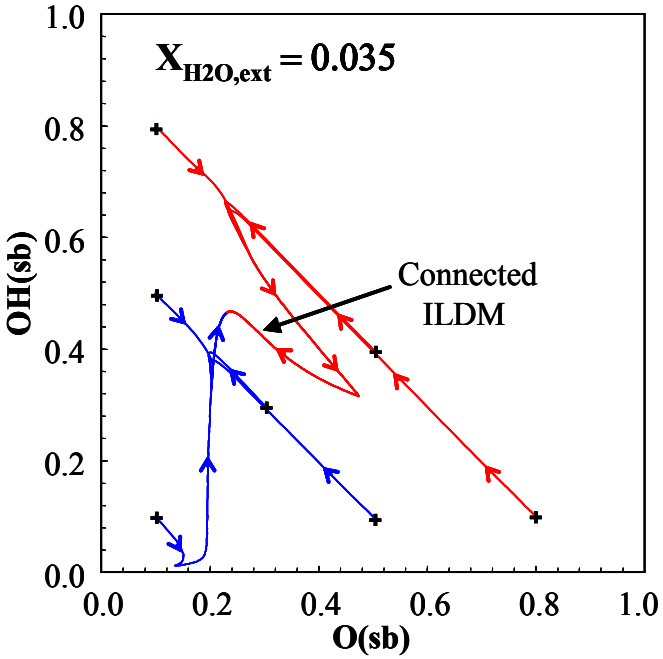

Figure 5.5 Projection of trajectories onto the OH(sb) vs. O(sb) plane for different initial surface conditions at T_{ext} = 150 °C, ϕ = 0.1, X_{N2}/X_{O2} = 20.0
Red: initially more oxidized, Blue: initially more reduced

Plots of the trajectories in the OH(sb) versus O(sb) for $X_{H2O,ext}$ = 0.035 and T_{ext} = 150 °C in Figure 5.5 indicates that the initially oxidized and reduced state manifolds are connected. Although the shape of the manifold is not significantly impacted by the additional gas phase H_2O, the rate of movement along the trajectories is accelerated for the more oxidized states.

The effect of external temperature on the shape of the manifolds in O(sb) vs. OH(sb) space is very significant. By increasing T_{ext} to 200ºC, the location of the manifold is shifted to higher O(sb) surface fractions as indicated in Figure 5.6. The higher surface temperatures accelerate the arrival to steady-state conditions where the trajectories collapse to a point. Furthermore, the mechanism predicts that the increased temperature

causes a steady-state with a much higher O(sb) surface site fraction. This suggests that as temperature rises in this range, surface oxide formation is more significant relative surface hydroxylation and reduction by the H_2. This has also been observed in our experiments where 200ºC maintains steady mass-transfer limited conversion for a range of reactor conditions.

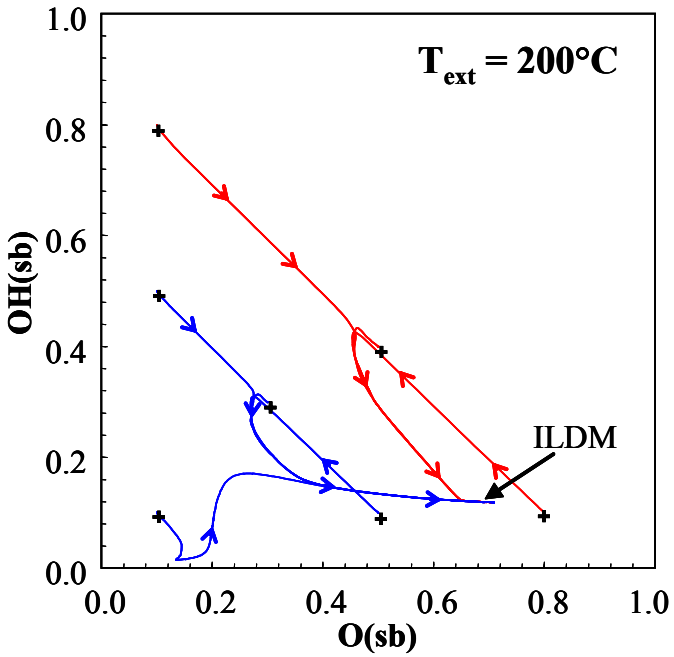

Figure 5.6 Projection of trajectories onto the OH(sb) vs. O(sb) plane for different initial surface site fractions at ϕ = 0.1, $X_{H2O,ext}$ = 0.0, X_{N2}/X_{O2} = 20
Red: initially more oxidized, Blue: initially more reduced

Analysis, of the ILDM‘s for this range of operating conditions for the Pd-H_2 system was investigated and results were obtained by identifying ILDM solution with different number of fast modes which are already equilibrated (relaxed). Dimension of local manifold has been defined based on user-specified error between ILDM solution and full chemistry solution. Having fixed the dimension of manifold, manifold points are computed in state space with an input tolerance.

Figure 5.7 shows how transient profiles of H_2 conversion with different number of relaxed modes capture full chemistry conversion profile. In Figure 5.7, H_2 conversion from full system integration is compared with ILDM solution with various numbers of active modes. Integration of 3D manifold solution can capture full chemistry curve completely after 17 fast modes are went away at a given time with lower than 0.1%. 2D manifold can not follow the full chemistry curve, although the point in which fast modes are relaxed has started sooner than the 3D ILDM curve. It can be said at that point, those relaxed modes can not follow integration of full chemistry curve. 2D manifold fails to capture decay in full conversion curve at the time predicted by the full chemistry whereas the 3d manifold captures it really exactly. Also, 1D manifold shows just a constant conversion for whole duration of integration.

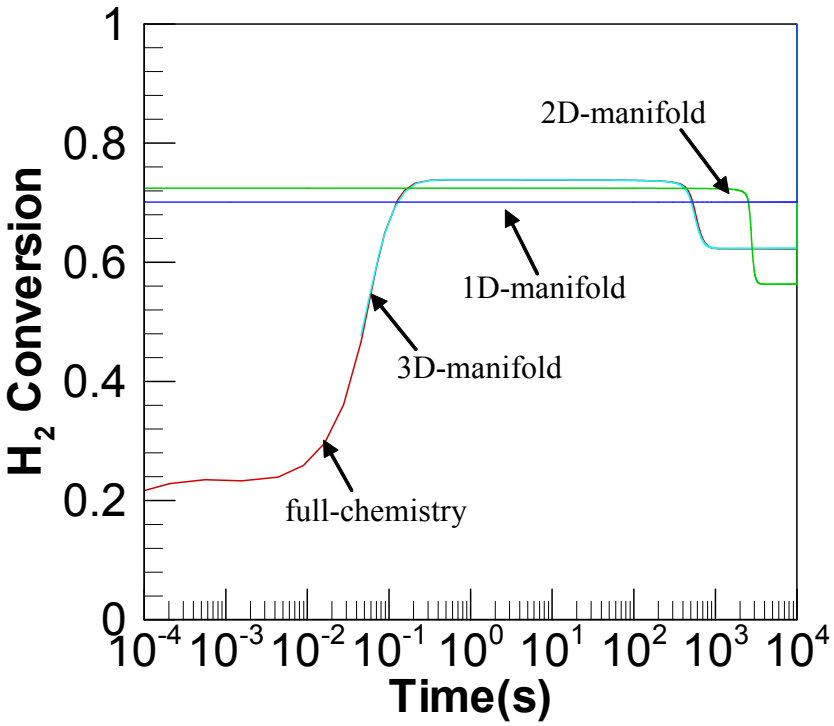

Figure 5.7 Transient profile of H_2 conversion by different number of relaxed modes, Red Plots: Full chemistry (20 modes), Blue Plots: 1D manifold, Green Plots: 2D manifold, Cyan Plots: 3D manifold, T_{ext} = 150 °C, ϕ = 0.1, X_{N2}/X_{O2} = 20, $X_{H2O,ext}$ = 0.035

Transient profiles of two major surface species, OH(sb), O(sb) in the washcoat layer are depicted in Figures 5.8a and 5.8b. As it is expected, ILDM with 17 relaxed mode can capture time functionality of two major surface species. It can be said for capturing full chemistry integration curve behavior in time scales larger than 0.1s, 3 equilibrating processes are critical. 2D manifold has already equilibrated some of processes that are necessary to capture full chemistry behavior.

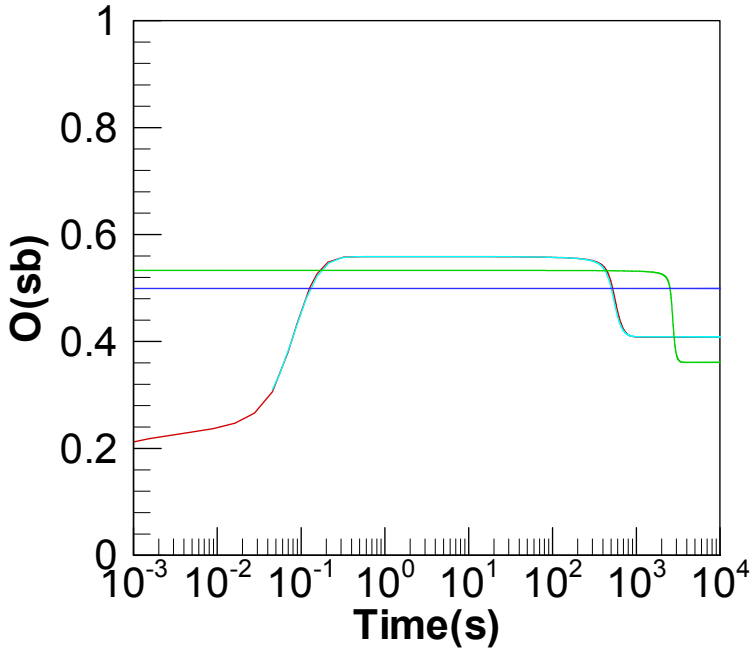

Figure 5.8a Time evolution of O(sb) with different number of relaxed modes Red Plots: Full chemistry (20 modes), Blue Plots: 1D manifold, Green Plots: 2D manifold, Cyan Plots: 3D manifold, T_{ext} = 150 °C, ϕ = 0.1, X_{N2}/X_{O2} = 20, $X_{H2O,ext}$ = 0.035

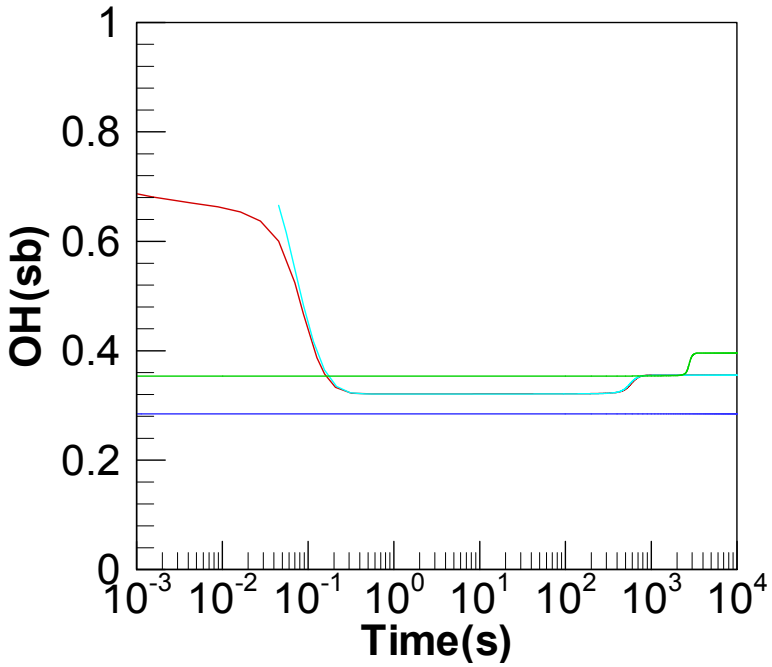

Figure 5.8b Time evolution of OH(sb) with different number of relaxed modes Red Plots: Full chemistry (20 modes), Blue Plots: 1D manifold, Green Plots: 2D manifold, Cyan Plots: 3D manifold, T_{ext} = 150 °C, ϕ = 0.1, X_{N2}/X_{O2} = 20, $X_{H2O,ext}$ = 0.035

5.6 ILDM analysis of surface chemistry mechanism

While it is clear many surface reactions on Pd achieve equilibrium in time scales < 1 ms, long time scale phenomena (> 10 s) are evident in H_2 oxidation on Pd catalysts as observed both in experiments and in modeling results. ILDM's can also provide a very powerful tool for evaluating uncertainties in complex chemical mechanisms through identification of combinations of chemical species that influence rate controlling processes. This is particularly valuable for surface chemistry where much remains uncertain about the thermochemistry and in particular, species interaction potentials, which play a decisive role in influencing experimentally observable phenomena at long time scales (Imbihl and Ertl 1995; McCarty 1995; Wolf et al. 2003).

The two Pd-H_2-O_2 surface chemistry mechanisms presented in Tables 4.1 and 4.2 (Mechanism A) and Tables 5.1 and 5.2 (Mechanism B) are analyzed by the uniform differential reactor model. Full simulations of the differential washcoat reactor were carried out for both mechanisms in different conditions with T_{ext} = 100, 125 and 150ºC, ϕ = 0.05 and 0.1, and $X_{H2O,ext}$ = 0.0 (dry) and 0.022 (wet). Results for Mechanism B (Table 5.2) were shown in section 5.2.

Figure 5.9a shows how the slight difference in surface mechanism A (Table 4.2) suppress the oscillations entirely for the dry case at T_{ext} = 100ºC and ϕ = 0.1, but only a single rapid transition after about 5 s when a build-up of H(sb) and H(s) rapidly oxidize and is removed from the surface. The lack of predicted oscillations with surface Mechanism A can be attributed to the reduced stability of the surface species OH(sb) and H_2O(sb) which prevents the build-up of these species as conversion increases. Surface mechanism A, for the dry feed simulation at 100°C shows more stable distribution of

dominated surface species OH(sb), OH(s) and O(sb) after a long time. At the same temperature and wet feed, Mechanism B in Figure 5.3b shows a similar fast transient behavior after around 48 s. This transient in surface coverage does not show the same little spike in conversion because the surface is initially dominated with H_2O(s) and H_2O(sb), and the rapid desorption of these species is not substituted by rapid H_2 adsorption, whereas, O and OH species rapidly cover the surface. Surface mechanism A with added external gas phase water only shows a confined milder rapid transient from H-dominant to O-dominant surface coverage. However, long time conversion is magnificently reduced as shown in Figure 5.9b.

The oscillatory conversion for Mechanism B (Table 5.2) in the dry case at 100ºC is related to the stability of surface species H_2O (primarily H_2O(sb) and H_2O(s)) which as conversion and washcoat temperature increase finally becomes unstable and rapidly desorbs. The desorption is followed by a rapid surface coverage of the O-rich species, OH(sb) and OH(s), indicated in Figure 5.3a and the subsequent build-up of OH(sb) on the surface and another rapid transition back to H-rich species, H_2O(sb), H_2O(s) and H(s). This oscillation between the two states continues as a limit cycle appears to be reached. Comparison of the H-rich species history for both mechanisms in Figures 5.3a and 5.9a respectively indicates that with the slight changes in surface energies, surface mechanism in Table 5.2 has significantly more H_2O coverage whereas surface mechanism in Table 4.2 with the less stable H_2O surface species shows a build-up of H(s) and H(sb) without significant H_2O buildup on the surface. This difference indicates how the minor changes in the surface energies for the two mechanisms can result in dramatic differences in surface coverages during transient conditions. This also suggests the value of surface

spectroscopy as a tool for validating surface chemistry mechanisms when catalysts are operating under kinetically controlled conditions.

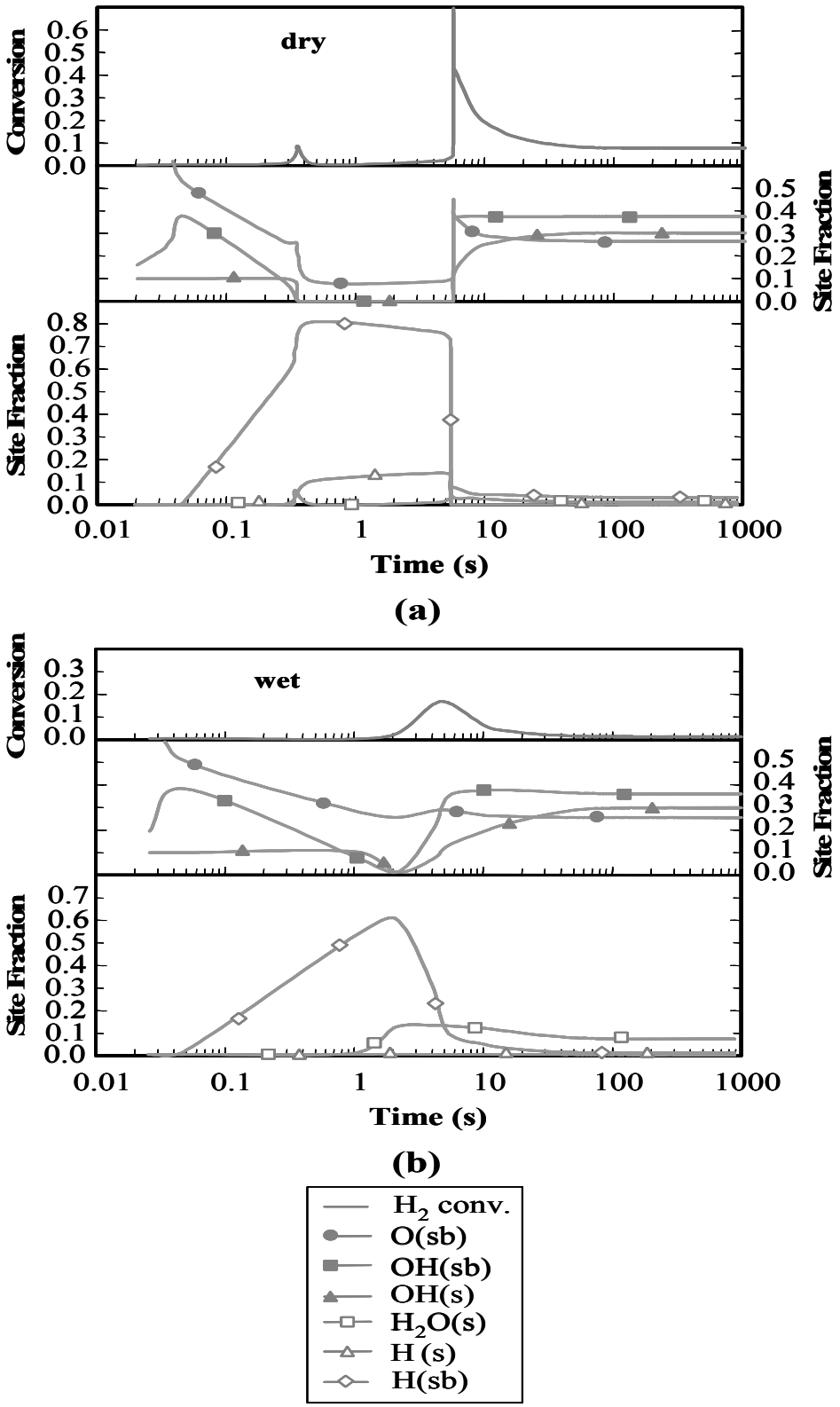

Figure 5.9 Transient profiles of H_2 conversion and surface site fractions at T_{ext} = 100ºC and ϕ = 0.1 with Mechanism A, for (a) dry and (b) wet ($X_{H2O,ext}$ = 0.022)

To verify ILDM's, it is useful to plot trajectories from several initial surface conditions for the dynamical system on the planes of dominant surface species such as O(sb) and OH(sb) or OH(s). Figures 5.10a and 5.10b shows such trajectories for the dry and wet conditions plotted in Figures 5.3. The oscillatory behavior of Mechanism B, Table 5.2, at the dry condition results in a complex limit cycle behavior in which the Pd-catalyst surface cycles between an H_2O(sb)/H2O(s)/H(s) dominated state and a state dominated by O(sb), OH(sb), and OH(s) based on Figure 5.3a. This limit cycle behavior is approached regardless of initial surface site distributions including conditions dominated initially by chemisorbed species on Pd-metal (dark curves in Figure 5.10a) and conditions dominated initially by oxide species (gray curves in Figure 5.10a). The trajectories in Figure 5.10b for the wet condition illustrate how additional gas-phase water impacts the catalyst behavior predicted by Mechanism B and doesn't show periodic limit cycle. Although initially the trajectories in the O(sb) and OH(sb) plane qualitatively follow the trajectories for the dry cases, the additional water causes the slowest mode in the ILDM to reach a high enough OH(sb) site fraction to avoid the instabilities associated with H_2O adsorption/desorption cycles. It was observed increasing temperature to 125ºC or 150ºC results in an alternative means of suppressing the oscillatory behavior by increased desorption rates of H_2O from the surface. Similarly, the lower H_2O desorption enthalpy barrier in surface mechanism Table 4.2 suppresses the oscillatory behavior even at 100ºC as discussed earlier.

The limited impact of initial surface conditions on long-term steady-state catalyst behavior indicated in Figure 5.10 has been observed for all conditions in this study. The multiple steady-states as observed in experiments with reduced bulk phases

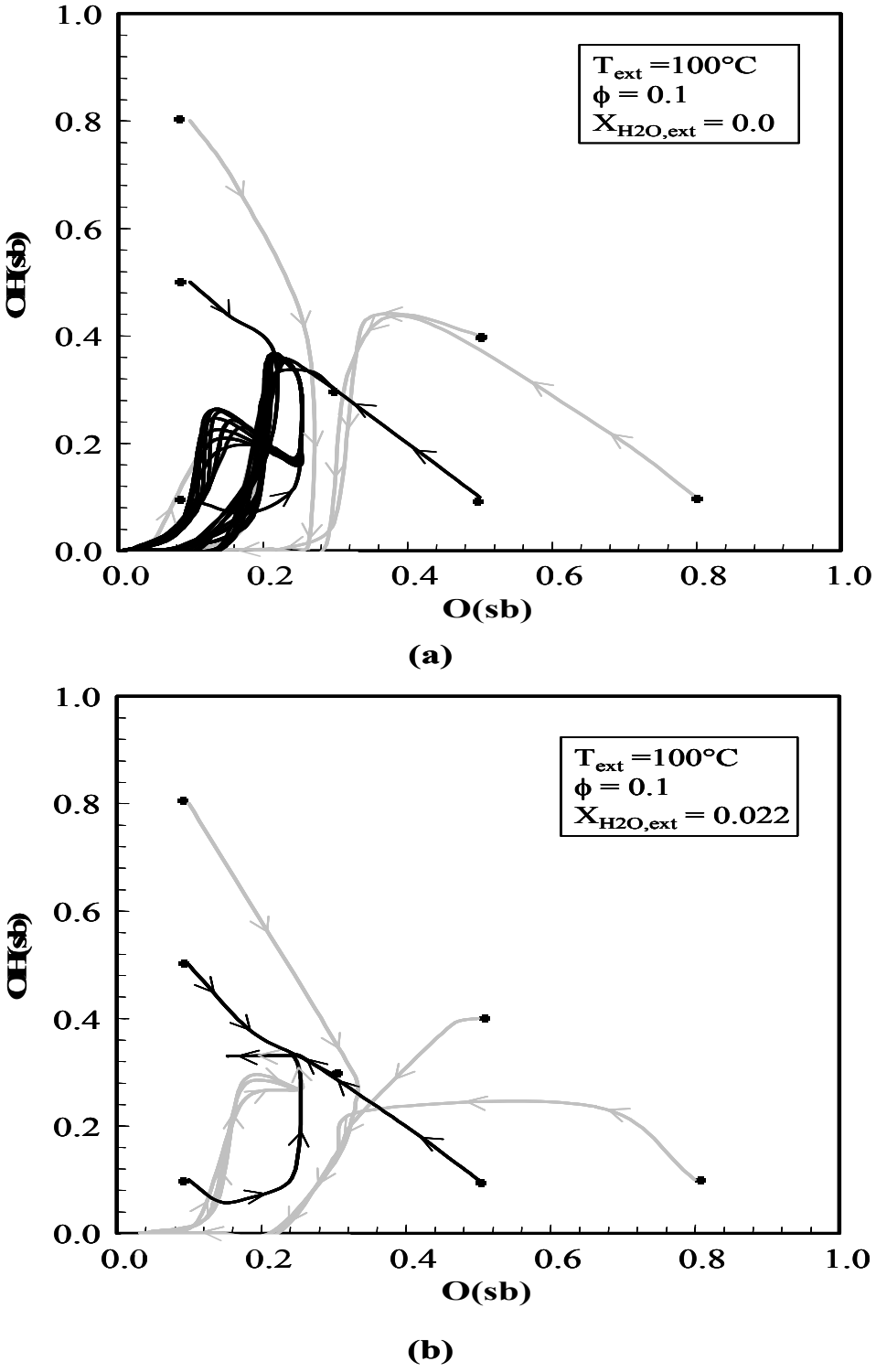

Figure 5.10 Projection of trajectories onto the $\theta_{OH(sb)}$ vs. $\theta_{O(sb)}$ plane for simulations with Mechanism B with different initial surface fractions indicated by ✚: (a) dry external conditions and (b) wet external conditions

(Dus and Nowicka 1998; Kramer et al. 2003) may require incorporation of bulk species in the model as demonstrated in the earlier study of Pd-O_2 chemistry (Wolf et al. 2003).

Figures 5.11a and 5.11b show the influence of ϕ on H_2 conversion and major surface site fractions for $\phi = 0.05$ and 0.1 at $T_{ext} = 125$ºC for both mechanisms. The differences in conversion with ϕ for both mechanisms indicate that the effective kinetics are not first order with respect to H_2 for $T_{ext} \leq 150$°C. Instead, there is a rapid increase in conversion with ϕ (27% at $\phi = 0.1$ compared to 2.1% at $\phi = 0.05$ for modified mechanism in Table 5.2 and 25% at $\phi = 0.1$ compared to 1.4% at $\phi = 0.05$ for mechanism A (Table 4.2). This increase with ϕ can be attributed to the higher H_2 concentrations destabilizing the O(sb)-dominated surface and exposing more vacancies for H_2 adsorption as described in full channel simulations in Chapter 3. Comparison of the surface site fractions in Figure 5.11a and 5.11b illustrates this observation. It has shown the lower concentration of H_2 has not changed time history of surface species. This might be related to the fact that oxidized dominant surface doesn't change too much in low ϕ. In higher ϕ both mechanisms predict the same long time behavior.

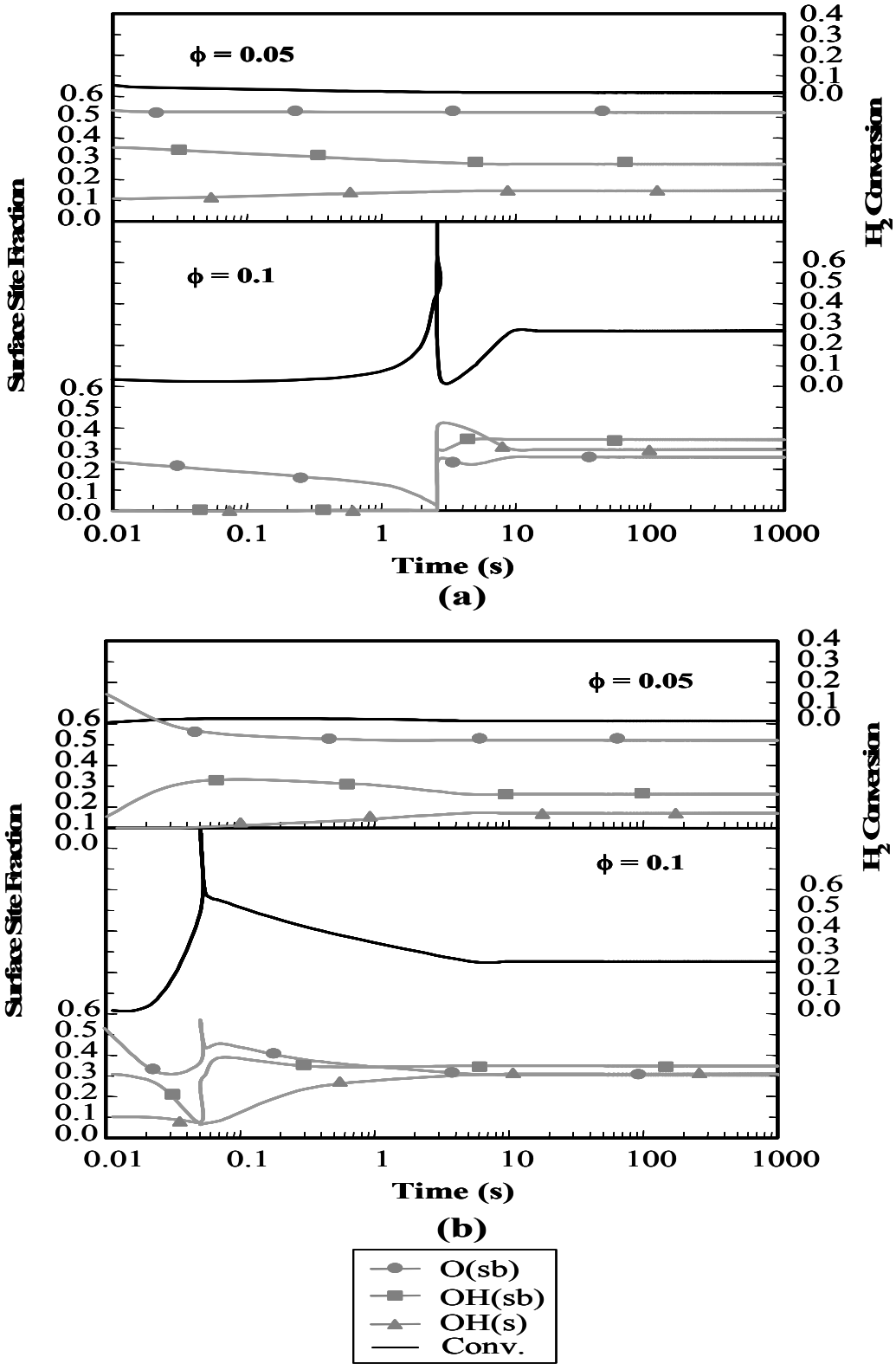

Figure 5.11 Transient profiles of H_2 conversion and surface site fractions at T_{ext} = 125ºC and ϕ = 0.05 and ϕ = 0.1: (a) with Mechanism B and (b) with Mechanism A

5.7 Identifying slow chemical modes using ILDM's

Using ILDM analysis for the uniform single cell washcoat model, system eigenvalues have been evaluated for a range of conditions and for both mechanisms. The slowest modes of the system are identified, and eigenvectors of these modes can provide a basis for identifying reactions (or groups of reactions) that control the catalytic combustion processes. The real part of the eigenvalues λ_{real} for the slowest modes for both mechanisms are shown in Figures 5.12 and 5.13 for both dry and wet conditions for T_{ext} = 100, 125, and 150ºC. The results in Figure 5.12 and 5.13 reveal that the addition of water always increases the time constant ($\tau = 1/|\lambda_{real}|$) of the slowest mode with the exception of 100ºC for modified mechanism, where the $\phi = 0.1$ simulation produces the oscillatory behavior. The oscillations in Figure 5.12a result from the switching between dominant modes controlled by different surface species. The slowest modes reduce their time scales rapidly as temperature increases from 100 to 150°C. For example, for the slowest modes with mechanism in Table 4.2 at 100ºC for dry and wet conditions, $\tau =$ 19.4 and 23.3 s respectively, both of which are time scales accessible to numerous experimental measurements. However, at 150ºC, $\tau = 0.11$ and 0.16 s for dry and wet cases, and these time scales are more than an order of magnitude faster than most standard gas-phase sampling measurement techniques, e.g. mass spectrometers used in this study. This suggests the importance of operating under conditions where kinetics are adequately slow to validate surface chemistry mechanisms.

To understand what surface and gas-phase species are involved in the slowest modes, the eigenvectors associated with the slowest eigenvalues for the range of

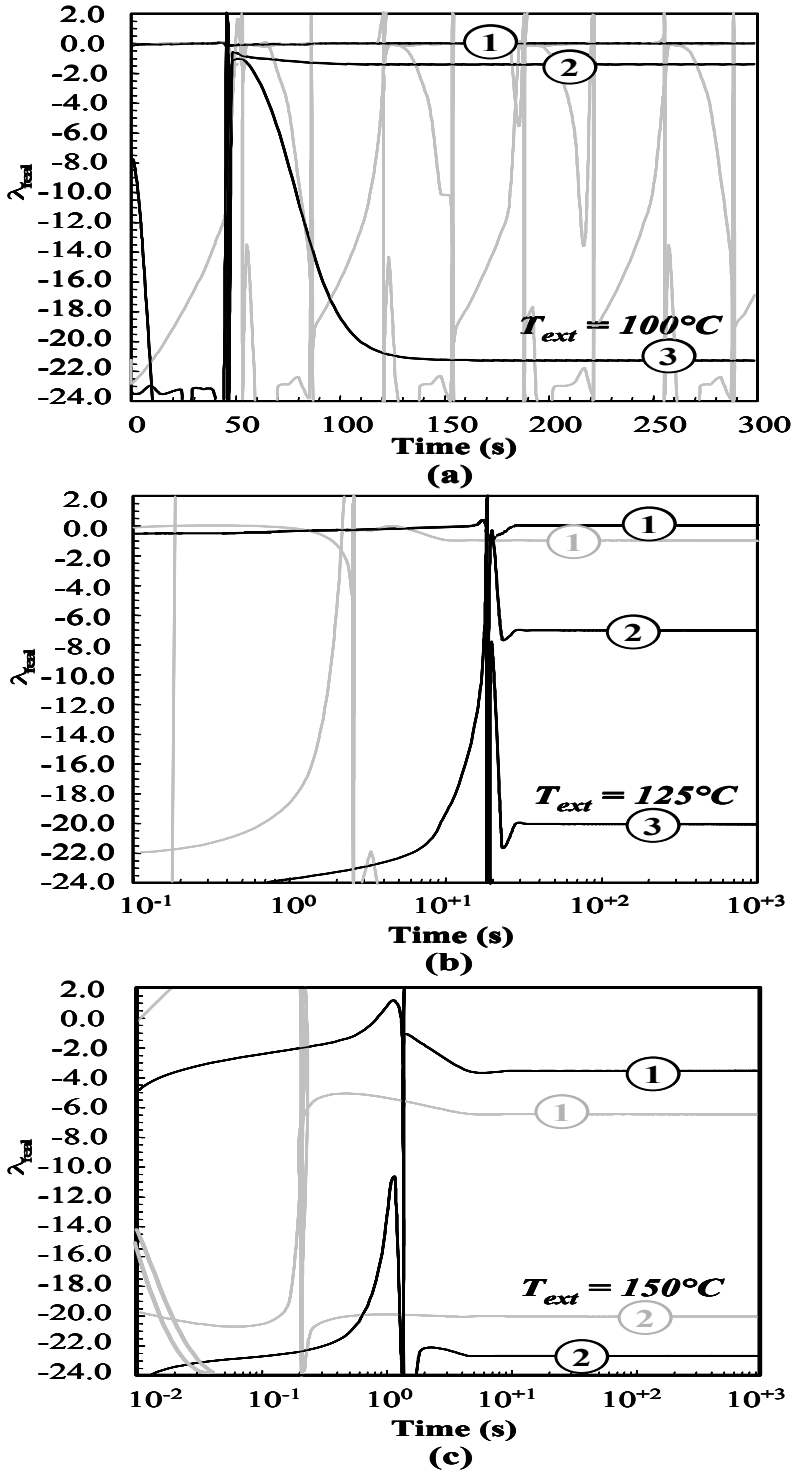

Figure 5.12 Transient eigenvalues for slowest active modes at $\phi = 0.1$ for dry (gray) and wet (black) conditions using Mechanism B at T_{ext} = (a) 100ºC, (b) 125ºC, (c) 150ºC $X_{H2O,ext} = 0.022$ for wet conditions. ① ② ① ② indicate slowest and 2nd slowest modes

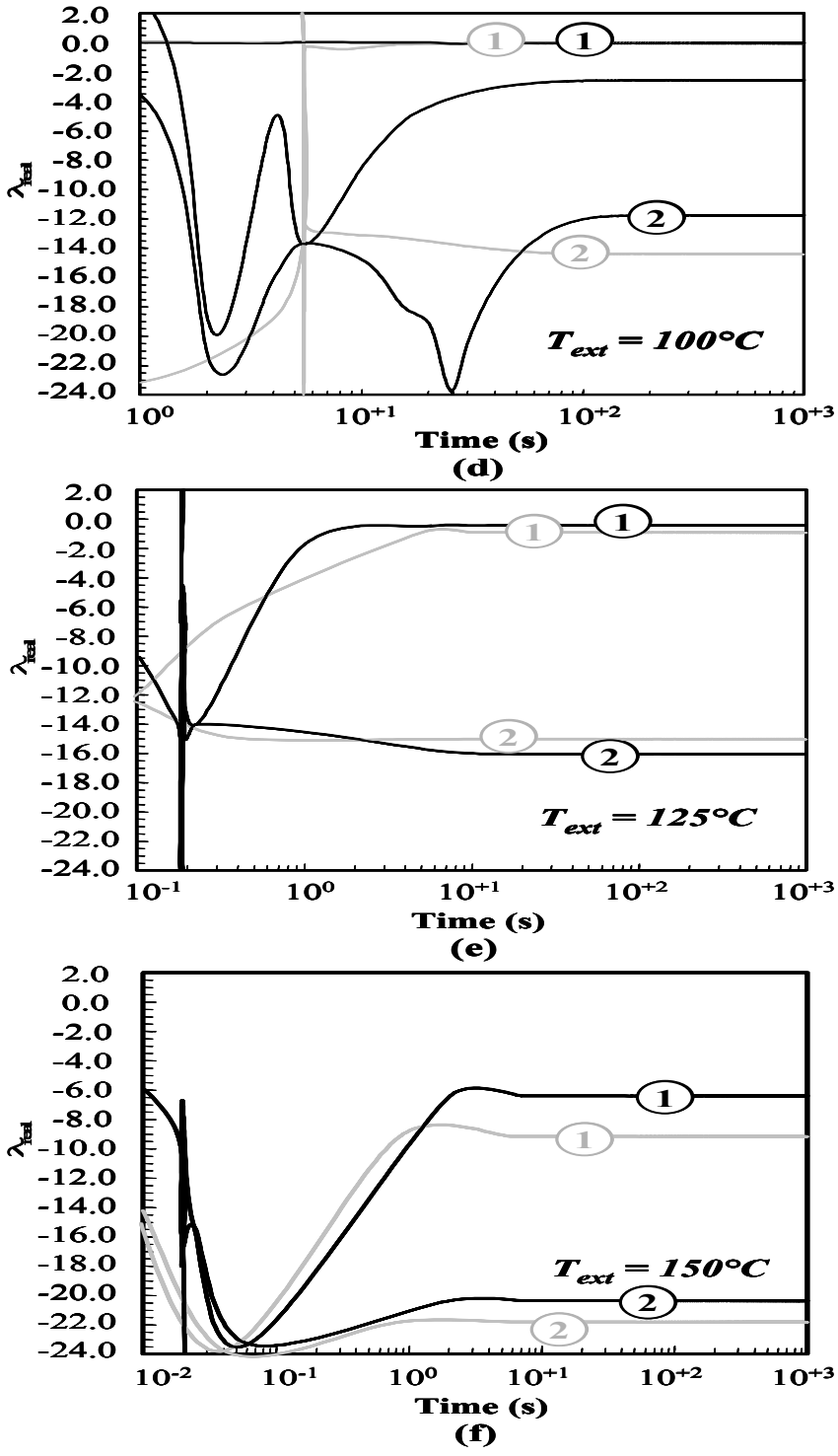

Figure 5.13 Transient eigenvalues for slowest active modes at $\phi = 0.1$ for dry (gray) and wet (black) conditions using Mechanism A at T_{ext} = (d) 100ºC, (e) 125ºC, (f) 150ºC $X_{H2O,ext} = 0.022$ for wet conditions. ① ② ① ② indicate slowest and 2nd slowest modes

conditions studied with the differential reactor simulation are depicted in Figure 5.14. For both mechanisms under all non-oscillatory conditions, the slowest mode is dominated by surface species and in particular the adsorbed species on a reduced Pd(s) surface (H(s), O(s), OH(s), and H_2O(s)). Various surface reactions that control the distribution of these species must take the longest time to equilibrate under the O_2-net environment. In an attempt it was tried to isolate the contributed group of reactions in the slowest mode based on the generated linear space by local eigenvectors. Based on the singular value decomposition (SVD) algorithm, it was found that reactions are linearly dependent, but they didn't make any projection on the eigenvector linear space. The impact that this slowest mode has on conversion is not clearly revealed by the eigenvalue/eigenvector analysis.

For $T_{ext} \leq 125°C$, the slowest mode is more than an order of magnitude slower than the other modes, which suggests that all other modes should maintain equilibrium as this mode progresses along its one-dimensional manifold. Figure 5.15 shows the effect of conditions on the second slowest mode for both mechanisms, and it is clear that fewer generalizations can be drawn from the diversity of contributions to the second slowest mode at the various conditions. A small contribution from gas phase H_2 under some of the higher T conditions suggests that H_2 adsorption becomes part of a rate limiting process according to the surface chemistry mechanism at these conditions.

ILDM analysis can also be useful for assessing the importance of the various modes on actual H_2 conversion. To this end, H_2 conversion from dynamical simulations using equation 5.12 with varying number of relaxed (fast) modes is compared with the

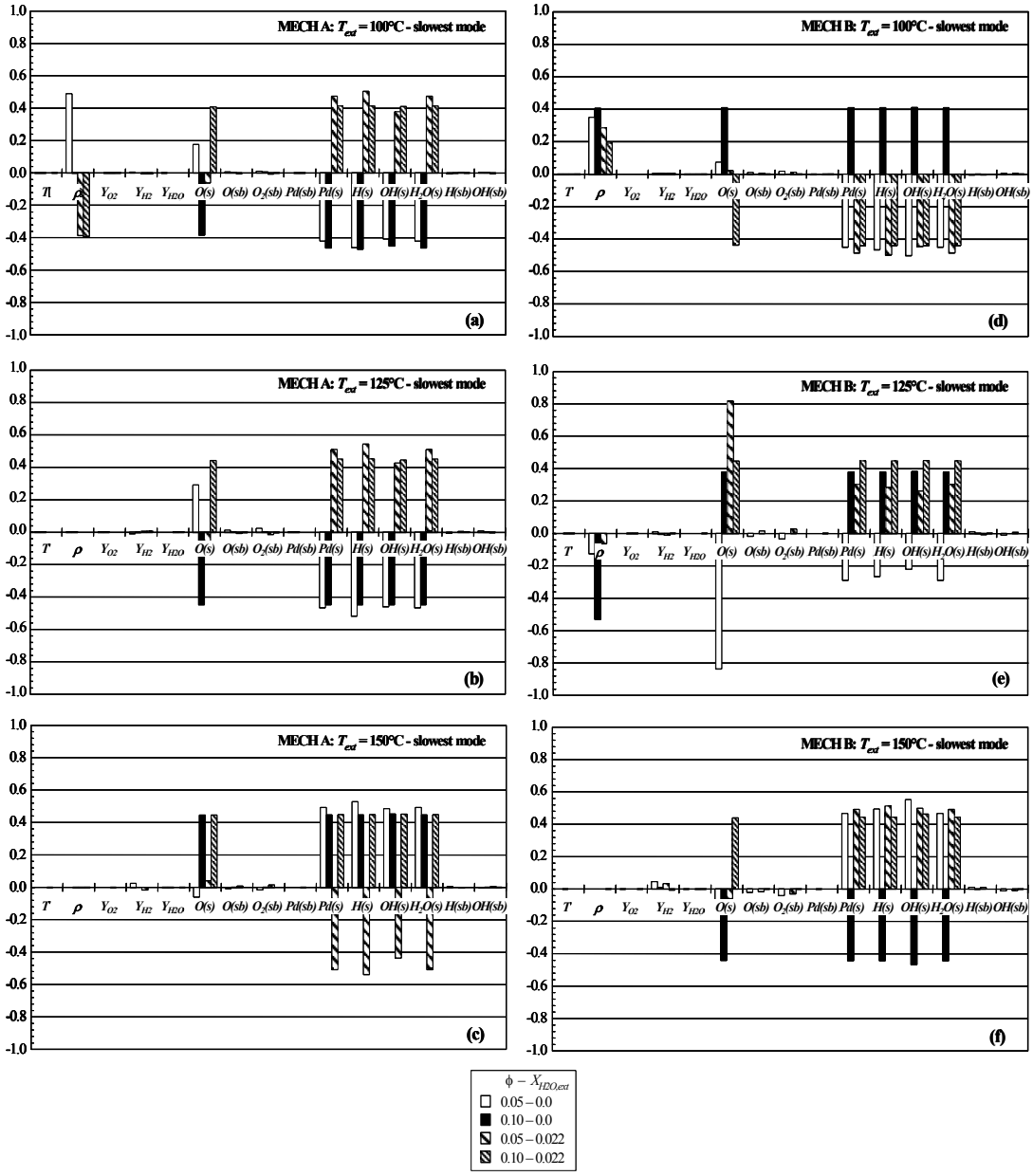

Figure 5.14 Contribution of state space variables in the slowest active mode for dry and wet conditions at $\phi = 0.05$ and $\phi = 0.1$ using Mechanism B with (a) T_{ext} = 100ºC, (b) T_{ext} = 125ºC, (c) T_{ext} = 150ºC and Mechanism A with (d) T_{ext} = 100ºC, (e) T_{ext} = 125ºC, (f) T_{ext} = 150ºC

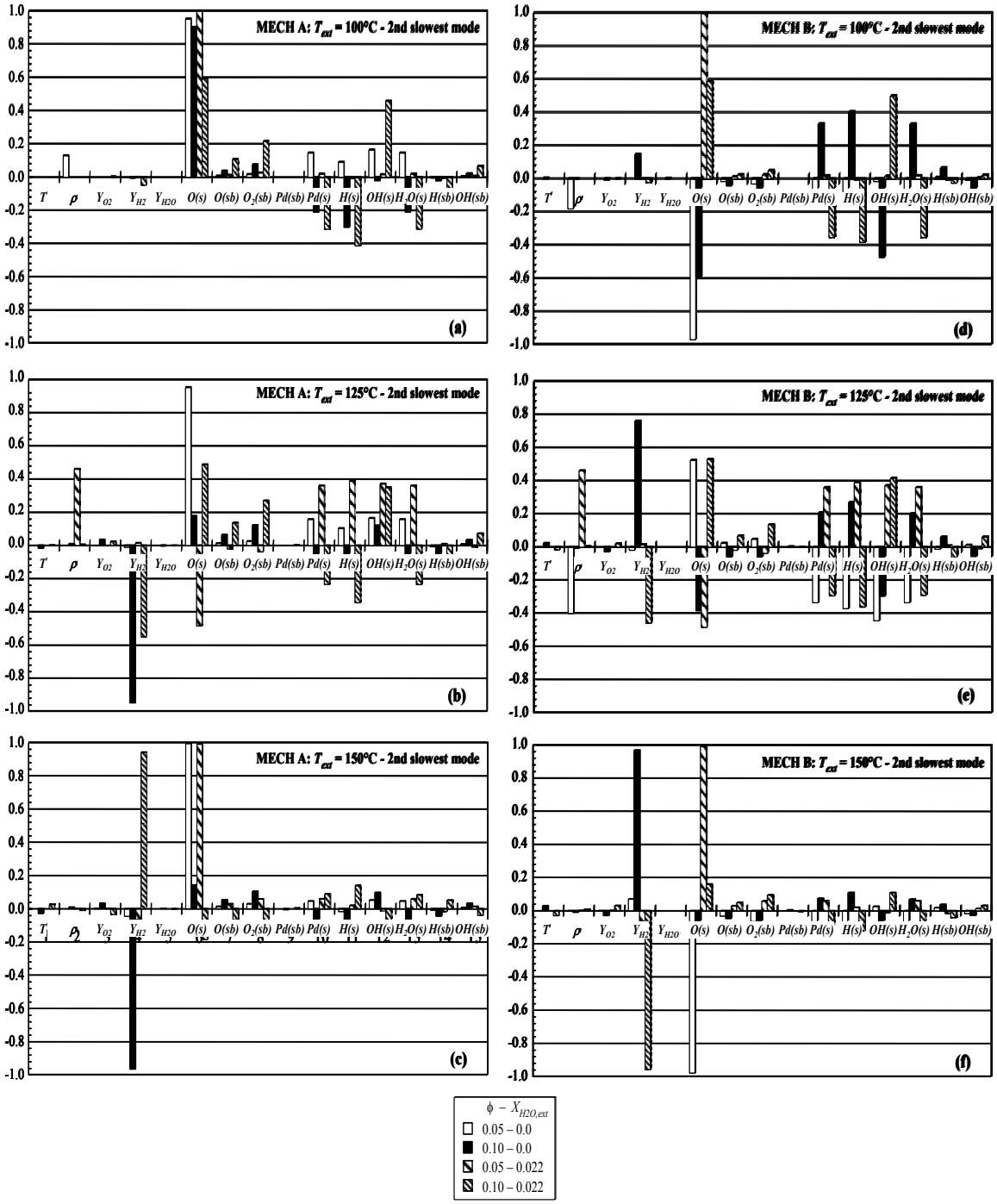

Figure 5.15 Contribution of state space variables in the 2nd slowest active mode for dry and wet conditions at $\phi = 0.05$ and $\phi = 0.1$ using Mechanism B with (a) T_{ext} = 100ºC, (b) T_{ext} = 125ºC, (c) T_{ext} = 150ºC and Mechanism A with (d) T_{ext} = 100ºC, (e) T_{ext} = 125ºC, (f) T_{ext} = 150ºC

full surface chemistry simulations. For this study, the number of relaxed modes at a given time is found by assessing whether the remaining slow modes integrated from that time can track the H_2 conversion calculated from the full chemistry simulations for all subsequent times to within 0.1%. Using this criterion, the number of relaxed modes with mechanism of Table 4.2 for dry external conditions with $\phi = 0.1$ is calculated. Figure 5.16 shows how the number of relaxed modes increase with time for T_{ext} = 100°C and 150°C. For 100°C, the final two modes remain slow (or active) for t > 20 s, whereas for 150°C, all 15 modes are relaxed before t = 2 s. This reiterates the importance of using low temperature data for dynamic kinetic mechanism assessment.

Figures 5.17a and 5.17b show comparisons at T_{ext} = 100°C and $\phi = 0.1$ between full chemistry simulations and ILDM simulations using equation 5.12 after determining varying number of relaxed modes as discussed above. The starting point for the ILDM simulations, which is also where the modes are calculated, are indicated and these points indicate the earliest times where the specified number of slow or active modes can track the full chemistry. For the oscillatory behavior with modified mechanism, no less than four active modes are required for the ILDM to capture the full chemistry simulation as indicated in Figure 5.17a. This four-mode (or four-dimensional) ILDM could not be identified until the first transition in the oscillatory behavior (at t = 53 s). The four modes have fluctuating time scales, as indicated in the eigenvalues plots in Figure 5.12a. For mechanism from Table 4.2 under the same conditions of T_{ext} = 100°C and $\phi = 0.1$, ILDM's of two modes (dimensions) can be used to simulate the full chemistry after a t = 8 s as indicated in Figure 5.17b. Furthermore, as steady state is approached (t > 23 s) a one-dimensional ILDM can match the full mechanism. The ability to assess H_2

conversion experimentally at shorter time intervals than the equilibration of the slower modes is critical for the usefulness of ILDM's as a tool for surface chemistry validation. Such transient experiments can be used to evaluate small changes in uncertain surface thermochemistry that can lead to substantial changes in catalyst behavior – as indicated by the extensive comparison of the two very similar mechanisms in this study.

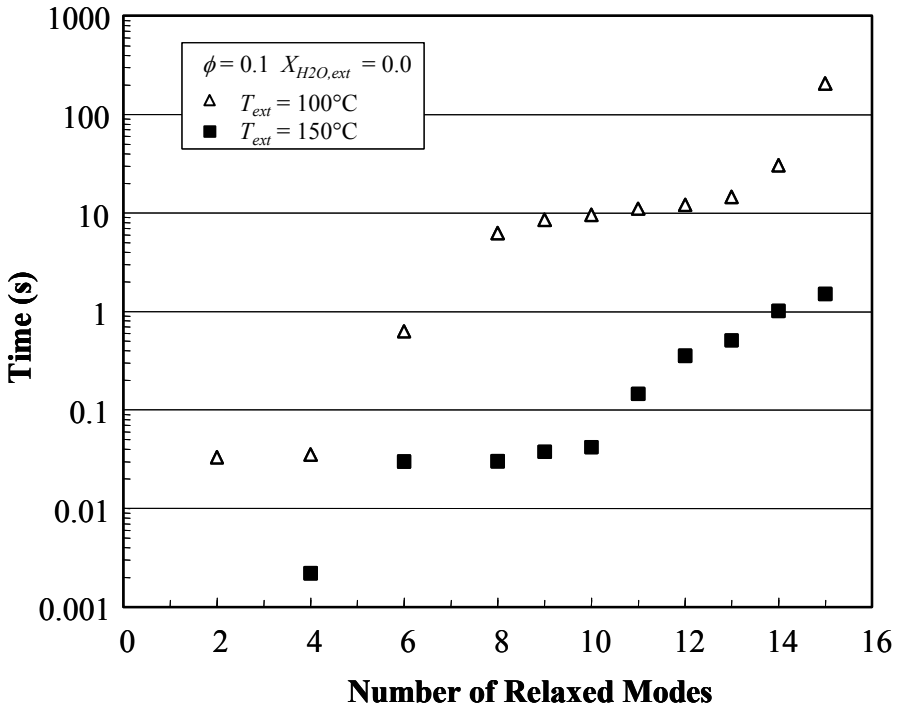

Figure 5.16 Number of relaxed modes for Mechanism A at two different T_{ext} for $\phi = 0.10$

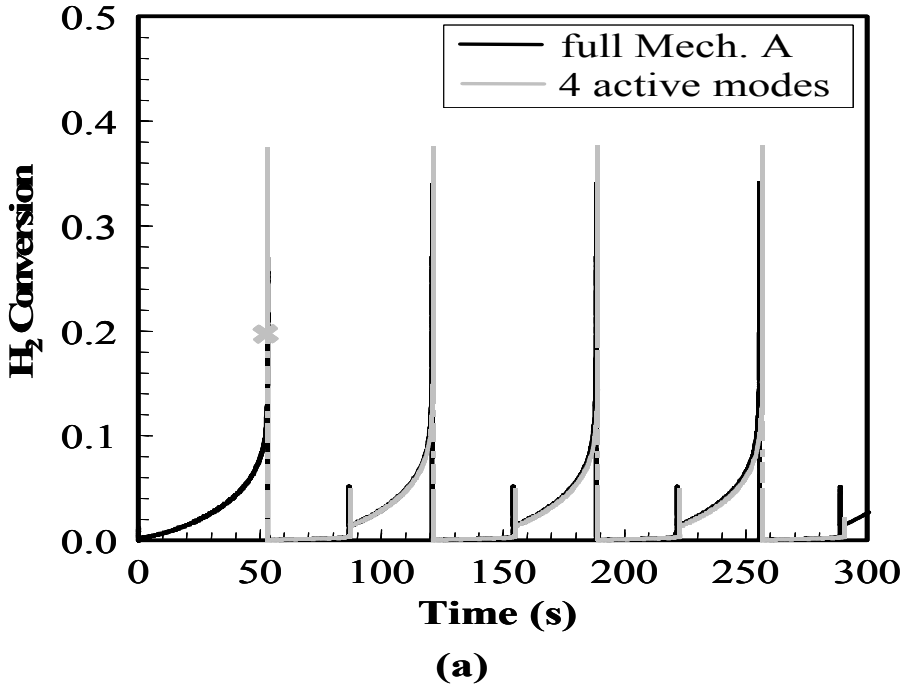

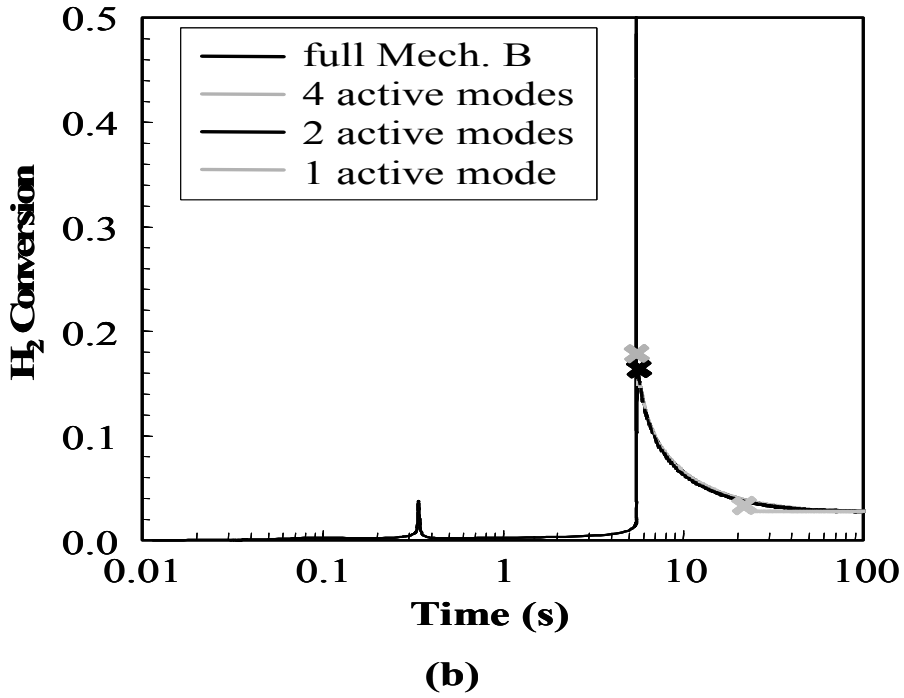

Figure 5.17 H_2 conversion for simulations using full chemistry and ILDM-reduced chemistry for T_{ext} = 100ºC, ϕ = 0.1, and $X_{H2O,ext}$ = 0.0 with (a) Mechanism (A) and (b) Mechanism (B). ✖,✖ indicates times at which ILDM simulations were initiated

5.8 Conclusion

The value of dynamical system analysis of differential reactors for understanding the complex surface chemistry of Pd-based H_2 catalytic combustion has been demonstrated. ILDM's provide a basis for assessing the rate controlling processes arising from complex interactions between surface and gas-phase species in porous washcoats. The simulated differential reactor allows for surface chemistry to be probed without variation in channel flow conditions, which otherwise obscures the dynamic analysis of the surface chemistry-driven processes. Such a reactor is very difficult to establish experimentally and requires adequately fast gas-sampling techniques to capture the dynamics associated with surface species changes. However, the differential reactor may be approximated experimentally with very low residence time (< 1 ms) reactors, and with isotopic tagging and/or *in situ* surface spectroscopy, many uncertainties associated in surface thermochemistry on Pd-based catalysts (and other systems) may be refined by using ILDM analysis similar as presented here. Such studies can validate mean field approaches for computationally efficient combustion mechanisms.

Comparison of two similar mechanisms, shows how relatively small changes in surface thermodynamics can lead to significant changes in surface chemistry. While these changes may not lead to extremely large changes in global H_2 conversion for the limited range of conditions explored in this study, the differences in surface thermodynamics may lead to substantial differences in global catalyst behavior under more complex conditions where bulk catalyst reduction occurs or where hydrocarbons are added to the Pd-O_2-H_2 thermochemistry.

The ILDM analysis of differential reactors provides a means for exploring the slowest processes that influence the chemistry and thus for identifying ways to validate some critical aspects of the surface thermodynamics and chemistry needed for accurate modeling of catalytic combustion. Based on the Figures 5.13 and 5.14 for both mechanisms some general results can be derived:

- Inlet water increases time constant of slowest mode
- Generally vectors of slowest modes contain predominantly surface species and are associated with adsorbates on metallic surfaces Pd(s), H(s), OH(s), H_2O(s), O(s)
- Slowest mode time constant decrease rapidly with increasing T
- Lower equivalence ratio show more slow modes than higher equivalence ratio.

Chapter 6

Experimental Results for Pd-CH_4

6.1 Introduction

Superior activity of Pd for oxidation of CH_4 has attracted many researchers to study Pd-based catalysts for lean oxidation of CH_4 – particularly for catalytic combustion in gas turbine applications. However, the complex interactions between CH_4 oxidation kinetics and Pd oxidation/reduction cycles (Ciuparu et al. 2002), requires multi-step reaction schemes where different steps becoming rate limiting at different reactor inlet temperatures (T_{in}) and CH_4 equivalence ratios (ϕ), and these mechanisms have not as of yet been resolved.

Pd-based catalysts have superior low-temperature activity (for $T_{in} < 500$ºC) for CH_4 oxidation (Forzatti 2003; Carroni et al. 2004). However, the Pd-PdO_x transients at temperatures > 650°C can cause significant transient variation in catalytic combustion activity (McCarty 1995; Ciuparu et al. 2002). This chapter presents well-characterized experiments in a microreactor similar to the reactor presented in Chapter 2. These experiments are used to provide a basis for evaluating Pd-CH_4 kinetics for temperatures ranging from 400 to 850°C. This range was chosen to observe the coupling between Pd/PdO reduction kinetics and CH_4 activity. Furthermore, effects of inlet H_2O and contribution of gas phase in CH_4 conversion will be addressed.

6.2 Experimental techniques

The current experimental investigation of CH_4 over Pd/PdO catalysts utilizes the same experimental set-up described in Chapter 2 with only minor modifications. In contrast, the earlier experiments a new magnetic sector mass spectrometer (VG Prima δB) was implemented to acquire real time measurements of reactants and products during time-on-stream tests and temperature programmed reactor studies. The real-time mass-spectrometer measurements with VG Prima δB provided measurements once every 10 s.

The length of the catalytically coated region was reduced from 20 mm used for low-temperature H_2 oxidation to 10 mm in this study for higher temperatures CH_4 oxidation. Because differential conversions are not maintained at the highest temperature conditions in this study, temperature rise in the catalytically active region was monitored by thermocouples placed inside the α-Al_2O_3 support tube. The K-type thermocouples contacted the tube inner wall at axial locations corresponding to the upstream and downstream boundaries of the catalytic section. Heat-loss in the reactor was desired to maintain the reactor at as near as possible to isothermal conditions. For the high conversions in this study, the measured reactor temperature rise remained below 10ºC.

N_2 and CO, as one of combustion products, both with molecular weight 28, have overlapping signals in mass spectrometry. In order to facilitate accurate interpretation of the MS histograms, Ar was used to dilute CH_4 and O_2 flows through the microreactor. Flow rates were controlled using electronic mass flow controllers. In most cases represented here, the Ar/O_2 ratio was maintained at 10 to keep temperature rises across the reactor low. For several runs H_2O was added to the flow to assist the effects of humidity on CH_4 oxidation rates by bubbling a portion of the O_2/Ar mixture through a

temperature-controlled saturator upstream of the fuel injection. For the conditions reported here, the saturator was held at 30 ± 3ºC such that for the conditions with H_2O addition, the mole fraction into the reactor $X_{H2O,in}$ = 0.04± 0.005. In all cases, the reactor inlet flow velocity was 1.5 m/s, which corresponds to a reactor residence time of 7 ms or a space velocity of 80 s^{-1}.

The γ-Al_2O_3-supported Pd catalysts were prepared from a slurry mixture supplied by Dr. William Retallick from Catacel. Although some γ-Al_2O_3- supported Pd-based catalysts for the high temperature CH4 oxidation were made in house as described in Chapter 2, the Retallick catalysts were found to have superior stability due to some stabilizers added. The content of the Catacel catalyst was 3% by weight Pd and other details for the catalyst can be obtained from Dr. Retallick. Washcoats were prepared by diluting the Pd/γ-Al_2O_3 slurry in nitric acid and then coating the outer diameter of the α-Al_2O_3 tube with intermediate drying to achieve a porous washcoat between 10-20 μm thick. The catalytic washcoat was then calcined in air at 500°C for 8+ hours and then at 450°C with a low flow of O_2 inside the tube furnace to insure that the Pd was in a fully oxidized state.

Results from the real-time transient analysis of the mass spectrometer measurements are presented in Figures 6.1a and 6.1b. The plots show the measured transient response of CH_4 conversion over the γ-Al_2O_3-supported Pd-based catalyst during time-on-stream studies at various inlet temperatures characteristic of gas turbine combustors. The results in Figures 6.1a and 6.1b show the importance of transient real time measurements as the slow decay of the T_{in} = 600ºC case at both ϕ = 0.2 and 0.4 as

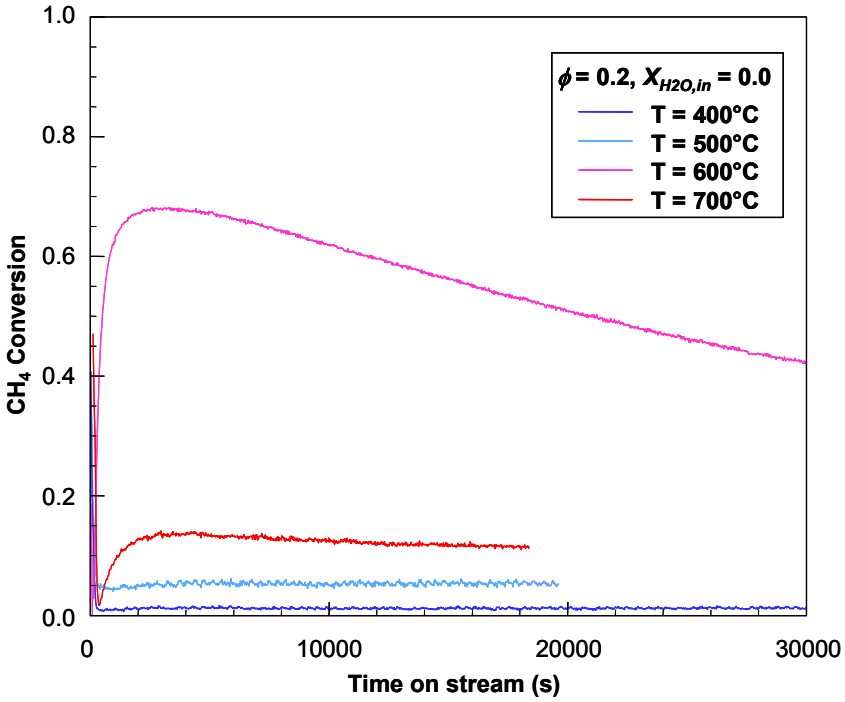

Figure 6.1a Isothermal activity of catalyst in time on stream (TOS) experiment

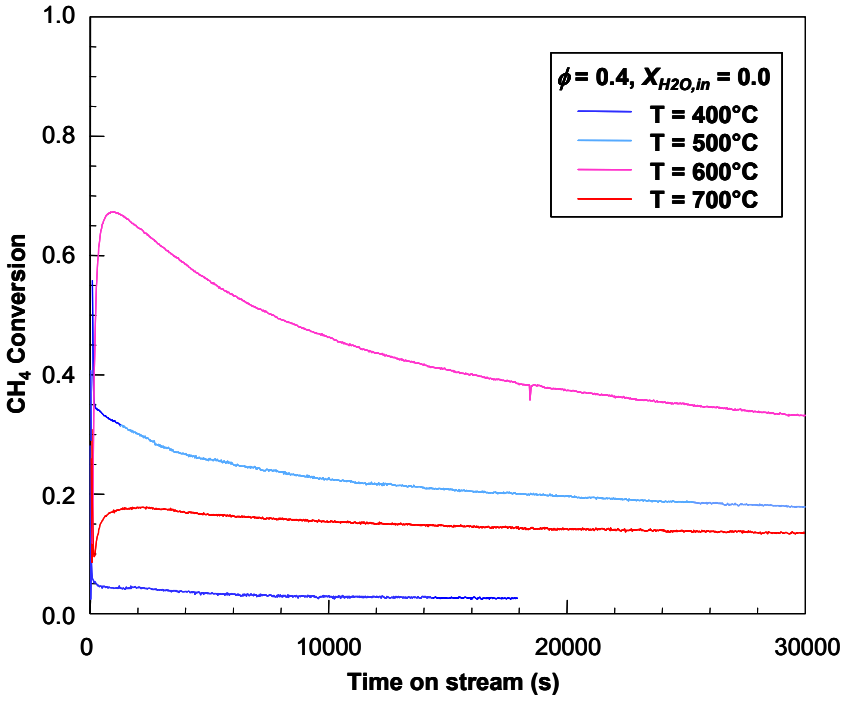

Figure 6.1b Isothermal activity of catalyst in time on stream (TOS) experiment

well as for the T_{in} = 500ºC at ϕ = 0.4 provides quantitative measures of the impact of PdO_x reduction on the CH_4 oxidation activity.

For the current study, two types of transient experiments were conducted: 1) time-on-stream studies where the inlet conditions remained fixed for as much as 10-12 hours and the transient response of the catalyst was observed and 2) temperature-programmed reactor (TPR) studies where T_{in} was cycled between 400ºC and 850ºC. Observations from the TPR studies were highly dependent on whether the maximum T_{in} was above the point where PdO_x began to undergo reduction for that particular combination of ϕ and $X_{H2O,in}$. If the maximum T_{in} was high enough such that significant PdO_x reduction occurred, then a hysteresis in activity like that observed in previous studies (McCarty 1995; Ciuparu et al. 2002) was identified. However, the current study extends the previous work by providing a more quantitative assessment of the effects of H_2O and CH_4 equivalence ratio ϕ.

The results shown in Figure 6.2 indicate that gas phase reactions are not significant until T_{in} > 850°C with full conversion occurring suddenly at T_{in} = 890°C. This result suggests that the catalytic conversion tests for $T_{in} \leq$ 850°C is certainly not due to gas phase reactions. Furthermore, the catalytic activity will suppress gas-phase reactions due to radical adsorption (Schlegel et al. 1996). Thus, conversion for $T_{in} \leq$ 850°C can be attributed to Pd catalyst activity.

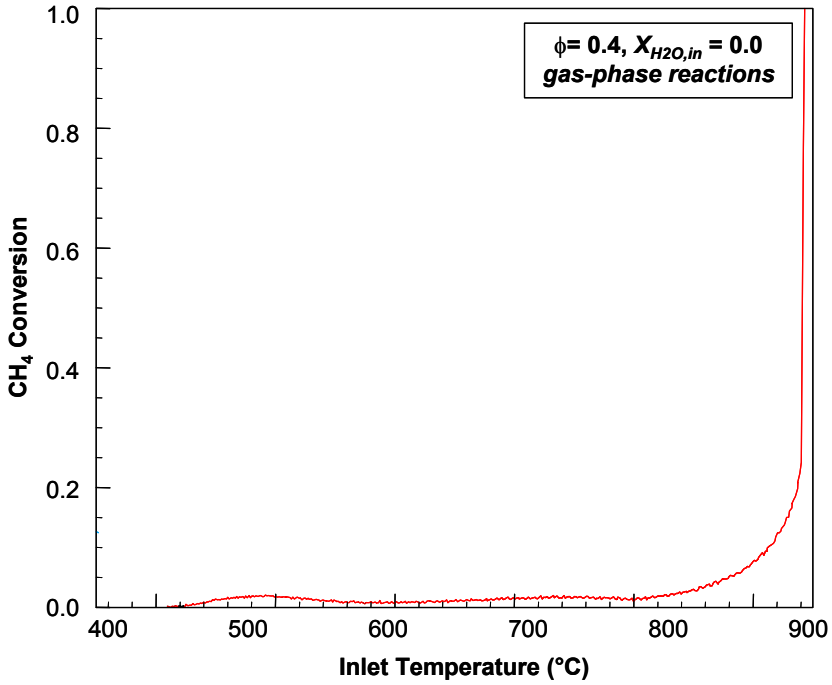

Figure 6.2 Contribution of gas phase reaction in CH_4 activity

6.3 Combustion of CH_4 on PdO catalyst

The experimental results show a strong correlation between CH_4 oxidation activity for the supported Pd-based catalysts and the expected content of PdO in the catalysts as suggested from the previous PdO_x oxidation/reduction studies (Wolf et al. 2003). For the current study when $P_{O2,in}$ = 0.1 atm.; and T_{in} is rises above 750°C, CH_4 conversion begins to decrease. If T_{in} continues to rise 800°C, CH_4 conversion begins to rise again shows a clockwise hysteresis loop for heating and cooling cycles, shown in Figure 6.4. The reduction of CH_4 conversion upon heating occurs at a temperature, $T_{red,}$ where it is expected that PdO undergoes rapid reduction to Pd both on the surface and in sub-surface regions (Ciuparu and Pfefferle 2001). As observed in heating and cooling of γ-Al_2O_3-supported PdO_x in O_2/diluent mixtures, the apparent reoxidation temperature T_{ox}

of PdO_x in 1% CH_4/ 9% O_2 / Ar balance mixtures during cooling from a high-temperature reduced state does not occur until between 150°C-200°C lower than T_{red} for the heating ramp.

The γ-Al_2O_3-supported catalyst was submitted to time-on-stream tests for four different inlet temperatures, T_{in}. Inlet velocity, u_{in}, is held constant for all tests at 1.5 m/s in order to maintain a constant residence time 6 ms. To ensure an initially fully oxidized PdO catalyst (surface and bulk) for all tests, the catalyst was held in a 10% O_2 in Ar mixture 450°C for 10 hrs before starting all tests. For T_{in} up to 500°C, CH_4 conversion remains stabilized after 8 hrs of time-on-stream as shown in Figure 6.1a. At the inlet temperature of 600°C for the same reactant mixture, the catalyst shows a decline in conversion. A slow reduction of PdO in the downstream regions of the catalyst may cause this slow decay in conversion because the measured temperature rise in the support is relatively small (< 10°C). Experiments with recovered catalyst confirmed the assumption. All the same at T_{in} = 600°C conversion remains significantly higher than for the T_{in} = 700°C case. The drop in activity for the 700°C correlates with an observed reduction of the PdO_x catalyst at this high inlet temperature and changes in color of catalyst.

Increasing the CH_4 inlet concentration to a ϕ = 0.4 (still with $P_{O2,in}$ = 0.1 atm.) was done to assess the effects of ϕ on the high temperature time-on-stream results. Experimental results are represented in Figure 6.1b. Trends for T_{in} at 700°C are almost the same for those cases in Figure 6.1a. This suggests that the high temperature chemistry on the reduced metal surface is likely first order in CH_4 concentrations. However, for the lower T_{in} from 400°C and 600°C, interesting differences are noted between the two

different ϕ's. The higher ϕ results in increased conversion at T_{in} = 400 and 500°C suggesting that based on the redox mechanism the increased oxide vacancies may be accelerating the conversion as is the case for lower temperature H_2 oxidation. For the 600°C case, a higher temperature rise in the catalyst bed (not detected by the thermocouples along the support) may have caused an increased reduction of the oxide-dominated surface which results in the faster decay in CH_4 conversion. These cases suggest that increased O_2 pressure is necessary to sustain high conversion for $T_{in} \geq 600$°C as it has been observed in Figure 6.9 (McCarty 1995).

Experimental TPR tests were performed where T_{in} was cycled up and down between 400°C and 650°C at 1°C/min with constant inlet feeds of 1% CH_4 / 9% O_2 (ϕ = 0.2) and 2% CH_4 / 9% O_2 (ϕ = 0.4) in Ar balances. The high temperature limit for these tests was chosen so as to avoid significant bulk phase transformation of PdO to Pd.

Figure 6.3a shows the CH_4 conversion for five consecutive cycles. With the high GHSV and low residence time (6 ms), CH_4 conversions remain at or below 50%. Nonetheless, this value is much lower than the estimated value of ~ 99% for the mass-transfer limited conversion based on approximate CH_4 diffusivities and Sherwood numbers indicating that kinetics control the conversion process as desired. The five heating and cooling cycles show slight differences in conversion with the initial cycle exhibiting higher conversion than the second and the other cycles. The second and third cycles exhibit very similar conversion with a slight increase in conversion for the third. In this temperature range (< 650°C) and O_2 partial pressures (~ 0.1 bar), the lack of hysteresis in activity or a region of negative apparent E_{act} suggests that bulk (subsurface) PdO does not undergo significant reduction which would influence the catalytic activity.

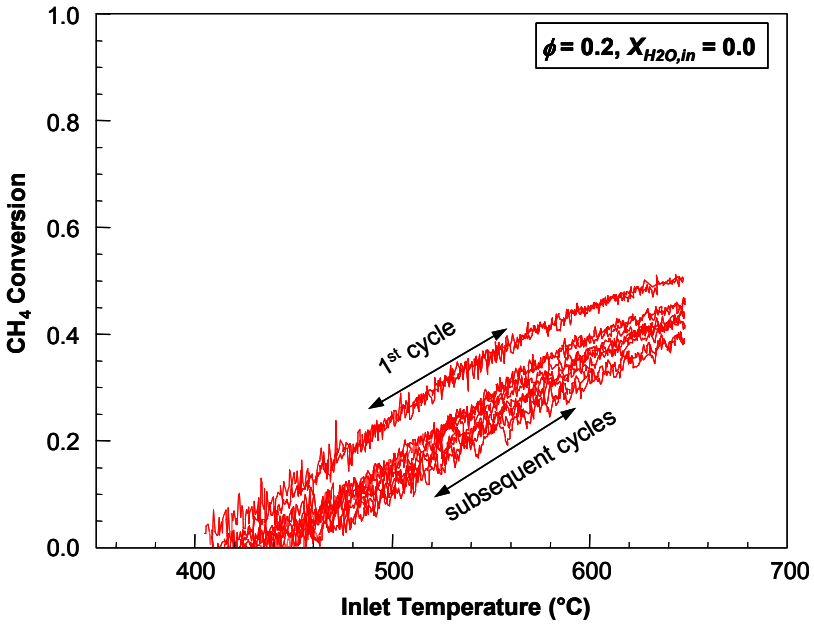

Figure 6.3a Change in CH_4 activity during TPR test

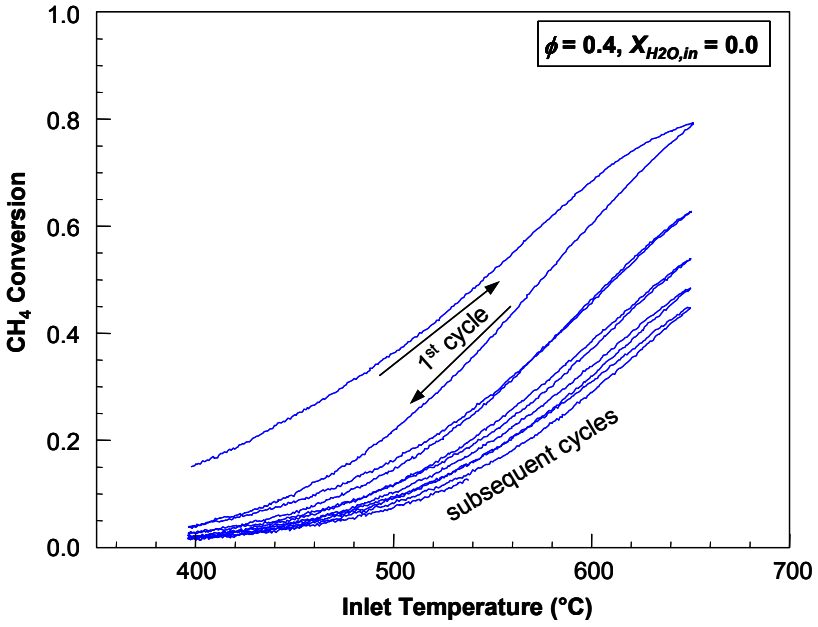

Figure 6.3b Change in CH_4 activity during TPR test

The differences in conversion during the five cycles can be attributed to partial reduction of PdO in higher temperatures of the cycle and not due to particle sintering as the catalyst regained its original activity upon full reoxidation. This reduction causes an activity drop for the next cycles. Increasing ϕ in flow over catalyst shows a distinguishable activity drop in consecutive cycles where difference between cycles decreases, shown in Figure 6.3b, suggesting the increased propensity for partial reduction of the PdO with the increased ϕ.

To study excursions in catalytic activity and the previously observed hysteresis in oxidation-reduction cycles, TPR tests, with heating rate 1.2 °C/min, were performed where T_{in} was cycled from 400°C to 850°C for both $\phi = 0.2$ with dry inlet ($X_{H2O,in} = 0.0$) and wet inlet ($X_{H2O,in} = 0.04$) flows. Experimental results are shown in Figures 6.4a and 6.4b. For the dry inlet, during the initial heating ramp, combustion starts after $T_{in} = 550$°C and the rates peak around 720°C. Above 720°C, PdO reduction begins to decrease CH_4 conversion until $T_{in} = 800$°C, at which point a second mechanism for CH_4 oxidation begins to cause a rapid increase with temperature in total CH_4 conversion. Upon cooling back down to 400°C inlet, the low temperature light-off drops almost 100°C from the initial ramp light-off ($T_{in} \approx 550$°C), to $T_{in} \approx 450$°C. During the cooling after the high-temperature reduction of the PdO_x, the activity decreases to a point where very limited conversion is sustained for T_{in} between 720°C and 620°C. However as T_{in} cools below 620°C, conversion increases as the catalyst appears to undergo reoxidation and

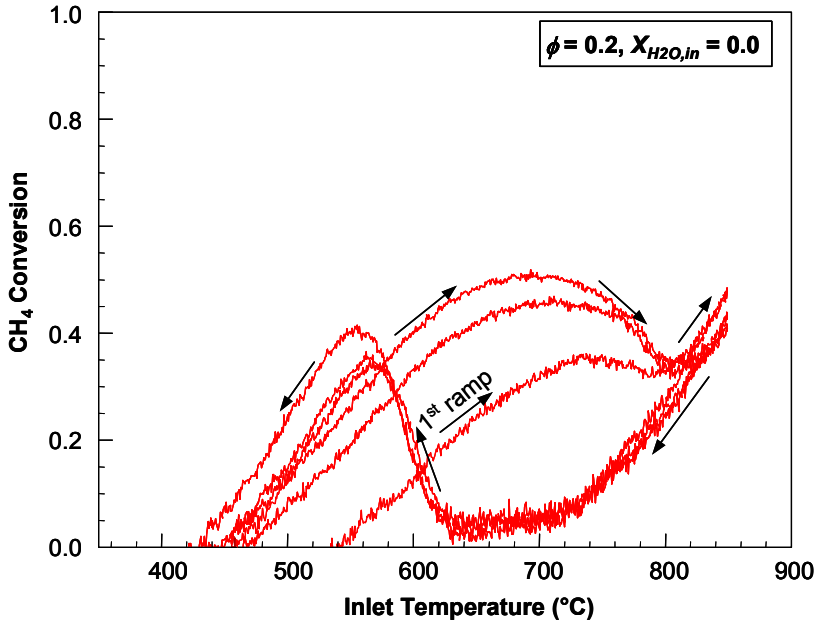

Figure 6.4a Catalytic activity in hysteresis test

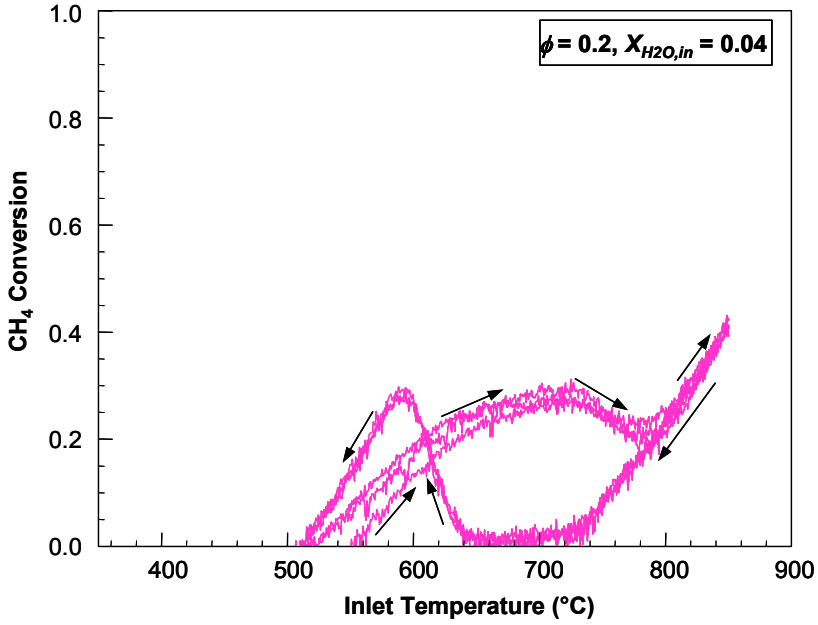

Figure 6.4b Catalytic activity in hysteresis test

thereby regains full activity in a somewhat similar manner observed in other studies (McCarty 1995; Ciuparu and Pfefferle 2001; Ciuparu et al. 2002). The region that activity increases while temperature decreasing suggests a negative activation energy and has been observed in the other investigations for CH_4 combustion over PdO catalysts (McCarty 1995; Lyubovsky et al. 1999).

Activity values recorded for the cooling ramp in the 600-400 °C region are higher than those observed for the heating ramp in the same temperature ramp in Figures 6.4 and 6.5, which determines a second activity hystresis and suggests that the catalysts undergoes an activation process (Ciuparu and Pfefferle 2001). Reactivation of the PdO_x catalyst initially results in a higher conversion at the same T_{in} in comparison with the heating half of the cycle. The increased activity upon initial reoxidation may arise from the restructuring of the catalyst due to increased oxide vacancies on the surface for CH_4 adsorption (Baldwin and Burch 1990). This conclusion is supported by the result that under low-temperature reaction conditions, “amorphous” PdO present initially transforms to a crystalline phase with a consequent increase in activity (Carstens et al. 1998). The second and third heating-cooling cycles also show higher activity during heating than the first cycle in agreement with results of other researchers (McCarty 1995; Ciuparu et al. 2002). Ciuparu et al. mention this effect is possibly result of the surface roughening noted by TEM and STM that occurs on reoxidation (Ciuparu et al. 2002), although it has been shown flowing a dry reaction mixture composed of 1% CH4, 4% O2 in He for 12 hrs over a zirconia-supported Pd catalyst at room temperature returned the TPR activity profile to the initial form (Ciuparu and Pfefferle 2001).

The cooling half of the second and third cycles also shows the same activity during the reduced and reoxidized states. For all cycles during the cooling part, there is an observed kinetic passivation (less reactive state) of the reduced surface Pd to reoxidation in oxygen uptake process. This persists until the temperature reaches between 620-640C, when apparent catalyst reactivation is driven by oxygen uptyake into the reduced Pd.

For the catalytic activity hysteresis gap for the $P_{O2,in}$ = 0.1 atm., T_{red} - T_{ox} (difference between reduction temperature and reoxidation temperature) for the γ-Al_2O_3-supported PdO_x is shown in the Table 6.1. These values seems relatively independent of ϕ but not so much inlet water $X_{H2O,in}$ as shown by comparing Figure 6.4a with Figure 6.5a and Figures 6.4b and 6.5b (which show the similar activity hysteresis for ϕ = 0.4). This multiplicity steady states may arise from the species interaction potentials giving multiple steady state or from kinetics of buk PdO being too slow. From Wolf et. al and Datye et al. (Datye et al. 2000) analysis has suggested that thermodynamics of surface and subsurface soecies provide more than one equilibrium state 1) with predominantly an oxide bulk and surface and 2)with a reduced metallic subsurface and surface. The most common source of multiplicity in catalytic reactors is due to the nonmonotonic dependency of the intrinsic reaction rate on the concentration of reactants

Table 6.2 Hysteresis temperature gap at different inlet conditions

Test Inlet Conditions	$T_{red} - T_{ox}$ °(C)
ϕ = 0.2, $X_{H2O,in}$ = 0.0	80
ϕ = 0.2, $X_{H2O,in}$ = 0.04	120
ϕ = 0.4, $X_{H2O,in}$ = 0.0	80
ϕ = 0.4, $X_{H2O,in}$ = 0.04	20

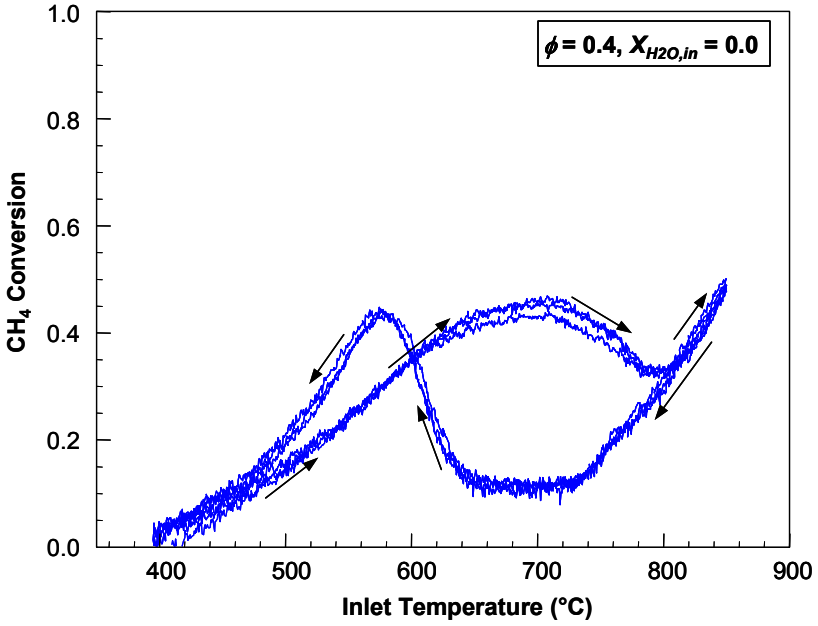

Figure 6.5a Change of CH_4 activity in hysteresis test with higher ϕ

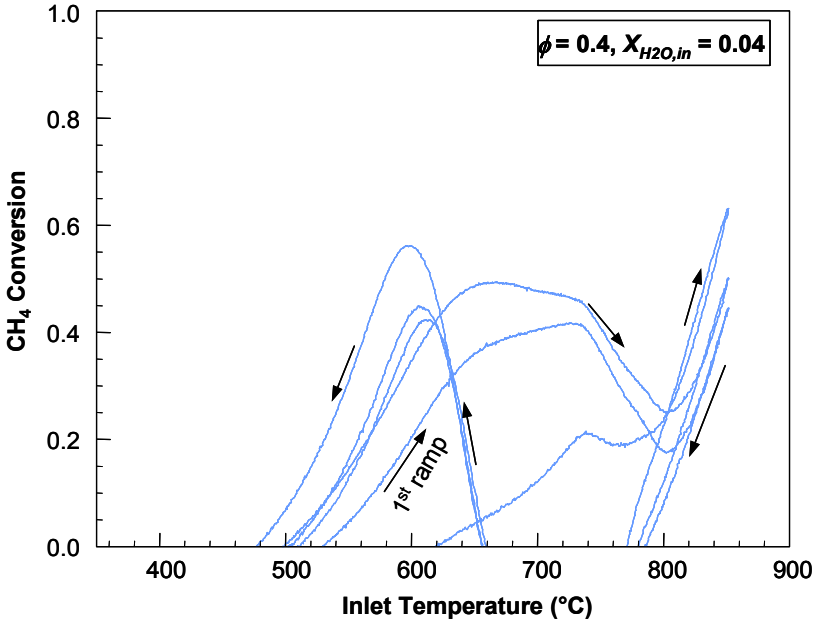

Figure 6.5b Change of activity CH_4 of in hystresis test with higher ϕ

and products (concentration (isothermal) multiplicity) within the boundaries of the system (reactor).

In Figure 6.6 the reoxidation data are shown in the Arrhenius coordinates. The activation energy of CH_4 oxidation reaction at the beginning of the cooling ramp is found to be $E_a \approx 45$ kcal/mol, consistent with metallic Pd state (Lyubovsky and Pfefferle 1998). In the middle of test where the conversion increases while temperature decreasing the apparent activation energy has a negative value. The experimental data doesn't show a line to define activation energy for this range of temperature. At the end of the run experimental data can be fitted in a line to find activation energy. The slope of the line gives activation energy $E_a \approx 20$ kcal/mol corresponding to the PdO state of the catalyst. These values are pretty well in the other literatyre (McCarty 1995; Lyubovsky and Pfefferle 1998; Ciuparu et al. 2002)

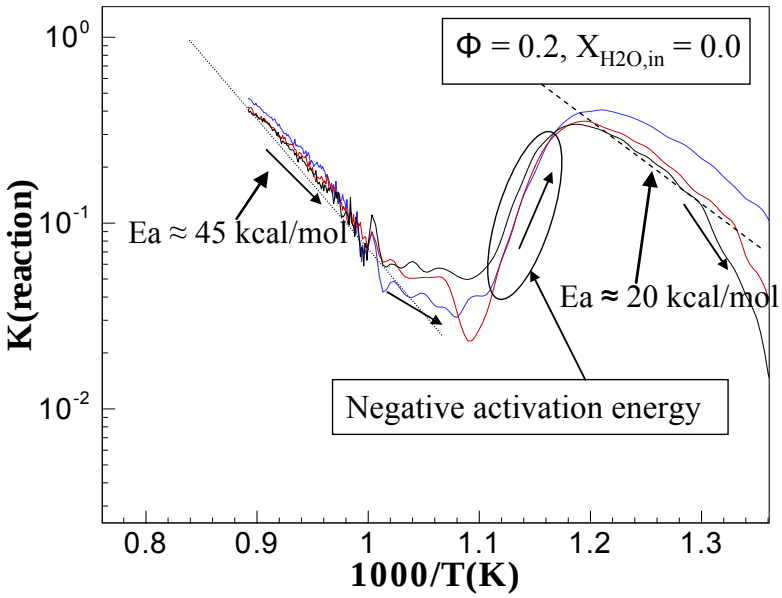

Figure 6.6 Activation energy calculated from the slope of the correspondent lines for cooling cycles

It is generally accepted H_2O has an inhibiting effect on CH_4 activity of supported Pd-based catalysts (Ciuparu and Pfefferle 2001; Ciuparu et al. 2002). It has been proposed the formation of palladium hydroxide (OH(sb)) blocks active sites for CH_4 adsorption. The TPR profiles obtained for the supported catalyst using a wet feed with 4 vol.% of water, depicted in Figure 6.4b and Figure 6.5b. The profiles are qualitatively the same as the dry inlet feed, but water can be seen to have a strong effect of reducing activity for conditions where activity is controlled by surface oxide chemistry.

Interestingly, H_2O has no noticeable effect on PdO decomposition temperature or on CH_4 activity at the higher T_{in} where reduced metal catalysis dominates conversion as shown in Figures 6.4b and Figure 6.5b. As it is shown in Figure 6.5b, it shows conversion very small, when catalyst is in reduced form. This is compatible with the blocked sites by water in this high temperatures (Ciuparu and Pfefferle 2001). These observations are also

observed in the time-on-stream experiments shown in Figure 6.7. For T_{in} = 700°C, $X_{H2O,in}$ has a very minor impact on long-term CH_4 conversion whereas for the lower T_{in} = 500°C, the 4 % H_2O has a profound reduction in CH_4 conversion (from > 20% to < 5%). Nonetheless, for the γ-Al_2O_3 supported catalysts, the H_2O inhibition was found to be fully recoverable after several hours of dry inlet feed. The reduction in low temperature activity due to H_2O is observed in the heating cycles for both ϕ's as indicated in both Figures 6.4 and 6.5 where low temperature light-off is delayed by as much as 100°C. This has profound implications for gas turbine operation in humid environments as the 4% H_2O inlet is comparable to what is found in air on a warm humid day.

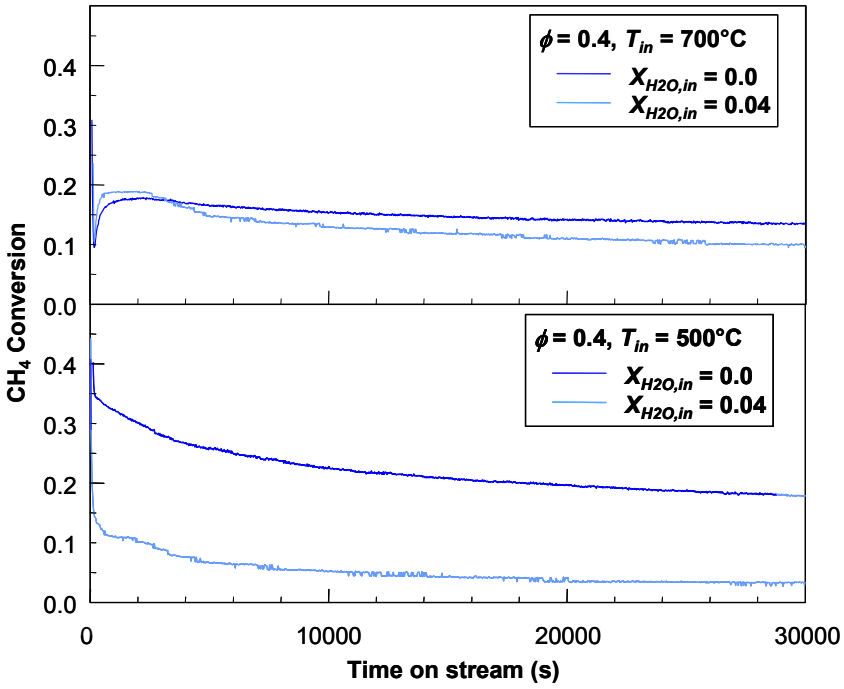

Figure 6.7 Effect of water in time on stream experiment

The slow transient decay of the catalyst activity observed in the time-on-stream experiments for $T_{in} \geq 500°C$, as shown in Figures 6.1, 6.3, and 6.7 was not found to be permanent, but rather activity could be completely recovered by reoxidation for no more than 4 hours at 450°C. This is indicated in Figure 6.8 which shows that for both dry and wet inlet feeds transient activity profiles can be fully recovered after reoxidation (2nd run in Figure 6.8). This result shows the amazing stability of the catalyst formulation and indicates that this catalyst will likely be a good candidate for front end reactors in the demanding gas turbine applications.

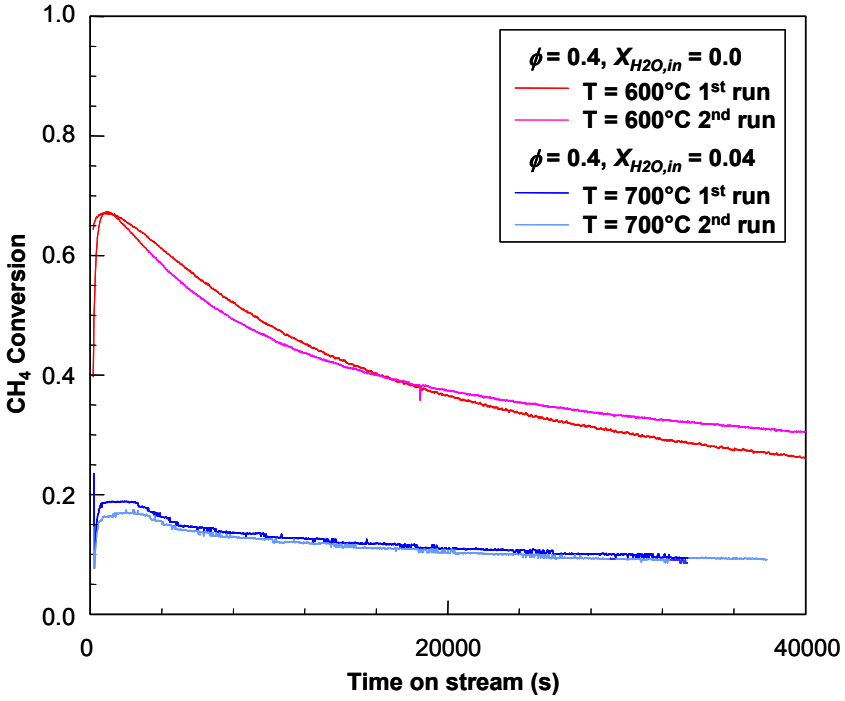

Figure 6.8 Repeatability of time on stream experiments

Figure 6.9 shows how increasing the partial $P_{O2,in}$ to 0.2 atm impacts the CH_4 activity in the heating and cooling cycles from 400 to 850°C. The increase in $P_{O2,in}$ also increases the $P_{CH4,in}$ which increases the heat load on the reactor and may cause the

higher conversion and improved low temperature light-off (T_{in} < 400°C) for the catalyst in the oxidized state. Some interesting features are observed by comparing the $P_{O2,in}$ = 0.1 atm. and $P_{O2,in}$ = 0.2 atm cases in Figure 6.9. The high temperature reduction is increased only by about 20°C with the increased $P_{O2,in}$, and the high temperature chemistry appears to be either zero or first order with respect to O_2 concentration as both cases fall on top of each other for the high temperature reduced chemistry. Upon cooling, the higher $P_{O2,in}$ case does not completely lose activity and in fact begins to reoxidize the catalyst (as signified by increasing conversion) at temperatures around 680°C, i.e. 60°C higher than the $P_{O2,in}$ = 0.1 atm. case. In general upon subsequent ramps, the CH_4 conversion for both $P_{O2,in}$ cases are similar in the temperature range of 400-500°C.

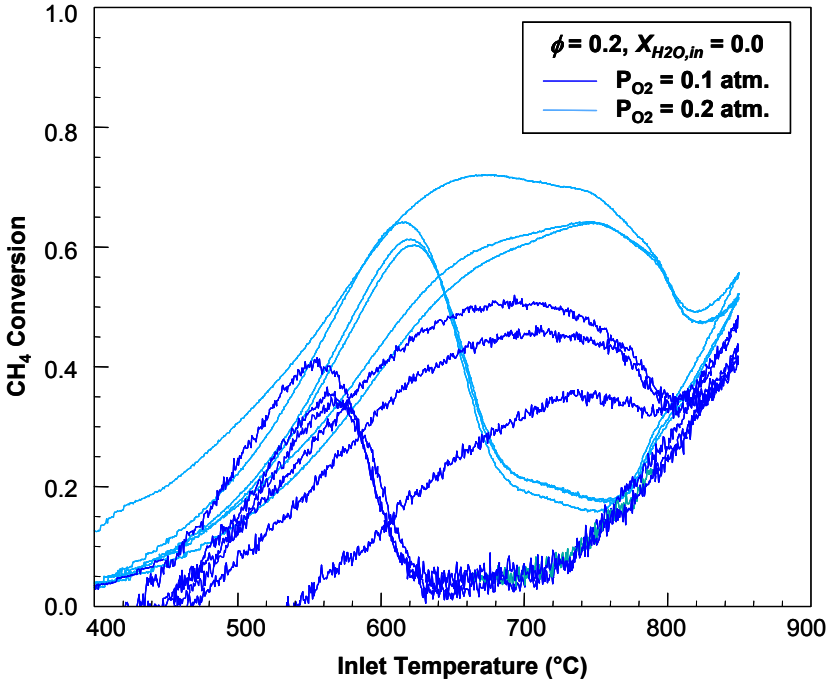

Figure 6.9 Effect of partial pressure of O_2 in TPR tests

6.4 Conclusion

The extended experimental effort has been implemented to provide some clear fundamental results that will help in validation of a detailed chemical mechanism for lean CH_4 combustion over Pd-based catalysts for developing predictive tools for catalytic reactor design. It was revealed contribution of gas phase to catalytic activities limited to $T_{in} > 850°C$. Also, repeatability of experimental data was shown. Hysteresis temperature gap (80°C) was not changed by fuel concentration, ϕ. However, with $X_{H2O,in}$ =0.04, the temperature gap has dropped from 120°C in $\phi = 0.2$ to around 20°C at $\phi = 0.4$. Also, effect of O_2 partial pressure on temperature gap was revealed.

Chapter 7

Assessment of Pd-CH_4 Surface Chemistry

7.1 Introduction

To capture the unique transient behavior of the Pd-PdO_x thermochemistry (McCarty 1995) and its effect on CH_4 combustion activity, efforts have been ongoing to develop a detailed chemistry model for CH_4 combustion on Pd-based catalysts. Such a detailed mechanism will allow to explore reactor optimization strategies for the broad range of performance and to implement transient reactor models of lean catalytic combustor performance which will capture the complex behavior of the catalyst at expected combustor operating conditions.

In this chapter, surface chemistry of CH_4 over the Pd-based catalysts is developed based on the surface chemistry subsets for Pd-O_2, Pd-O_2-H_2 , Pd-O_2-CO and CH_4 decomposition on PdO/Pd. Then numerical model predictions and experimental results in different conditions are compared. Finally, to identify critical chemical pathways in the CH_4 surface chemistry, sensitivity analysis is conducted.

7.2 Model description

The modeling approach is follows that presented in Chapter 3. The model integrates a 1-D gas-phase flow channel model with a radially discretized porous washcoat model that includes detailed surface chemistry and thermal transport through the porous media. Mass and heat transport from the gas-phase channel flow is modeled using the equations 3.41 and 3.42 (Beretta et al. 1999). Although there are some

uncertainties to the accuracy of these models, it was found that a 50% increase in the Sh_k for the fuel (the most important transport) resulted in less than a 10% increase in conversion. The test was run under a temperature ramp 400-850C at $\phi = 0.2$. These results suggest that designed surface kinetics are predominantly controlling the rate of fuel conversion for the conditions in this study. Such conditions are critical to compare surface chemistry mechanism predictions with experimental results. Thus, all the correlations were considered accurate enough for the heat and mass transport between the porous washcoat and the channel flow such that the computationally efficiency of the 1D gas-phase flow could be implemented for investigating surface chemistry model. The 1D channel flow model facilitated rapid simulations for assessing complex surface chemistry with a relatively large number of surface species (~ 20).

7.3 Surface mechanism of Pd-CH_4 combustion

The complicated nature of the Pd-PdO_x chemistry (Wolf et al. 2003) and its hysteretic influence on activity for CH_4 oxidation has made surface chemistry modeling of CH_4 on Pd catalysts a challenging problem. This has caused efforts to focus on the more well understood system of CH_4 combustion on Pt. In order to make a surface chemistry valid on a broad range of operating conditions, surface model must include significant details. A full surface chemistry of Pd-CH_4 involves several key subsets of surface chemistry mechanisms and their interactions: 1) Pd/O_2, 2) Pd/H_2/O_2 and 3) Pd/O_2/CO. The first surface chemistry is well validated for hysteretic surface chemistry of Pd-O_2 over a wide range and included in the surface chemistry model of Pd-CH_4 (Wolf et al. 2003). The second one which was proposed and validated in Chapter 4 for temperatures less than 200°C provides a portion of the Pd-O_2-H_2 needed for higher

temperature CH_4 combustion. In higher temperatures, H_2 can reduce bulk phase oxide. Development of surface chemistry mechanism for Pd-CH_4 follows the same method that was applied for Pd-O_2-H_2 in Chapter 4.

The kinetics of CH_4 combustion on Pd catalysts at low temperatures are believed to follow a redox mechanism, where CH_4 is oxidized by lattice oxygen, and reduced catalyst is subsequently reoxidized by gas phase O_2 (Fujimoto et al. 1998; Muller et al. 1999). The oxygen lost from the catalyst during dissociative adsorption of CH_4 can be replenished by dissociative adsorption of O_2 from the gas phase or diffusion from bulk oxide of catalyst (Au-Yeung et al. 1999).

For CH_4, two different chemical decomposition pathways are postulated for the mechanism: 1) dissociative adsorption of CH4 on Pd metallic sites and oxide vacancies Pd(sb) , 2) oxygen-assisted hydrogen abstraction from CH_x species due to CH_4 adsorption on oxide site of Pd, O(sb). Under oxidizing envitonments (i.e. $\phi << 1$), these H abstraction processes can be modeled as irreversible (Hei 1998). In pyrolytic pathways, abstracted hydrogen atoms are in form of chemisorbed hydrogen, H(s) or hydrogen on oxide vacancy, H(sb). E_{act} for the first activated adsorption process on Pd metal is estimated at 197 kJ/mol (Lyubovsky and Pfefferle 1998), however, the subsequent H abstractions have different energy barriers (Hei 1998).

$$CH_4 + Pd(sb) + Pd(sb) \rightarrow CH_3(sb) + H(sb) \tag{7.1}$$

$$CH_4 + Pd(s) + Pd(s) \rightarrow CH_3(s) + H(s) \tag{7.2}$$

For oxygen-assisted CH_4 dissociative adsorption, a dual site reaction involving O(sb) and the oxide vacancy Pd(sb) must take place and the estimated E_{act} for this activated adsorption is 81 kJ/mol (Lyubovsky and Pfefferle 1998):

$$CH_4 + Pd(sb) + O(sb) \rightarrow CH_3(sb) + OH(sb) \quad (7.3)$$

Sticking coefficients for CH_4 adsorption were tuned for the conditions in the current study. For the Pd-O_2-CO surface chemistry, previous mechanism developed by others (Hartmann et al. 1994) ha sbeen adapted in a thermodynamically consistent manner with the Pd-O_2 and Pd-H_2-O_2 surface chemistry.

The thermodynamics that governs the reversible reaction rates are given in Table 7.1 where species enthalpies relative to zero energy levels defined by gas phase enthalpies and pure Pd metal. Where possible these thermodynamics are taken from the desorption enthalpies of adsorbates, otherwise they are tuned by a parametric study. The interaction potentials are all based on some physical intuition or tuned as a parameter. The surface reaction mechanism is given in Table 7.2. It is combined with bulk-surface interface reactions that are provided in Table 7.3. The interaction between the bulk reactions and the surface reactions is largely driven by the instability of the oxide-based species ((sb) species) as the bulk mole fraction of reduced Pd $Z_{Pd(b)}$ increases. This instability which shows up in the surface thermodynamics causes a very significant change in the nature of the surface reactions when the bulk undergoes reduction. The surface reactions are coupled to the bulk through the H(sb) abstraction of bulk O(b) (reaction 33f) and through the creation of vacancies by fuel oxidation reactions.

Table 7.1 – Surface thermodynamics with interaction potentials for surface and bulk species in Pd/PdO_x catalyst; h_k relative to standard gas phase enthalpies

Surface Species	**h_k (in kJ/gmol)**
Pd(s)	0.0
Pd-O(s)	$-115.0+57.5\theta_{O(s)}+29.0\theta_{OH(s)}$
Pd-O(sb)	$-115.0+35.0Z_{Pd(b)}$
Pd(sb)	$-35.0+208\theta_{Pd(sb)}+147\theta_{H2O(sb)}+208\theta_{H(sb)}+104\theta_{OH(sb)}+35.0Z_{Pd(b)}+35.0Z_{H(b)}$
Pd-O_2(sb)	$-105.0+35.0Z_{Pd(b)}$
Pd-H(s)	$-42.0+8.0\theta_{H(s)}$
Pd-OH(s)	$-214.0+29.0\theta_{O(s)}+14.5\theta_{OH(s)}$
Pd-H_2O(s)	-302.0
Pd-H(sb)	$-57.0+208\theta_{Pd(sb)}+147\theta_{H2O(sb)}+208\theta_{H(sb)}+104\theta_{OH(sb)}+35.0Z_{Pd(b)}+35.0Z_{H(b)}$
Pd-OH(sb)	$-229.0+104\theta_{Pd(sb)}+73.5\theta_{H2O(sb)}+104\theta_{H(sb)}+52\theta_{OH(sb)}+35.0Z_{Pd(b)}+35.0Z_{H(b)}$
Pd-H_2O(sb)	$-332.0+147\theta_{Pd(sb)}+104\theta_{H2O(sb)}+147\theta_{H(sb)}+73.5\theta_{OH(sb)}+35.0Z_{Pd(b)}+35.0Z_{H(b)}$
Pd-C(s)	-40.0
Pd-CO(s)	$-274.0+10.5\theta_{CO(s)}$
Pd-CH(s)	N/A
Pd-CH_2(s)	N/A
Pd-CH_3(s)	N/A
Bulk Species	**h_k (in kJ/gmol)**
Pd(b)	$-25.0+25.0Z_{O(b)}$
Pd-O(b)	$-80.0+25.0Z_{Pd(b)}+25.0Z_{H(b)}$
Pd-H(b)	$-45.0+25.0Z_{H(b)}$

Table 7.2 – Pd-O_2-H_2-CH_4 surface reactions for mechanism used in numerical model

Reactions	A or stick coeff	E_{act} [kJ/mol]
Adsorption/Desorption Rxns.		
1f) $O_2+2Pd(s) \Rightarrow 2O(s)$	$0.8*T^{-0.5}$	0.0
1r) $2O(s) \Rightarrow O_2+2Pd(s)$	$5.7*10^{21}$	$230 -115\theta_{O(s)}$
2f) $O_2+Pd(sb) \Rightarrow O_2(sb)$	$1.0*T^{-0.5}$	0.0
2r) $O_2(sb) \Rightarrow O_2+Pd(sb)$	$1.0*10^{13}$	70
3f) $H_2+2Pd(s) \Rightarrow 2H(s)$	$4.0*T^{-0.5}$	0.0
3r) $2H(s) \Rightarrow H_2+2Pd(s)$	$5.7*10^{21}$	$84 -16\theta_{H(s)}$
4f) $H_2+Pd(sb)+O(sb) \Rightarrow H(sb) +OH(sb)$	$8.0*T^{-0.5}$	0.0
4r) $OH(sb)+H(sb) \Rightarrow H_2+Pd(sb)+O(sb)$	$5.7*10^{21}$	$136 + C_{4r}$[a]
5f) $H_2O+Pd(s) \Rightarrow H_2O(s)$	0.50	0.0
5r) $H_2O(s) \Rightarrow H_2O+Pd(s)$	$1.0*10^{13}$	60.2
6f) $H_2O+Pd(sb) \Rightarrow H_2O(sb)$	0.50	0.0
6r) $H_2O(sb) \Rightarrow H_2O+Pd(sb)$	$1.0*10^{13}$	$55.2 + C_{6r}$[a]
7f) $CH_4+2Pd(s) \Rightarrow CH_3(s)+Pd(s)$	8.0	160.0
8f) $CH_4+Pd(sb)+O(sb) \Rightarrow CH_3(s)+OH(sb)$	0.08	45.0
9f) $CH_4+2Pd(sb) \Rightarrow CH_3(s)+H(sb)$	0.08	85.0
10f) $CO_2+2Pd(s) \Rightarrow CO(s)+O(s)$	0.005	81.0
10r) $CO(s)+O(s) \Rightarrow CO_2+2Pd(s)$	$5.7*10^{21}$	$185+57.5\theta_{O(s)}+29\theta_{OH(s)}+10.59\theta_{CO(s)}$
11f) $CO_2+2Pd(sb) \Rightarrow CO(s)+O(sb)$	0.005	121.0
11r) $CO(s)+O(sb) \Rightarrow CO_2+2Pd(sb)$	$5.7*10^{21}$	$46.5+ C_{11r}$[a]
Reversible Surface Rxns.	$5.0*10^{11}$	90
12) $O(s) \Leftrightarrow O(sb)$	$5.7*10^{21}$	0.0
13) $O_2(sb)+Pd(sb) \Leftrightarrow 2O(sb)$	$5.7*10^{21}$	$185 - 57.5\theta_{O(s)}$
14) $O_2(sb)+Pd(s) \Leftrightarrow O(sb)+O(s)$	$5.7*10^{20}$	60
15) $H(s)+Pd(sb) \Leftrightarrow H(sb)+Pd(s)$	$5.7*10^{21}$	50
16) $H(s)+O(s) \Leftrightarrow OH(s)+Pd(s)$	$5.7*10^{21}$	55
17) $H(s)+OH(s) \Leftrightarrow H_2O(s)+Pd(s)$	$5.7*10^{21}$	102
18) $OH(s)+OH(s) \Leftrightarrow H_2O(s)+O(s)$	$5.7*10^{20}$	$117 + 8\theta_{H(s)}$
19) $OH(sb)+Pd(s) \Leftrightarrow H(s)+O(sb)$	$5.7*10^{20}$	$45 + C_{15f}$[a]
20) $H(s)+OH(sb) \Leftrightarrow H_2O(sb)+Pd(s)$	$5.7*10^{21}$	122
21) $OH(sb)+Pd(sb) \Leftrightarrow H(sb)+O(sb)$	$5.7*10^{21}$	121
22) $H_2O(sb)+Pd(sb) \Leftrightarrow H(sb)+OH(sb)$	$5.7*10^{21}$	81
23) $OH(sb)+OH(sb) \Leftrightarrow H_2O(sb)+O(sb)$	$5.7*10^{20}$	95
24) $H_2O(sb)+O(s) \Leftrightarrow OH(sb)+OH(s)$	$5.7*10^{21}$	200
25) $CO(s)+Pd(sb) \Leftrightarrow C(s)+O(sb)$	$5.7*10^{21}$	$175+57.5\theta_{O(s)}+29\theta_{OH(s)}$
26) $CO(s)+Pd(s) \Leftrightarrow C(s)+O(s)$	$5.7*10^{21}$	$215+57.5\theta_{O(s)}+29\theta_{OH(s)}$
Essentially Irreversible Surface Rxns.		
27) $CH_3(s)+O(sb) \Rightarrow CH_2(s)+OH(sb)$	$5.7*10^{21}$	$103 + C_{4r}$[a]
28) $CH_2(s)+O(sb) \Rightarrow CH(s)+OH(sb)$	$5.7*10^{21}$	$94 + C_{4r}$[a]
29) $CH(s)+O(sb) \Rightarrow C(s)+OH(sb)$	$5.7*10^{21}$	9.0
29) $CH_3(s)+Pd(s) \Rightarrow CH_2(s)+H(s)$	$5.7*10^{21}$	51
29) $CH_2(s)+Pd(s) \Rightarrow CH(s)+H(s)$	$5.7*10^{21}$	20
29) $CH(s)+Pd(s) \Rightarrow CH(s)+H(s)$	$5.7*10^{21}$	51

[a] Coverage dependencies: $C_{4r} = -104\theta_{Pd(sb)} - 73.5\theta_{H2O(sb)} - 104\theta_{H(sb)} - 52\theta_{OH(sb)}$,

$C_{6r} = 61\theta_{Pd(sb)}+43\theta_{H2O(sb)}+61\theta_{H(sb)}+30.5\theta_{OH(sb)}$,

$C_{11r} = 416\theta_{Pd(sb)}+294\theta_{H2O(sb)}+416\theta_{H(sb)}+208\theta_{OH(sb)}-10.5\theta_{CO(s)}+35Z_{Pd(b)}+35Z_{H(b)}$

$C_{15f} = 43\theta_{Pd(sb)}+30.5\theta_{H2O(sb)}+43\theta_{H(sb)}+21.5\theta_{OH(sb)}$

Table 7.3 – Pd-O-H bulk reactions for mechanism used in numerical model

Bulk-Surface Interface Reactions	A or stick coeff	E_{act} [kJ/mol]
30f) Pd(b)+O(sb) ⇒ O(b)+Pd(sb)	$2.0*10^5$	$90 + C_{30f}$[a]
30r) O(b)+Pd(sb) ⇒ Pd(b)+O(sb)	$2.0*10^5$	$65+35\theta_{O(sb)} +35\theta_{O2(sb)}+25Z_{O(b)}$
31f) Pd(b)+H(sb) ⇒ H(b)+Pd(sb)	$8.0*10^5$	45
31r) H(b)+Pd(sb) ⇒ Pd(b)+H(sb)	$8.0*10^5$	$23+8\theta_{H(s)}$
32f) Pd(b)+H(s) ⇒ H(b)+Pd(s)	$8.0*10^5$	45
32r) H(b)+Pd(s) ⇒ Pd(b)+H(s)	$8.0*10^5$	43
33f) H(sb)+O(b) ⇒ OH(sb) +Pd(b)	$8.0*T^{-0.5}$	$40+25Z_{O(b)}$

[a] Surface coverage dependencies: $C_{30f} = 173\theta_{Pd(sb)}+173\theta_{H(sb)}+69\theta_{OH(sb)}+112\theta_{H2O(sb)}-10.5\theta_{CO(s)}+25Z_{Pd(b)}+25Z_{H(b)}$

7.4 Testing of numerical results for Pd-CH_4

The experimental results in Chapter 6 provide detailed kinetic information to assist in validation of a detailed chemical mechanism for lean CH_4 combustion over Pd-based catalysts. Such an effort is very challenging, and only preliminary mechanisms for predicting low temperature CH_4 light-off have been reported in the archival literature for Pd-based catalysts (Fujimoto et al. 1998; Sidwell et al. 2003). As a goal for this study was to go beyond those mechanisms and utilizing thermodynamic consistency and previous literature references develop a mechanism that captures not only low-temperature light-off but also the high temperature reduction and hysteretic reoxidation/reactivation of the catalyst. This has been considered critical for understanding the limits of Pd catalyst for high-pressure applications where the high temperature reduction will impact the short-term stability of the catalyst as well as its operational temperature limits. With such a detailed model, a lean combustor may be optimized and furthermore transient start-up issues can be addressed through detailed modeling studies.

As presented in Chapter 3, the model utilizes specific geometric properties including catalyst surface area per washcoat volume ratio a_{cat}, catalyst dispersion σ_{cat}, washcoat porosity ε and washcoat thickness δ_{wc}. It was observed final result of the full reactor model and the channel flow model with uniform washcoat doesn't shift final conversion, thereby allowing the radial discretization to be neglected as for the conditions of interest. This was beneficial because of the long-time scales for the modeling the heating and cooling cycles runs for exploring parametric modifications to the surface chemistry.

The model was run under both isothermal conditions at T_{in} and under conditions where heat generation and loss were simulated to calculate the temperature rise through the reactor. In both cases, time steps for the numerical integration were limited to time steps ≤ 0.2 s. For the 1 cm long reactor, a variable-spacing grid of 10 cells (finer near the reactor entrance) was sufficient to capture transient behavior of the surface along the reactor axis. Physical input parameters and inlet conditions are provided in Table 7.4.

Table 7.4 Flow conditions and physical parameters of the annular reactor

Physical Parameters:	
Length of the reactor	1.0 cm
Porosity of washcoat	0.5
Density of solid phase of washcoat	3.94 g/cm^3
Site density per unit washcoat surface area	1.75e-09 sites/cm^2
Dispersion of the Catalyst	10 %
Wall thermal conductivity	0.22 W/(cm.K)
Washcoat Thickness	20 μm
Annular channel height	0.068 cm
Specific heat at constant volume	0.765 kJ/kg.K
Specific area in washcoat	2000 cm^{-1}
Inlet Flow Conditions for Case of CH_4	
Pressure	1atm
Temperature	673.15 – 1123.15 K
Velocity	1.5m/s
CH_4 concentration	1.0mol%
O_2 concentration	9.0mol%
Ar concentration	90.0mol%

The preliminary mechanism presented in Tables 7.2-7.3 presents a thermodynamically consistent mechanism based on species enthalpies including surface species interaction potentials and simple assumptions about constant entropies of surface species. The mechanism has not been fully optimized, but it does predict qualitatively CH_4 light-off, high temperature Pd reduction and associated loss in CH_4 activity at the tested $P_{O2,in}$, and the hysteresis observed in reoxidation/reactivation upon cooling in temperature cycles. This is illustrated in Figure 7.1a which compares model predictions both assuming a uniform temperature (= T_{in}) and calculating the energy equation with expected heat losses where the catalyst temperature bed may rise as much as 50-100°C.

The difference in model predictions between how the reactor temperature is handled illustrates the challenges in validating complex chemical kinetics mechanism for phenomena as complex as CH_4 combustion over PdO_x catalysts. While both the uniform

T and the full energy equation simulations of the heating and cooling cycles between 400 and 850°C show the reduction in activity upon PdO reduction, they show reduction at different T_{in} with the energy equation simulation occurring in stages at T_{in} between 650 and 700°C. This reduction occurs because most of the catalyst bed is calculated to be100°C hotter than T_{in}. The sharp rise in CH_4 conversion for the energy equation simulation suggests that the thermal mass of the catalyst bed is underestimated and increasing this may give a conversion profile much more similar to the experimental conditions.

The uniform T simulations in Figure 7.1a for $\phi = 0.2$, $P_{O2,in} = 0.1$ atm., and $X_{H2O,\,in} = 0.00$ and in Figure 7.1b for $\phi = 0.2$ and $X_{H2O,\,in} = 0.04$ indicate how rapid reduction of PdO results in a similarly rapid drop in CH_4 oxidation rates which is not recovered upon cooling until T_{in} drops 200°C below the original T_{red}. This is a larger hysteresis loop than observed in the experiments.

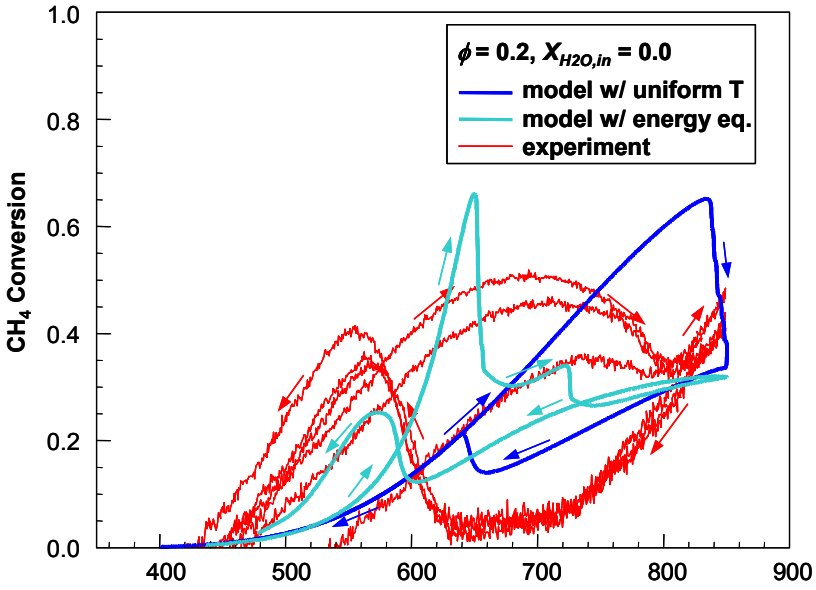

Figure 7.1a Comparison of experimental cycles with model predictions

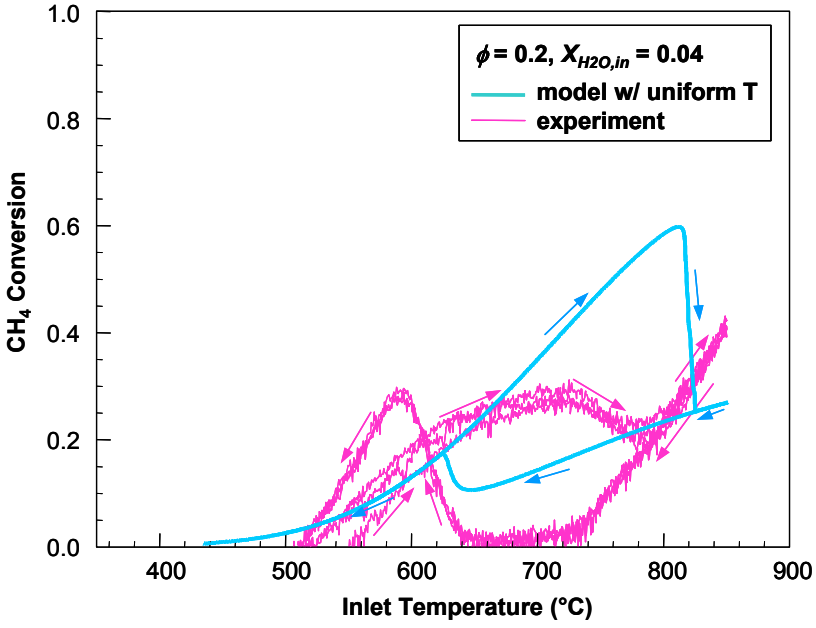

Figure 7.1b Comparison of experimental cycles with model predictions

Nonetheless, the mechanism does capture the qualitative trends including the minimal impact of X_{H2O} on the CH_4 oxidation over the reduced Pd at high T_{in}.
The conducted experiments showed a temperature rise < 10°C. Figure 7.2 compares the model predictions for the uniform T approximation at $\phi = 0.4$, $P_{O2,in} = 0.1$ atm, and $X_{H2O,\,in} = 0.00$, and trends are similar to those for $\phi = 0.2$. The model predictions agree with the experimental observations that ϕ does not play a significant role in high temperature activity at the low-pressure conditions. It was observed that the predicted fraction of bulk Pd oxidized at different inlet conditions correlates directly with the CH_4 oxidation hysteresis and this suggests the importance of the surface oxide coupling with the bulk phase on catalyst activity.

On the other hand, the current version of the mechanism fails to capture the effect of ϕ on light-off in low T_{in}. This suggests a need to tune the reversible surface reactions such that at low T_{in}, CH_4 adsorption is not solely the rate-limiting reaction as sensitivity analysis as discussed in next subsection.

As the experiment result showed, water delays low-temperature light-off. Also, it was shown, pressure of O_2 in reactor can impact greatly on conversion of CH_4 in higher temperatures (Figure 6.9). In this regard, Figure 7.3 compares how the model predictions for $\phi = 0.2$ and $\phi = 0.4$ with both dry and wet inlet feeds change with reactor pressure. The high-pressure simulation predicts that Pd reduction is completely avoided at the total pressure 10 atm (or $P_{O2} = 2.0$ atm) conditions even for T_{in} up to 850°C (above which is where gas phase reactions become significant). This result suggests that the reduction observed at low P_{tot} may be avoided at high-pressure conditions, if temperature does not rise significantly higher than at low-pressure. This is likely mass transfer scales with P

with an power less than 1 (Kolaczkowski 1995), but also because even with kinetically controlled conditions, the reduced vacancies at higher P_{tot} reduce the effective CH_4 adsorption rates.

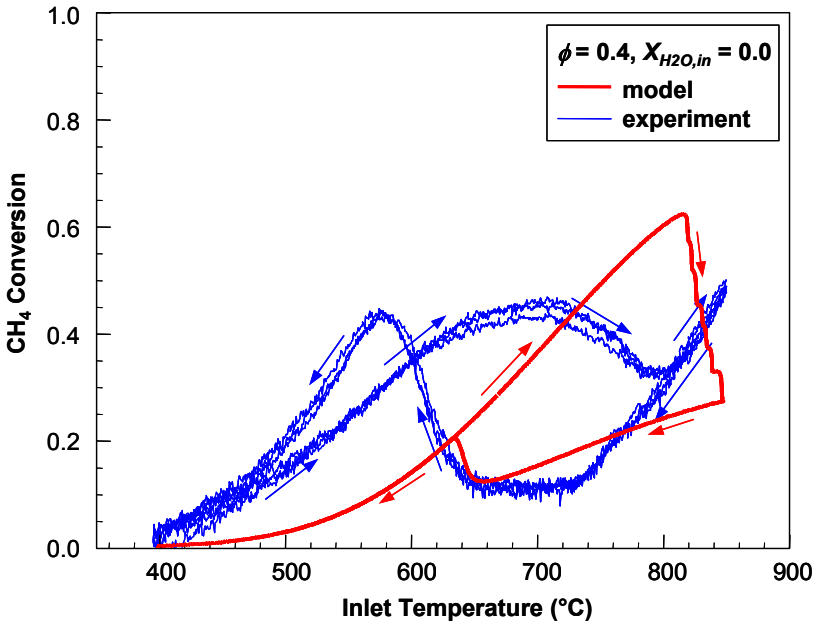

Figure 7.2 Comparison of experimental cycles with model predictions

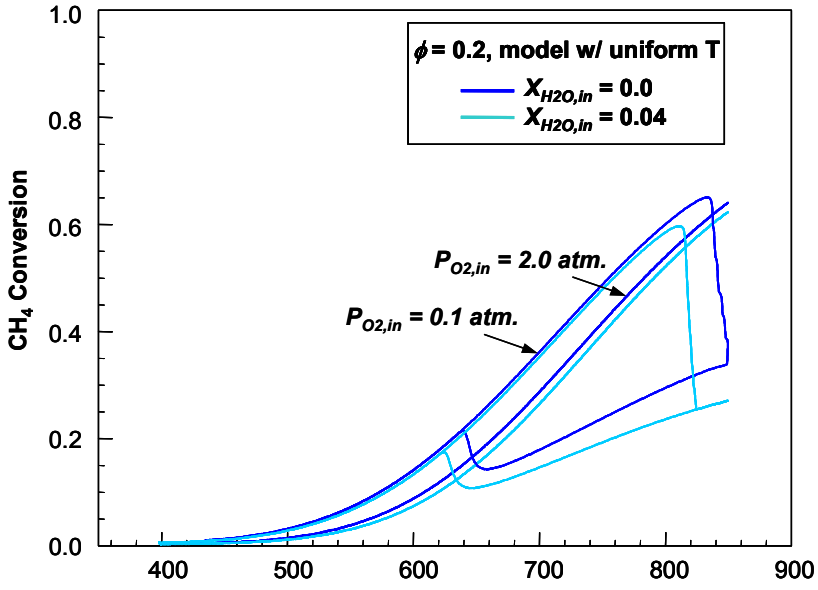

Figure 7.3 Model predictions for dry/wet feed for two different reactor pressures

7.5 Sensitivity analysis

The non-linear nature of chemical mechanisms, such as the Pd-CH_4 oxidation mechanism presented in this chapter, leads to kinetic rates that are very sensitive to the instantaneous species fractions as well as temperature. At any stage of process, kinetics is determined exclusively by the actual species concentrations and the rate coefficients. Therefore, kinetic problems should be analyzed by using quantities only depending on the concentrations and the kinetic parameters (Turanyi 1988). In this way, in conventional sensitivity analysis, the basic desired quantity is the sensitivity coefficient of concentration evaluated as the partial derivative of a species mass fraction Y_k with respect to a kinetic parameter k_i, $s_{ki} = \partial Y_k/\partial k_i$. Sensitivity coefficients can be either a function of time or quasi-stationary. The calculated coefficients provide a measure of the response of species concentrations and other physical variables with respect to the perturbation in the value of parameter k_j. The kinetic differential equations for a chemical

system consisting of *I* reactions and $K_{gas}+K_{surf}+K_{bulk}$ -3 species are given by the equation 5.6:

$$\frac{\partial \vec{y}}{\partial t} = \vec{F}(\vec{y}, \vec{k}) \tag{7.4}$$

Where $\vec{y}(0) = \vec{y}_0$ and $\vec{y}(t)$ is the K_{tot}-vector species including gas, surface and bulk phases and $\vec{k}$ is the *I*-vector of rate coefficients. Here only concentrations are considered as dependent variables; nevertheless other variables like temperature and pressure can be taken into account. To calculate local first order sensitivity coefficients, differentiation of the rate law equations (7.4) with respect to the parameters provides differential equations:

$$\frac{\partial}{\partial t}\left(\frac{\partial \vec{y}}{\partial k_i}\right) = \left(\vec{\vec{F}}_y\right)\frac{\partial \vec{y}}{\partial k_j} + \vec{F}_j \tag{7.5}$$

where $\vec{\vec{J}} = \vec{\vec{F}}_y$ and $\vec{F}_j = \partial \vec{F} / \partial k_j$, with $j = 1,2, \ldots, I$.

In non-linear systems, the sensitivity coefficients may be regarded as dynamic quantities according to equation 7.5. Dynamic response of the system to a differential change in k_j near to the steady point is given by time profiles of the dynamic response of the system. In reaction systems species concentrations are usually a function of time, it means $\vec{\vec{F}}_y$ and $\vec{F}$ are time dependent. Thus, sensitivity equation 7.5 is a system of linear differential equations with variable coefficients. Therefore, calculation of the sensitivity coefficients is not straightforward as it is in the case of equilibrium or stationary systems. Numerical integration of sensitivity equations can be done by different ODE stiff solver packages like, LSODE (Hindmarsh 1983), DASSL (Petzold 1983) and LIMEX (Deuflhard et al. 1987). Some more advanced mathematical methods like Green functions has been shown successfully (Turanyi 1990) but will not be discussed further here.

In systems with region of physical parameters with long time scales, constant concentration assumption will serve as a good assumption. Therefore, time profiles of the sensitivity coefficients converge to a steady-state curve. In other words, stationary sensitivity coefficients are the limits in time of the dynamic system, equation 7.5. This means steady state is asymptotically stable. For stationary conditions, matrices $\vec{\vec{F}}_y$, $\vec{F}$ are time invariant and the stationary sensitivity coefficients can be calculated from the following algebraic equations:

$$\frac{\partial \vec{y}}{\partial k_j} = -\vec{\vec{F}}_y^{-1} \vec{F}_j \qquad j = 1, \ldots..., I \tag{7.6}$$

The stationary sensitivity matrix represents the change of stationary species concentrations as a result of a differential change in parameters. For a chemical process, they are a function of temperature and chemical composition.

7.6 Observations from sensitivity analysis

Sensitivity study is applied to post-process the surface chemistry of Pd-CH_4 in different conditions. To compute sensitivity coefficients, the developed code for calculating sensitivity matrix was integrated with the channel flow model. Then the combined model was run for a range of inlet temperatures and compositions in dry feed. Quasi-steady sensitivity coefficients are calculated at temperatures from 400°C to 800°C for equivalence ratio ϕ = 0.2, 0.4 with dry/wet feeds. Each sensitivity coefficient is the

change of the solution variable with respect to change of pre-exponential factor of all reactions and is a function of variables.

Sensitivity analysis for ignition temperature in different points of a heating cycle is shown in Figures 7.4, 7.5 and 7.6. Contributed surface reactions have been specified based on the absolute value of sensitivity coefficients less than 10^{-3}. This lower bound has shown a convenient choice for the range of sensitivity coefficients calculated for the inlet conditions in the current study. The controlling surface reactions of ignition temperature are presented in Table 7.2 and 7.3. It is obvious adsorption of CH_4 on surface oxide (reaction 8f in Table 7.2) mainly control the ignition temperature. In temperatures $\leq 600°C$, dissociative adsorption O_2 on oxide vacancy (reactions 2 and 13 in Table 7.2) has shown relatively high contribution. The other reactions are sufficiently fast that they do not significantly affect the ignition temperature. In inlet temperature 800°C, more reactions in Table 7.2 have shown contribution in ignition temperature. Interestingly, at this temperature, surface reaction between O(s) and O(sb) is more important than O_2 adsorption. This is related to the time scales of these reactions. In high temperature rate of equilibration of adsorption/desorption is much faster than that of surface reaction between O(s) and O(sb) (surface nucleation).

Thus, a proper description of CH_4 adsorption is crucial for accurate prediction of ignition temperature. In particular, decreasing the pre-exponential of CH_4 adsorption (i.e. the sticking coefficient) decreases the ignition temperature, whereas decreasing the preexponential of O_2 adsorption (reaction 2 in Table 7.2) has the opposite effect on ignition temperature. This is consistent with our understandings from the system. For highly lean conditions, CH_4 acts as the limiting species. Also, CH_4 and O_2 adsorb

competitively on Pd surface which is dominantly covered by O(sb). Therefore any reaction that facilitates the adsorption CH_4 over that of O_2, in general increases the activity of catalyst surface, resulting in higher temperature.

Effect of higher concentration of CH_4 on ignition temperature has shown in Figures 7.7 thru 7.9. Increasing CH_4 concentration has activated more reactions, shown in Tables 7.2 and 7.3. In temperatures $\leq 600°C$, adsorption of CH_4 and O_2 mainly control the ignition temperature, whereas at $T_{in} = 800°C$, ignition temperature is controlled by different mechanisms including CH_4 adsorption, O_2 adsorption on oxide vacancies and Pd metal (small dependency) and bulk oxidation/reduction.

Sensitivity analysis for CH_4 conversion in simulated conditions, again showed very strong dependence on CH_4 adsorption presented in Figure 7.10 thru 7.12 for $\phi = 0.2$ and dry feed, although O_2 adsorption has some contribution to fuel concentration. Related surface reactions are brought in Table 7.2. In low temperatures surface chemistry mechanism is driven basically by CH_4 adsorption and O_2 mechanism. However, in 800°C Pd-O_2-H_2 surface reactions show contribution to conversion.

To further assess the surface chemistry, effect of prefacors of reaction was investigated for conversion in higher CH_4 concentration, $\phi = 0.4$. Figures 7.13 thru 7.15 depict this effect. Fuel concentration doesn't show any effect on conversion sensitivity in $T_{in} \leq 600°C$. In that range, conversion is significantly governed by CH_4 adsorption and O_2 mechanism. This is compatible with the other behaviors, increasing the fuel concentration increases competition between O_2 and CH_4. In $T_{in} = 800°C$, conversion is mainly impacted by O_2 mechanism. At this temperature, as the experimental result show, PdO_x

catalyst is reduced and effect of CH_4 adsorption on O(sb) decreases as it is shown in Figure 7.15 (reaction 8f in Table 7.2).

Another aspect of sensitivity analysis is calculation of sensitivity coefficients with respect to thermodynamic parameters like activation energies. This matter will not be covered here, although some calculations are done. These sensitivity coefficients are important in exploring the sensitivity of reactions with respect to their barriers in different temperatures and fuel concentrations. Also, this can be more helpful in identifying the critical chemical pathway to be considered.

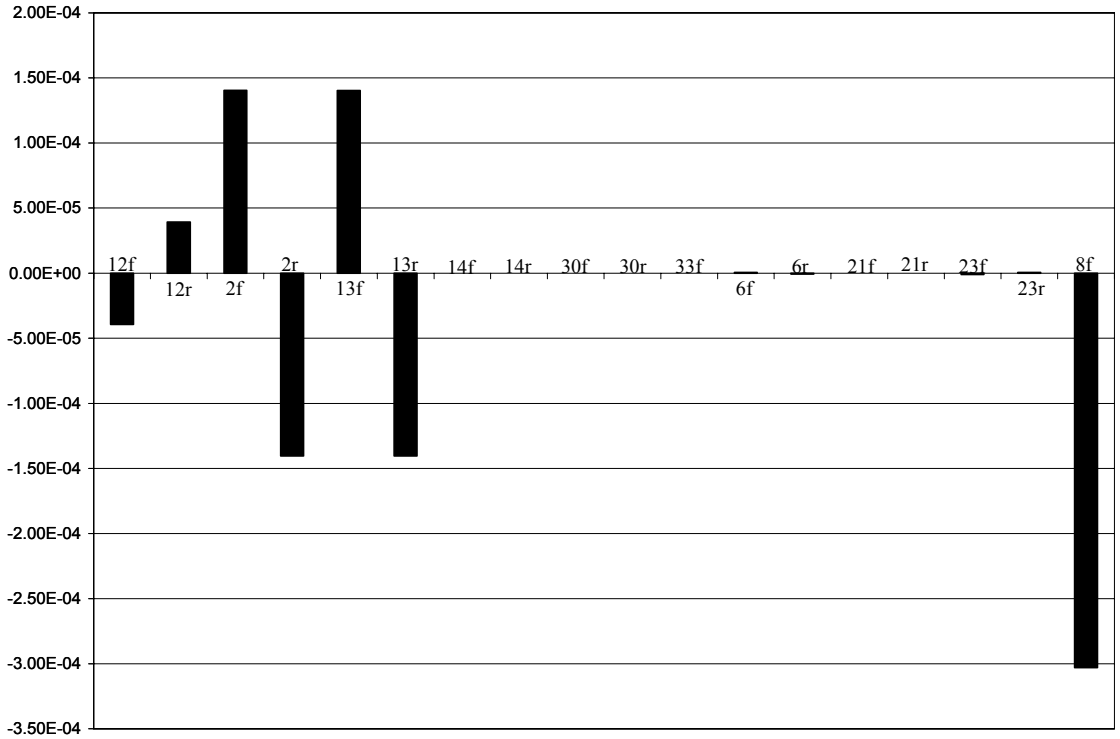

Figure 7.4 Sensitivity of gas temperature with respect to surface reaction rates at T_{in} = 400°C, ϕ = 0.2, $X_{H2O,in}$ = 0.0.

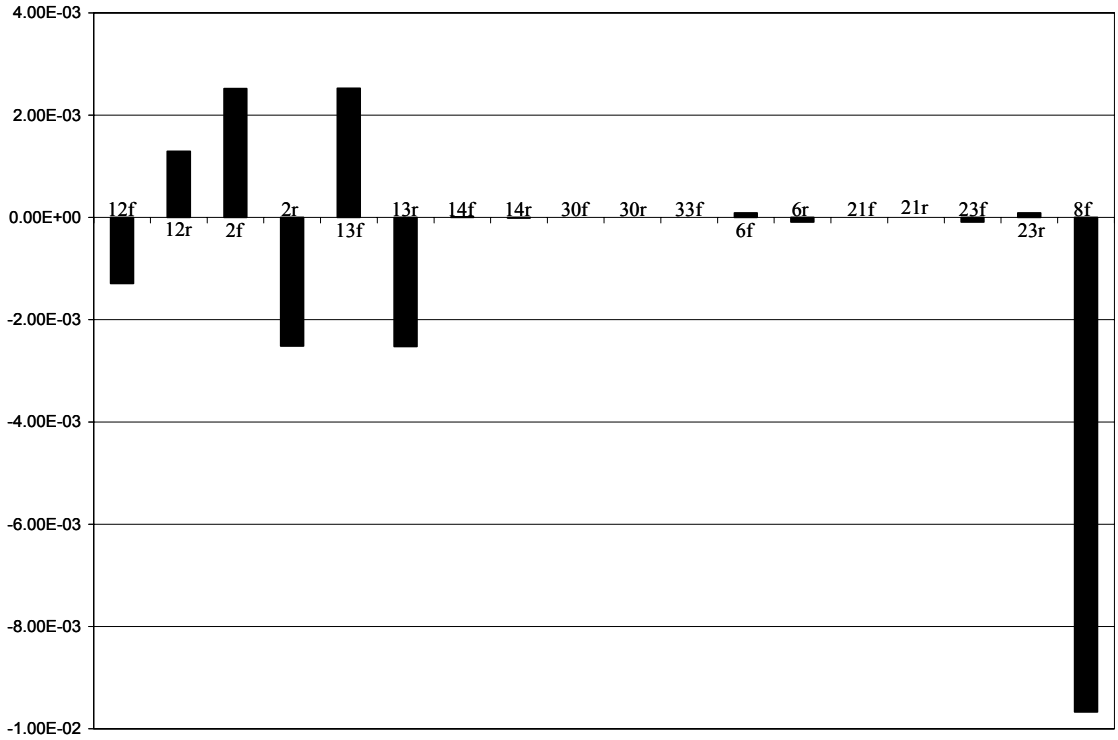

Figure 7.5 Sensitivity of gas temperature with respect to surface reaction rates at T_{in} = 600°C, ϕ = 0.2, $X_{H2O,in}$ = 0.00.

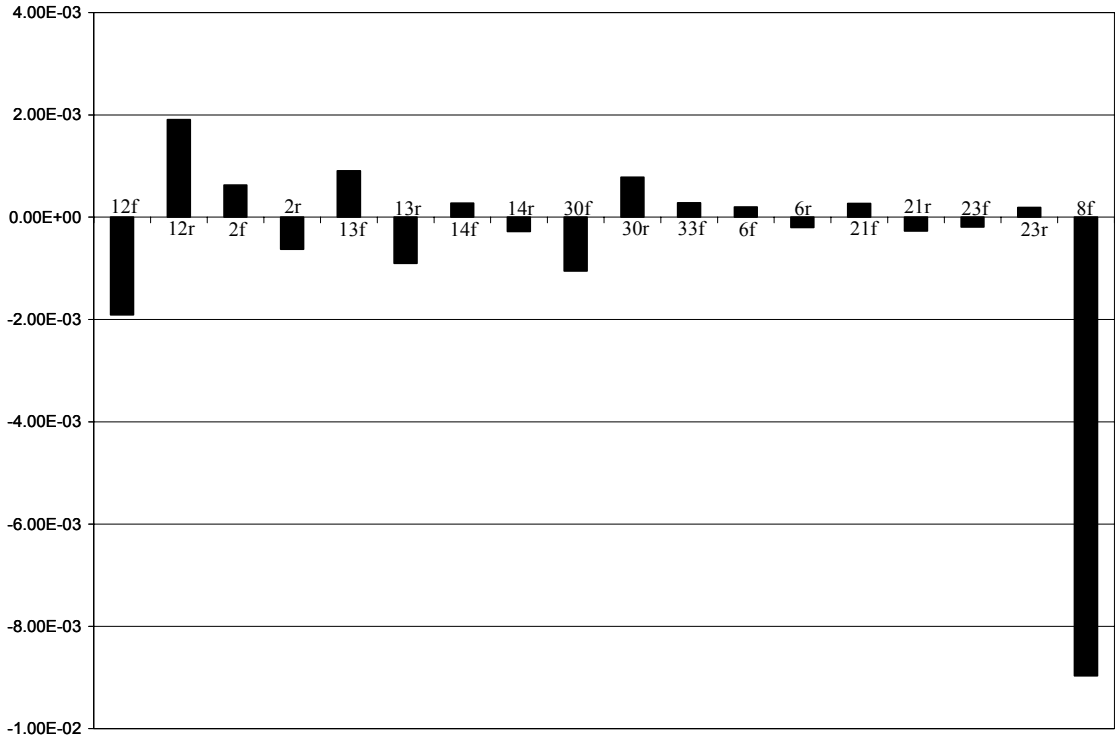

Figure 7.6 Sensitivity of gas temperature with respect to surface reaction rates at T_{in} = 800°C, ϕ = 0.2, $X_{H2O,in}$ = 0.0.

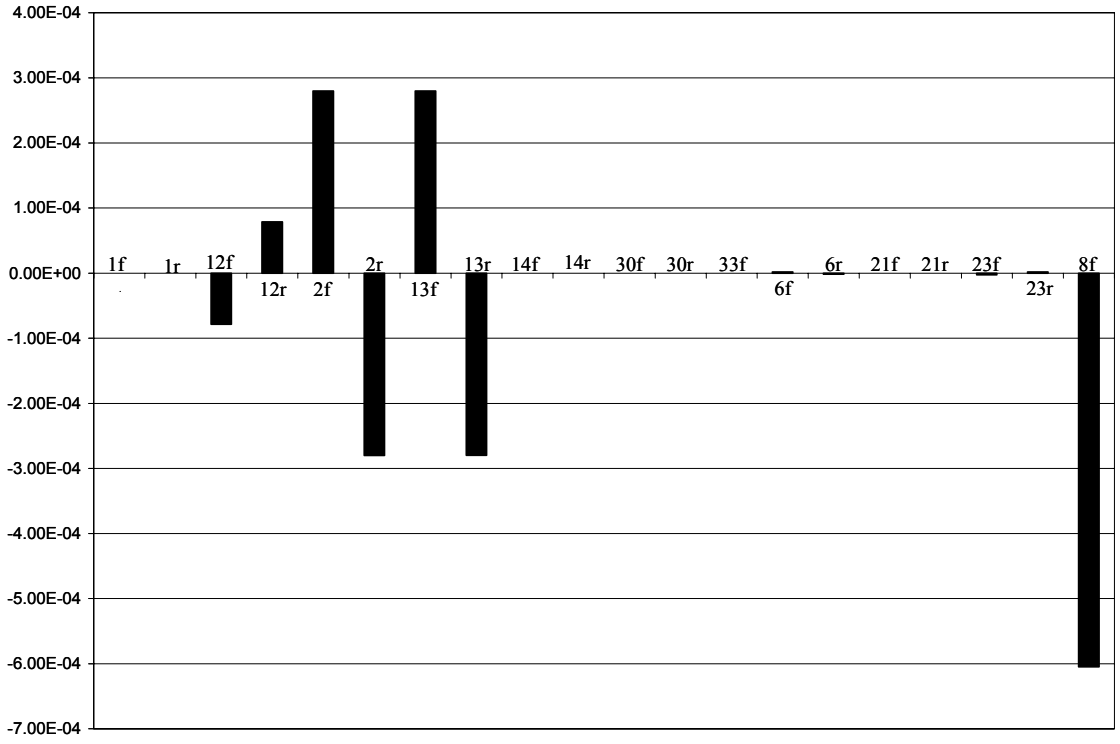

Figure 7.7 Sensitivity of gas temperature with respect to surface reaction rates at T_{in} = 400°C, ϕ = 0.4, $X_{H2O,in}$ = 0.0.

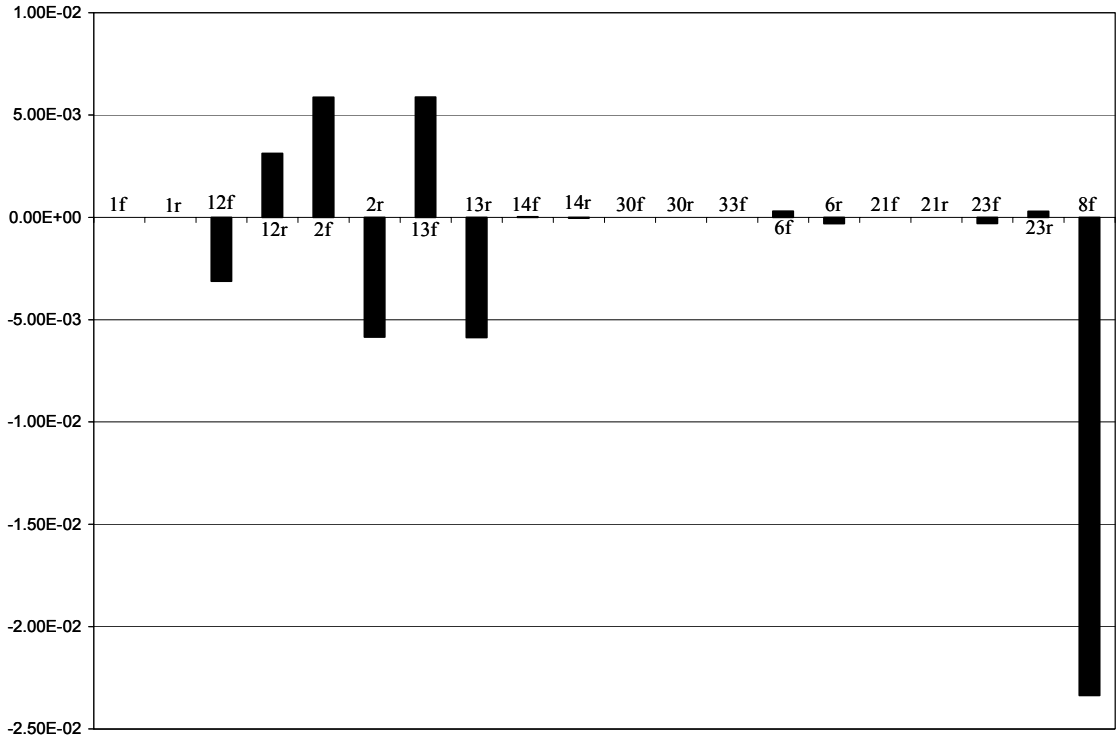

Figure 7.8 Sensitivity of gas temperature with respect to surface reaction rates at T_{in} = 600°C, ϕ = 0.4, $X_{H2O,in}$ = 0.0.

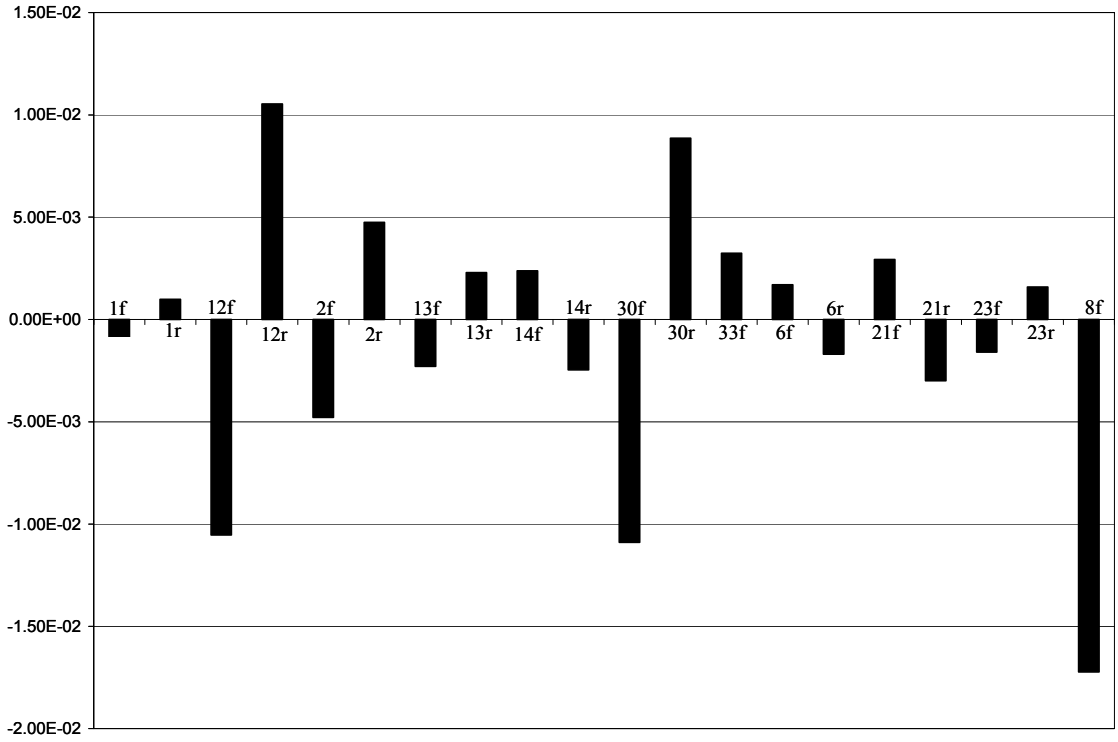

Figure 7.9 Sensitivity of gas temperature with respect to surface reaction rates at T_{in} = 800°C, ϕ = 0.4, $X_{H2O,in}$ = 0.0.

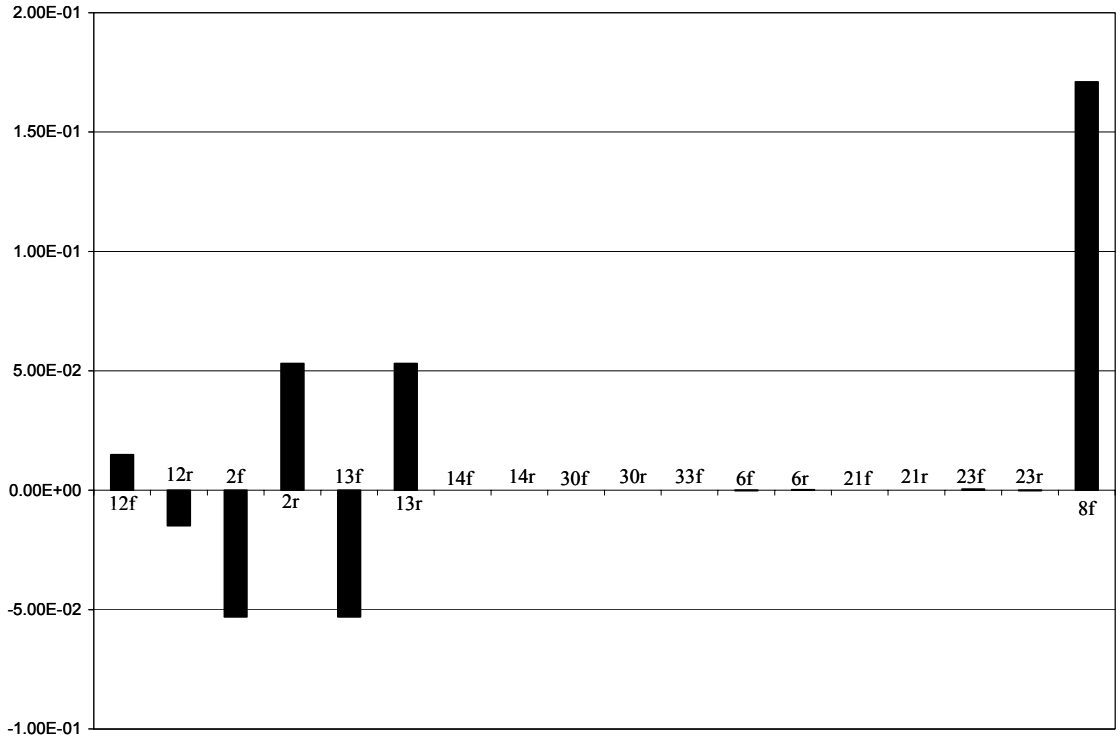

Figure 7.10 Sensitivity of conversion with respect to surface reaction rates at T_{in} = 400°C, ϕ = 0.2, $X_{H2O,in}$ = 0.00.

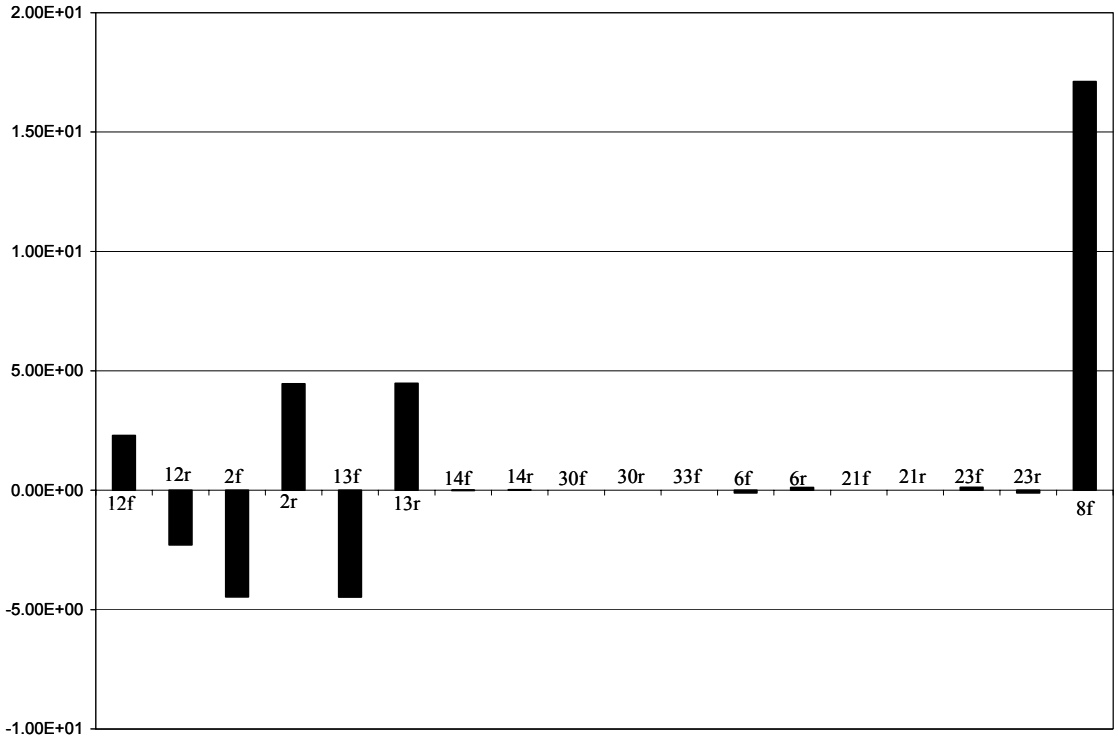

Figure 7.11 Sensitivity of conversion with respect to surface reaction rates at T_{in} = 600°C, ϕ = 0.2, $X_{H2O,in}$ = 0.00.

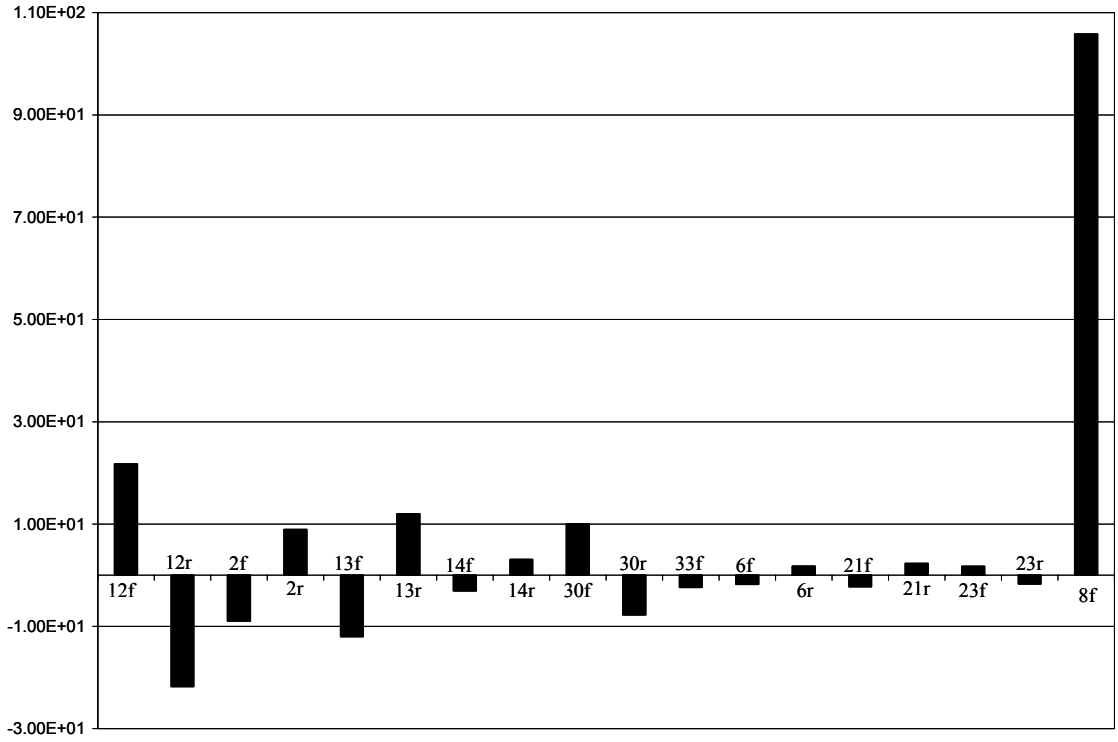

Figure 7.12 Sensitivity of conversion with respect to surface reaction rates at T_{in} = 800°C, ϕ = 0.2, $X_{H2O,in}$ = 0.00.

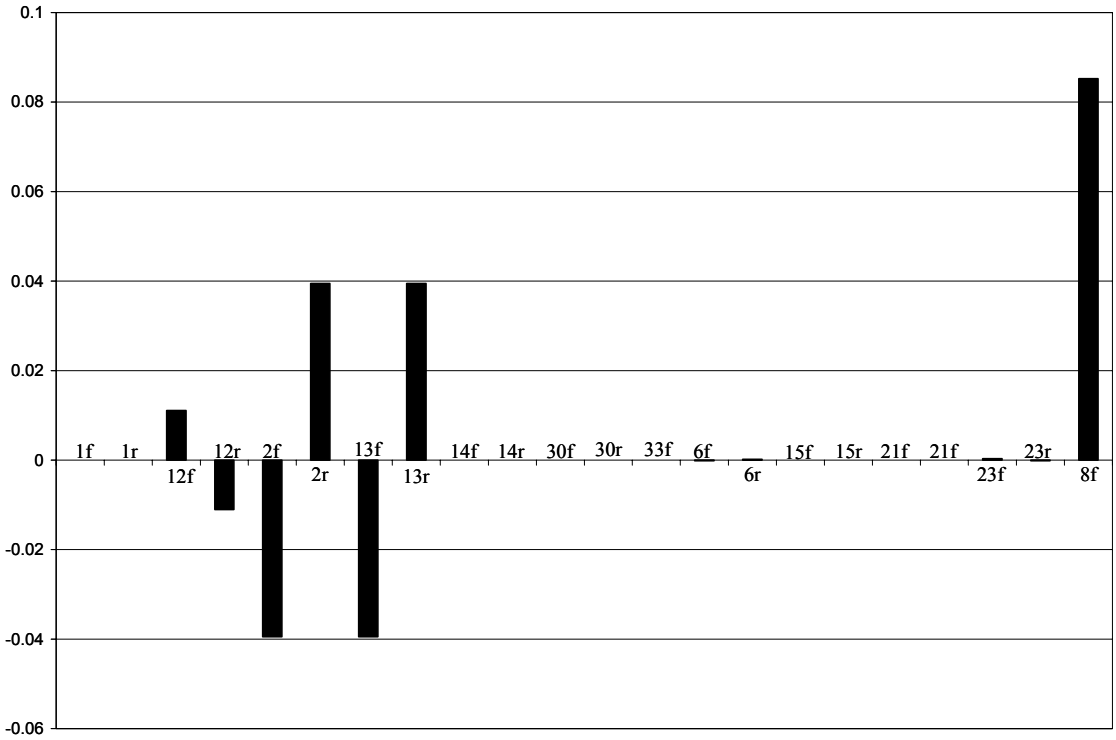

Figure 7.13 Sensitivity of conversion with respect to surface reaction rates at T_{in} = 400°C, ϕ = 0.4, $X_{H2O,in}$ = 0.00.

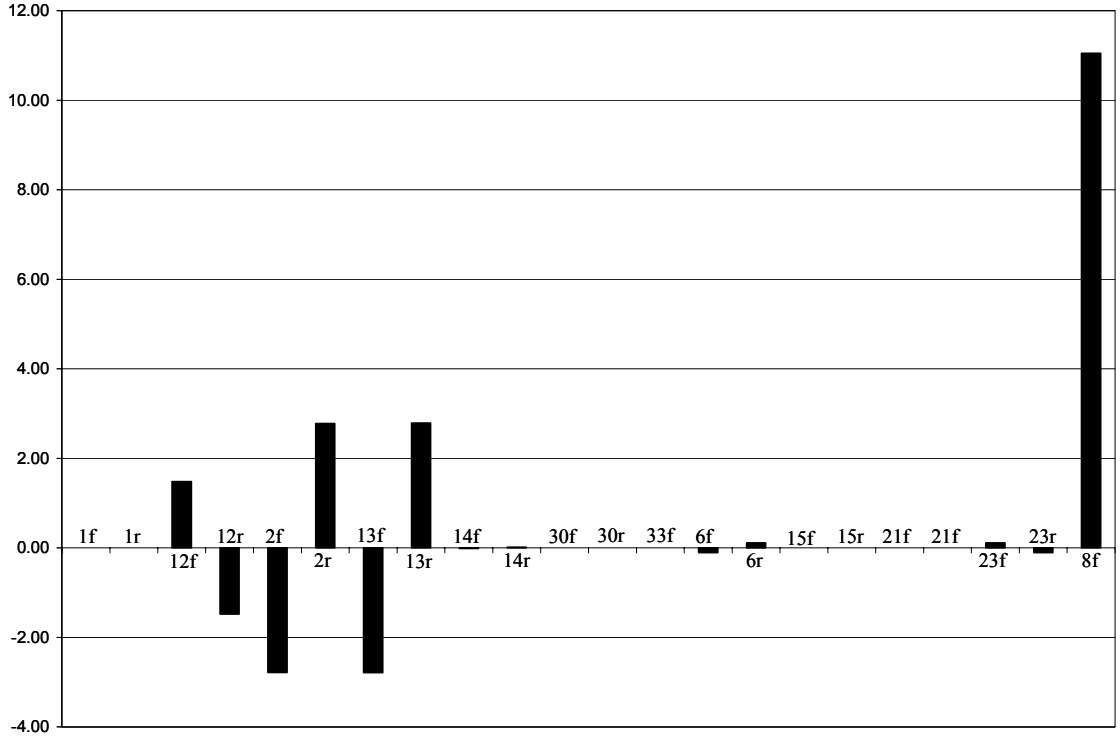

Figure 7.14 Sensitivity of conversion with respect to surface reaction rates at T_{in} = 600°C, ϕ = 0.4, $X_{H2O,in}$ = 0.00.

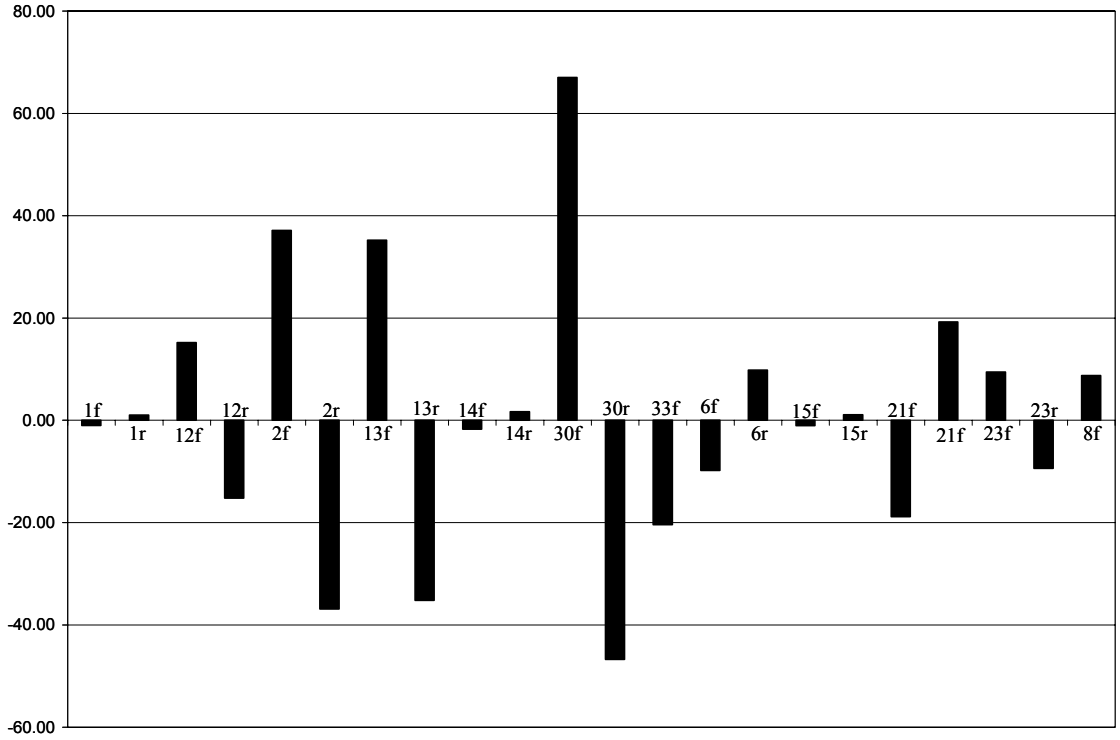

Figure 7.15 Sensitivity of conversion with respect to surface reaction rates at T_{in} = 800°C, ϕ = 0.4, $X_{H2O,in}$ = 0.00.

7.7 Conclusion

The preliminary proposed mechanism presents a thermodynamically consistent mechanism based on species enthalpies and simple assumptions about constant entropies of surface species. The mechanism has not been fully optimized, but it does qualitatively CH_4 light-off, high temperature Pd reduction and associated loss in CH_4 activity at the tested $P_{O2,in}$, and the hysteresis observed in reoxidation/reactivation upon cooling in temperature cycles.

Sensitivity analysis for a comprehensive C_1 mechanism for the oxidation of CH_4 over Pd-based catalysts has been conducted in order to determine the important reaction path ways at different conditions. It was seen adsorption of CH_4 has a great impact on ignition temperature and conversion at different temperatures.

Chapter 8

Conclusion and Recommendation for Direction of Future Works

8.1 Conclusions

Applications of fuel-lean catalytic combustion for power generation and exhaust heat recovery have motivated the desire for reactor optimization. Such optimization requires adequately detailed surface chemistry models to predict reactor performance over a broad range of conditions relevant to the application. This study presents experimental and numerical studies in well-defined micro-reactors for catalytic combustion of two systems:

- Pd-catalyzed H_2 combustion for 50°C < T_{in} < 250°C for $\phi < 0.2$
- Pd-catalyzed CH_4 combustion in 400°C < T_{in} < 900°C for $\phi < 0.4$

For the cases studied, experiments indicate that H_2 conversion depends on ϕ only at low temperatures (< 125°C) where conversion remains under 40%. For higher temperatures (> 125°C) mass transfer limitations prevails as temperature increases thus conversion becomes relatively independent of ϕ. Addition of H_2O vapor to the inlet flow causes a reduction in conversion for lower temperatures (< 125°C), but for higher than that it only delays catalyst light-off and the rapid transition to high steady-state conversion.

Detailed modeling of low-temperature H_2 combustion over the supported Pd-based catalysts by discretized porous washcoat model can capture the experimental results in low temperature range ≤ 250°C which is relevant to low-temperature heating and fuel cell anode exhaust combustion. The effect of intra-phase diffusion for channel-

flow oxidation reactors with washcoats ranging in thickness from 10 to 80 μm is explored in combination with a detailed surface chemistry for low-temperature (≤ 200°C) H_2 oxidation over supported Pd/PdO_x catalysts. The Pd-H_2-O_2 surface chemistry mechanism predicts non-linear behavior of conversion with respect to H_2 concentrations at the low equivalence ratios particularly at lower temperatures (< 150°C) in agreement with experiments. The catalytic washcoat model also shows that conversion and catalyst effectiveness are a strong function of the site fractions of vacancies available for H_2 adsorption, which is strongly dependent upon flow conditions and at higher conversions with depth in the porous washcoat. The results suggest that care should be taken in interpreting kinetic data for oxidation reactions even when relatively thin washcoats are employed for reaction rate studies. It was found the homogeneous gas phase chemistry can be neglected at the lean combustion conditions.

Capability of intrinsic low dimensional manifolds (ILDM's) for interpreting complex behavior of catalytic combustion chemistry has been revealed for low temperature combustion of H_2 over supported Pd-based catalysts. Two similar surface chemistry mechanisms, capture the negative influence of gas-phase H_2O on H_2 conversion and the non-linear behavior of H_2 conversion with respect to H_2 concentration. Analysis of these mechanisms and their differences by the dynamical model reveals complex behavior including strong oscillations for some conditions and rapid decomposition of states during approach to steady–state conversion. The differential reactor simulations reveal ILDM's with slow modes in the transient catalytic combustion. H_2O concentration in the external flow does not significantly alter the slowest modes, but does impact the rate or progress along the ILDM trajectories. The

system eigenvalues and eigenvectors identify qualitatively critical set of reactions and surface species controlling rate limiting processes.

The experimental study of CH_4 oxidation on γ-Al_2O_3 supported Pd catalysts revealed key features of surface kinetics for this reaction including reduction/reoxidation in higher temperatures. Temperature difference between reduction/reoxidation is relatively independent of ϕ, but dependent on inlet water content. Also, experiment showed partial pressure of O_2 impact greatly on reduction temperature of Pd and thus on activity of catalyst. Inhibiting effect of water on CH_4 conversion was not observed for cooling (reoxidation) cycle.

The detailed surface chemistry mechanism of CH_4 on supported Pd-based catalysts is evaluated against experiment measurements in the annular flow reactor for higher temperatures relevant to gas turbines combustion applications. It predicts complex behavior observed in experiments such as hysteretic effect of activity during heating and cooling cycles due to reduction/reoxidation of PdO, transient light-off in temperature ramp, water inhibiting effect and transient performance under high pressure atmospheres. Model does capture qualitative trends including the minimal effect of gas phase water on the CH_4 oxidation. Numerical model predict well that combustion equivalence ratio does not have a prominent role in high temperature activity at low pressure in agreement with the experiment. Model suggests that the reduction observed at low P_{tot} may be readily avoided at high pressure conditions by reducing mass transfer and vacancies, but it fails to capture well the differences for the two combustion equivalence ratio at low inlet temperature

Sensitivity analysis of surface chemistry of CH_4 over the supported Pd-based catalysts has shown at low temperature, although CH_4 adsorption is not solely the rate-limiting reaction, it has a strong impact on ignition temperature. Also, it was revealed at lower concentration of fuel surface chemistry is mainly driven by O_2 mechanism. Adding H_2O vapor to gas phase removes impact of CH_4 adsorption and surface chemistry is controlled solely by water adsorption/desoption and surface reactions including OH(sb).

8.2 Directions for future work

Despite the significant amount of research that has already been conducted in the current study, there is still work that can be done in this area. The surface chemistry mechanism of H_2 combustion over the supported Pd-based catalysts could b improved by incorporating processes for H_2 combustion on metallic Pd particles. For the current study, surface chemistry for Pd-O_2-H_2 has only been designed for Pd catalysts in deeply oxidized form. This was considered to be more important initially. However, a set of experiments performed on entirely reduced PdO_x to Pd metal indicated the tremendous increase in the activity of the reduced catalyst. In the reduced case, the controlling processes would be unlike of that in oxidized catalyst and sub-surface catalyst state would change. Incorporation of surface enthalpy interactions on metallic Pd for H_2 combustion surface species can provide a broad range for the validity of the Pd-O_2-H_2 surface mechanism. Despite a preliminary set of experiment was run in the current study, there is still a need to investigate sub-surface chemistry of reduced catalysts behavior and H uptake/abstraction.

As discussed in Chapter 3, the correlations for interphase heat and mass transfer processes in catalytic channel flows might have some room to improve to capture the light-off conversions, particularly in low equivalence ratios. The reactors used in this study have very short residence time and work in kinetically limited operating conditions. This means all correlations should have accurate enough for interphase heat and mass transfer. A 50% increase in the Sh_k for the fuel resulted in less than a 10% increase in conversion. Additional research into different correlations would be useful for the applications to ensure adequate accuracy in the correlations. As a suggestion modeling with a multi-dimensional flow model using a CFD package such as FLUENT would be a complementary study.

In the current study, the model for the catalytic combustion over the supported Pd-based catalyst was validated using an experimental setup. These validation studies were adequate for model validation, but they did not provide as much insight into the actual surface species status that experiment could provide. However, the differential reactor may be investigated experimentally with very low residence time reactors, and with isotopic tagging and/or in situ surface spectroscopy, many uncertainties associated in surface thermochemistry on Pd-based catalysts could be revealed.

It would be helpful to conduct further testing on catalytic characterization for the actual amount of catalyst surface area per unit volume of porous washcoat for a specific catalyst. This value has a large effect on the conversion since it controls the amount of reactant can adsorb and react in a catalytic cycle. The current study tuned this parameter from the experimental data. The actual value would provide a more accurate assessment of accrual activity. This can be done by CO adsorption method.

The current ILDM analysis was conducted for verified H_2 combustion on supported Pd-based catalysts results. ILDM can reveal contributed surface species in the slowest mode of a surface chemistry set of reactions. It would be helpful if the same analysis is conducted on the surface chemistry of CH_4 combustion to Pd-based catalysts.

8.3 Contributions and final points

The main objective of this study was application of intrinsic low dimensional method (ILDM) for evaluating surface chemistry for catalytic combustion. Based on the results of the current research, it seems ILDM needs another complementary tool in the order of meso- and/or micoscopic-scale (Raimondeau and Vlachos 2002) to be more useful and effective in appraising surface chemistry mechanisms. This is related to how to calculate activation barriers of adsorption/desorption processes, surface reactions and interaction potentials between different surface species. ILDM can show the time direction of the system, but it can not give an answer for energy barriers. In spite of the pros and cons of ILDM, the current study has developed two novel tools to analyze surface chemistry mechanisms.

To generate a reliable experimental data base, design of micro-reactor is a crucial issue in reactor design. Kinetics data can be easily masked by mass transfer limited conversions and operating condition of reactor. In designing a reactor for kinetics study two points must be satisfied, 1) isothermality of reactor; and 2) residence time of inlet fuel. The current study has shown that annular flow reactor has covered these two points.

In addition an integrated channel and porous washcoat model has been devised that can be effectively used to evaluate performance of reactors in different operating

conditions. This type of modeling has been absent from the reported literature in the analysis of catalytic combustion reactors. The validated numerical predictions against the experimental results in Chapters 4, 7 for low and high temperature catalytic combustion of H_2 and CH_4, respectively, indicate the significance of the developed model.

Appendix A

Adsorption & Desorption on Catalytic Surfaces

The first step in every heterogeneous catalytic reaction is the adsorption of reacting species on the active phase of the catalyst which consists of metal or metal oxide particles. Adsorption is the preferential concentration of a species at the interface between two phases. According to type of interaction one can differentiate two processes:

- Physisorption is based on the physical interaction and intermolecular forces (secondary valence forces) involving permanent dipole, induced dipole and quadrupole interactions. It includes van der Waals forces. The thermal energy, which becomes free with the physisorption of a particle, has the same order as the condensation enthalpy (order of 10 *kT* or 2-6 *kcal/mol*). This energy is not sufficient for breaking bonds.
- Chemisorption, on the other hand, involves a chemical linkage or covalent electron transfer (electrovalence) between adsorbent and adsorbate. Therefore, the adsorbed species is held to the surface by valence forces. It is almost always an exothermic process on the order of 100 *kT* or 10-50 *kcal/mol*. In some rare caeses such as dissociative chemisorption of hydrogen on glass, the process is endothermic.

Physisorption process is very fast due to its low activation barrier and it reaches equilibrium rapidly. However, chemisorption may occur at much slower rates, depending on the surface temperature. Chemisorption by a finite activation barrier proceeding at finite rates only above a minimum temperature is called activated chemisorption. However, in some systems chemisorption occurs very rapidly even at low temperatures

due to near zero activation energy such as chemisorption of H_2 and O_2 on many clean metal surfaces at liquid nitrogen temperature. These cases are called non-activated chemisorption. As another aspect, activation desorption barrier for physical adsorbates is much lower than that of the chemical adsorbates. Also, higher temperatures diminish the amount of physisorped gas monotonically. At temperatures higher than normal boiling point, physical adsorption should not occur, whereas appreciable chemisorption can take place at temperatures higher than boiling point. Due to finite rate of chemisorption, it may not be easy to determine the equilibrium concentration or even it may not be reversible.

After the reactants bind to the catalyst, the adsorbed species react with each other or with gas phase species. Then the system goes through a catalytic cycle where the intermediates are formed and destroyed. In order to react, the surface species must be able to move on the surface. The mechanism for this movement is that the adsorbed species overcome a small energy barrier and hop to an adjacent site. Interestingly, a strongly adsorbed species will not be mobile and thus the substrate in this case is a poor catalyst for that species. In the literature, heterogeneous catalytic reactions are treated by three mechanisms, the *Langmuir–Hinshelwood* (LH), the *Eley–Rideal* (ER) mechanism and a precursor mechanism. In the first case (LH), shown in Figure A.1, two or more thermally equilibrated adsorbed species react to form the product which is subsequently desorbed. The reaction is initiated by surface thermal energy. In the second case, (ER), shown in Figure A.1, the reaction is formed between an adsorbed species and an incoming gas phase molecule. Then the formed complex desorbs. In activated reactions, required energy to overcome the barrier is paid by the translational or internal energy of

the impinging molecule/atom. In the third case one of adsorbed species enters a mobile precursor state. The precursor rebounds along the surface until it reacts with the other adsorbed species. Then the formed complex desorbs. In catalytic research, results are discussed primarily in terms of LH mechanism (Masel 2001).

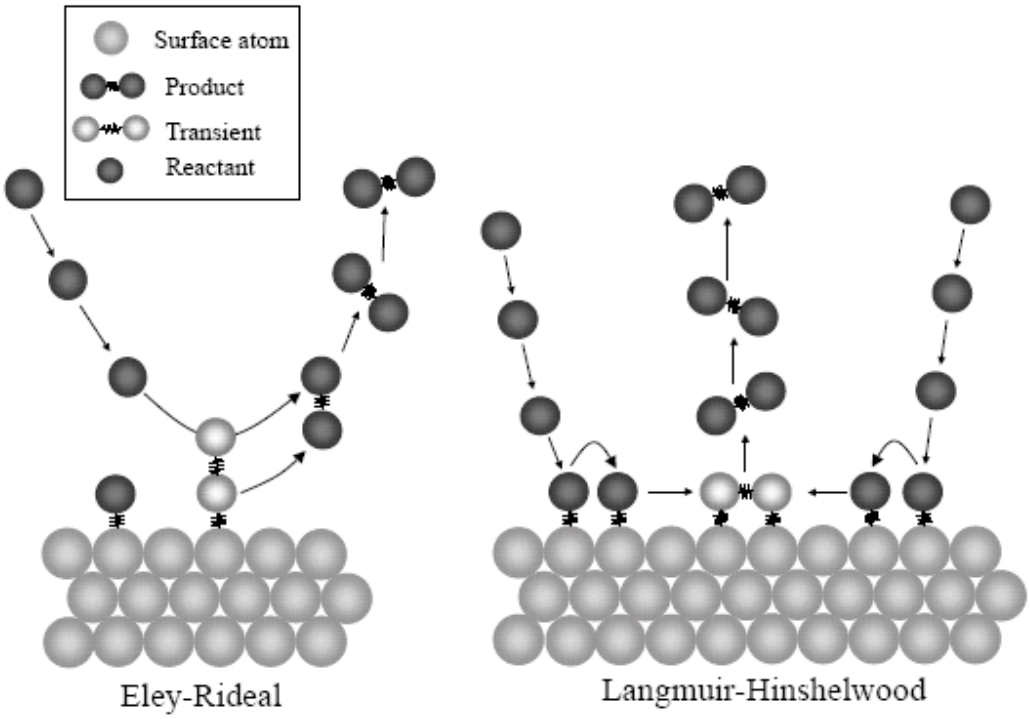

Figure A.1 Schematic of different surface reaction mechanisms

References

Aghalayam, P., et al., (2003). "A C1 mechanism for methane oxidation on platinum." Journal of Catalysis **213**(1): 23-38.

Ascher, U. M., Petzold, L.R. (1998). Computer Methods for Ordinary Differential Equations and Differential-Algebraic Equations, SIAM.

Au-Yeung, J., et al., (1999). "The dynamics of oxygen exchange with zirconia-supported PdO." Journal of Catalysis **185**(1): 213-218.

(1999). "Isotopic studies of methane oxidation pathways on PdO catalysts." Journal of Catalysis **188**(1): 132-139.

Bader, G., Deuflhard, P. (1983). "A Semi-Implicit Mi--Point Rule for Stiff Systems of Ordinary Differential Equations." Numerische Mathematik **41**: 373-398.

Baldwin, T. R. and R. Burch (1990). "Catalytic Combustion of Methane over supported Palladium Catalysts 1. Alumina supported catalysts." Applied Catalysis **66**(2): 337-358.

Bassett, M. R. and R. Imbihl (1990). "Mathematical-Modeling of Kinetic Oscillations in the Catalytic Co Oxidation on Pd(110) - the Subsurface Oxygen Model." Journal of Chemical Physics **93**(1): 811-821.

Beretta, A., et al., (1999). "Analysis of a catalytic annular reactor for very short contact times." Chemical Engineering Science **54**(6): 765-773.

(1999). "Potentialities and draw-backs of the experimental approach to the study of high T and high GHSV kinetics." Applied Catalysis a-General **187**(1): 49-60.

Boehman, A. L. (1998). "Radiation heat transfer in catalytic monoliths." AIChE Journal **44**(12): 2745-2755.

Brown, N. J., Li, G., Koszykowski, L. (1997). "Mechanism Reduction Via Principal Component Analysis." International Journal of Chemical Kinetics **29**(6): 393-414.

Bui, P. A., et al., (1997). "Modeling ignition of catalytic reactors with detailed surface kinetics and transport: Oxidation of H-2/air mixtures over platinum surfaces." Industrial & Engineering Chemistry Research **36**(7): 2558-2567.

(1997). "Hierarchical reduced models for catalytic combustion: H-2/air mixtures near platinum surfaces." Combustion Science and Technology **129**(1-6): 243-275.

Buki, A., et al., (2002). "Repro-modelling based generation of intrinsic low-dimensional manifolds." Journal of Mathematical Chemistry **31**(4): 345-362.

Burch, R. (1997). "Low NOx options in catalytic combustion and emission control." Catalysis Today **35**(1-2): 27-36.

Burch, R. and P. K. Loader (1994). "Investigation of Pt/Al2o3 and Pd/Al2o3 Catalysts for the Combustion of Methane at Low Concentrations." Applied Catalysis B-Environmental **5**(1-2): 149-164.

Burch, R. and F. J. Urbano (1995). "Investigation of the Active State of Supported Palladium Catalysts in the Combustion of Methane." Applied Catalysis a-General **124**(1): 121-138.

Canu, P. and S. Vecchi (2002). "CFD simulation of reactive flows: Catalytic combustion in a monolith." Aiche Journal **48**(12): 2921-2935.

Carroni, R., et al., (2004). "Cathlean: catalytic, hybrid, lean-premixed burner for gas turbines." Applied Thermal Engineering **24**(11-12): 1665-1676.

(2003). "High-pressure experiments and modeling of methane/air catalytic combustion for power-generation applications." Catalysis Today **83**(1-4): 157-170.

Carstens, J. N., et al., (1998). "Factors affecting the catalytic activity of Pd/ZrO2 for the combustion of methane." Journal of Catalysis **176**(1): 136-142.

Ciuparu, D., et al., (2001). "Temperature and time dependence of the water inhibition effect on supported palladium catalyst for methane combustion." Applied Catalysis a-General **216**(1-2): 209-215.

(2002). "Catalytic combustion of methane over palladium-based catalysts." Catalysis Reviews-Science and Engineering **44**(4): 593-649.

Ciuparu, D. and L. Pfefferle (2001). "Support and water effects on palladium based methane combustion catalysts." Applied Catalysis a-General **209**(1-2): 415-428.

Cobden, P. D., et al., (1999). "Field emission microscope study of the initial behaviour of the palladium-hydrogen system at low temperatures." Surface Science **432**(1-2): 61-68.

Datye, A. K., et al., (2000). "Catalyst microstructure and methane oxidation reactivity during the Pd <-> PdO transformation on alumina supports." Applied Catalysis A-General **198**(1-2): 179-196.

de Persis, S., et al., (2004). "Classical and dynamic analysis of gas phase reactivity - Influence of carbon precursor in the CVD of SiC." Journal of the Electrochemical Society **151**(4): C236-C244.

Demmel, J. W. (1997). Applied Numerical Linear Algebra, SIAM.

Deuflhard, P., et al., (1987). "One-Step and Extrapolation Methods for Differential-Algebraic Systems." Numerische Mathematik **51**(5): 501-516.

Deutschmann, O., et al., (1998). "Formal treatment of catalytic combustion and catalytic conversion of methane." Catalysis Today **46**(2-3): 155-163.

(2000). "Hydrogen assisted catalytic combustion of methane on platinum." Catalysis Today **59**(1-2): 141-150.

Deutschmann, O. and L. D. Schmidt (1998). "Modeling the partial oxidation of methane in a short-contact-time reactor." Aiche Journal **44**(11): 2465-2477.

Deutschmann, O., Schwiedernoch, R, Maier, L.I., Chatterjee, D. (2001). Natural gas Conversion in Monolithic Catalysts: Interaction of Chemical Reactions and Transport Phenomena. 6th Natural Gas Conversion Symposium, Girdwood, USA.

Dus, R. and E. Nowicka (1998). "Hydrogen segregation on a palladium hydride surface." Progress in Surface Science **59**(1-4): 289-300.

Emonts, B. (1999). "Catalytic radiant burner for stationary and mobile applications." Catalysis Today **47**(1-4): 407-414.

Etemad, S., et al., (1999). "Advanced technology catalytic combustor for high temperature ground power gas turbine applications." Catalysis Today **47**(1-4): 305-313.

Fant, D. B., et al., (2000). "Status of catalytic combustion R&D for the Department of Energy Advanced Turbine Systems program." Journal of Engineering for Gas Turbines and Power-Transactions of the Asme **122**(2): 293-300.

Farrauto, R., et al., (2003). "New material needs for hydrocarbon fuel processing: Generating hydrogen for the PEM fuel cell." Annual Review of Materials Research **33**: 1-27.

Farrauto, R. J., Bartholomew, C.H. (1997). Fundamentals of industrial catalytic processes, Blackie Academic & Professional.

Farrauto, R. J., et al., (1992). "Catalytic Chemistry of Supported Palladium for Combustion of Methane." Applied Catalysis a-General **81**(2): 227-237.

Fedkiw, R. P., et al., (1997). "High accuracy numerical methods for thermally perfect gas flows with chemistry." Journal of Computational Physics **132**(2): 175-190.

Fernandes, N. E., et al., (1999). "The autothermal behavior of platinum catalyzed hydrogen oxidation: Experiments and modeling." Combustion and Flame **118**(1-2): 164-178.

Fiorina, B., et al., (2003). "Modelling non-adiabatic partially premixed flames using flame-prolongation of ILDM." Combustion Theory and Modelling **7**(3): 449-470.

Fogelberg, J. and L. G. Petersson (1996). "Kinetic modelling of the H-2-O-2 reaction on Pd and of its influence on the hydrogen response of a hydrogen sensitive Pd metal-oxide-semiconductor device." Surface Science **350**(1-3): 91-102.

Forzatti, P. (2003). "Status and perspectives of catalytic combustion for gas turbines." Catalysis Today **83**(1-4): 3-18.

Forzatti, P. and G. Groppi (1999). "Catalytic combustion for the production of energy." Catalysis Today **54**(1): 165-180.

Fujimoto, K., et al., (1998). "Structure and reactivity of PdOx/ZrO2, catalysts for methane oxidation at low temperatures." Journal of Catalysis **179**(2): 431-442.

Gicquel, O., et al., (1999). "Direct numerical simulation of turbulent premixed flames using intrinsic low-dimensional manifolds." Combustion Theory and Modelling **3**(3): 479-502.

Goralski, C. T. and L. D. Schmidt (1999). "Modeling heterogeneous and homogeneous reactions in the high-temperature catalytic combustion of methane." Chemical Engineering Science **54**(24): 5791-5807.

Groppi, G. (2003). "Combustion of CH4 over a PdO/ZrO2 catalyst: an example of kinetic study under severe conditions." Catalysis Today **77**(4): 335-346.

Groppi, G., et al., (1995). "Analysis of Multidimensional Models of Monolith Catalysts for Hybrid Combustors." Aiche Journal **41**(10): 2250-2260.

(1995). "A Comparison of Lumped and Distributed Models of Monolith Catalytic Combustors." Chemical Engineering Science **50**(17): 2705-2715.

(1999). "Effect of ceria on palladium supported catalysts for high temperature combustion of CH4 under lean conditions." Catalysis Today **50**(2): 399-412.

(2001). "Structured reactors for kinetic measurements in catalytic combustion." Chemical Engineering Journal **82**(1-3): 57-71.

(2001). "High-temperature combustion of CH4 over PdO/Al2O3: kinetic measurements in a structured annular reactor." Chemical Engineering Science **56**(3): 831-839.

(1999). "Mathematical models of catalytic combustors." Catalysis Reviews-Science and Engineering **41**(2): 227-254.

Handrock-Meyer, S., et al., (2001). "A method to determine the dimension of long-time dynamics in multi-scale systems." Journal of Mathematical Chemistry **30**(2): 133-160.

Hartmann, N., et al., (1994). "The Role of Adsorbate-Adsorbate Interactions in the Rate Oscillations in Catalytic Co Oxidation on Pd(110)." Journal of Chemical Physics **101**(8): 6717-6727.

Hayes, R. E., et al., (1999). "Catalytic combustion of methane in a monolith washcoat: Effect of water inhibition on the effectiveness factor." Canadian Journal of Chemical Engineering **77**(4): 688-697.

Hayes, R. E. and S. T. Kolaczkowski (1994). "Mass and Heat-Transfer Effects in Catalytic Monolith Reactors." Chemical Engineering Science **49**(21): 3587-3599.

(1999). "A study of Nusselt and Sherwood numbers in a monolith reactor." Catalysis Today **47**(1-4): 295-303.

Hayes, R. E., et al., (2001). "The palladium catalysed oxidation of methane: reaction kinetics and the effect of diffusion barriers." Chemical Engineering Science **56**(16): 4815-4835.

(1992). "Finite-Element Model for a Catalytic Monolith Reactor." Computers & Chemical Engineering **16**(7): 645-657.

(1995). "Intraphase Diffusion and Interphase Mass-Transfer Effects During the Catalytic-Oxidation of Co in a Tube Wall Reactor." Proceedings of the Royal Society of London Series a-Mathematical and Physical Sciences **448**(1933): 321-334.

Heath, M. T. (2002). Scientific computing : an introductory survey, McGraw-Hill.

Heck, R. H., Wei, J., Katzer, J. (1976). "Mathematical modeling of monolithic catalysts." AIChE **22**(3): 477-484.

Hegedus, L. L. (1975). "Temperature excursions in catalytic monoliths." AIChE **21**(5): 849-853.

Hei, M. J., Chen, H.B., Yi, J. (1998). "CO2 reforming of CH4 on transition metal surfaces." Surface Science **417**: 82-96.

Hill, C. G. (1977). Chemical Engineering Kinetics & Reactor Design, John Wiley & Sons.

Hindmarsh, A. (1983). ODEPACK, A Systemized Collection of ODE Solvers**:** 55-64.

Holmgren, A. and B. Andersson (1998). "Mass transfer in monolith catalysts - CO oxidation experiments and simulations." Chemical Engineering Science **53**(13): 2285-2298.

Ibashi, W., et al., (2003). "Kinetic measurements of CH4 combustion over a 10% PdO/ZrO2 catalyst using an annular flow microreactor." Catalysis Today **83**(1-4): 115-129.

Imbihl, R. and G. Ertl (1995). "Oscillatory Kinetics in Heterogeneous Catalysis." Chemical Reviews **95**(3): 697-733.

Johansson, M. and L. G. Ekedahl (2001). "The water formation rate on platinum and palladium as a function of the surface hydrogen pressure from three-dimensional hydrogen pressure distributions." Applied Surface Science **180**(1-2): 27-35.

Kajita, S. and R. D. Betta (2003). "Achieving ultra low emissions in a commercial 1.4 MW gas turbine utilizing catalytic combustion." Catalysis Today **83**(1-4): 279-288.

Kaper, H. G. and T. J. Kaper (2002). "Asymptotic analysis of two reduction methods for systems of chemical reactions." Physica D **165**(1-2): 66-93.

Kee, R., J., Dixon-Lewis, G., Warnatz, J., Coltrin, M.E., Miller, J.A., Moffat, H.K. (1998). A Fortran Computer Code Package for the Evaluation of Gas-Phase, Multicomponent Transport Properties, SANDIA National Lab.

Kissel-Osterrieder, R., et al., (2000). "Dynamic Monte Carlo simulations of catalytic surface reactions." Proceedings of the Combustion Institute **28**: 1323-1330.

Kolaczkowski, S. T. (1995). "Catalytic Stationary Gas-Turbine Combustors - a Review of the Challenges Faced to Clear the Next Set of Hurdles." Chemical Engineering Research & Design **73**(A2): 168-190.

Kramer, J. F., et al., (2003). "Low-temperature combustion of hydrogen on supported Pd catalysts." Proceedings of the Combustion Institute **29**: 989-996.

Landenfeld, T., et al., (2002). "A turbulence-chemistry interaction model based on a multivariate presumed beta-PDF method for turbulent flames." Flow Turbulence and Combustion **68**(2): 111-135.

Leung, D., et al., (1996). "Diffusion limitation effects in the washcoat of a catalytic monolith reactor." Canadian Journal of Chemical Engineering **74**(1): 94-103.

Lischka, M. and A. Gross (2002). "Hydrogen adsorption on an open metal surface: H-2/Pd(210)." Physical Review B **65**(7).

Ljungstrom, S., et al., (1989). "An Experimental-Study of the Kinetics of Oh and H2o Formation on Pt in the H2+O2 Reaction." Surface Science **216**(1-2): 63-92.

Lopez, E., et al., (2001). "Influence of the methane combustion kinetic model on the operating conditions of an autothermal catalytic reactor." Industrial & Engineering Chemistry Research **40**(23): 5199-5205.

Lopez, N., et al., (2004). "When Langmuir is too simple: H-2 dissociation on Pd(111) at high coverage." Physical Review Letters **93**(14).

Lyubovsky, M. and L. Pfefferle (1998). "Methane combustion over the alpha-alumina supported Pd catalyst: Activity of the mixed Pd/PdO state." Applied Catalysis a-General **173**(1): 107-119.

(1999). "Complete methane oxidation over Pd catalyst supported on alpha-alumina. Influence of temperature and oxygen pressure on the catalyst activity." Catalysis Today **47**(1-4): 29-44.

Lyubovsky, M., et al., (1999). "TEM study of the microstructural modifications of an alumina-supported palladium combustion catalyst." Journal of Catalysis **187**(2): 275-284.

(2003). "Catalytic combustion over platinum group catalysts: fuel-lean versus fuel-rich operation." Catalysis Today **83**(1-4): 71-84.

Maas, U. (1998). "Efficient calculation of intrinsic low-dimensional manifolds for the simplification of chemical kinetics." Computing and Visualization in Science **1**: 69-81.

Maas, U. and S. B. Pope (1992). "Simplifying Chemical-Kinetics - Intrinsic Low-Dimensional Manifolds in Composition Space." Combustion and Flame **88**(3-4): 239-264.

Mantzaras, J., et al., (2000). "Numerical modelling of turbulent catalytically stabilized channel flow combustion." Catalysis Today **59**(1-2): 3-17.

Masel, R. I. (2001). Chemical Kinetics and Catalysis, wiley-Interscience.

McCarty, J. G. (1995). "Kinetics of PdO combustion catalysis." Catalysis Today **26**(3-4): 283-293.

Meusel, I., et al., (2001). "The interaction of oxygen with alumina-supported palladium particles." Catalysis Letters **71**(1-2): 5-13.

Mhadeshwar, A. B., et al., (2003). "Thermodynamic consistency in microkinetic development of surface reaction mechanisms." Journal of Physical Chemistry B **107**(46): 12721-12733.

Morfin, F., et al., (2004). "Catalytic combustion of hydrogen for mitigating hydrogen risk in case of a severe accident in a nuclear power plant: study of catalysts poisoning in a representative atmosphere." Applied Catalysis B-Environmental **47**(1): 47-58.

Muller, C. A., et al., (1997). "Combustion of methane over palladium/zirconia derived from a glassy Pd-Zr alloy: Effect of Pd particle size on catalytic behavior." Journal of Catalysis **166**(1): 36-43.

(1999). "Combustion of methane over palladium/zirconia: effect of Pd-particle size and role of lattice oxygen." Catalysis Today **47**(1-4): 245-252.

Nafe, J. and U. Maas (2002). "A general algorithm for improving ILDMs." Combustion Theory and Modelling **6**(4): 697-709.

Nomura, K., et al., (1999). "Combustion of a trace amount of CH4 in the presence of water vapor over ZrO2-supported Pd catalysts." Catalysis Letters **58**(2-3): 127-130.

Norris, A. T. and S. B. Pope (1995). "Modeling of Extinction in Turbulent-Diffusion Flames by the Velocity-Dissipation-Composition Pdf Method." Combustion and Flame **100**(1-2): 211-220.

Nuckols, M. L., VanZandt, K., and Finlayson, W.S. (2000). Diver heating using hydrogen catalytic reactions. Oceans Conference Record (IEEE), Providence, RI, IEEE.

Nutzenadel, C., et al., (2000). "Critical size and surface effect of the hydrogen interaction of palladium clusters." European Physical Journal D **8**(2): 245-250.

Ozawa, Y., et al., (2003). "Test results of a catalytically assisted combustor for a gas turbine." Catalysis Today **83**(1-4): 247-255.

Perdigon-Melon, J. A., et al., (2003). "Calorimetric study of methane interaction with supported Pd catalysts." Journal of Thermal Analysis and Calorimetry **72**(2): 443-451.

Peskov, N. V., et al., (2003). "Stochastic model of reaction rate oscillations during CO oxidation over zeolite-supported catalysts." Chemical Engineering Science **58**(21): 4797-4803.

Petzold, L. (1983). A discription of DASSL: a differential/algebraic system solver, Scientific Computing.

Pfefferle, L. D. and W. C. Pfefferle (1987). "Catalysis in Combustion." Catalysis Reviews-Science and Engineering **29**(2-3): 219-267.

Raimondeau, S. and D. G. Vlachos (2002). "Recent developements on multiscale, hierarchical modeling of chemical reactors." Chemical Engineering Journal **90**: 3-23.

(2002). "Recent developments on multiscale, hierarchical modeling of chemical reactors." Chemical Engineering Journal **90**(1-2): 3-23.

(2002). "The role of adsorbate-layer nonuniformities in catalytic reactor design: multiscale simulations for CO oxidation on Pt." Computers & Chemical Engineering **26**(7-8): 965-980.

Raja, L. L., et al., (2000). "A critical evaluation of Navier-Stokes, boundary-layer, and plug-flow models of the flow and chemistry in a catalytic-combustion monolith." Catalysis Today **59**(1-2): 47-60.

Ribeiro, F. H., et al., (1994). "Kinetics of the Complete Oxidation of Methane over Supported Palladium Catalysts." Journal of Catalysis **146**(2): 537-544.

Rinnemo, M., et al., (1997). "Experimental and numerical investigation of the catalytic ignition of mixtures of hydrogen and oxygen on platinum." Combustion and Flame **111**(4): 312-326.

Roussel, M. R., Fraser, S.J. (1990). "Geometry of the steady-state approximation: Perturbation and accelerated convergence method." Chemical physics **93**(2): 1072-1081.

Salomonsson, P., et al., (1995). "Methane Oxidation over Pdox - on the Mechanism for the Hysteresis in Activity and Oxygen-Content." Catalysis Letters **33**(1-2): 1-13.

Schlegel, A., et al., (1996). "Catalytic stabilization of lean premixed combustion: Method for improving NOx emissions." Combustion and Flame **105**(3): 332-340.

Schmidt, D., et al., (1998). "Intrinsic low-dimensional manifolds of strained and unstrained flames." Combustion Theory and Modelling **2**(2): 135-152.

Schuurman, Y. and C. Mirodatos (1997). "Uses of transient kinetics for methane activation studies." Applied Catalysis a-General **151**(1): 305-331.

Schwiedernoch, R., et al., (2003). "Experimental and numerical study on the transient behavior of partial oxidation of methane in a catalytic, monolith." Chemical Engineering Science **58**(3-6): 633-642.

Sekizawa, K., et al., (1993). "Catalytic Properties of Pd-Supported Hexaaluminate Catalysts for High-Temperature Catalytic Combustion." Journal of Catalysis **142**(2): 655-663.

Shaikhutdinov, S., et al., (2001). "Structure-reactivity relationships on supported metal model catalysts: Adsorption and reaction of ethene and hydrogen on Pd/Al2O3/NiAl(110)." Journal of Catalysis **200**(2): 330-339.

Sheng, P. Y., et al., (2002). "H-2 production from ethanol over Rh-Pt/CeO2 catalysts: The role of Rh for the efficient dissociation of the carbon-carbon bond." Journal of Catalysis **208**(2): 393-403.

Sidwell, R. W., et al., (2003). "Catalytic combustion of premixed methane/air on a palladium-substituted hexaluminate stagnation surface." Proceedings of the Combustion Institute **29**: 1013-1020.

Singh, S., et al., (2001). "Viscous detonation in H-2-O-2-Ar using intrinsic low-dimensional manifolds and wavelet adaptive multilevel representation." Combustion Theory and Modelling **5**(2): 163-184.

Skodje, R. T. and M. J. Davis (2001). "Geometrical simplification of complex kinetic systems." Journal of Physical Chemistry A **105**(45): 10356-10365.

Soderberg, D. and I. Lundstrom (1983). "Competition between Hydrogen and Oxygen Dissociation on Palladium Surfaces at Atmospheric Pressures." Solid State Communications **45**(5): 431-434.

Strang, G. (1968). SIAM Journal of Numerical Analysis **5**(3): 506-517.

Tomlin, A. S., Turanyi, T., Pilling, M.J. (1997). Mathematical tools for the construction, investigation and reduction of combustion mechanisms. Low-Temperature Combustion and Autoignition, Elsevier.

Turanyi, T. (1990). "Sensitivity Analysis of Complex Kinetic Systems: Tools and Applications." Journal of Mathematical Chemistry **5**: 203-248.

(1994). "Parameterization of Reaction-Mechanisms Using Orthonormal Polynomials." Computers & Chemistry **18**(1): 45-54.

Turanyi, T., Berces, T. (1988). "The Method of Quasi-Stationary Sensitivity Analysis." Journal of Mathematical Chemistry **2**: 401-409.

Uberoi, M. and C. J. Pereira (1996). "External mass transfer coefficients for monolith catalysts." Industrial & Engineering Chemistry Research **35**(1): 113-116.

van Giezen, J. C., et al., (1999). "The effect of water on the activity of supported palladium catalysts in the catalytic combustion of methane." Catalysis Today **47**(1-4): 287-293.

Veser, G., et al., (1999). "On the oxidation-reduction kinetics of palladium." Catalysis Letters **58**(4): 199-206.

Vlachos, D. G. and P. A. Bui (1996). "Catalytic ignition and extinction of hydrogen: Comparison of simulations and experiments." Surface Science **364**(3): L625-L630.

Wanker, R., et al., (2000). "A fully distributed model for the simulation of a catalytic combustor." Chemical Engineering Science **55**(20): 4709-4718.

Warnatz, J., Maas, U., Dibble, R.W. (1999). Combustion, Springer.

Wolf, M. M., et al., (2003). "Kinetic model for polycrystalline Pd/PdOx in oxidation/reduction cycles." Applied Catalysis a-General **244**(2): 323-340.

Yagi, K., et al., (1999). "Adsorption and desorption kinetics of oxygen on the Pd(110) surface." Surface Science **442**(2): 307-317.

Yan, X. and U. Maas (2000). "Intrinsic low-dimensional manifolds of heterogeneous combustion processes." Proceedings of the Combustion Institute **28**: 1615-1621.

Yetter, R. A., et al., (1991). "A Combined Stability-Sensitivity Analysis of Weak and Strong Reactions of Hydrogen Oxygen Mixtures." International Journal of Chemical Kinetics **23**(3): 251-278.

Zerkle, D. K., et al., (2000). "Understanding homogeneous and heterogeneous contributions to the platinum-catalyzed partial oxidation of ethane in a short-contact-time reactor." Journal of Catalysis **196**(1): 18-39.

Zhu, H. Y. (2001). Numerical Modeling of Methane Combustion on Palladium Catalyst for Gas Turbine Applications. Department of Mechanical Engineering. College Park, University of Maryland**:** 289.